FOOD ENGINEERING SERIES

Sterilization of Food in Retort Pouches

A.G. Abdul Ghani Al-Baali
Mohammed M. Farid

STERILIZATION OF FOOD IN RETORT POUCHES

FOOD ENGINEERING SERIES

Series Editor

Gustavo V. Barbosa-Cánovas, Washington State University

Advisory Board

Jose Miguel Aguilera, Pontifica Universidad Catolica de Chile
Pedro Fito, Universidad Politecnica
Richard W. Hartel, University of Wisconsin
Jozef Kokini, Rutgers University
Michael McCarthy, University of California at Davis
Martin Okos, Purdue University
Micha Peleg, University of Massachusetts
Leo Pyle, University of Reading
Shafiur Rahman, Hort Research
M. Anandha Rao, Cornell University
Yrjö Roos, University College Cork
Walter L. Spiess, Bundesforschungsanstalt
Jorge Welti-Chanes, Universidad de las Américas-Puebla

Titles

Jose M. Aguilera and David W. Stanley, *Microstructural Principles of Food Processing and Engineering*, Second Edition (1999)
Stella M. Alzamora, María S. Tapia, and Aurelio López-Malo, *Minimally Processed Fruits and Vegetables: Fundamental Aspects and Applications* (2000)
Gustavo Barbosa-Cánovas and Humberto Vega-Mercado, *Dehydration of Foods* (1996)
Gustavo Barbosa-Cánovas, Enrique Ortega-Rivas, Pablo Juliano, and Hong Yan, *Food Powders: Physical Properties, Processing, and Functionality* (2005)
P.J. Fryer, D.L. Pyle, and C.D. Reilly, *Chemical Engineering for the Food Industry* (1997)
A.G. Abdul Ghani Al-Baali and Mohammed M. Farid, *Sterilization of Food in Retort Pouches* (2006)
Richard W. Hartel, *Crystallization in Foods* (2001)
Marc E.G. Hendrickx and Dietrich Knorr, *Ultra High Pressure Treatments of Food* (2002)
S.D. Holdsworth, *Thermal Processing of Packaged Foods* (1997)
Lothar Leistner and Grahame Gould, *Hurdle Technologies: Combination Treatments for Food Stability, Safety, and Quality* (2002)
Michael J. Lewis and Neil J. Heppell, *Continuous Thermal Processing of Foods: Pasteurization and UHT Sterilization* (2000)
Jorge E. Lozano, *Fruit Manufacturing* (2006)
R.B. Miller, *Electronic Irradiation of Foods: An Introduction to the Technology* (2005)
Rosana G. Moreira, M. Elena Castell-Perez, and Maria A. Barrufet, *Deep-Fat Frying: Fundamentals and Applications* (1999)
Rosana G. Moreira, *Automatic Control for Food Processing Systems* (2001)
Javier Raso Pueyo and Volker Heinz, *Pulsed Electric Fields Technology for the Food Industry: Fundamentals and Applications* (2006)
M. Anandha Rao, *Rheology of Fluid and Semisolid Foods: Principles and Applications* (1999)
George D. Saravacos and Athanasios E. Kostaropoulos, *Handbook of Food Processing Equipment* (2002)

STERILIZATION OF FOOD IN RETORT POUCHES

A.G. Abdul Ghani Al-Baali
The University of Auckland
Auckland, New Zealand

Mohammed M. Farid
The University of Auckland
Auckland, New Zealand

Springer

A.G. Abdul Ghani Al-Baali
Department of Chemical and
Materials Engineering
The University of Auckland
Private Bag 92019, Auckland
New Zealand
ghanialbaali@hotmail.com

Mohammed M. Farid
Department of Chemical and
Materials Engineering
The University of Auckland
Private Bag 92019, Auckland
New Zealand
m.farid@auckland.ac.nz

Series Editor:
Gustavo V. Barbosa-Cánovas
Department of Biological Systems Engineering
Washington State University
Pullman, WA 99164-6120
USA

Cover illustration: Velocity vector profile in a top-insulated can filled with CMC and heated by condensing steam after 1157 s. Created by A.G. Abdul Ghani Al-Baali.

Library of Congress Control Number: 2005938492

ISBN-10: 0-387-31128-9 e-ISBN-10: 0-387-31129-7
ISBN-13: 978-0387-31128-9 e-ISBN-13: 978-0387-31129-6

Printed on acid-free paper.

9 8 7 6 5 4 3 2 1

springer.com

To our families for their patience and understanding

PREFACE

Sterilization of canned food is a well-known technology that has been in practice for many decades. Food sterilization has been well studied in a large number of textbooks. This book is not about the science of sterilization or food safety but rather about the important interaction between fluid mechanics, heat transfer, and microbial inactivation. Such interaction is complex and if ignored would lead to incorrect information not only on food sterility but also on food quality. The book is written by engineers for both food engineers and scientists. However, it may also be of interest to those working in computational fluid dynamics (CFD). It presents an elementary treatment of the principles of heat transfer during thermal sterilization, and it contains sufficient material presented at a high level of mathematics. A background in the solution of ordinary and partial differential equations is helpful for proper understanding of the main chapters of this book. However, we have avoided going into a detailed numerical analysis of the finite volume method (FVM) of solutions used to solve the sets of equations. Some familiarity with fluid dynamics and heat transfer will also be helpful but not essential.

In this book, conduction and convective heat transfer is treated such that the reader is offered the insight that is gained from analytical solutions as well as the important tools of numerical analysis, which must be used in practice. Analysis of free convection is used to present a physical picture of the convection process.

The first three chapters present a brief historical review of thermal sterilization of food, fundamentals of heat transfer, and principles of thermal sterilization, in order to acquaint the reader with those materials to establish more firmly the important analogies between heat, mass, and momentum transfer. These chapters provide the reader with a good balance between fundamentals and applications; they provide adequate background information to the point. The computer is now the preferred tool for the solution of many heat transfer problems. Personal computers with powerful software offer the engineer the power for the solutions of most problems. Chapter 4 deals with numerical modeling and fundamentals of CFD and is one of the highlights in this book. Sterilization of canned liquid food in a three-dimensional (3-D) can sitting horizontally and heated at 121°C from all sides and the effect of using different retort temperatures on bacteria and vitamin C destruction are also predicted and studied in Chapter 5.

The subject of sterilization of food in cans has been well studied both experimentally and theoretically, but very limited work has been undertaken to study the sterilization of food in pouches. In this book, natural convection heating of viscous liquid foods of different types (broccoli-cheddar soup, carrot-orange soup, and beef-vegetable soup) in a uniformly heated 3-D pouch is presented in Chapter 6 for the first time in the literature. The slowest heating zone (SHZ) and its migration for each case of cans and pouches are presented and analyzed. The results of a simulation performed for the same pouch, but based on conduction heating, are also presented to illustrate the importance of free convective heat transfer in sterilization. In all the simulations, the retort temperature is assumed to rise instantaneously and remain at 121°C. The effect of retort come-up time (the time required for the temperature of the retort to reach a selected constant processing temperature after steam is turned on) is also studied in one of the simulations presented in Chapter 6. The cooling process following

the holding period is also simulated for the purpose of understanding its effect on the temperature distribution and the degree of sterilization achieved in the pouch.

Thermal sterilization of liquid food always results in important biochemical changes such as bacteria inactivation and nutrient concentration changes. The concentration distribution of live bacteria and vitamins C (ascorbic acid), B_1 (thiamine), and B_2 (riboflavin) in a pouch filled with different liquid food materials during thermal sterilization is presented in Chapters 7 and 8. In these simulations, the governing equations for continuity, momentum, and energy are solved numerically together with the equations defining the concentration of live bacteria and vitamins. The Arrhenius equation is used to describe the kinetics of these biochemical changes and was incorporated in the CFD software package PHOENICS via user-written FORTRAN code.

Although the main theme of the book is to present a theoretical analysis of the sterilization process and nutrient quality, some experimental validation was necessary. However, this was merely to validate the theoretical prediction and may not be considered as a thorough analysis of the sterilization process, which is the subject of other published textbooks on sterilization. In Chapter 9, experimental measurements are presented to validate the theoretically calculated temperature distribution in the pouch. These measurements were conducted at Heinz Watties Australasia Research and Development Laboratories in New Zealand, using an Easteel Pilot Plant Retort, which operates using steam at 121°C. The predicted temperatures are compared with those measured at different locations in the pouch and subsequently analyzed.

The analysis of sterilization of liquid food in pouches and cans is complicated by the important effect of free convective heat transfer, which requires the numerical solution of the Navier Stokes equations as presented in Chapters 5 to 8. This numerical solution is time-consuming and challenging. Such facilities and expertise may not be always available to those working in the food industry. Chapter 10 presents a simplified analysis of the thermal sterilization in vertical and horizontal cans, utilizing the vast information available from the detailed simulations. An effective thermal conductivity is used to account for convection similar to the approach usually used to describe free convection heat transfer in cavities. The analysis provides a quick and simple prediction for sterilization time.

This text presents for the first time the analysis of sterilization of liquid foods in 3-D pouches. The emphasis is to develop numerical techniques that can lead to a computer solution for such realistic engineering problems. The book is useful for engineers and food scientists where heat transfer is one of the basic disciplines. However, the book is more suitable as a text for postgraduate students and researchers; it provides a reference to the analysis of sterilization of cans and pouches, using CFD. In addition to the black and white figures contained in the book, color figures will be posted on the publisher's Web site, at springer.com/0-387-31128-9.

A.G. Abdul Ghani Al-Baali
Mohammed M. Farid

ACKNOWLEDGMENTS

The authors would like to express their thanks and gratitude to Professor Peter Richard at the Department of Mechanical Engineering, The University of Auckland, for his valuable contribution and advice on the major parts of the book, especially those related to CFD. We would also like to thank Professors Dong Chen and Gordon Mallinson for their valuable discussions and comments. Special thanks go to Professor Gustavo V. Barbosa-Cánovas for encouraging us to write this book. Finally, we would like to thank our families for being patient and very supportive during the writing of this book and the many years of work prior to that.

A.G. Abdul Ghani Al-Baali
Mohammed M. Farid

CONTENTS

LIST OF FIGURES

LIST OF TABLES

LIST OF ABBREVIATIONS

2-D	two-dimensional
3-D	three-dimensional
AA	ascorbic acid
BFC	body-fitted coordinates
CDS	central differencing scheme
CFU	colony-forming unit
CFD	computational fluid dynamics
CMC	carboxyl methyl cellulose
DAD	diode array detector
DHAA	dehydroascorbic acid
FAD	flavin adenine dinucleotide
FDA	Food and Drug Administration
FDE	finite difference equation
FDM	finite difference method
FEM	finite element method
FMN	flavin mononucleotide
FVE	finite volume equation
FVM	finite volume method
HBCZ	high bacteria concentration zone
HDS	hybrid-differencing scheme
HPLC	high-performance liquid chromatography
HTST	high temperature short time
HVCZ	high vitamin concentration zone
NLABS	Natick research and development laboratories
NSA	nutrient sporulation agar
PDE	partial differential equation
PHOENICS	parabolic hyperbolic or elliptic numerical integration code series
R&D	research and development
SCZ	slowest cooling zone
SHZ	slowest heating zone
SO	spores only
TDT	thermal death time
TN	too numerous
UDS	upwind differencing scheme
UHT	ultrahigh temperature
USDA	U.S. Department of Agriculture
UV	ultraviolet
WOS	without spores
WS	with spores

CHAPTER 1

THERMAL STERILIZATION OF FOOD

Historical Review

Thermal sterilization has been used to achieve long-term shelf stability for canned foods and is now used for a broad range of products. The majority of shelf-stable foods are thermally processed after being placed in the final containers. A relatively small percentage of shelf-stable foods are processed before packaging, using aseptic filling (Heldman and Hartel, 1997). Thermal sterilization of canned foods has been one of the most widely used methods for food preservation during the twentieth century and has contributed significantly to the nutritional well-being of much of the world's population (Teixeira and Tucker, 1997).

The objective of thermal sterilization is to produce safe and high-quality food at a price that the consumer is willing to pay. It is a function of several factors such as the product heating rate, surface heat transfer coefficient, initial food temperature, heating medium come-up time, Z value for the quality factor, and target F_{ref} value (Silva et al., 1992). The sterilization process not only extends the shelf life of the food but also affects its nutritional quality such as vitamin content. Optimal thermal sterilization of food always requires a compromise between the beneficial and destructive influences of heat on the food. One of the challenges for the food canning industry is to minimize these quality losses, meanwhile providing an adequate process to achieve the desired degree of sterility. The optimization of such a process is possible because of the strong temperature dependence of bacteria inactivation as compared to the rate of quality destruction (Lund, 1977). For this reason an estimate for the heat transfer rate is required in order to obtain optimum processing conditions and to maximize product quality. Also, a better understanding of the mechanism of the heating process will lead to an improved performance in the process and perhaps to energy savings. Basic principles for determining the performance of different but related processes have been presented by May (1997) and Wilbur (1996).

In thermal sterilization of food, the heating medium temperature (steam or hot water) can deviate significantly from the design value during the heating phases. Such deviations may seriously endanger public safety due to under-processing of food (under-sterilization), waste energy, or reduce quality because of overprocessing of food (Datta et al., 1986). For these reasons, online retort control in thermal sterilization has been well studied by Datta et al., 1986; Gianoni and Hayakawa, 1982; Teixeira and Manson, 1982; and Teixeira and Tucker, 1997, to assure safety, quality, and process efficiency of thermally processed canned foods.

In the design of thermal food process operations, the temperature in the slowest heating zone (SHZ) and the thermal center of the food during the process must be known. Traditionally this temperature is measured using thermocouples. The placement of thermocouples to record the temperature at various positions in a container during heating disturbs the flow patterns, causing errors in the measurements (Stoforos and Merson, 1990). Also, it is difficult to measure the temperature at the SHZ because this is a nonstationary region, which keeps moving during the heating progress, as

will be shown in the analysis presented in the following chapters. For this reason, there is a growing interest toward the use of mathematical models to predict the food temperature during the thermal treatment (Datta and Teixeira, 1987, 1988; Naveh et al., 1983; Nicolai et al., 1998; Teixeira et al., 1969). Mathematical models for prediction of temperature during heat sterilization are invaluable tools to help assure safer production and control of thermally processed foods. With the development of desktop computers, these models developed rapidly, and the facility to solve a complex series of equations made online process and monitoring feasible (Tucker, 1991).

Several studies have been performed on the numerical simulation of foods undergoing thermal processing. These studies include (1) Transient natural convection heat transfer in a cylindrical container (Datta and Teixeira, 1988); (2) Transient natural convection heat transfer (constant low viscosity fluid foods) in a bottle-shaped container (Engelman and Sani, 1983); (3) Heat transfer in a can (non-Newtonian foods with temperature-dependent viscosity) (Kumar and Bhattacharya, 1991; Kumar et al., 1990; Yang and Rao, 1998); (4) Continuous sterilization (Datta, 1999; Jung and Fryer, 1999); (5) Improvement of thermal process control (Tucker, 1991); and (6) Sterilization of more complicated nonhomogenous food products (Scott et al., 1994).

Saturated steam is the most commonly used heating medium for commercial sterilization of packaged foods because of several advantages. During the heating period, steam condenses on the surface of the package resulting in very large values of the surface heat transfer coefficient (h). The rate of heat transfer from the heating medium (steam) through the package wall into the outer layer of the food is controlled by the thermal properties of food itself (Bhowmik and Tandon, 1987) and the shape and size of the can or pouch containing it. Although steam is a highly desirable heating medium, its application in certain cases is not possible.

1.1. THERMAL STERILIZATION OF FOOD IN CANS

Canned foods have a long history and are likely to remain popular in the foreseeable future owing to their convenience, long shelf life, and low cost of production. The technology is receiving increasing attention from thermal processing specialists to improve both the economy and quality of some canned foods (Durance, 1997).

The heat transfer mechanism through liquid food in cans is classified as convection-heated, conduction-heated, or combined convection and conduction-heated mechanism. This will be discussed in Chapter 2. Typically, conduction is assumed as the only mode of heat transfer, because of the relative simplicity of the analytical and numerical solutions for this case. This analysis is acceptable for the heating of solid food but not for liquid. If heat transfer is controlled by conduction only, then the so-called SHZ will remain at the geometric center of the can during the heating process. In conduction-heated food, the heating rate at the SHZ is controlled by the resistance to heat transfer within the product, which is a function of the thermophysical properties of the product as well as the geometry and dimensions of the container (Silva et al., 1992). The external and surface thermal resistances may be neglected when condensing steam is used to heat foods in metal containers (Tucker and Holdsworth, 1991). In the case of using steam/air mixtures as a source of heating or water during the cooling cycle, it is necessary to consider a finite surface heat transfer coefficient. Also, the use of glass or plastic containers requires the inclusion of conduction resistance of the container wall (Deniston et al., 1987; Deniston et al., 1991; Heldman and Singh, 1981; Ramaswamy et al., 1983; Shin and Bhowmik, 1990; Stoforos and Merson, 1990; Tucker and Clark, 1990; Tung et al., 1984).

Foods such as canned tuna, thick syrups, purees, and concentrates are usually assumed to be heated by pure conduction. For these foods, the required processing time is generally determined

by analytical or numerical solutions to the heat conduction equation (Datta et al., 1986). For example, Dincer et al. (1993) analyzed transient conduction heat transfer during sterilization of canned foods in order to determine the heat transfer rate. Their model was based on solving the conduction equation by using the boundary condition of the first kind in the transient heat mode, which expresses a simple relationship between time and temperatures. Lanoiselle et al. (1986) developed a linear recursive model to represent the heat transfer inside a can during sterilization in a retort and predicted the internal temperature distribution in canned foods during thermal processing. Akterian (1994) developed a numerical model for the determination of the unsteady-state temperature field in conduction-heated canned foods of various shapes and boundary conditions. The heat conduction equation is solved using finite differences. Silva et al. (1992) studied the optimal sterilization temperatures for conduction-heated foods, considering finite surface heat transfer coefficients. Different one-dimensional heat transfer shapes were considered, and it was found that the initial temperature and the heating medium come-up time had little influence on the optimal processing temperature. Banga et al. (1993) also studied the thermal processing of conduction-heated canned foods. Numerical simulations were performed using finite difference method (FDM) and finite element method (FEM). The simulation results were validated with some experimental data available for sterilization of canned tuna.

Because of the complex nature of heat transfer in natural convection heating, the observation of the SHZ is a difficult task and requires the prediction of detailed transient flow patterns and temperature profiles. Natural convection occurs due to density differences within the liquid caused by the temperature gradient. Natural convection causes the SHZ to move toward the bottom of the can. The velocity in the momentum equations is coupled with the temperature in the energy equation because the movement of fluid is solely due to the buoyancy force. Because of this coupling, the energy equation needs to be solved simultaneously with the momentum equations, requiring the use of appropriate software, which will be discussed in later chapters. Basic heat transfer principles needed to determine the thermal processing methods have been presented in several books. A number of numerical heat transfer studies have been published in the literature in an effort to model sterilization processes and to determine temperature and flow distributions in the cans. It has been established experimentally that during heating, the fluid rises along the can wall and falls in the can center (Hiddink, 1975). It was also established both experimentally (Nickerson and Sinskey, 1972) and theoretically (Datta and Teixeira, 1988) that the SHZ in convection-heated food in a cylindrical can is a torroid that continuously alters its location. Most of these studies have been carried out for water-like liquid food products, assuming constant viscosity (Kumar and Bhattacharya, 1991). The numerical predictions of the transient temperature and velocity profiles during natural convection heating of water in a cylindrical can have been well studied by Datta et al. (1987, 1988). The liquid food was found to be stratified inside the container with increasing temperatures toward the top. Datta et al. predicted distinct internal circulation at the bottom of the can and showed that the SHZ is a doughnut-shaped region located close to the bottom of the can at about one-tenth of the can height.

The influence of natural convection heating during the sterilization process of sodium carboxyl methyl cellulose (CMC) as a model liquid food has been studied in detail by Kumar et al. (1990) and Kumar and Bhattacharya (1991). Kumar and Bhattacharya carried out a simulation for the sterilization of viscous liquid food in a metal can sitting in an upright position and heated from the side wall in a still retort. Equations of mass, momentum, and energy conservation using a cylindrical coordinate system were solved using the FEM to simulate heating of non-Newtonian liquid foods in cans. The plots of temperature, velocity, and streamlines were presented for natural convection heating. The liquid was assumed to have a temperature-dependent viscosity but constant

specific heat and thermal conductivity. They also presented a simulation for the same can when its bottom and top surfaces were insulated (Kumar et al., 1990). The results indicated that natural convection tends to push the SHZ (the coldest region) to the bottom of the can. Yang and Rao (1998) solved the energy, mass, and momentum-governing equations for a stationary vertical can filled with 3.5 wt % of cornstarch dispersion during thermal possessing. They found that the increase in viscosity during starch gelatinization diminished the buoyancy-driven flow and hence lowered the heat transfer rate.

Retortable plastic cans, which consist of several thin layers of polymeric materials, have been used by many food industries to produce shelf-stable foods. Bhowmik and Shin (1991) and Lu et al. (1991) studied the thermal processing of conduction-heated foods in plastic cylindrical cans. A mathematical model was developed by Bhowmik and Shin to evaluate thermal processing of foods in plastic cylindrical cans. The model included external convective heat transfer coefficients for heating and cooling, and the temperatures estimated by the model at the coldest point in a can agreed closely with those determined. It was found that the thermal diffusivity of the can wall and the heat transfer coefficients of the heating and cooling media considerably influenced the sterilizing values of the processed food. Lu et al. presented a comparison between the sterilization of metal cans and retortable plastic containers. In their study, the SHZ was mathematically determined and found to be influenced by the container material and the lid orientation of the plastic containers. The results indicated that the design of thermal processes in plastic containers must take into account nonsymmetrical external heat transfer due to the presence of the metal lid.

In all simulations, the temperature distribution at the end of the heating process in the cans was assumed to be an important measure of sterility of food products. However, it is necessary to keep the food under these conditions for a specified period to ensure that microorganisms are efficiently killed. In reality, the death of microorganisms is expected to begin at early stages of heating, especially at locations near the wall, where the temperature approaches the retort temperature (121°C) very quickly. Hence it is necessary to solve the partial differential equation (PDE), governing bacteria concentration, coupled with the equations of continuity, momentum, and energy. Datta (1991) followed this approach to study sterilization of liquid food in a nonagitated cylindrical enclosure heated from all sides and described the computational procedure for obtaining the full range of biochemical changes during processing without explicitly following the liquid elements. Datta showed that the lowest sterilization achieved by any portion of the fluid in the system was considerably more than the sterilization level normally calculated by using the temperature of the SHZ. In conduction heating, it is sufficient to know the transient temperature at various fixed locations in order to calculate the distribution of bacteria concentration. However, the situation is quite difficult for fluid under continuous motion. In this case, following the temperature distribution with time is very important.

Chemical and biochemical reactions in liquid food during heating are temperature-dependent. Such reactions not only destroy microorganisms but also destroy some of the valuable nutrients such as vitamins. The destruction of vitamins follows a first-order reaction similar to microbial destruction. In general, the decimal reduction time (the time needed to destroy 90 percent of the species) of vitamins is significantly higher than that of microorganisms and enzymes. As a result, nutritional properties may be retained well by the use of higher temperatures and shorter times during heat processing (Fellows, 1996). Because these destruction processes are all temperature-dependant, the distribution of temperature results in unavoidable spatial distributions of the reaction products. These distributions can be easily quantified in the case of conductive heating of solid materials. However, the situation becomes quite complex when the fluid is in motion. In this case, temperature and concentration profiles are influenced strongly by the natural convection in the liquid food.

The effect of the thermal sterilization process on the quality and nutrient retention of food has been of major concern for food processors since Nicholas Appert first discovered the art of canning for food preservation in 1809. Later, this concern led to several experimental and computer simulation studies to investigate the effect of thermal sterilization on vitamins. Teixeira et al. (1969) developed a numerical computer model to simulate the thermal processing of canned food. The model simultaneously predicted the lethal effect of the heat process on the destruction of thiamine in pea puree, which is usually rich in thiamine. The experimental evidence to support the accuracy and validity of the mathematical method and computer model of Teixeira et al. (1969) for thermal process evaluation with respect to thiamine retention was subsequently shown by Teixeira et al. (1975a). Because the can size was expected to be a strong factor that would limit the response of interior temperatures to any variable control action on the surface, Teixeira et al. (1975b) also studied the effects of various container geometries of equal volume on the level of thiamine retention for both constant and time-varying surface temperature. Saguy and Karel (1979) investigated and developed a method for calculating the optimum temperature profile for a reaction in a retort as a function of the time needed to achieve a specified level of sterilization with maximum nutrient retention. Saguy and Karel used a computational scheme to determine the optimum temperature profile for thiamine retention in canned foods during the sterilization process.

Thermal processing of liquid food materials always results in biochemical changes, depending on sterilization time and temperature. These changes include the change in food color, which is associated with heat treatment of the food. Retention of food color after thermal processing may be used to predict the extent of quality deterioration of food, resulting from exposure to heat. Shin and Bhowmik (1995) studied the thermal kinetics of color changes in pea puree. In this work, samples of green pea puree were heat-treated for different lengths of time at various temperatures to determine the thermal destruction of color. Barreiro et al. (1997) also studied the kinetics of color changes of double-concentrated tomato paste during thermal treatment. The order of the reaction and the constants E_a (activation energy) and k_T (reaction rate constant) of the Arrhenius equation (Chapter 3) were determined. It was found that all the color change followed apparent first-order kinetics.

1.2. RETORT POUCHES (HISTORICAL REVIEW)

Retortable flexible containers are laminate structures that are thermally processed like a can. The materials of the flexible containers provide superior barrier properties for a long shelf life, seal integrity, toughness, and puncture resistance and also withstand the rigors of thermal processing. Generally, any product currently packaged in cans or glass can be packaged in flexible containers. The retort pouch is perhaps the most significant advance in food packaging since the development of the metal can (Mermelstein, 1978). The structure of the retortable pouch used today is made from a laminate of three materials: an outer layer of 12 μm polyester film for strength, an adhesive laminated to a middle layer of 9–18 μm aluminum foil as a moisture, light, and gas barrier, which is laminated to the inner layer of 76 μm polypropylene film as the heat seal and food-contact material. The use of the polyester film is to provide high temperature resistance, toughness, and printability (Rahman, 1999). The retort pouch with its multilayer polymer foil is shown in Figure 1.1.

1.2.1. Benefits of the Pouch

The retort pouch has many advantages over canned and frozen food packages for the food processor, distributor, retailer, and consumer.

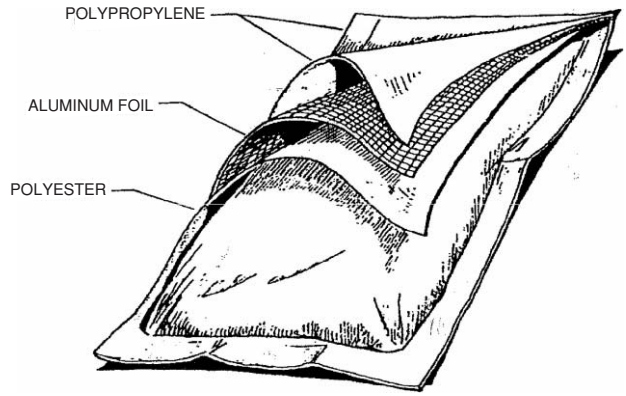

Figure 1.1. Retort pouch (Lampi, 1980).

These advantages are as follows (Mermelstein, 1978):

1. A pouch takes less time to reach sterilization temperature than cans or jars, which is due to the thinner pouch profile and its larger surface area per unit volume. In addition, because the product near the surface is not overcooked, as it can be with cans and jars, the product quality is better maintained. The product retains its color, remains firmer in texture and fresher in flavor, and experiences less nutrient loss. The pouch is especially beneficial for such products as delicate sauces, seafood, and entrees, where color and texture are important. Also, products such as vegetables can be packed in retort pouches with less brine (required for improving the heat transfer processes). Thus, there is less shipping weight and less discarding of the brine (Mermelstein, 1978).
2. A pouch product is commercially sterile, does not require refrigeration or freezing, and is shelf-stable at room temperature.
3. Pouched food can be eaten without heating, or it can be heated quickly by placing the pouch in boiling water for a few minutes. Frozen foods, in contrast, require heating for about half an hour. Thus, less energy is required for heating a retort pouch. Pouched food can also be heated in a microwave oven simply by removing it from the pouch before heating.
4. A pouch can be easily and safely opened by tearing it across the top at a notch in the side seal or by cutting it with scissors. There is no need for a can opener and no danger from can lids or broken glass. There is also no problem in handling a pouch immediately after removal from boiling water.
5. There is no need to get pots or pans—or even dishes—messy. The food can be eaten directly from a pouch or served on dishes.
6. Pouches weigh less than comparable cans and jars, thus reducing distribution costs.
7. Pouches, empty and full, take up less storage space than comparable cans, jars, and trays. Empty pouches, for example, occupy up to 85 percent less storage space than cans.
8. Pouches, including paperboard cartons, will most likely require less energy to manufacture than cans, jars, and trays. In addition, studies indicate that the total energy required from harvesting to consumption is about 60 percent lower for a vegetable packaged in a retort pouch than for a frozen vegetable and about 15 percent lower than for canned vegetable.
9. The combination of shelf stability without refrigeration and the light weight of a pouch make retort-pouched products ideal for military use as well as for recreational camping.

10. The capability of serving single portions of foods makes the retort pouch desirable for the singles market and the hospital-feeding market.
11. The ease of preparation and opening, as well as the elimination of the need for much storage space and refrigeration, makes the retort pouch desirable for use in feeding the elderly.
12. The ability to package large quantities of foods in less brine makes the retort pouch desirable for use in institutional feeding.

For all the reasons above, the retort pouch is expected to enter almost all areas of food marketing.

1.2.2. Steps to Regulatory Acceptance

Development of the retort pouch in the United States ranged from lab work in the early 1950s to use in the Apollo space program beginning in 1968 to the demonstration of commercial feasibility in 1968–1972. In mid 1974, the U.S. Department of Agriculture (USDA) gave its approval to a number of manufacturers for marketing meat and poultry products in retort pouches on the basis that the materials involved met the Food and Drug Administration (FDA) regulations. However, in early 1975, studies indicated that the components of the adhesive used to hold the three layers of the pouch material together migrated through the food contact layer at retort temperatures. Consequently, the FDA asked the USDA to withdraw its approval and asked the material suppliers to submit data identifying and quantifying the components.

Reynolds Co. and Continental Can Co. responded in late 1975 by submitting the requested data along with petitions to amend the food additive regulations to provide for the "safe use components of flexible laminated pouch under retort conditions." In early 1976, the FDA asked for additional safety testing data on the adhesive components. Both Continental Can and Reynolds developed modified versions of their pouch material, using different thermal adhesives, or bonding agents, that already complied with the existing FDA regulations. Continental Can and Reynolds pouches are similar in construction but differ in relative thickness of the three component layers.

In mid-1977, the FDA notified the companies that their models were acceptable. A week later the USDA approved the pouches for use with meat and poultry products.

1.2.3. Natick's Role

The U.S. military began working on the retort pouch in 1959 at the Quartermaster Food and Container Institute, the predecessor of the U.S. Army Natick R&D Command by whom most of the development work on retort pouch packaging and processing has been done. Natick worked closely with material and equipment suppliers as well as food companies.

Natick's goal was to find a package that would be lighter than the metal can, could be carried by a soldier without interfering with normal movement, would fit into combat uniform pockets conveniently and not harm the soldiers if they fell on it, and would be durable and easy to open and dispose. In addition, the food within the package would be stable without refrigeration, ready to eat without thawing, acceptable when hot or cold, and at least equal in quality to canned foods.

From 1959 to 1966, Natick screened more than 200 materials to be used in the manufacturing of pouches. The type and amount of the extractable substances that might migrate to the food were studied to determine whether over-wrapping of the pouch by a paperboard envelope or carton would be necessary or preferable. The durability during handling was also tested. The results of a field test of 50,000 filled pouches in 1965–1966 indicated that if a pouch was made well, it would perform well.

In 1968–1972, Natick undertook a manufacturing reliability project, it made a contract with Swift & Co. to provide meat product technology as a prime contractor. Swift subcontracted with Pillsbury Co. to provide baked goods and with Continental Can Co. to provide packaging material as well as vacuum-generating equipments, seal closure systems, dryers, and pouch carriers. Continental Can in turn subcontracted with Rexham Corp. for form, fill, and seal equipment and with FMC Corp. for retorting equipment.

A feasibility phase lasting about 1.5 years involved the study of existing equipment and the design of new equipment. The results indicated that it would be feasible to produce pouches with the same low failure rate as metal cans. This phase was followed by a confirmatory phase, lasting about 2.5 years, in which the recommended equipment in the feasibility phase was engineered, built, and used. The recommended equipment was installed in a pilot plant at Swift's Research and Development Center in Oak Brook, IL in 1970 and received USDA approval for army usage and testing.

The reliability project and a subsequent project culminated in the running of the pilot plant for 8 months in 1972 to produce more than 400,000 pouches containing more than 22 different food items. These pouches were tested for seal integrity, sterility, and defects, and the results showed performance at least equal to that of metal cans. Thus the reliability project proved the feasibility of the retort pouch. As far as Natick is concerned, the retort pouch came out of the R&D stages, and the military at that time considered it as a standard food package that could be handled by regular procurement procedures for use in its Meal Ready-to-Eat (MRE) ration that was replaced by the Meal Combat Individual (MCI) ration. The MRE differs from the MCI not only in using retort pouches instead of metal cans but also in containing more familiar as well as a great variety of food items. Natick developed 12 basic menus for the MRE, including 22 entrees and dessert items that were packaged in retort pouches. The pouches were then rolled over at the top (headspace portion) and glued at one spot to the cartons to immobilize them (Mermelstein, 1978).

Most Natick activities at that time were devoted to test the pouch materials, which had been cleared by the FDA, to determine whether they met military requirements. Natick conducted 24-month tests to monitor the physical properties of the pouch materials, including integrity of bonding of the three layers, seal strength, and resistance to internal pressure. The FDA accepted pouch materials from Continental and Reynolds that had been in Natick's tests for 4–18 months and had performed satisfactorily. Based on Natick's testing, the original and modified versions performed equally well, and both met military requirements. Natick also tested similar materials from other suppliers.

1.2.4. Continental's Role

Continental Flexible Packaging, Chicago, IL, began work on retort pouch materials in 1958 and, in conjunction with Ohio State University, tested sample pouches under simulated retort conditions in 1959 in Ohio. In 1962 Continental's pouch material was used in Natick's first commercial procurement of 40,000 performed pouches. Continental's licensees began using Continental's material in Denmark and England in 1967, Japan in 1968, and Canada in 1975. Continental's material was also used in Natick's reliability project in 1968–1972, the Apollo space program in 1969, and a hospital-feeding study in 1971. As already mentioned, Continental was responsible for the material and equipment phase of Natick's reliability project (Mermelstein, 1978). The pilot plant, which is USDA approved, included food preparation equipment; pouch formers and dispensers; filling capable of handling solids, liquids, and mixtures; vacuum impulse sealers capable of sealing 40–45 pouches/min; two batch retorts that held 2,400 pouches each and were operated by hot water with overriding air pressure; pouch-testing equipment; and cartoning and casing equipment. Laboratory scales fillers, sealers, and retorts were also available for producing smaller quantities of pouches.

Continental's Canadian division also had a pilot plant, which incorporated automatic pouch dispensing and filling equipment and had a retort capable of being operated by water or a steam/air mixture with overriding pressure. Continental offered at that time the use of the pilot plant to interested food processors for the production of samples for testing and market research purposes.

1.2.5. Reynolds's Role

Reynold's flexible packaging division began working on the retort pouch concept in the mid-1950s, and in the early 1960s it ran two trials in New York and Florida, using performed pouches. These studies were followed in 1967 by test runs of packaging vegetables products in Wisconsin. In 1968, in Wisconsin, Reynolds successfully used roll stock pouch material in the commercial packaging of vegetables in pouches. These products were used for consumer testing. Reynolds officially opened its food processing center in Bellwood to aid food processors in reaching the market with the retort pouches. The center had three connecting areas: food preparation area, packaging area, and processing area.

The food processing center produced about 1,500–2,000 finished pouches in a day. Reynold's flexible packaging division offered at that time the use of the center to food processors interested in evaluating the retort pouch for their products.

The retort pouch had become a commercial reality in the United States by the end of 1970s, and much of the credit is due to the three groups (Natick, Continental, and Reynolds) that were named as joint recipients of the 1978 IFT Food Technology Industrial Achievement Award. At that time (late 1970s), and in addition to the huge production of retort pouches in the United States, about 350 million food retort pouches were marketed annually in Japan and about 50 million in England.

The commercial and technical aspects of the pouch are described by the Natick Research and Development Laboratories (NLABS). The successful laboratory results and the potential advantages led to the use of the retort pouch for the military and civilians. The basic incentives for the use of the pouch in the U.S. military were the convenience of shape to carry with negligible constraint to movement; softness that precluded injury during crawling; a convenient opening; ready-to-eat products; and some weight savings. In the United States, the military has taken the lead in both the development and adoption of the retort pouch. The Japanese, primarily, are continuing to advance the art and to make refinements to the product, package, and process, and the state of commercialization is highest in Japan (Lampi, 1980).

1.3. THERMAL STERILIZATION OF FOOD IN POUCHES

The research interest in thermal sterilization of pouches was stimulated by its approval for use in commercial sterilization of low-acid foods. Numerous articles on the benefits of using pouches in food processing were published (Lampi, 1980; Mermelstein, 1978). Sterilization of food in cans has been well studied both experimentally and theoretically since the 1920s. The theory and practice of establishing and evaluating thermal processes for cans can be found in several sources, and the mathematical modeling of thermal processing has also been thoroughly reviewed (Hayakawa, 1977a, 1977b, 1978; Holdsworth, 1985). Even though pouches were introduced in the 1960s, little information is available on the temperature distribution within the pouches during the sterilization process. The results of sterilization of food in cans cannot be extended to pouches because of the more complicated geometry of the latter. Pouch analysis will require computer modeling in a 3-D domain.

Most studies conducted on thermal processing of pouches were based on conduction-heated foods. Ohlsson (1980) presented a numerical solution to the heat conduction equation in one dimension to obtain an optimal temperature profile for the pouches and to achieve a minimum loss in sensory and nutritional quality of the processed food. In the study, the geometrical configuration of the pouches was assumed to be an infinite slab in order to apply the FDM to the solution. Calculations were performed at different sterilization temperatures and processing conditions in order to find the optimal sterilization temperature that produced minimal quality changes. Ohlsson also showed that the low initial temperature and the retort come-up time (i.e. the time required for the temperature of the retort to reach a preselected constant processing temperature after steam is first turned on) have only a minor influence. Manson et al. (1970) developed a model to evaluate thermal processing of conduction-heated foods in a rigid rectangular container by solving the heat conduction equation in three dimensions by using the FDM. The time-temperature history predicted at different locations inside the container was used to estimate lethality and nutrient retention during sterilization. In the simulation by Castilo et al. (1980), an analytical method was presented to predict the nutrient retention in conduction heating of foods in a rectangular pouch. The nutrient degradation during the retort come-up time and cooling time of the process cycle was neglected. The result showed that the deviation between the predicted and the measured nutrient retention values was 2–16 percent. Hayakawa (1977b) developed computerized models to estimate the proper thermal processes of canned foods, based on the Ball formula method. This method can be applied to pouches subject to thermal sterilization at a constant retort temperature. Comparisons of general and Ball formula methods were also studied for pouches processed under water in a still, vertical retort (Spinak and Wiley, 1982).

All the methods described above are applicable to rectangular containers. However, when a pouch filled with food was placed in a cassette during the sterilization process, it always conformed to a shape similar to a pillow. The assumption of a rectangular configuration was necessary to simplify the numerical solution of the heat conduction equation so that the FDM could be applied to the solution. These assumptions led to an overestimation of processing time, resulting in less retention of nutrients in and greater loss of sensory quality from the food (Tandon and Bhowmik, 1986).

Bhowmik and Tandon (1987) developed a mathematical model to evaluate the thermal processing of a two-dimensional (2-D) pouch containing conduction-heated food. Hot water was used as the heating medium in this study. The temperature predicted by the model compared well with the experimentally measured temperatures at the center of the pouch. The nutrient retention estimated in this model showed close agreement with the experimental measurements. In the simulation of Tandon and Bhowmik (1986), a computer model was developed to evaluate thermal processing of a pouch containing conduction-heated food. In this model, the transient 2-D heat conduction equation was solved using a modified FDM for a pouch filled with food. Temperature distributions and degree of sterilization predicted in this simulation were compared with those obtained by applying an FEM, and the results were found in a close agreement.

Critical processing factors, which have been identified in the thermal processing of retort pouches, include pouch thickness, presence of residual gas, type of heating media, and operating pressure (Beverly et al., 1980). However, research quantifying these critical factors under conditions of practical processing operation is limited in scope. The overall heat transfer coefficient from the heating medium (steam and water) to a pouch containing liquid products (curry sauce) was studied both theoretically and experimentally by Terajima (1975). It was found that the overall heat transfer coefficient from the heating medium to the food in the pouch is governed mainly by the heat transfer coefficient from the inner surface of the pouch to its contents. However, the circulation rate of the water used for heating was identified as a critical processing factor for maintaining a uniform retort temperature during processing.

The effect of the sterilization process on the quality of canned food has been a major concern since the beginning of the canning industry. Castillo et al. (1980) developed a model to predict the retention of nutrients, using first-order kinetics of thermal degradation in foods packaged in retortable pouches, assuming conduction heating. The model was effective in predicting the temperature at the center of the container at the end of the heating period. The validity of the model was verified experimentally on simulated food. However, the work was based on heat conduction and cannot be extended to cases in which convection may be important.

1.4. COMPUTATIONAL FLUID DYNAMICS AND THE FOOD INDUSTRY

Computational fluid dynamics (CFD) is undergoing a desktop revolution similar to that which revolutionized computers in 1980s (Scott, 1994). CFD is a tool used to simulate fluid flow, heat transfer, chemical reactions, and related phenomena, using numerical solutions to the equations describing such transport phenomena—for example, the Navier–Stokes equations, which describe the flow of fluids inside or around defined flow geometry. CFD offers a powerful design and investigative tool to process engineers. Its application would assist in the better understanding of the complex physical mechanisms that govern the thermal, physical, and rheological properties of food materials (Scott and Richardson, 1997).

CFD has wide applications in the areas of fluid and heat transfer outside the food industry. CFD has only recently been applied to food processing applications. It has seen applications in many different processing industries, including airflow in clean rooms, ovens and chillers, flow of foods in continuous-flow systems, and convection patterns during thermal processing (Scott and Richardson, 1997). CFD models can be of great use in a variety of food engineering applications. It can also be used, for example, for predicting mixing efficiency for specific mixer geometry, determining the average residence times of turbulent flows through heat exchangers, and determining the flow patterns of airborne microorganisms in a clean room in a factory environment. Advances in computing speed and memory capacity of computers are allowing ever more accurate and rapid calculations to be performed. A number of commercial software packages are available to conduct these calculations, such as FIDAP, FLUENT, FLOW 3-D, and PHOENICS, which were used for the simulations presented in this book.

Other examples on the use of CFD codes are as follows:

In engineering applications such as aerospace, automotives, chemicals and processes, combustion, electronics, marine, metallurgical, nuclear, petroleum, power, radiation, and water treatment

In environment applications such as atmospheric pollution, natural water pollution, safety, and fire spread

In architecture and building science such as flow in a football stadium, flow around bus shelters, pollutant dispersion near a tower block, dispersion of ammonia spill within a city complex, flow around a group of buildings, and flow around inline wind turbines

In internal flows such as airport terminal ventilation, display-case design, optimization of air flow in a clean room, baby cot ventilation, tunnel ventilation, smoke movement in a tunnel—computed by means of the parabolic option—ventilation of concert halls, and ventilation in a gas turbine plant

A commercial fluid dynamics analysis software package PHOENICS (Concentration, Heat and Momentum Limited [CHAM], London) was used in the analysis presented in the following chapters.

The following are some recent engineering applications of this code:

- Split-pipe performance (CHAM for FIAT Research, Italy)
- Modeling of downwind sail (University of Auckland, New Zealand)
- Thermal and nonthermal sterilization of food (University of Auckland, New Zealand)
- Silicon micro-hotplate structure (NRC/CHAM, Canada/U.K.)
- Internal waves in the ocean (Winfrith Technology Centre, U.K.)
- Currents in water intake (*Ecole Nationale d'Ing_nieurs de Tunis*)
- Two-phase exhaust plumes (S&C Thermofluids Ltd., U.K.)
- Contaminant dispersion in the ocean (Petrobras/Chemtec, Brazil)
- Solid oxide fuel cells (NRC/CHAM, Canada/U.K.)
- Diffuser augmented wind turbine (Vortec Energy, New Zealand)
- Application-oriented interface (Petrobras/Chemtec, Brazil)
- Pharmaceutical clean rooms (Clean-room construction/Flowsolve Ltd., U.K.)
- Mixed flow pump (Lloyd's Register, U.K.)
- Ventilation of a roadway tunnel (Vortex de Mexico, Mexico)
- Convection zone of a boiler (University of Zaragoza, Spain)
- Hypolimnetic aerator (Vortex de Mexico, Mexico)
- Two-phase flow in annuals (Vortex de Mexico, Mexico)
- Reactor pressure vessel (DNST, HMS Sultan, U.K.)
- Packed bed filters (S&C Thermofluids/DERA, U.K.)

The equations that PHOENICS solves are algebraic equations, which result from the application of the conservation law of physics to finite volumes of space and time. The PHOENICS code is based on the finite volume method (FVM), as developed by Patankar and Spalding (1972). The key characteristic of this method is the immediate discretization of the integral equation for flow into the physical 3-D space—that is, the computational domain covers the entire can or pouch, which is divided into a number of divisions in the three dimensions, as will be discussed later in Chapter 4. The details of this code can be found in the PHOENICS manuals, especially the PHOENICS Input Language (PIL) manual, and the PHOENICS beginner's menu system user guide by Radosavljevic and Wu (1990). The FVM and its uses have been well explained by Versteeg and Malalasekera (1995). The computational methods for fluid dynamics can also be found in details in several books (Versteeg and Malalasekera, 1995; Wendit, 1992; Ferziger and Peric, 1996).

Some recent studies have been done on the application of CFD to thermal processing of foods. Verboven et al. (1997) calculated the surface heat transfer coefficient during thermal processing of foods of different shapes and for different heating conditions. The calculated results were compared with the experimental results obtained from the literature. In the study of Jung and Fryer (1999), a computational model for continuous food sterilization was used, and a model system for a laminar flow in circular pipes with uniform wall temperatures was developed. Temperature and velocity profiles were modelled using the FIDAP CFD package. The data obtained from the model was used to study the efficiency of a continuous sterilization process. Verboven et al. (2000a and 2000b) discussed the validation of a CFD model against measurements of heat transfer in an industrial electrical forced-convection oven. The results of the calculated oven temperatures were in good qualitative agreement with the measured temperature distribution.

1.5. OBJECTIVES

The objective of this book is to discuss, for the first time, the important application of CFD on thermal sterilization of pouches filled with different viscous liquid foods and at different conditions

of sterilization. The results of the computations will be compared with those obtained by previous studies as well as with some experimental measurements conducted at the department of Chemical and Materials Engineering at the University of Auckland, New Zealand, and at Heinz Watties Australasia located in Hasting, New Zealand.

The book will illustrate the following cases of sterilization of food in pouches:

1. Study the transient temperature, velocity profiles, and the migration of the SHZ during the natural convection heating of food in a 3-D pouch, a newly designed shape currently used in the canning industry.
2. Investigate the inactivation of bacteria in canned liquid food by developing a computational procedure for describing the changes in live bacteria concentrations and their transient spatial distributions during the sterilization. The liquid food will be tagged and monitored, which is computationally difficult for most flow situations of interest (Datta, 1991). The PDEs describing the conservation of mass, momentum, and energy will be solved numerically together with those for bacterial concentrations using an FVM. The kinetics of bacterial death and the influence of temperature on the destruction rate constant will be introduced to the software package by using FORTRAN code via PHOENICS ground facility that allows user code to be incorporated.
3. Study the effect of natural convection currents during thermal sterilization on the rate of destruction of vitamin C (ascorbic acid), B_1 (thiamine), and B_2 (riboflavin). This will require the prediction of the concentration of vitamins in the different locations in the pouch.

The results of these investigations can be used to optimize the industrial sterilization process with respect to sterilization temperature and time. Using the CFD model developed in the above-mentioned simulations for pouches, it will be possible to predict the necessary sterilization time required for pouches containing any new food products. Such analysis will save both energy and time, which are of great value for the large production capacity in the canning industry.

REFERENCES

Akterian, S.G. (1994). Numerical simulation of unsteady heat conduction in arbitrary shaped canned foods during sterilization processes. *Journal of Food Engineering, 21*, 343–354.

Banga, J.R., Alonso, A.A., Gallardo, J.M., & Perez-Martin, R.I. (1993). Mathematical modeling and simulation of the thermal processing of anisotropic and non-homogeneous conduction-heated canned foods: Application to canned tuna. *Journal of Food Engineering, 18*, 369–387.

Barreiro, J.A., Milano, M., & Sandoval, A.J. (1997). Kinetics of color changes of double concentrated tomato paste during thermal treatment. *Journal of Food Engineering, 33*, 359–371.

Beverly, R.G., Strasser, J., & Wright, B. (1980). Critical factors in filling and sterilizing of institutional pouches. *Food Technology, 34*(9), 44.

Bhowmik, S.R., & Tandon, S. (1987). A method of thermal process evaluation of conduction heated foods in retortable pouches. *Journal of Food Science, 52*(1), 202–209.

Bhowmik, S.R., & Shin, S. (1991). Thermal sterilization of conducted-heated foods in plastic cylindrical cans using convective boundary condition. *Journal of Food Science, 56*(3), 827–830.

Castillo, P.F., Barreiro, J.A., & Salas, G.R. (1980). Prediction of nutrient retention in thermally processed heat conduction food packaged in retortable pouches. *Journal of Food Science, 45*, 1513.

Datta, A.K., Teixeira, A.A., & Manson, J.E. (1986). Computer based retort control logic for on-line correction process deviations. *Journal of Food Science, 51*(2), 480–483.

Datta, A.K., & Teixeira, A.A. (1987). Numerical modeling of natural convection heating in canned liquid foods. *Transaction of American Society of Agricultural Engineers, 30*(5), 1542–1551.

Datta, A.K., & Teixeira, A.A. (1988). Numerically predicted transient temperature and velocity profiles during natural convection heating of canned liquid foods. *Journal of Food Science, 53*(1), 191–195.

Datta, A.K. (1991). Mathematical modeling of biochemical changes during processing of liquid foods and solutions. *Biotechnology Progress, 7*, 397–402.

Datta, A.K. (1999). Heat transfer coefficient in laminar flow of non-Newtonian fluid in tubes. *Journal of Food Engineering, 39*, 285–287.

Deniston, M.F., Hassan, B.H., & Merson, R.L. (1987). Heat transfer coefficients to liquids with food particles in axially rotating cans. *Journal of Food Science, 52*(2), 962.

Deniston, M.F., Kimball, R.N., Pedersen, L.D., Gee, M., Parkinson, K.S., & Jones, H.C. (1991). Effects of steam/air mixtures on a convection-heating product processed in a steritort. *Journal of Food Science, 56*(1), 27.

Dincer, I., Varlik, C., & Gun, H. (1993). Heat transfer rate variation in a canned food during sterilization. *International Comm. Heat Mass Transfer, 20*, 301–309.

Durance, T.D. (1997). Improving canned food quality with variable retort temperature process. *Trends in Food Science & Technology, 8*, 113–118.

Engelman, M.S., & Sani, R.L. (1983). Finite-element simulation of an in-package pasteurization process. *Numerical Heat Transfer, 6*, 41–54.

Fellows, P.J. (1996). *Food processing technology (principles and practice)*. U.K.: Woodhead Publishing Series in Food Science and Technology.

Ferziger, J.H., & Peric, M. (1996). *Computational methods for fluid dynamics*. New York: Springer-Verlag.

Giannoni-Succar, E.B., & Hayakawa, K.A. (1982). Correction factor of deviant thermal processes applied to packaged heat conduction food. *Journal of Food Science, 47*(2), 642–646.

Hawakawa, K. (1977a). Review on computerized prediction of nutrients in thermally processed canned food. *Journal of the AOAC, 60*, 1243.

Hawakawa, K. (1977b). Mathematical models for estimating proper thermal processes and their computer implementation. *Advanced Food Research, 23*, 75.

Hawakawa, K. (1978). A critical review of the mathematical procedures for determining proper heat sterilization processes. *Food Technology, 32*(3), 59.

Heldman, D.R., & Singh, R.P. (1981). *Food process engineering* (2nd ed.). Westport, CT: AVI.

Heldman, D.R., & Hartel R.W. (1997). *Principles of food processing*. New York: Chapman & Hall.

Hiddink, J. (1975). Natural convection heating of liquids, with reference to sterilization of canned food (Agricultural Research Report No. 839). Wageningen, The Netherlands: Center for Agricultural Publishing and Documentation.

Holdsworth, S.D. (1985). Optimization of thermal processing-a review. *Journal of Food Engineering, 4*, 89.

Junge, A., & Fryer, P.J. (1999). Optimizing the quality of safe food: Computational modeling of a continuous sterilization process. *Chemical Engineering Science, 54*, 717–730.

Kumar, A., Bhattacharya, M., & Blaylock, J. (1990). Numerical simulation of natural convection heating of canned thick viscous liquid food products. *Journal of Food Science, 55*(5), 1403–1411.

Kumar, A., & Bhattacharya, M. (1991). Transient temperature and velocity profiles in a canned non-Newtonian liquid food during sterilization in a still—cook retort. *International Journal of Heat & Mass Transfer, 34*(4/5), 1083–1096.

Lampi, R.A. (1980). Retort pouch: The development of a basic packaging concept in today's high technology era. *Food Processing Engineering, 4*, 1–18.

Lanoiselle, J.L., Candau, Y., & Debray, E. (1986). Predicting internal temperature of canned food during thermal processing using a linear recursive model. *Journal of Food Science, 60*(3), 715–719.

Lu, Q., Mulvaney, S.J., & Hsieh. (1991). Thermal processes for metal cans compared to retortable plastic containers. *Journal of Food Science, 56*(3), 835–837.

Lund, D.B. (1977). Maximising nutrient retention. *Food Technology, 31*(2), 71–80.

Manson, J.E., Stumbo, C.R., & Zahradnik, J.W. (1970). Evaluation of lethality and nutrient retentions of conduction heating foods in rectangular containers, *Food Technology, 24*(11), 109–113.

May N. (1997). Guidelines No.13, 16, and 17. Campden & Chorleywood Food Research Association.

Mermelstein, N.H. (1978). Retort pouch earns 1978 IFT food technology industrial achievement award. *Food Technology, 32*(6), 22.

Naveh, D., Kopelman, I.J., & Pflug, I.J. (1983). The finite element method in thermal processing of foods. *Journal of Food Science, 48*, 1086.

Nickerson, J.T., & Sinskey, A.J. (1972). *Microbiology of foods and food processing*. New York: Elsevier.

Nicolai, B.M., Verboven, B., Scheerlinck, N., & De Baerdemaeker, J. (1998). Numerical analysis of the propagation of random parameter fluctuations in time and space during thermal food processes. *Journal of Food Engineering, 38*, 259–278.

Ohlsson, T. (1980). Optimal sterilization temperature for flat containers. *Journal of Food Science, 45*, 848–852.

Patankar, S.V., & Spalding, D. B. (1972). A calculation procedure for heat, mass and momentum transfer in three-dimensional parabolic flows. *International Journal of Heat and Mass Transfer, 15*(10), 1787–1806.

PHOENICS Reference Manual, Part A. PIL. TR 200 A Bakery House, London SW 19 5AU, U.K.: CHAM.

Radosavljevic, D., & Wu, J.Z. (1990). The PHOENICS beginner's menu system user guide. TR 217 A Bakery House, London SW 19 5AU, U.K.: CHAM.

Rahman, M.S. (1999). *Handbook of food preservation. Food science and technology. A series of monographs, textbooks, and reference books*. New York: Marcel Dekker.

Ramaswamy, H.S., Tung, M.A., & Stark, R. (1983). A method to measure surface heat transfer from steam/air mixtures in batch retorts. *Journal of Food Science, 48*, 900.

Saguy, I., & Karel, M. (1979). Optimal retort temperature profile in optimizing thiamine retention in conduction-type heating of canned foods. *Journal of Food Science, 44*, 1485–1490.

Scott, G.M., Tucker, G.S., Kassim, H.O., Bewaji, E., Best, R., & Richardson, P. (1994). Process simulation techniques for batch and continuous thermal processing operations (Technical memorandum No. 710). Campden, England: Campden Food & Drink Research Association.

Scott, G.M. (1994). Computational fluid dynamics for the food industry. *Journal of Food Technology International Europe*, 49–51.

Scott G.M., & Richardson P. (1997). The application of computational fluid dynamics in the food industry. *Trends in Food Science & Technology, 8*, 119–124.

Shin, S., & Bhowmik, S.R. (1990). Computer simulation to evaluate thermal processing of food in cylindrical plastic cans. *Journal of Food Engineering, 12*, 117.

Shin, S., & Bhowmik, S.R. (1995). Thermal kinetics of color changes in pea puree. *Journal of Food Engineering, 24*, 77–86.

Silva, C., Hendrickx, M., Oliveira, F., & Tobback, P. (1992). Optimal sterilization temperatures for conduction heating foods considering finite surface heat transfer coefficients. *Journal of Food Science, 57*(3), 743–748.

Spinak, S.H., & Wiley, R.C. (1982). Comparisons of the general and Ball formula methods for retort pouch process calculations. *Journal of Food Science, 47*, 880–884.

Stoforos, N.G., & Merson, R.L. (1990). Estimation heat transfer coefficients in liquid/particulate canned food using only liquid temperature data. *Journal of Food Science, 55*(2), 478.

Tandon, S., & Bhowmik, S.R. (1986). Evaluation of thermal processing of retortable pouches filled with conduction-heated foods considering their actual shapes. *Journal of Food Science, 51*(3), 709–714.

Teixeira, A.A., Dixon, J.R., Zahradnik, J.W., & Zinsmeister, G.E. (1969). Computer optimization of nutrient retention in thermal processing of conduction-heated foods. *Food Technology, 23*(6), 134–140.

Teixeira, A.A., Stumbo, C.R., & Zahradnik, J.W. (1975a). Experimental evaluation of mathematical and computer models for thermal process evaluation. *Journal of Food Science, 40*, 653–655.

Teixeira, A.A., Zinsmeister, G.E., & Zahradnik, J.W. (1975b). Computer simulation of variable retort control and container geometry as a possible means of improving thiamin retention in thermally processed foods. *Journal of Food Science, 40*, 656–659.

Teixeira, A.A., & Manson, J.E. (1982). Computer control of batch retort operations with on-line correction of processes deviations. *Food Technology, 36*, 85–90.

Teixeira, A.A., & Tucker, G.S. (1997). On-line retort control in thermal sterilization of canned foods. *Food Control, 8*(1), 13–20.

Terajima, Y. (1975). Over-all heat transmission from the heating medium (steam and water) to the content of the retortable pouch. *Canners Journal, 54*(1), 73–79.

Tucker, G.S., & Clark, P. (1990). Modelling the cooling phase of heat sterilization processes, using heat transfer coefficients. *International Journal of Food Science Technology, 25*, 668.

Tucker, G.S. (1991). Development and use of numerical techniques for improved thermal process calculations and control. *Food Control, 2*, 15–19.

Tucker, G.S., & Holdsworth, S.D. (1991). Mathematical modelling of sterilization and cooking processes for heat preserved foods-applications of a new heat transfer model. *Transaction of Institution of Chemical Engineers, 69*(3), 5.

Tung, M.A., Ramaswamy, H.S., Smith, T., & Stark, R. (1984). Surface heat transfer coefficients for steam/air mixtures in two pilot scales retorts. *Journal of Food Science, 49*, 939.

Verboven, P., Nicolai, B.M., Sheerlinck, N., & Beardmeaker, J.D. (1997). The local surface heat transfer coefficient in thermal food process calculations: A CFD approach. *Journal of Food Engineering, 33*, 15–35.

Verboven, P., Sheerlinck, N., Beardmeaker, J.D., & Nicolai, B.M. (2000a). Computational fluid dynamics modeling and validation of the temperature distribution in a forced convection oven. *Journal of Food Engineering, 43*, 41–53.

Verboven, P., Sheerlinck, N., Beardmeaker, J.D., & Nicolai, B.M. (2000b). Computational fluid dynamics modeling and validation of the temperature distribution in a forced convection oven. *Journal of Food Engineering, 43*, 61–73.

Versteeg, H.K., & Malalasekera (1995). *An introduction to computational fluid dynamics. The finite volume method*. Harlow, England: Longman Scientific and Technical.

Wendt, J.F. (1992). *Computational fluid dynamics. An introduction*. Berlin and New York: von Karmen Institute, Springer-Verlag.

Wilbur, A. (1996). *Unit operation for the food industries, Food processing and technology*. Ohio State University, 125–136.

Yang, W.H., & Rao, M.A. (1998). Transient natural convection heat transfer to starch dispersion in a cylindrical container: numerical solution and experiment. *Journal of Food Engineering, 36*, 395–415.

CHAPTER 2

HEAT TRANSFER PRINCIPLES

Food preservation remains to be one of the important food processing industries. Early approaches to food preservation applied the methods of preservation naturally available, such as sun drying, salting, and fermentation, which were used to provide food in periods when fresh foods were not available. As civilization developed, demand for large quantities of better quality processed food also increased. This led to the development of a large food preservation industry aimed at supplying food of high quality in an economical way. Thermal sterilization of foods is the most significant part of this industry (Karel et al., 1975). Other methods of sterilization such as a pulsed electric field (Barbosa-Canovas et al., 1998; Barbosa-Canovas and Zhang, 2000; Jia et al., 1999; Martin et al., 1997; Qin et al., 1994, 1998; Sepulveda-Ahumada et al., 2000; Vega-Mercado et al., 1997, 1999; Zhang et al., 1995), ultrahigh hydrostatic pressure (Barbosa-Canovas et al., 1997a; Furukawa and Hayakawa, 2000; Paloua et al., 1999; Sancho et al., 1999), and ultraviolet (UV) treatment (Farid et al., 2000) have been widely studied. However, with the exception of high-pressure processing, these technologies have not yet reached commercialization stage.

2.1. INTRODUCTION TO THERMAL STERILIZATION

Two different methods of conventional thermal processing are known: aseptic processing, in which the food product is sterilized prior to packaging, and canning in which the product is packed and then sterilized (Barbosa-Canovas et al., 1997b). Food after being canned has to undergo thermal treatment to deactivate most organisms (i.e. sterilization). In 1981, the food industry in the United States alone processed more than 16.3 billion kg of food products in approximately 37 billion containers (Kumar et al., 1990).

Thermal sterilization is one of the most effective means of preserving a large part of our food supply. The objective of sterilization is to extend the shelf life of food products and make the food safe for human consumption by destroying harmful microorganisms. A sterilizer is a unit in which food is heated at high temperature and then held at that temperature for a period sufficient to kill the microorganisms of concern from the foodproduct. A sterile product is one in which no viable microorganisms are present. A viable organism is one that is able to reproduce when exposed to conditions that are optimum for its growth. Temperature slightly higher than the maximum for bacterial growth results in the death of vegetative bacterial cells, whereas bacterial spores can survive at much higher temperatures. Since bacterial spores are far more heat resistant than vegetative cells, they are of primary concern in most sterilization processes. Saturated steam is the most commonly used and highly desirable heating medium for commercial sterilization of canned foods. Conventional canning consists of the following operations:

1. Preparing the food (cleaning, cutting, grading, blanching, etc.)
2. Filling the container
3. Sealing the container

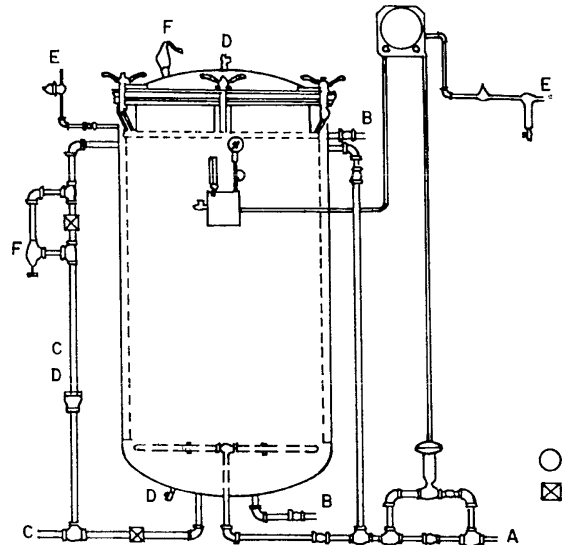

Figure 2.1. Vertical retort (Rahman, 1999).

4. Placing the container in a batch or continuous retort where it is heated for a time sufficient for commercial sterility
5. Cooling of the container, which is usually done using a cold shower

The still retort is the oldest type of equipment used for thermal processing. It is still used in large canning plants for metal- and glass-packed products. The sterilization method using a still retort consists of loading the containers, which are placed into baskets immediately after seaming and then into an appropriately designed iron vessel (retort), closing the vessel, and heating the containers with steam. A controller regulates the temperature, and the duration of heating is determined by the rate of heat transfer into the containers. Introduction of steam into the retort should be done with care since it is necessary to displace all of the air in the retort. The presence of air during thermal sterilization processing can result in under-processing since steam–air mixtures result in lower heat transfer rates (Karel et al., 1975).

Still retorts are usually arranged either vertically (Figure 2.1) or horizontally (Figure 2.2). The metal shell pressure vessel is fitted with a steam inlet (A), a water inlet (B), outlet ports for venting

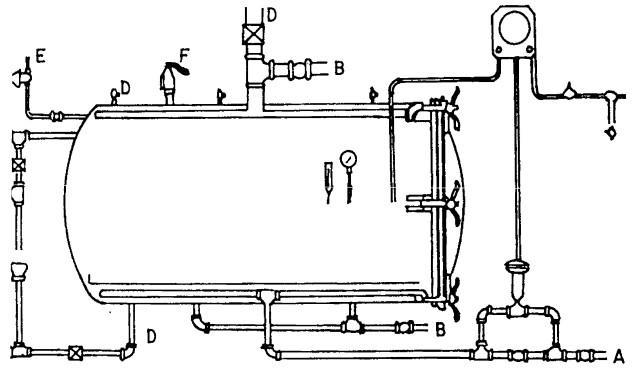

Figure 2.2. Horizontal retort (Rahman, 1999).

air during retort come-up and for draining (D), outlet ports for venting the retort at the end of the cycle (C), and a safety and pressure relief valve (F). A pocket for instruments, a thermometer, a temperature-recording probe, and a pressure gauge is located on the side of the vessel.

The operating cycle of this type of a retort involves bringing the retort up to a temperature of around 121°C. Steam is then allowed to pass through the vessel so that all air in the retort and between the cans is removed (venting) before the retort is finally brought up to the operating pressure and processing temperature (Rahman, 1999). At the end of the processing time, the steam is turned off, and a mixture of cooling water and air is introduced into the retort to cool the cans. The purpose of the air is to maintain the pressure in the retort, following the condensation of the residual steam after the initial introduction of cooling water. The containers may deform because of the pressure difference between inside and outside of the container if this pressure is not maintained.

The recent focus on thermal sterilization of foods is to improve the rates of heating, in order to increase production rates and minimize damage to product quality.

2.2. HEAT TRANSFER

In the sterilization of canned food, the heat transfer mechanism through liquid food in cans is classified as convection-heated, conduction-heated, or combined convection- and conduction-heated mechanism (Herson and Hulland, 1980). *Conduction* is the movement of heat by direct transfer of molecular energy within solids. *Free convection* is the transfer of heat in fluid by groups of molecules or fluid bulk that moves as a result of differences in the density of the fluid. In most applications these two types of heat transfer occur simultaneously, but one type may be more important than the other. *Steady-state* heat transfer takes place when there is no change in temperature with time. However, in most food processing applications, the temperature of the food or of the heating or cooling medium is constantly changing, and *unsteady-state* heat transfer is found more commonly. Calculations of heat transfer under these conditions are complicated but are simplified by making a number of assumptions (Fellows, 1996). *Forced convection* heat transfer will not be discussed in this chapter since it is not applicable to a number of objectives stated in this book. The subject of forced convection heat transfer is well described in most heat transfer textbooks. Also, the analysis of heat transfer presented in this chapter does not cover heat transfer with phase change such as freezing or evaporation. In retorting, steam condensation occurs at the surface of the cans or pouches. However, the condensation heat transfer coefficient is large enough to allow the assumption that the surface temperature is the same as the condensing steam temperature. The calculation of evaporation and condensation heat transfer coefficients is well described in most textbooks of heat transfer (Holman, 1992; Incropera and DeWitt, 1996). Radiation heat transfer does not play an important role in heat transfer in retorting since the heating temperature does not exceed 121°C and hence will not be considered in the analysis presented in this book.

The thermal conductivities of a variety of food materials are available in the literature. A notable feature of food products is their low value of thermal conductivity compared to metals. In metals, electrons transmit most of the heat energy, whereas in foods, where water is the main constituent, the free electron concentration is low, and the transfer mechanism involves primarily vibration of atoms and molecules (Karel et al., 1975). Moreover the thermal conductivity of liquid food is close to that of water.

2.2.1. Unsteady-State Heat Conduction

In food processing, there are many situations where temperature is a function of time. The most notable examples of unsteady-state heat transfer are heating and cooling of particulate materials,

such as cooling and heating of products in containers (canning). If the heated or cooled materials are solid, then heat will transfer by conduction only. The calculations of unsteady-state heat transfer are usually complicated and involve solving the Fourier equation, written in terms of the partial differential equation in three dimensions (Karel et al., 1975). In unsteady-state heat transfer, the temperature within a food during processing depends on the time and position. The temperature changes are influenced by

1. the initial temperatures of the heated body
2. the temperature of the heating medium
3. the surface heat transfer coefficient (heat transfer coefficient at all interfaces as well as where convection is involved)
4. the thermal conductivity, specific heat, and density of the food and their variation with temperature and composition
5. thickness of the heated body

The basic equation for unsteady-state heat conduction in one-space dimension (x) is

$$\frac{\partial T}{\partial t} = \frac{k}{\rho C_p}\frac{\partial^2 T}{\partial x^2} \tag{2.1}$$

where $\partial T/\partial t$ is the change of temperature with time, ρ is the density (kg m^{-3}), C_p is the specific heat capacity (J $kg^{-1}K^{-1}$), and k is the thermal conductivity (W $m^{-1}K^{-1}$).

When a solid piece of food is heated or cooled by a fluid, the resistance to heat transfer is mainly controlled by the surface heat transfer coefficient (h) and the thermal conductivity of the food (k). These two factors are related by the *Biot number* (*Bi*):

$$Bi = \frac{h\delta}{k} \tag{2.2}$$

where δ is the characteristic dimension or heat transfer path length in the solid (m). At small *Bi* values (>0.2), the surface film is the main resistance to heat flow; in this case, the assumption of a negligible internal (conductive) heat transfer resistance in the solid food is valid (Barbosa-Canovas et al., 1997b). However, in most applications the thermal conductivity of the food limits the rate of heat transfer ($Bi > 1$). The calculations in these cases are complex, and a series of charts is available to solve the unsteady-state equations for simple-shaped foods, as described in the following section.

2.2.1.1. Convection Boundary Conditions

In most practical situations, a transient heat conduction problem is connected with a convection boundary condition at the surface of the solid. Naturally, the boundary conditions for the differential equation must be modified to take into account this convective heat transfer at the surface (Holman and White, 1992). The most important cases are plates whose thickness is smaller than their other dimensions, cylinders whose diameter is smaller than their length, and spheres. Results for these geometries have been presented in a graphical form known as *Heisler charts* (Heisler, 1947; Holman, 1992). In all cases the convection temperature is designated as T_∞ and the center temperature for plate ($x = 0$) or cylinder and sphere ($r = 0$) as T_0. At time zero, each solid is assumed to have a uniform temperature T_i. Temperatures in the solids are given in Heisler charts as a function of time and spatial position. The calculations for the Heisler charts are performed by truncating the infinite series solutions for the problems into a few terms. This restricts the applicability of the charts to values of the Fourier number (Fo) greater than 0.2.

Heisler charts may be used to obtain the temperature distribution in the infinite plate, the long cylinder, or the sphere. When a wall whose height and depth dimensions are not large compared with the thickness or a cylinder whose length is not large compared with its diameter is encountered, additional space coordinates are necessary to specify the temperature, and the above charts no longer apply. In this case we have to seek another solution (Holman and White, 1992). Fortunately, it is possible to combine the solution for the one-dimensional system in a very straightforward way to obtain solutions for the multidimensional problems. There are many other practical heating and cooling problems of interest. The solutions for a large number of cases are presented in graphical form by Schneider (1955).

The charts described above are very useful for calculating temperatures in certain regular-shaped solids under transient heat flow conditions. Unfortunately, many geometric shapes of practical interest do not fall into these categories, and we are also frequently faced with problems in which the boundary conditions vary with time. These transient boundary conditions as well as the geometric shape of the body do not allow analytical solutions. In these cases the problems are best handled by numerical techniques such as those used and presented in detail in this book for the cases of thermal sterilization in cans and pouches.

2.2.2. Free Convection

When a fluid's temperature changes, the resulting changes in density establish natural convection currents, which occur as a result of bulk movement of the fluid, such as the movement of liquid inside a can during sterilization. Obviously, heat transfer by conduction occurs simultaneously but is generally negligible compared to convection heat transfer (Karl et al., 1975). The rate of convection heat transfer is governed by Newton's law of cooling. This law states that the rate of heat transfer by convection is directly proportional to the heat transfer area and the temperature difference between the fluid and heating/cooling surface:

$$Q = h_s a\ (T_{bu} - T_s) \tag{2.3}$$

where Q is the rate of heat transfer (W), a is the surface area (m^2), T_s is the surface temperature, T_{bu} is the bulk fluid temperature, and h_s is the surface or film heat transfer coefficient (W m^{-2} K^{-1}). The surface heat transfer coefficient is inversely related to heat flow resistance, caused by the boundary film near the surface, and is therefore equivalent to the term $k/\Delta x$ in the conduction equation. The heat transfer coefficient is a function of the physical properties of the liquid food used in thermal processing, such as the density, viscosity, specific heat, and thermal expansion coefficient. It is also related to the gravity, which causes circulation due to the changes in density; the temperature difference; and the length or diameter of the container under investigation. The formulae, which relate these factors, are expressed as dimensionless numbers as shown below:

$$\text{Nusselt number Nu} = \frac{h d_v}{k} \tag{2.4}$$

$$\text{Prandtl number Pr} = \frac{C_p \mu}{k} \tag{2.5}$$

$$\text{Grashof number Gr} = \frac{d_v^3 \rho^2 g \beta \Delta T}{\mu^2} \tag{2.6}$$

where h is the heat transfer coefficient at the solid liquid interface (W m^{-2} K^{-1}); d_v is the characteristic dimension (m), which may be the height or diameter of the can, as will be discussed later; k is the thermal conductivity of the fluid (W $m^{-1}K^{-1}$); ρ is the density (kg m^{-3}); C_p is the specific heat

capacity (J $kg^{-1}K^{-1}$); μ is the viscosity (N s m^{-2}); g is the acceleration due to gravity (m s^{-2}); β is the thermal expansion coefficient (K^{-1}); and ΔT is the temperature difference (°C).

There are large numbers of empirical correlations available in literatures describing the relationship between Nu, Gr, and Pr for many cases (Holman, 1992; Incropera and DeWitt, 1996; Mills, 1995). These cases include fluid heated or cooled by vertical and horizontal solid cylinders, inclined surfaces, etc. These correlations are approximate and purely empirical and can be used only for the geometries for which they have been developed. Such empirical correlations are not available in literatures for liquid heated in cylinders or pouches. The only approach left to account for the free convection of liquid in these geometries is to solve the Navier–Stokes equations of continuity, momentum, and energy conservation in a cylinder and pouch space, as described in the following chapters of this book.

NOMENCLATURE

a	area, m^2
Bi	Biot number, $Bi = \frac{h\delta}{k}$, dimensionless
C_P	specific heat of liquid food, J $kg^{-1}K^{-1}$
d_v	vertical dimension, m
Gr	Grashof number, $\mathrm{Gr} = \frac{d_v^3 \rho^2 g \beta \Delta T}{\mu^2}$, dimensionless
g	acceleration due to gravity, m s^{-2}
h	heat transfer coefficient, W $m^{-2}K^{-1}$
k	thermal conductivity, W m^{-1} K^{-1}
Nu	Nusselt number, $\mathrm{Nu} = \frac{h_c d_v}{k}$, dimensionless
Pr	Prandtl number, $\mathrm{Pr} = \frac{C_p \mu}{k}$, dimensionless
F_o	Fourier number
Q	rate of heat transfer, J s^{-1}
t	time, s
T	temperature, °C
β	thermal expansion coefficient, K^{-1}
μ	viscosity, Pas
ρ	density, kg m^{-3}
δ	diameter, m

Subscripts

bu	bulk
s	surface
x, y, z	coordinates

REFERENCES

Barbosa-Canovas, G.V., Gongora-Nieto, M.M., & Swanson B.G. (1998). Nonthermal electrical methods in food preservation. *Food Science and Technology International, 4*(5), 363–370.

Barbosa-Canovas, G.V., Ma, L., & Barletta B. (1997b). *Food engineering laboratory manual*. Lancaster, PA: Technomic.

Barbosa-Canovas, G.V., Pothakamury, U.R., Palou, E., & Swanson, B.G. (1997a). *Nonthermal preservation of foods*. New York: Marcel Dekker.

Barbosa-Canovas, G.V., & Zhang Q.H. (2000). *Pulsed electric field in food processing: fundamentals aspects and applications*. Lancaster, PA: Technomic.

Farid, M.M., Chen, X.D., & Dost, Z. (2000). Ultraviolet sterilization of orange juice. Eighth International Congress on Engineering and Food, April 2000, Pueblo, Mexico.

Fellows, P.J. (1996). *Food processing technology (principles and practice)*. U.K.: Woodhead Publishing Series in Food Science and Technology.

Furukawa, S., & Hayakawa, I. (2000). Investigation of desirable hydrostatic pressure required to sterilize Bacillus stearothermophilus IFO 12550 spores and its sterilization properties in glucose, sodium chloride and ethanol solutions. *Journal of Food Research International, 33*, 901–905.

Heisler, M.P. (1947). Temperature charts for induction and constant temperature heating. *Transaction of American Society of Mechanical Engineers, 69*, 227–236.

Herson, A.C., & Hulland, E.D. (1980). *Canned foods. Thermal processing and microbiology*. Edinburgh: Churchill Livingstone.

Holman, J.P. (1992). *Heat transfer*. U.K.: McGraw-Hill International Limited.

Incropera, F.B., & DeWitt, D.B. (1996). *Fundamentals of heat & mass transfer*. USA: Wiley.

Jia, M., Zhang, Q.H., & Min, D.B. (1999). Pulsed electric field processing effects on flavor compounds and microorganisms of orange juice. *Journal of Food Chemistry, 65*, 445–451.

Karel, M., Fennema, O.R., & Lund, D.B. (1975). *Principles of food science, Part II*. New York: Marcel Dekker.

Kumar, A., Bhattacharya, M., & Blaylock, J. (1990). Numerical simulation of natural convection heating of canned thick viscous liquid food products. *Journal of Food Science, 55*(5), 1403–1411.

Martin, O., Qin, B.L., Chang, F.J., Barbosa-Canovas, G.V., & Swanson, B.G. (1997). Inactivation of Escherichia coli in skim milk by high intensity pulsed electric fields. *Journal of Food Processes Engineering, 20*, 317–336.

Mills, A.F. (1995). *Basic heat and mass transfer*. USA: Irwin.

Paloua, E., Lopez-Malo, A., Barbosa-Canovas, G.V., & Swanson, B.G. (1999). High pressure treatment in food preservation. In *Handbook of food preservation* by Rahman, M.S. (1999). New York: Marcel Dekker.

Qin, B.L., Barbosa-Canovas, G.V., Swanson, B.G., Pedrow, P.D., & Olsen, R.G. (1998). Inactivating microorganisms using a pulsed electric field continuous treatment system. *IEEE Transactions on Industry Applications, 34*(1), 43–50.

Qin, B.L., Zhang, Q., Barbosa-Canovas, G.V., Swanson, B.G., & Pedrow, P.D. (1994). Inactivation of microorganisms by pulsed electric fields with different waveforms. *IEEE Trans. on Dielectrics and Electrical Insulation, 1*(6), 1047–1057.

Rahman, M.S. (1999). *Handbook of food preservation. Food science and technology. A series of, monographs, textbooks, and reference books.* New York: Marcel Dekker.

Sancho, F., Lambert, Y., Demazeau, G., Largeteau, A., Bouvier, M., & Narbonne, J.F. (1999). Effect of ultra-high hydrostatic pressure on hydrosoluble vitamins. *Journal of Food Engineering, 39*, 247–253.

Schneider, P.J. (1955). *Conduction heat transfer*. Reading, MA: Addison-Wesley.

Sepulveda-Ahumada, D.R., Ortega-Revas, E., & Barbosa-Canovas, G.V. (2000). Quality aspects of cheddar cheese obtained with milk pasteurized by pulsed electric fields. *Journal of Institution of Chemical Engineers, 78*, 65–71.

Vega-Mercado, H., Gongora-Nieto, M.M., Barbosa-Canovas, G.V., & Swanson, B.G. (1999). Non-thermal preservation of liquid foods using pulsed electric fields. In *Handbook of food preservation* by Rahman, M.S. (1999). New York: Marcel Dekker.

Vega-Mercado, H., Martin, O., Qin B.L., Chang, F.J., Gongora-Nieto, M.M., & Barbosa-Canovas, G.V. (1997). Non-thermal food preservation: Pulsed electric fields. *Trends in Food Science and Technology, 5*(8), 151–157.

Zhang, Q., Barbosa-Canovas, G.V., & Swanson B.G. (1995). Engineering aspects of pulsed electric field pasteurization. *Journal of Food Engineering, 25*(2), 261–281.

CHAPTER 3

PRINCIPLES OF THERMAL STERILIZATION

3.1. EFFECTS OF HEAT TREATMENT DURING STERILIZATION

The rate of heat transfer from the heating medium (steam) through the can wall into the outer layer of food is high. Hence, penetration of heat into the slowest heating zone (SHZ) (i.e., the location of the lowest temperature) in the food is controlled by thermal properties of the food itself (Bhowmik and Tandon, 1987). The severe heat treatment during sterilization produces substantial changes in nutritional and sensory qualities of foods. In order to determine the process time for a given food, it is necessary to have information on both the rate of heat penetration and its effect on the inactivation of microorganisms.

3.1.1. Heat Penetration

In thermal processing, which represents the most common technique used in food preservation today, the study of heat penetration into foods is of great importance. The factors that influence the rate of heat penetration are as follows:

1. *Product specification*. Liquid or particulate foods in which natural convection is established heat faster than solid foods in which heat is transferred by conduction. The low thermal conductivity of foods is a major limitation to the conduction heat transfer.
2. *Size of the container.* Heat penetration to the center is faster in small containers than in large containers.
3. *Temperature of the retort*. A higher temperature difference between the heating medium and the foods causes faster heat penetration.
4. *Shape of the container*. Tall containers promote free convection currents in convective heating of foods and hence faster heat penetration.
5. *Type of the container*. Heat penetration is faster through metal walls than glass or plastics walls of the container because of the higher thermal conductivity of metal than that of glass and plastic.

The rate of heat penetration is measured by placing a thermocouple at the thermal center of a container to record the temperature of the food during sterilization, assuming that all other points in the container receive more heat and are therefore adequately processed. Fellows (1996) stated that in cylindrical containers, the thermal center is at the geometric center of the cylinder for conduction-heated foods and approximately one third up from the base of the container for convection-heated foods (Figure 3.1). This is in agreement with the finding of Barbosa-Canovas et al. (1997), who also stated that the coldest point for a solid product will be at the center of the can, whereas in liquid-type

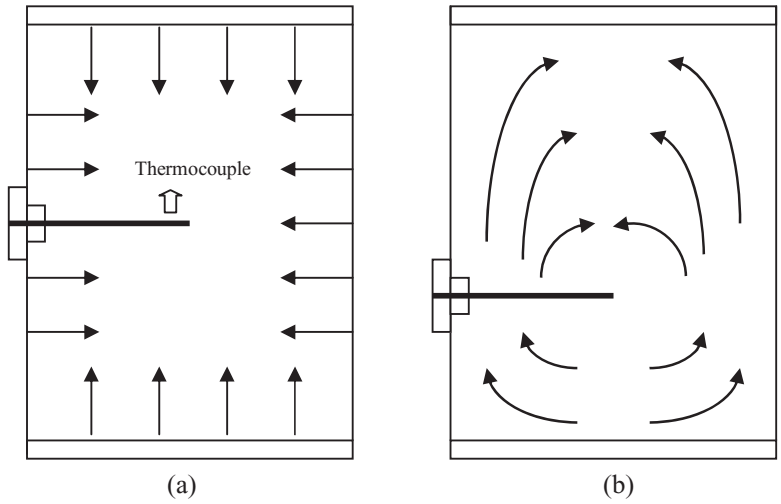

Figure 3.1. Heat transfer in container by (a) conduction and (b) convection (Fellows, 1996).

products it is usually at a lower location. However, in convection heating, the exact position of the SHZ may change progressively, as will be discussed in this book.

3.1.2. Heat Resistance of Microorganisms

In low-acid foods (pH > 4.5), *Clostridium botulinum* is the most dangerous heat-resistant and spore-forming pathogen likely to be present. Strict regulations and procedures are established by government agencies for the thermal processing of low-acid canned foods because of widespread public health concern about the anaerobic *C. botulinum*, which produces a toxin deadly to humans, even in very small amounts (Barbosa-Canovas et al., 1997). It can grow under anaerobic conditions inside a sealed container and produce a potent exotoxin; therefore its destruction is a minimum requirement in the sterilization of foods. Normally, foods receive more than this minimum treatment, as other more heat-resistant spoilage bacteria may also be present (Table 3.1). In low-acid foods, processing could be based on inactivation of spores, which are more heat resistant than those of *C.*

Table 3.1. Heat resistance of some spore-forming bacteria used as a basis for heat sterilization processes for low-acid foods (Fellows, 1996)

Microorganism	Z (°C)	D_{121}(min)	Typical foods
Thermophilic (35–55°C)			
Bacillus stearothermophilus	10	4.0	Vegetables, milk
Thermosaccharolyticum	7.2–10.0	3.0–4.0	Vegetables
Mesophilic (10–40°C)			
Clostredium sporogenes	8.8–11.1	0.8–1.5	Meats
Bacillus subtilis	4.1–7.2	0.50–0.76	Milk products
Clostridium botulinum toxins A and B	5.5	0.1–0.3	Low-acid foods
Psychrophilic (−5–1.5°C)			
Clostridium botulinum toxin E	10	3.0 (60°C)	Low-acid foods

botulinum, such as *Bacillus stearothermophilus*. Spores of this organism are extremely heat resistant (up to 20 times more resistant than *C. botulinum* spores). Growth of these spores results in "flat sour" spoilage because acid is produced with little or no gas. Optimum growth temperatures for these flat sour thermophiles vary from about 35°C to 55°C, as shown in Table 3.1. The parameters Z (°C) and D_{121} (min) are fully described in the following section.

3.2. EFFECT OF HEAT ON MICROBIAL POPULATION

Thermal destruction of microorganisms takes place logarithmically, and a sterile product cannot therefore be produced with certainty no matter how long the process time. However, the probability of survival of a single microorganism can be predicted using details of heat resistance of the microorganisms, temperature distribution, and time of heating. This gives rise to a concept known as commercial sterility. In canning factories, accelerated storage trials on randomly selected cans of food ensure that these levels of commercial sterility are maintained before foods are released for retail sale.

The effect of heat on microbial population causes denaturation of proteins, which destroys enzyme activity and enzyme-controlled metabolism in microorganisms. The rate of destruction is usually taken as a first order. Differences between the vegetative microbial populations as compared to the populations of microbial spores are evident within short periods of time after initial exposure to elevated temperatures. The pattern of reduction for both of them is the same, following logarithmic reduction. When the microbial populations are presented on semi-logarithmic coordinates as a function of time on standard coordinates, a linear decrease in microbial population with time is observed at a given temperature. This is known as the *logarithmic order of death* and is described by a *death rate curve* or *survivor curve*. A typical relationship for a microbial spore population versus time on semi-logarithmic coordinates is shown in Figure 3.2 (Fellows, 1996).

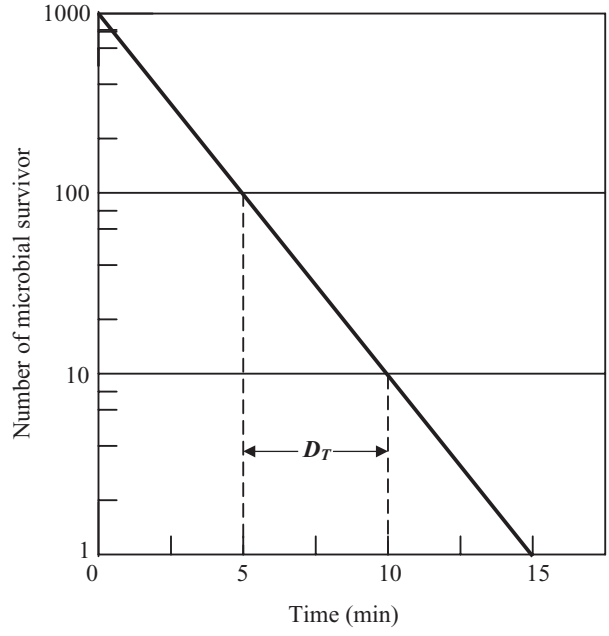

Figure 3.2. Death rate curve of microbial population (Fellows, 1996).

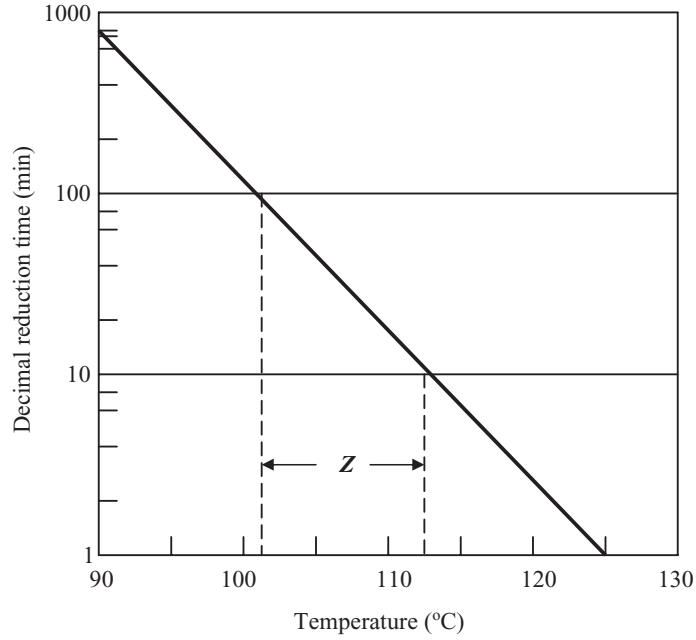

Figure 3.3. TDT curve of microbial population (Fellows, 1996).

The time needed to destroy 90% of the microorganisms (to reduce their numbers by a factor of 10) is defined as the *decimal reduction time* (D_T). It is the time required for a one-log cycle reduction in microbial population. D_T value has been used throughout thermal processing literature to quantify the effect of temperature on microbial populations. D_T values differ for different microbial species (Table 3.1). The larger D_T value at a given temperature indicates higher thermal resistance of the microbial population. A plot of decimal reduction time as a function of temperature on semi-log coordinates results in a linear relationship, which is referred to as the *thermal death time (TDT) curve* for a given microbial population (Figure 3.3).

The slope of the TDT curve is termed the Z value and is defined as the temperature increase required to cause a one-log cycle reduction in the decimal reduction time. It is also defined as the temperature difference that causes a tenfold change in the rate of microbial destruction. The value of Z can be used to estimate the effect of changing temperature on the processing time, using the equation (Fryer et al., 1997)

$$\text{Time required at temperature } T = \frac{\text{Time required at temperature } T_{\text{ref}}}{10^{(T-T_{\text{ref}})/Z}} \tag{3.1}$$

The destruction of microorganisms is temperature dependant, and the D_T value will decrease with increasing temperature. The decimal reduction time is a characteristic of the type of microorganisms and is found experimentally to vary with temperature according to

$$D_T = D_{T_{\text{ref}}} 10^{(T_{\text{ref}}-T)/Z} \tag{3.2}$$

where D_T is the decimal reduction time at temperature T, T_{ref} is an arbitrary reference temperature,

$D_{T_{\text{ref}}}$ is the decimal reduction time at T_{ref}, and Z is a temperature-dependent characteristic of microorganisms, assumed to be constant over normal processing conditions (David et al., 1996).

D_T and Z values are important parameters normally used to characterize the heat resistance of an enzyme, a microorganism, or a chemical component of foods. They are also used to quantify the thermal process required for a given microbial population. A large Z value suggests that a given increase in the temperature of exposure for the microbial population results in a small change in decimal reduction time. This is due to the microbial population containing vegetative cells or microbial spores that have greater heat resistance to elevated temperatures than populations characterized by a lower Z value (Heldman and Hartel, 1997).

The third important quantitative parameter in the thermal processing is the *thermal death time (F)*, or F value. It is defined as the time required to destroy a given percentage of microorganisms at a given temperature and Z value. This parameter states the reduction in the population of microbial pathogens required to establish product safety. The F value represents the total time-temperature combination received by a food and is quoted with suffixes indicating the retort temperature and the Z value of the target microorganism. A reference F value F_{ref} is used to describe processes that operate at 121°C, which are based on a microorganism with a Z value of 10°C. The F value is defined by Equation (3.3), which gives the relationship between F and the change in the concentration of microorganism in a containerized food, as a result of heating or cooling (David et al., 1996; Karel et al., 1975).

$$F^{Z}_{T_{\text{ref}}} = D_{T_{\text{ref}}}(\log n_1 - \log n_2) \tag{3.3}$$

where n_1 is the initial concentration of microorganisms at the beginning of the thermal process, and n_2 is the final concentration of microorganisms at the end of the thermal process. For the spores of *C. botulinum*, researchers have experimentally used n_1 less than or equal to 10^{12} spores per milliliter with an end point of n_2 less than 1 spore per milliliter, at a D_{121} value of 0.1 to 0.2 minutes and a Z value of 10°C. Thus Equation (3.3) can be written as

$$F^{Z}_{T_{\text{ref}}} = D_T(\log 10^{12} - \log 1) = 12D \tag{3.4}$$

which shows the most common relationships ($F = 12D$) for *C. botulinum* in commercial sterilization. A $12D$ process reduces cell numbers by twelfth decimal reductions. When this process is applied to a raw material, which contains for example 10^{12} spores per container, it reduces the microbial numbers to 1.0 spore per container. The type of microorganism that is expected to contaminate the raw material determines the level of survival. In foods that contain less heat-resistant spoilage microorganisms than *C. botulinum*, the application of $12D$ would result in overprocessing and excessive loss of quality. In practice a $5D$ or $8D$ process is therefore used to give the most economical level of food spoilage consistent with adequate food quality and safety (David et al., 1996; Karel et al., 1975).

Equation (3.3) forms the basis for the definition of a *process F* value (F_{process}), which is defined as the time-temperature effect of a thermal process expressed as time in minutes at a single reference temperature T_{ref} and for a given value of microorganisms. It is defined by the equation (David et al., 1996)

$$\left(F^{Z}_{T_{\text{ref}}}\right)_{\text{pocess}} = \int_{t_{\text{i}}}^{t_{\text{f}}} \frac{1}{10^{(T_{\text{ref}} - T_t)/Z}}\, dt \tag{3.5}$$

where t_{i} is the time at the beginning of the thermal process (min), and t_{f} is the time at the end of

the thermal process, i.e., at end of cooling (min). For sterilization to be deemed successful, this time must be greater than or equal to the required F value at temperature T_{ref}. This approach is widely used in the food industry. An F value of 3 min is taken as acceptable industrially, although process design values of at least 6 min are used in practice (Fryer et al., 1997).

3.3. EFFECT OF HEAT ON NUTRITIONAL PROPERTIES OF FOOD

Food contains a large number of nutrients. These are used for growth maintenance, tissue repair, and cell reproduction in the human body. Water, vitamins, proteins, fats, carbohydrates, and minerals comprise the general classes of nutrients. Many food processing operations, especially those that do not involve heat, have little or no effect on the nutritional quality of foods. Examples include mixing, cleaning, sorting, freeze-drying, and pasteurization. Heat processing is a major cause of change to the nutritional properties of food. It destroys some types of heat-labile vitamins, for example (Fellows, 1996). The destruction of many vitamins by heat follows a first-order reaction similar to microbial destruction. In general, both D_T and Z values of nutrients are higher than those of microorganisms and enzymes. As a result nutritional properties are better retained by the use of higher temperatures and shorter times during the sterilization process. It is therefore possible to select a particular time-temperature combination from a TDT curve to optimize a process for nutrient retention. This concept forms the basis of individual quick blanching, high-temperature short-time (HTST) pasteurization, and ultrahigh-temperature (UHT) sterilization.

3.4. REACTION KINETICS OF QUALITY CHANGES

Thermal sterilization of food causes changes in the food quality (biochemical changes). These changes include positive impact such as the reduction in the microbial population and negative impact such as the loss of nutrients, as discussed earlier. Most reactions occurring in food are represented by simple reaction kinetics. The thermal destruction of microorganisms, most nutrients, quality factors (texture, color, and flavor), and enzymes generally follow first-order reaction kinetics. That is the destruction rate of each of these components is linearly dependent on the concentration of the component. This relationship is frequently referred to as a "logarithmic order of inactivation or destruction" since this is regardless of the initial concentration. The first-order response describing the changes occurring during processing of food can be expressed mathematically by

$$-\frac{dC}{dt} = k_T C \tag{3.6}$$

where C is the concentration of the quality attribute, t is the time of exposure, and k_T is the reaction rate constant. In fact most changes occurring during thermal processing of food are more complex (Heldman and Hartel, 1997). However, it has been accepted in practice to use relatively simple expressions to describe quality changes in food and to use parameters similar to the rate constant (k_T). Integrating Equation (3.6) gives

$$Ln\frac{C}{C_0} = -k_T t \tag{3.7}$$

where C_0 is the initial concentration of the quality attribute. From the values of the reaction rate

constant (k_T) and the initial concentration of the quality attribute, the amount of the attribute remaining can be estimated for any time of exposure to a process.

The relationships between microbial populations and time are very similar to the relationships used to describe the kinetic parameters in first-order chemical reactions described above. The reaction rate constant (k_T) was used to describe the change in concentration of a reactant as a function of time. In microbial populations, D_T value is used to describe the same relationship. It follows that the relationship between the reaction rate constant (k_T) and the decimal reduction time (D_T) is given by the equation

$$k_T = \frac{2.303}{D_T} \tag{3.8}$$

There are two principal methods of describing the dependence of the reaction rate constant on temperature: (1) the Arrhenius equation and (2) TDT curves, presented in 3.3. The dependence of the reaction rate constant on temperature as described by the Arrhenius equation is

$$k_T = A \exp(-E/R_g T) \tag{3.9}$$

where

A = preexponential factor (s^{-1})
E = activation energy [kJ (kg mol)$^{-1}$]
R_g = universal gas constant [kJ (kg mol)$^{-1}$ K^{-1}]
T = temperature (°C)
k_T = reaction rate constant at temperature T (s^{-1})

The Arrhenius equation is useful in describing the effect of temperature on the rate constant of change in product quality during processing and storage (Fellows, 1988). It has a sounder theoretical base compared to that of the F value (Fryer et al., 1997).

In conclusion, the information provided by D_T and F values are valuable as they provide information on how fast a specific microorganism can be destroyed and model the effect of temperature on the rate of destruction. Equations (3.6) and (3.9) couple the effect of both time and temperature on the death rate. However, none of the mentioned approaches can be used to measure the required sterilization temperature in cans or pouches. This is because of the large variation in temperature with position in these containers. Direct application of these equations is appropriate only to small samples or in containers with a high degree of agitation. In stationary cans and pouches, there are significant spatial temperature distributions. In both cans and pouches, this requires the solution of the Navier–Stokes equations of continuity, momentum, and energy conservation.

NOMENCLATURE

A preexponential factor, s^{-1}
C concentration of bacteria (number of bacteria m^{-3}) and vitamin (kg m^{-3})
n_1 initial concentration of bacteria (number of bacteria m^{-3})
n_2 final concentration of bacteria (number of bacteria m^{-3})
D_T decimal reduction time, min
E activation energy, kJ (kg mol)$^{-1}$

F TDT, min
k_T reaction rate constant, s^{-1}
R_g gas constant, kJ $(kg\ mol)^{-1}\ K^{-1}$
t time, s
T temperature, °C
T_{ref} reference temperature, °C
Z temperature required to change the TDT by a factor of 10, °C

Subscripts

0 initial
ref reference

REFERENCES

Barbosa-Canovas, G.V., Ma, L., & Barletta B. (1997). *Food engineering laboratory manual*. Lancaster, PA: Technomic.
Bhowmik, S.R., & Tandon, S. (1987). A method of thermal process evaluation of conduction heated foods in retortable pouches. *Journal of Food Science, 52*(1), 202–209.
David, J.R.D., Graves, R.H., & Carlson, V.R. (1996). *Aseptic processing and packaging of food*. Boca Raton, FL: CRC Press.
Fellows, P.J. (1996). *Food processing technology (principles and practise)*. U.K.: Woodhead Publishing Series in Food Science and Technology.
Fryer, J.P., Pyle, D.L., & Rielly, C.D. (1997). *Chemical engineering for the food industry*. Blackie Academic & Professional.
Heldman, D.R., & Hartel R.W. (1997). *Principles of food processing*. New York: Chapman & Hall.
Karel, M., Fennema, O.R., & Lund, D.B. (1975). *Principles of food science, Part II*. New York: Marcel Dekker.

CHAPTER 4

FUNDAMENTALS OF COMPUTATIONAL FLUID DYNAMICS

In this chapter, a general description of mathematical modeling using computational fluid dynamics (CFD) is presented. The numerical approximation to the conservation equations is presented in accordance with the form used by the commercial CFD code "PHOENICS." The modifications required to adapt PHOENICS for the analysis of momentum and energy transfer in thermal sterilization are also presented.

4.1. INTRODUCTION TO COMPUTATIONAL FLUID DYNAMICS

CFD is a numerical technique used for the solution of the equations governing fluid flow and heat transfer problems inside a defined flow geometry (Scott, 1994). CFD has wide applications in the areas of fluid and heat transfer within the aerospace and nuclear industries backed by the availability of powerful supercomputers. It has expanded into other industries such as the chemical and petrochemical industries. It is only in recent years that it has been applied to the food industry, with a limited variety of food-related problems being investigated (Scott and Richardson, 1997).

CFD offers a powerful design and investigative tool to the process engineer in many applications. However, at present little use of this technology has been reported in the food industry. Its application in such areas would be beneficial for the better understanding of the complex interactions occurring in food systems. The development of CFD packages came from a need to solve complex fluid flow problems of a general nature for a wide range of geometry and boundary conditions (Hatton and Carpenter, 1976). CFD works by dividing the physical environment of interest into a two or three-dimensional (3-D) grid or mesh. It contains a number of discrete cells and can evaluate fluid velocities, temperature, and pressure inside every one of the cells where fluid flows. This is done by the simultaneous solution of the equations describing fluid flow, heat, and mass transfer.

The use of CFD techniques to solve a fluid flow and heat transfer problem is split into three discrete parts: *pre processing, processing, and post processing*. In general, different computer programs that form the CFD code must undertake each of the three tasks.

4.1.1. Definition of a CFD Problem (Preprocessor)

The first stage in solving a CFD problem is to define all the relevant parameters required by the CFD code prior to the numerical solution process, as follows:

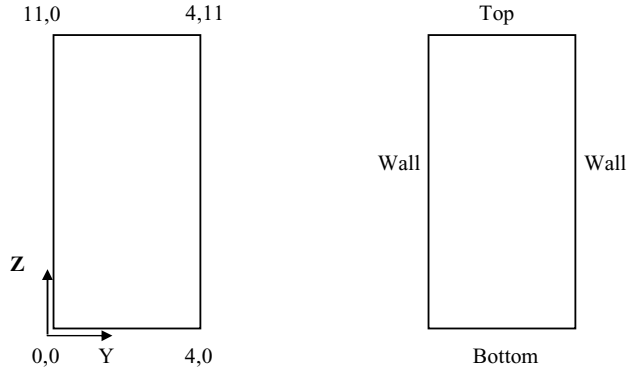

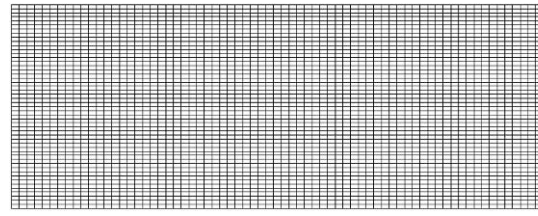

(a) Orthogonal structured mesh with uniform spacing (50x70)

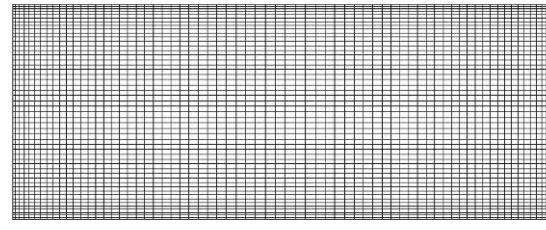

(b) Orthogonal structured mesh with non-uniform spacing (50x70)

Construction of a computational grid

Figure 4.1. Defining geometry for a CFD simulation.

1. Definition of the physical geometry of the environment in which the fluid flows, which is normally done by building up a geometric representation of the environment. "Create the shape of the problem domain that needs to be analysed."
2. Declaration of the boundary conditions of the physical environment. These boundary conditions will include defining certain areas such as the inlets and outlets for the fluid flow and the boundary areas of solids where heat transfer from or to the fluid can occur.
3. Construction of a mesh or grid as a geometric representation of the physical environment. This mesh or grid will form the computational grid that will be used in the solution of the problem by the powerful mathematical techniques around which CFD is based.

A uniform spacing mesh has regular rectangular cells with second-order accuracy. A nonuniform mesh (Figure 4.1) provides smaller cells where rapid changes are taking place within the solution domain (e.g., close to the boundaries); however, it is only of first-order accuracy (Mallinson, 1999).

In any CFD problem, the definition of boundary conditions is essential because they will define the flow conditions inside the flow domain. In general, at any top, bottom, inlets, or outlets, the flow domain needs to be defined to set the appropriate boundary conditions. For example, in the case of heating a fluid in a can, the velocity of the fluid and its temperature are set at the top, bottom, and wall of the can. Other types of boundary conditions that may need to be set are those for walls and solids particularly if they act as heat transfer boundaries (Scott and Richardson, 1997).

After defining the computational mesh and boundary conditions, the user needs to define the assumptions need to be made—for example, whether the flow is laminar or turbulent and whether heat transfer takes place or not. This usually involves writing a command file in PHOENICS that ties any other information required by the CFD solver, such as the type of model used and the number of iterations required.

There are two methods of generating the grid and the setup data for any problem. The first is to define the problem using FORTRAN. The second and more elegant method is based on a graphical user interface. In this method, the data is entered via a menu-driven procedure, which guides the user through all the separate stages in setting up a CFD simulation.

All CFD packages offer a variety of coordinate systems from which the computational grid is defined and generated, such as strict Cartesian, cylindrical polar, curvilinear, body fitted, or moving/rotating coordinate systems. The choice of the coordinate system, the resolution of the computational grid, and the method of its generation will be dependent on the complexity of the simulation.

4.1.2. Solution of the Problem (Processor)

The solution of the problem by the CFD code is where a host of mathematical techniques is used to approximate the differential equations into algebraic form, which can be solved directly or iteratively. Different CFD codes employ different solution techniques, but the physics is the same if it can be well defined and understood. The solution of the transport equations for the geometry under study is not a trivial matter and cannot be solved readily, if at all, by analytical techniques. CFD uses numerical techniques to solve discretized representations of the transport equations.

Direct or explicit numerical methods, which can be both extremely accurate and rapid, may be used if sufficient computing power is available. Many codes use iterative methods to solve the equations because they tend to be more robust, although they can take longer to converge. Standard texts are available that provide good background material on numerical simulation and CFD.

4.1.3. Analysis of the Results (Postprocessor)

The results can be analyzed both numerically and graphically. The postprocessor takes the numerical results and displays them as a visual representation. It displays a visual image of the physical geometry through which the fluid flows, with the option of printing a hard copy of all the results as tables of numbers and other means. It is possible to superimpose the velocity, pressure, and temperature distributions within the fluid. The format of this display is a graphical contour with the option of displaying scaled arrows for vector quantities. The output file can contain all sorts of information, including the spatial coordinates of all of the cells in the computational mesh and the solved transport variables for each cell. In the case of a large CFD problem, say greater than 100,000 cells, it is obvious that the user does not want to read through this file. Thus, the second method offers the user the ability to visualize the results. This method, often referred to as postprocessing, takes the results from the CFD solver and allows the user to display variables graphically on the computer screen, for all or part of the flow domain. These graphical presentation methods include vector plots

(a scaled arrow pointing in the direction of flow), contour plots on a two-dimensional (2-D) slice through the domain, and iso-surface plots (a 3-D surface on which a variable is constant). The user has the option to rotate the image in 3-D space or to zoom into areas of interest to extract the most useful information from the image. Combining both visual and numerical results allows the optimal solution to be achieved for the problem under investigation.

In this work, PHOENICS, a commercial CFD package developed by Concentration, Heat and Momentum Limited (CHAM), London, was used to solve the equations governing natural convection in liquid canned food during thermal sterilization. PHOENICS is a well-known CFD code. It is a computer code, which simulates fluid flow, heat transfer, chemical reactions, and related phenomena. It uses the finite volume method (FVM), which is one of several computational methods used for solving heat transfer and fluid flow problems. The details of this code and the various options and values of significant parameters are discussed in the PHOENICS Reference Manual.

For solving the equations governing natural convection, Nield and Bejan (1992), after examining a range of numerical techniques, concluded that the FVM is more appropriate than other methods of solution.

4.2. FINITE VOLUME METHOD AND PARTICULAR FEATURES OF PHOENICS

The FVM, which is also known as the finite domain method, is one of several computational methods for solving fluid flow among many other problems. The principle behind this numerical method is based on the control volume idea used in many fluid texts. This idea is applied on a cell basis and used to derive the conservation equations of mass, momentum, and energy from basic laws into a mathematical form known as finite volume equations (FVE).

In order to specify a problem, it is necessary to identify the computational domain, which totally covers the region of flow to be studied. The computational domain may contain some sections where there is no fluid flow since these may be blocked. The computational domain must then be subdivided into a number of divisions in the three dimensions (i.e. filled with NX $\times$ NY $\times$ NZ cells). In general, topologically Cartesian grids take three forms which are as follows:

a. *Strict Cartesian*
   A Cartesian grid is composed of cells formed by the intersection of three sets of mutually perpendicular parallel planes, on any one of which either x, y, or z is constant, these quantities being the distances in the three coordinate directions.
b. *Cylindrical (polar) grids*
   A cylindrical (polar) grid consists of cells formed by the intersection of
   - planes of constant z perpendicular to the axis of rotation
   - planes of constant x, which all pass through and thus intersect on that axis so that x now represents an angle in radius and not distance
   - concentric cylindrical surfaces of constant radial coordinate y
c. *Body-fitted coordinates (BFC)*
   A BFC is best imagined by supposing that a regular Cartesian grid is first embedded in a jellylike medium, which is then squeezed, bent, and twisted in an arbitrary way. All the cells in contact with another remain so.
   1. The position of each grid corner must be stored, which requires the storage of 3 $\times$ (NX + 1) $\times$ (NY + 1) $\times$ (NZ + 1) pieces of information, which represents the number of grids in the different direction values of I, J, and K for each corner in the cell.

2. The velocities are directed along lines joining cell nodes and are therefore perpendicular to the cell faces for strict Cartesian and cylindrical polar grids. In body-fitted grids, this is not necessarily true, and hence careful calculation of flows across faces is required.
3. In body-fitted grids, some form of a grid generation technique is required in order to specify the grid corner positions.

In cylindrical polar and body-fitted grids, the ideas behind the FVM are the same as those for strict Cartesian grids, but the mathematics is harder.

The FVM may treat time in a manner that is similar to that used for the other dimensions with a Cartesian grid. This means that the time dimension is subdivided into NT discrete time planes at which a solution is obtained. These may be spaced in any desired manner but should obviously be concentrated at times when the flow is changing rapidly, such as the fine mesh time steps used in our work at the beginning of heating. Three-dimensional notation will be discussed here for the geometry of the can and pouch being investigated in this book. Grid nomenclature used in PHOENICS is shown in Figure 4.2.

For the cell with its node at P, which adjoins cells with their nodes at E, W, N, S, H, and L (east, west, north, south, high, and low), the centers of the adjoining faces are e, w, n, s, h, and l having face areas of A_e, A_w, A_n, A_s, A_h, and A_l, respectively.

Most properties are stored as values at the cell nodes, while velocities are stored at the cell faces. This has computational advantages both in terms of stability and computational ease since the velocity related to flow across a face is specified at its center. This is done by assuming a staggered grid passing through the cell nodes and having the velocity at the face centers (e, w, n, s, h, and l), as shown in the dashed lines in Figure 4.3 for the XY plane.

In the course of defining the computational domain, the optimum meshing arrangement should be decided upon. The geometrical and time mesh subdivides the computational domain into small cells at which values of the medium properties, and solved variables, are stored (Mallinson, 1999).

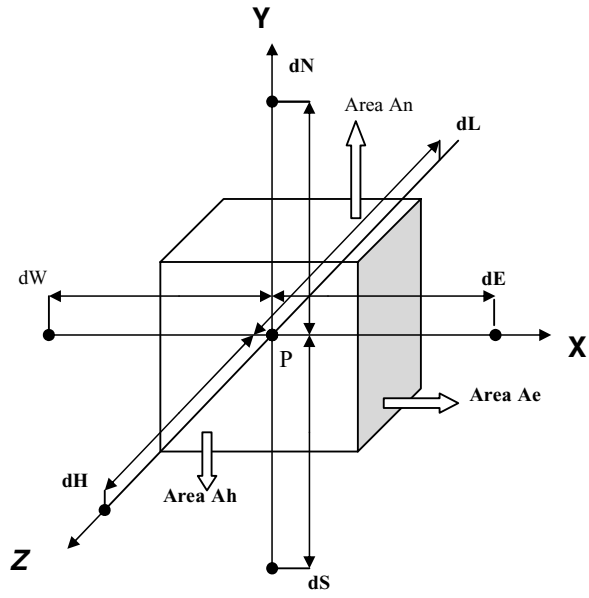

Figure 4.2. Cell nomenclature showing cell nodes and staggered grid.

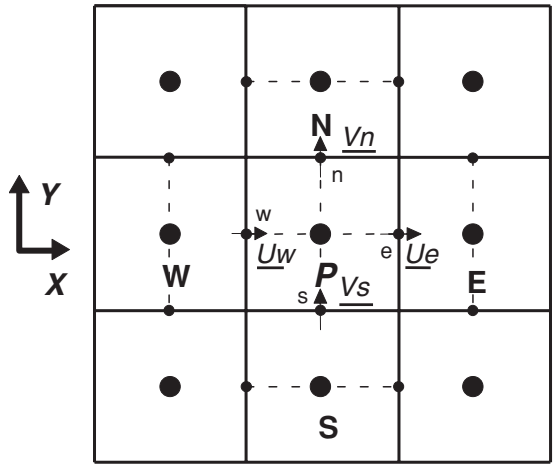

Figure 4.3. Cell nomenclature showing staggered grid.

Several meshing arrangements will be considered throughout this work. Most of the cases presented in this work were checked using both mesh types (uniform and nonuniform spacing) and for a different numbers of cells to prevent any discretization error and also to make sure that the results were consistent.

4.2.1. The Conservation Equations

In order to obtain a solution to a fluid flow problem, it is necessary to relate what is happening within one cell to that that is happening in its neighbours. This is achieved through the principles of conservation of mass, momentum, energy, etc. The basic principle of conservation as applied to a control volume is "The change in what is contained within a control volume must have come from or gone somewhere."

When deriving the conservation equation for cell P, the net change within the cell equals the net convection transfer plus the net diffusive transfer and any other sources. The transfer process is subdivided into three categories.

Convection:	The net amounts of a conserved property carried into or taken out of the control volume by the movement of fluid across the control surface (the cell faces)
Diffusion:	The transfer of a conserved property by diffusion
Other sources:	Sources from outside the solution domain as well as terms such as the pressure gradient–related source of momentum

The conservation equation for a control volume is therefore

$$\text{Net change within the control volume} = \text{Net convective transfer} + \text{Net diffusive transfer} + \text{Sources}$$

4.2.1.1. Conservation of Mass (Continuity)

In the software used in our work, we have only three components in the equation of conservation of mass:

1. The net change of mass in cell P during a time interval Δt is $\rho_P \forall_P - \rho_T \forall_T$, where subscript P denotes the present value and T denotes the previous value.
2. The net convective mass transfer through the faces of the cell is

$$(\rho_w A_w U_w - \rho_e A_e U_e + \rho_s A_s V_s - \rho_n A_n V_n + \rho_l A_l W_l - \rho_h A_h W_h)\,\delta t.$$

3. The net transfer from external sources, such as sources or sinks, is $m_{\text{source}}\delta t$.

Then the conservation of mass equation will be

$$\begin{aligned}\rho_P \forall_P &= \rho_T \forall_T + (\rho_w A_w U_w - \rho_e A_e U_e + \rho_s A_s V_s - \rho_n A_n V_n + \rho_l A_l W_l \\ &\quad - \rho_h A_h W_h + m_{\text{source}})\,\delta t \end{aligned} \tag{4.1}$$

4.2.1.2. Conservation of General Intensive Properties

For any general intensive property Φ (specific property used here for energy and concentration), the conservation equation can be written in a similar manner to equation (4.1):

1. The change of Φ in the cell is $\rho_P \forall_P \Phi_P - \rho_T \forall_T \Phi_T$.
2. The net convection is

$$(\rho_w A_w U_w \Phi_w - \rho_e A_e U_e \Phi_e + \rho_s A_s V_s \Phi_s - \rho_n A_n V_n \Phi_n + \rho_l A_l W_l \Phi_l - \rho_h A_h W_h \Phi_h)\,\delta t$$

3. The source of Φ associated with mass sources is $m_{\text{source}} \Phi_{\text{source}} \delta t$.
4. The other sources with no mass transfer is $\sum_f \text{CO}_f Tp_f (\text{Val}_f - \Phi_P)$.

The final term to be included is the diffusion term. In general the diffusion of Φ across any area A_f (f = e, w, n, s, h, or l) is equal to $\Gamma_f A_f \dfrac{\Phi_F - \Phi_P}{d_F} \delta t$.

If strong convection exists, the amount of diffusion is reducing. This is achieved by using

$$\text{Diffusion} = \langle 1 - D_f \rangle \Gamma_f A_f \frac{\Phi_F - \Phi_P}{d_F} \delta t$$

$$D_f = Dc\ ABS\left[\frac{\text{convection flux}}{\Gamma_f A_f / d_F}\right]$$

and where

$$D_f = Dc\ ABS\left[\frac{\text{convection flux}}{\Gamma_f A_f / d_F}\right]$$

Φ = specific property
CO = coefficient
d_F = the distance between nodes P and F (F = E, W, N, S, H, and L)
Dc = diffusion cut-off, which cuts the diffusion when convection becomes high
Tp = patch type multiplier (e.g., area or volume of the cell)
Val = value of Φ associated with the nonconvective source
$\forall$ = volume of the cell

δt = time interval
Γ = exchange coefficient = $\dfrac{\mu}{\mathrm{Pr}}$
Pr = Prandtl number = $\dfrac{\mu Cp}{k}$

Combining these five terms gives the full FVE (4.2):

$$\begin{aligned}\rho_{\mathrm{P}}\forall_{\mathrm{P}}\Phi_{\mathrm{P}} - \rho_{\mathrm{T}}\forall_{\mathrm{T}}\Phi_{\mathrm{T}} = (&\rho_{\mathrm{w}}A_{\mathrm{w}}U_{\mathrm{w}}\Phi_{\mathrm{w}} - \rho_{\mathrm{e}}A_{\mathrm{e}}U_{\mathrm{e}}\Phi_{\mathrm{e}} + \rho_{\mathrm{s}}A_{\mathrm{s}}V_{\mathrm{s}}\Phi_{\mathrm{s}} - \rho_{\mathrm{n}}A_{\mathrm{n}}V_{\mathrm{n}}\Phi_{\mathrm{n}}\\ &+ \rho_{\mathrm{l}}A_{\mathrm{l}}W_{\mathrm{l}}\Phi_{\mathrm{l}} - \rho_{\mathrm{h}}A_{\mathrm{h}}W_{\mathrm{h}}\Phi_{\mathrm{h}}\\ &+ \langle 1 - D_{\mathrm{w}}\rangle\Gamma_{\mathrm{w}}A_{\mathrm{w}}\left(\frac{\Phi_{\mathrm{W}} - \Phi_{\mathrm{P}}}{d_{\mathrm{W}}}\right) + \langle 1 - D_{\mathrm{e}}\rangle\Gamma_{\mathrm{e}}A_{\mathrm{e}}\left(\frac{\Phi_{\mathrm{E}} - \Phi_{\mathrm{P}}}{d_{\mathrm{E}}}\right)\\ &+ \langle 1 - D_{\mathrm{s}}\rangle\Gamma_{\mathrm{s}}A_{\mathrm{s}}\left(\frac{\Phi_{\mathrm{S}} - \Phi_{\mathrm{P}}}{d_{\mathrm{S}}}\right) + \langle 1 - D_{\mathrm{n}}\rangle\Gamma_{\mathrm{n}}A_{\mathrm{n}}\left(\frac{\Phi_{\mathrm{N}} - \Phi_{\mathrm{P}}}{d_{\mathrm{N}}}\right)\\ &+ \langle 1 - D_{\mathrm{l}}\rangle\Gamma_{\mathrm{l}}A_{\mathrm{l}}\left(\frac{\Phi_{\mathrm{L}} - \Phi_{\mathrm{P}}}{d_{\mathrm{L}}}\right) + \langle 1 - D_{\mathrm{h}}\rangle\Gamma_{\mathrm{h}}A_{\mathrm{h}}\left(\frac{\Phi_{\mathrm{H}} - \Phi_{\mathrm{P}}}{d_{\mathrm{H}}}\right)\\ &+ m_{\mathrm{source}}\Phi_{\mathrm{source}} + \mathrm{CO}Tp(\mathrm{Val} - \Phi_{\mathrm{P}})\delta t\end{aligned} \tag{4.2}$$

For the FVE to be solved in all the cells and for all the intensive properties, the coefficients of Φ_{P} must be coupled with all Φ_{F} at the nearby cells. This is performed by substituting Equation (4.1) into Equation (4.2) to eliminate $\rho_{\mathrm{P}}\forall_{\mathrm{P}}$ and then dividing by δt to get the FVE (4.3) of the form

$$\begin{aligned}0 = &\frac{\rho_{\mathrm{T}}\forall_{\mathrm{T}}}{\delta t}(\Phi_{\mathrm{T}} - \Phi_{\mathrm{P}})\\ &+ \rho_{\mathrm{w}}A_{\mathrm{w}}U_{\mathrm{w}}(\Phi_{\mathrm{w}} - \Phi_{\mathrm{P}}) - \rho_{\mathrm{e}}A_{\mathrm{e}}U_{\mathrm{e}}(\Phi_{\mathrm{e}} - \Phi_{\mathrm{P}})\\ &+ \rho_{\mathrm{s}}A_{\mathrm{s}}V_{\mathrm{s}}(\Phi_{\mathrm{s}} - \Phi_{\mathrm{P}}) - \rho_{\mathrm{n}}A_{\mathrm{n}}V_{\mathrm{n}}(\Phi_{\mathrm{n}} - \Phi_{\mathrm{P}})\\ &+ \rho_{\mathrm{l}}A_{\mathrm{l}}W_{\mathrm{l}}(\Phi_{\mathrm{l}} - \Phi_{\mathrm{P}}) - \rho_{\mathrm{h}}A_{\mathrm{h}}W_{\mathrm{h}}(\Phi_{\mathrm{h}} - \Phi_{\mathrm{P}})\\ &+ \langle 1 - D_{\mathrm{W}}\rangle\Gamma_{\mathrm{W}}A_{\mathrm{W}}\left(\frac{\Phi_{\mathrm{W}} - \Phi_{\mathrm{P}}}{d_{\mathrm{W}}}\right) + \langle 1 - D_{\mathrm{e}}\rangle\Gamma_{\mathrm{e}}A_{\mathrm{e}}\left(\frac{\Phi_{\mathrm{E}} - \Phi_{\mathrm{P}}}{d_{\mathrm{E}}}\right)\\ &+ \langle 1 - D_{\mathrm{s}}\rangle\Gamma_{\mathrm{s}}A_{\mathrm{s}}\left(\frac{\Phi_{\mathrm{S}} - \Phi_{\mathrm{P}}}{d_{\mathrm{S}}}\right) + \langle 1 - D_{\mathrm{n}}\rangle\Gamma_{\mathrm{n}}A_{\mathrm{n}}\left(\frac{\Phi_{\mathrm{N}} - \Phi_{\mathrm{P}}}{d_{\mathrm{N}}}\right)\\ &+ \langle 1 - D_{\mathrm{l}}\rangle\Gamma_{\mathrm{l}}A_{\mathrm{l}}\left(\frac{L_{\mathrm{L}} - \Phi_{\mathrm{P}}}{d_{\mathrm{L}}}\right) + \langle 1 - D_{\mathrm{h}}\rangle\Gamma_{\mathrm{h}}A_{\mathrm{h}}\left(\frac{\Phi_{\mathrm{H}} - \Phi_{\mathrm{P}}}{d_{\mathrm{H}}}\right)\\ &+ m_{\mathrm{source}}(\Phi_{\mathrm{source}} - \Phi_{\mathrm{P}}) + \mathrm{CO}Tp(\mathrm{Val} - \Phi_{\mathrm{P}})\end{aligned} \tag{4.3}$$

By normalizing the influence coefficients

$$a_{\mathrm{T}} = \frac{\rho_{\mathrm{T}}\forall_{\mathrm{T}}}{\delta t}$$

$$a_{\mathrm{F}} = \rho_{\mathrm{f}}A_{\mathrm{f}}\langle V_{\mathrm{f}}\rangle + \langle 1 - Dc_{\mathrm{f}}\rangle\frac{\Gamma_{\mathrm{f}}A_{\mathrm{f}}}{d_{\mathrm{F}}}$$

$$a_{\mathrm{P}} = a_{\mathrm{T}} + \sum_{\mathrm{F}} a_{\mathrm{F}} + m_{\mathrm{source}} + \mathrm{CO}Tp$$

where V_f is the velocity directed into the cell and F = W, E, S, N, L, and H, the FVE (4.3) becomes much simpler as follows:

$$a_P\Phi_P = a_T\Phi_T + \sum_F a_F\Phi_F + m_{source}\Phi_{source} + COTpVal$$

or

$$a_P\Phi_P = a_T\Phi_T + \sum_F a_F\Phi_F + b$$

4.2.1.3. Conservation of Momentum

The momentum equation is approximated in a manner similar to the mass and energy equations, except that the velocity is stored at the cell faces rather than the cell nodes, using the staggered grids (Figure 4.3) mentioned earlier. Simple mathematical interpolation must be carried out to obtain the values of fluxes and properties at these faces.

In addition to possible externally applied forces, the momentum equations also need a pressure-related source (generally automatically built into codes such as PHOENICS), for example for the V_s velocity, the momentum source for these terms has the form $A_s(P_P - P_S)$.

This is simple enough if the pressure is known, but so far we do not have an equation for the pressure. If the pressure is unknown, an additional equation of pressure (pressure correction equation) should be considered that affects all momentum equations and interlinks the three velocity components through the pressure.

To update the pressure, the momentum equations are solved using the in-store pressure field P^*. Then we can compute the error in the conservation Equation (4.1) as a rate of gaining or losing mass as follows:

$$\begin{aligned} R_{\dot{m}} &= \frac{\rho_P\forall_P - \rho_T\forall_T}{\delta t} \\ &\quad - (\rho_w A_w U_w - \rho_e A_e U_e + \rho_s A_s V_s - \rho_n A_n V_n + \rho_l A_l W_l - \rho_h A_h W_h) - \dot{m}_{source} \end{aligned}$$

If $R_{\dot{m}} > 0$ then the cell is gaining mass and the pressure needs to increase to counteract the flow and drive it out of the cell. If the cell is losing mass, $R_{\dot{m}} < 0$, dropping the pressure will induce mass inflow. The net change in the rate of gaining or losing mass induced by modifying the pressure field is calculated from

$$\begin{aligned} \Delta\dot{m} &= \rho_W A_W \frac{\partial U_W}{\partial(P_W - P_P)}\left(P'_W - P'_P\right) - \rho_e A_e \frac{\partial U_e}{\partial(P_P - P_E)}\left(P'_P - P'_E\right) \\ &\quad + \rho_s A_s \frac{\partial V_s}{\partial(P_S - P_P)}\left(P'_S - P'_P\right) - \rho_n A_n \frac{\partial V_n}{\partial(P_P - P_N)}\left(P'_P - P'_N\right) \\ &\quad + \rho_l A_l \frac{\partial W_l}{\partial(P_L - P_P)}\left(P'_L - P'_P\right) - \rho_h A_h \frac{\partial W_h}{\partial(P_P - P_H)}\left(P'_P - P'_H\right) \end{aligned}$$

Note that

$$P = P^* + P'$$

where P^* is the current in-store value of the pressure (from the previous sweep) and P' is the correction needed to obtain the new pressure (P).

The partial derivatives are obtained from the momentum equation corresponding to each velocity. For example the FVE for velocity component V_s is as follows:

$$a_{PV} V_s = A_s (P_P - P_S) + \text{Other terms}$$

so that $\frac{\partial V_s}{\partial (P_P - P_S)} = \frac{A_s}{a_{PV}}$.

By normalizing the influence coefficients similar to the energy and continuity equations, we can find a correction equation for P':

$$a_P P'_P = a_W P'_W + a_E P'_E + a_S P'_S + a_N P'_N + a_L P'_L + a_H P'_H + R_{\dot{m}} \tag{4.4}$$

This equation will be solved along with Equations (4.1) and (4.2).

Having obtained the pressure correction P', there are associated velocity corrections such as

$$V_s^{'} = \frac{A_s}{a_{PV}} (P_P^{'} - P_S^{'}) \tag{4.5}$$

which should be added to the velocities.

The normalized form of all the conservation equations can be solved explicitly by using a Jacobi point-by-point solver. PHOENICS has available a Jacobi point-by-point solver, which is not generally used, but it is useful when coefficients change greatly from "sweep to sweep." This method is easy to program but is generally slow to converge and may diverge. Alternatively, the most frequently used solution in PHOENICS is the slab-wise simultaneous solver, which is fully implicit. The slab-wise solution is one of the particular features of this code. In this technique a constant Z slab is solved simultaneously, while the off-slab values are treated as temporarily known (Richards, 1998). For example, consider the situation where conditions are specified at any one time for all blocks. For a particular horizontal row i, this solution method is solved by using old values for the rows $i + 1$ and $i - 1$ immediately above and below. When the solution moves to deal with row $i + 1$, the values used for row i are the old values not the new ones. When all rows are completed all old values are replaced with new ones and another "sweep" through the rows is undertaken.

4.2.2. The Transport Equations and Related Physics

The flow of any fluid can be described using transport equations that define the conservation of mass (continuity), momentum, and energy. They are derived by considering mass, momentum, and energy balances in an element of fluid as it flows. From these the appropriate partial differential equations are derived. These balances and equations are discussed in more detail by Bird et al. (1960). The transport equations are completed by adding two algebraic equations from thermodynamics, which are the equation of state and the constitutive equation.

4.2.2.1. Equation of State

The equation of state relates the density of a fluid to its thermodynamic state (temperature and pressure). A commonly used assumption for buoyancy problems is the Boussinesq approximation (Quarini, 1995). All fluid properties are assumed to be constant except for the density. The equation

of state (Boussinesq approximation) can be written as follows:

$$\rho = \rho_{\text{ref}}[1 - \beta(T - T_{\text{ref}})] \tag{4.6}$$

where β is the thermal expansion coefficient of the liquid, and T_{ref} and ρ_{ref} are the temperature and density at reference condition.

4.2.2.2. Constitutive Equation

The constitutive equation relates the static enthalpy of a fluid to its thermodynamic state. A discussion of such relationships can be found in any standard thermodynamics textbook such as that by Smith and Van Ness (1975).

4.2.2.3. Body Force

The body force (B) depends on the type of flow. For the Boussinesq buoyancy approximation, the body force becomes $B = \rho g$. Other body forces could include rotation forces, electrostatic forces, and resistances, such as those imposed on a fluid as it flows through a porous medium.

4.2.2.4. Turbulence

The transport equations presented can be applied to both laminar and turbulent flow conditions. Where turbulent flow conditions prevail, a suitable turbulence model is required to describe the turbulence and its influence on flow conditions. Several turbulence models are available in PHOENICS that attempt to solve the time-dependent nature of turbulence flow. The inclusion of turbulence in a CFD problem makes its solution more complex because turbulence modeling is difficult.

4.2.2.5. Non-Newtonian Fluid Behavior

When considering the flow of food products, it is often necessary to take the rheological nature of food into account because this will dictate its flow behavior. Most foods exhibit some form of non-Newtonian behavior, and many different fluid models have been used to describe such behavior (Holdsworth, 1993).

NOMENCLATURE

a	normalized influence coefficient
b	source and sink term
CO	coefficient
d_{F}	distance between nodes P and F (F = S, N, L, and H).
Dc	diffusion cut-off
P^*	current in-store pressure
P'	the correction needed to obtain the new pressure
R_m	rate of gaining or losing mass
Tp	patch type multiplier (e.g., area or volume of the cell)
V	velocity in the horizontal direction (y-direction)
Val	value
W	velocity in the vertical direction (z-direction)

Greek Symbols

δ_t time interval
Φ specific property
$\forall$ volume of the cell
Γ exchange coefficient $= \frac{\mu}{\mathrm{Pr}}$

Subscripts

F S, N, L, and H for the adjoining cell in the mesh
f s, n, l, and h for the adjoining faces in the mesh
H high cell
h high face
L low cell
l low face
N north cell
n north face
P present best-known value
S south cell
s south face
source external source term
T past best-known value
o initial state

REFERENCES

Bird, R.B., Stewart, W.S., & Lightfoot, E.N. (1960). *Transport phenomena*. New York: John Wiley & Sons.

Hatton, A.P., & Carpenter, C. (1976). *Sixth thermodynamics and fluid mechanics convention* (Institution of Mechanical Engineers, pp 81–89). London and New York: Mechanical Engineering Publication.

Holdsworth, S.D. (1993). Rheological model used in the prediction of the flow properties of food products. A literature Review. *Transaction of Institute of Chemical Engineers, 71*(C4), 139–179.

Mallinson, G.D. (1999). Computational fluid dynamics lecture notes. Department of Mechanical Engineering, University of Auckland.

Nield, D.A., & Bejan, A. (1992). *Convection in porous media*. New York: Springer-Verlag.

PHOENICS Reference Manual, Part A: PIL. TR 200 A, Bakery House, London SW 19 5AU, U.K: CHAM.

Quarini, G.L. (1995). Application of computational fluid dynamics in food and beverage production. *Journal of Food Science Technology Today, 4*, 234–236.

Richards, P.J. (1998). Computational fluid dynamics lecture notes. Department of Mechanical Engineering, University of Auckland.

Scott, G.M. (1994). Computational fluid dynamics for the food industry. *Journal of Food Technology International Europe,* 49–51.

Scott, G.M., & Richardson, P. (1997). The application of computational fluid dynamics in the food industry. *Trends in Food Science & Technology, 8*, 119–124.

Smith, J.M., & Van Ness, H.C. (1975). *Introduction to chemical engineering thermodynamic*. McGraw-Hill International.

CHAPTER 5

THERMAL STERILIZATION OF FOOD IN CANS

5.1. INTRODUCTION TO THE THEORETICAL ANALYSIS OF THERMAL STERILIZATION OF FOOD IN CANS

In this chapter, sterilization of canned liquid food in a two-dimensional (2-D) can sitting in an upright position and a three-dimensional (3-D) can lying horizontally were analyzed using computational fluid dynamics (CFD). In all the simulations, saturated steam at 121°C was assumed as the heating medium, except in Section 5.4 where the effect of sterilization temperature was studied. The different liquid foods studied were assumed to have a constant specific heat, thermal conductivity, and volume expansion coefficient, while the viscosity was taken as a function of temperature. Density variations were governed by the Boussinesq approximation (a commonly used assumption for buoyancy problems whereby the density variations are not explicitly modeled, but their effect is represented by a buoyancy force, which is proportion to the temperature variation). The CFD code PHOENICS was used, which is based on the finite volume method (FVM) of solution, as developed by Patankar and Spalding (1972). The results of the simulations were presented in the form of transient temperature, velocity, bacteria, and vitamin concentration profiles. The shape of the slowest heating zone (SHZ) during natural convection heating of canned liquid foods was also simulated and studied in all cases.

5.2. SIMULATIONS OF HIGH- AND LOW-VISCOSITY LIQUID FOOD

In this section, sterilization of canned liquid food in a metal can sitting in an upright position and heated at 121°C from all sides is presented. Sodium carboxyl methyl cellulose (CMC) and water were used as the model liquids having high and low viscosities respectively. The objective was to study the effect of natural convection currents on the movement of the SHZ in a can filled with different liquid food models (high and low viscosity).

5.2.1. Basic Model Equations and Solution Procedure

The computations were performed for a can with a radius of 40.5 mm and height of 111.0 mm for the viscous liquid, similar to that used in the study of Kumar and Bhattacharya (1991). For water, a can with a radius of 42 mm and height of 107 mm was used, similar to that used in the study of Datta and Tiexiera (1988). The choices of the can dimensions were purely for the purpose of comparison. The can outer surface temperature (top, bottom, and side) was assumed to rise instantaneously and to be maintained at 121°C throughout the heating period.

5.2.1.1. Computational Grid

The boundary layer adjacent to the heated walls and its thickness is one of the very important parameters affecting the numerical convergence of the solution of the governing equations (Equations (5.1)–(5.4)). Temperature and velocities have their largest variations in this region. To adequately resolve this boundary layer flow, i.e., to keep discretization error small, the mesh should be optimized, and a large concentration of grid points is needed in this region. If the boundary layer is not resolved adequately, the underlying physics of the flow is lost, and the simulation will be less accurate. On the other hand, in the rest of the domain where the variations in the temperature and velocity are small, the use of a fine mesh will lead to increases in the computation time without any significant increase in accuracy. Thus a nonuniform grid system is needed to resolve the physics of the flow properly.

A nonuniform grid system was used in the simulations with 3,519 cells: 69 in the axial direction and 51 in the radial direction (Figure 5.1), graded in both directions with a finer grid near the wall. The natural convection heating of CMC in the can was simulated for 2,574 s. It took 100 steps to

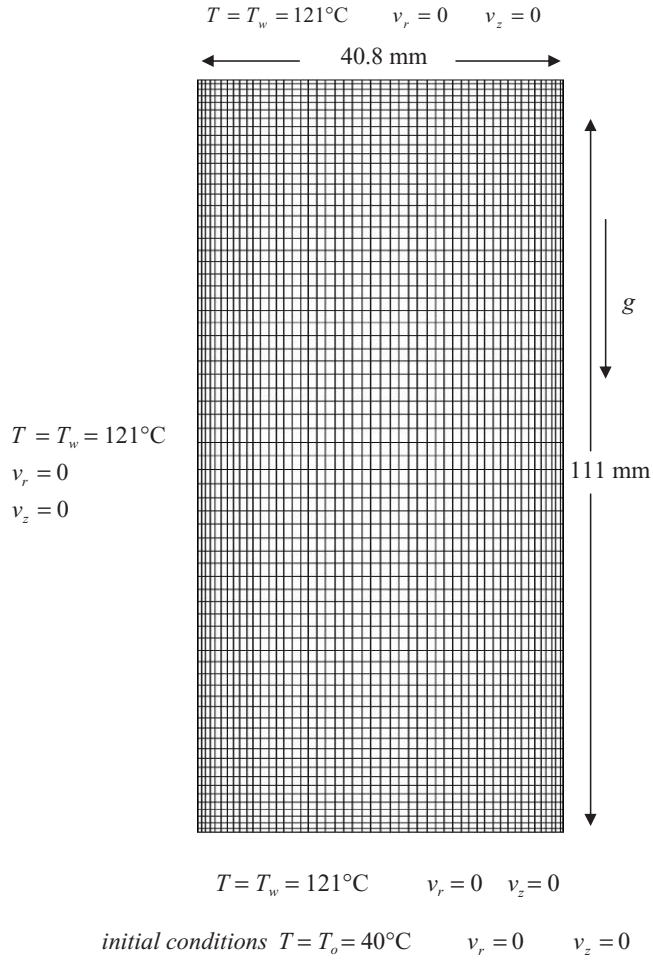

Figure 5.1. Grid mesh used in the simulations with 3,519 cells: 69 in the axial direction and 51 in the radial direction (the mesh is for a full can).

achieve the first 180 s of heating, another 100 steps for the next 820 s, and 100 steps for the remaining 1,574 s (Appendix A). In the simulation of a can containing water as a model liquid food, the natural convection heating was simulated for 1,800 s only, which was divided into 300 time steps. The time interval was increased progressively with heating; it took 100 steps to achieve the first 200 s of heating, another 100 steps for the next 400 s, and 100 steps for the remaining 1,200 s. This required 63 h and 18 h respectively of CPU time on the UNIX IBM RS6000 workstations at the University of Auckland, New Zealand.

To test the effect of mesh size on convergence, transient heating of a Newtonian fluid with temperature-dependent viscosity in a can at constant wall temperature (121°C) was simulated using a finer mesh. The use of a finer mesh of more than 3,519 cells showed no significant difference in the calculated temperature distribution in the can. For all cases analyzed in this chapter, solutions have been obtained using a variety of grid sizes and time steps, and the results showed that the solutions are time-step-independent and weakly dependent on grid variation.

5.2.1.2. Governing Equations and Boundary Conditions

The partial differential equations (PDEs) governing natural convection motion in cylindrical space are the Navier–Stokes equations in cylindrical coordinates (Bird et al., 1976).

Continuity equation:

$$\frac{1}{r}\frac{\partial}{\partial r}(r\rho v_r) + \frac{\partial}{\partial z}(\rho v_z) = 0 \tag{5.1}$$

Energy conservation:

$$\frac{\partial T}{\partial t} + v_r\frac{\partial T}{\partial r} + v_z\frac{\partial T}{\partial z} = \frac{k}{\rho C_\mathrm{p}}\left[\frac{1}{r}\frac{\partial}{\partial r}\left(r\frac{\partial T}{\partial r}\right) + \frac{\partial^2 T}{\partial z^2}\right] \tag{5.2}$$

Momentum equation in the vertical direction:

$$\rho\left(\frac{\partial v_z}{\partial t} + v_r\frac{\partial v_z}{\partial r} + v_z\frac{\partial v_z}{\partial z}\right) = -\frac{\partial p}{\partial z} + \mu\left[\frac{1}{r}\frac{\partial}{\partial r}\left(r\frac{\partial v_z}{\partial r}\right) + \frac{\partial^2 v_z}{\partial z^2}\right] + \rho g \tag{5.3}$$

Momentum equation in the radial direction:

$$\rho\left(\frac{\partial v_r}{\partial t} + v_r\frac{\partial v_r}{\partial r} + v_z\frac{\partial v_r}{\partial z}\right) = -\frac{\partial p}{\partial r} + \mu\left[\frac{\partial}{\partial r}\left(\frac{1}{r}\frac{\partial}{\partial r}(rv_r)\right) + \frac{\partial^2 v_r}{\partial z^2}\right] \tag{5.4}$$

The same set of governing equations describes a wide variety of flow situations in liquids and gases.

The *boundary conditions* used were as follows:

At the can boundary, $r = R$,

$$T = T_\mathrm{w}, \qquad v_r = 0, \qquad v_z = 0, \quad \text{for } 0 \le z \le H \tag{5.5}$$

At the bottom of the can, $z = 0$,

$$T = T_\mathrm{w}, \qquad v_r = 0, \qquad v_z = 0, \quad \text{for } 0 \le r \le R \tag{5.6}$$

At symmetry, $r = 0$,

$$\frac{\partial T}{\partial r} = 0, \qquad v_r = 0, \qquad \frac{\partial v_z}{\partial r} = 0, \qquad \text{for } 0 \le z \le H \tag{5.7}$$

At the top of the can, $z = H$,

$$T = T_{\mathrm{w}}, \qquad v_r = 0, \quad v_z = 0, \qquad \text{for } 0 \le r \le R \tag{5.8}$$

Initially the fluid is at rest and is at a uniform temperature:

$$T = T_{\mathrm{ref}} = 40^{\circ}\mathrm{C}, \qquad v_r = 0, \qquad v_z = 0 \quad \text{at } 0 \le r \le R, \qquad 0 \le z \le H \tag{5.9}$$

The boundary and the initial conditions are the most important parameters that specify the desired solution. To obtain satisfactory convergence of the numerical solution to these governing PDEs, it is necessary to apply a proper underrelaxation or overrelaxation. The improper use of the overrelaxation or underrelaxation parameter can easily make the computations impracticably long. Many of these optimum parameters are not known initially and can only be found through numerical experimentation. Different values of underrelaxation were also used to keep the computation stable.

5.2.1.3. Physical Properties

In the simulation of water and CMC, the viscosity was assumed a function of temperature. A second-order polynomial of the form shown in Equation (5.10) was used in the PHOENICS program.

$$\mu = a + bT + cT^2 \tag{5.10}$$

In the literature, the viscosity is usually expressed in exponential form; PHOENICS requires the expression to be in a polynomial form. In the simulation of water, values of a, b, and c were 1.6×10^{-3} Pa s, -2.988×10^{-5} Pa s K^{-1}, and 7.8×10^{-8} Pa s K^{-2}. These values were obtained from the curve fitting of viscosity versus temperature available in the literature (Holman, 1992).

Food materials are in general non-Newtonian, and hence the viscosity is a function of shear rate and temperature, with a flow behavior index typically less than one. Sodium CMC suspended in water was used as the model liquid food. Due to the high viscosity of CMC, which causes liquid velocities to be very low, the shear rate calculated in this work was found to be of the order of 0.01 s^{-1}, which was in agreement with values reported by Kumar and Bhattacharya (1991). Because of the low shear rate the viscosity may be assumed independent of shear rate, and the fluid will behave as Newtonian fluid. This Newtonian approximation is valid for most liquid food materials, such as tomato puree, carrot puree, green bean puree, apple sauce, apricot puree, and banana puree, whenever the shear rate is small, which is true for all cases of natural convection heating of viscous liquid foods (Steffe et al., 1986).

Kumar and Bhattacharya (1991) used the following viscosity model in their simulation work:

$$\mu = \eta_0 \gamma^{n-1} \exp\left(\frac{nE}{R_{\mathrm{g}} T}\right) \tag{5.11}$$

Equation (5.11) with the constants given in Table 5.1 was used to calculate the values of viscosity of CMC at different temperatures. This was done to maintain the same values of viscosity that was

Table 5.1. Properties of the liquid food (CMC) measured at room temperature used in the simulation (Kumar and Bhattacharya, 1991).

Property	Value
Density (ρ)	950 kg m^{-3}
Specific heat (C_p)	4100 J kg^{-1} K^{-1}
Thermal conductivity (k)	0.7 W m^{-1} K^{-1}
Volumetric expansion coefficient (β)	2×10^{-4} K^{-1}
Flow behavior index (n)	0.57
Consistency index (η_0)	2.23×10^{-3} Pa s^n
Activation energy (E)	3.08×10^4 kJ $(kg\ mol)^{-1}$

used by Kumar and Bhattacharya for the purpose of comparison. These values were correlated in a second-order polynomial of the form similar to that for water, with a, b, and c having the values of 4.135 Pa s, -6.219×10^{-2} Pa s K^{-1}, and 2.596×10^{-4} Pa s K^{-2}.

The variation of the density with temperature is usually expressed (Adrian, 1993) as

$$\rho = \rho_{ref}[1 - \beta(T - T_{ref})] \tag{5.12}$$

where β is the thermal expansion coefficient of the liquid, and T_{ref} and ρ_{ref} are the temperature and density at the reference condition. The density was assumed constant in the governing equations except in the buoyancy term (Boussinesq approximation), where Equation (5.12) was used to describe its variation with temperature.

For viscous liquids, the viscous forces are high, and thus the Grashof number (Gr) is low. This can be shown clearly for CMC at which the Grashof number is in the range 10^{-2}–10^{-1} (using maximum temperature difference) as compared to water in which the Grashof number is in the range of 10^9–10^{10}. The magnitude of the Grashof number gives a good indication whether the natural convection flow is laminar, transitional, or turbulent.

5.2.1.4. Assumptions Used in the Numerical Simulation

To simplify the problem, the following assumptions were made:

1. Axisymmetric geometry, which reduces the problem from 3-D to 2-D.
2. Heat generation due to viscous dissipation is negligible; this is due to the use of high-viscosity liquid with very low velocities (Mills, 1995).
3. Boussinesq approximation is valid.
4. Specific heat (C_p), thermal conductivity (k), and volume expansion coefficient (β) are constants (Table 5.1).
5. No-slip condition is present at the inside wall of the can.
6. The condensing steam maintains a constant temperature condition at the can outer surface.
7. The thermal boundary conditions are applied to liquid boundaries rather than to the outer boundaries of the can because of the low thermal resistance of the can wall.
8. The fluid is non-Newtonian; however due to the low shear rate, it is approximated as a Newtonian fluid for CMC.

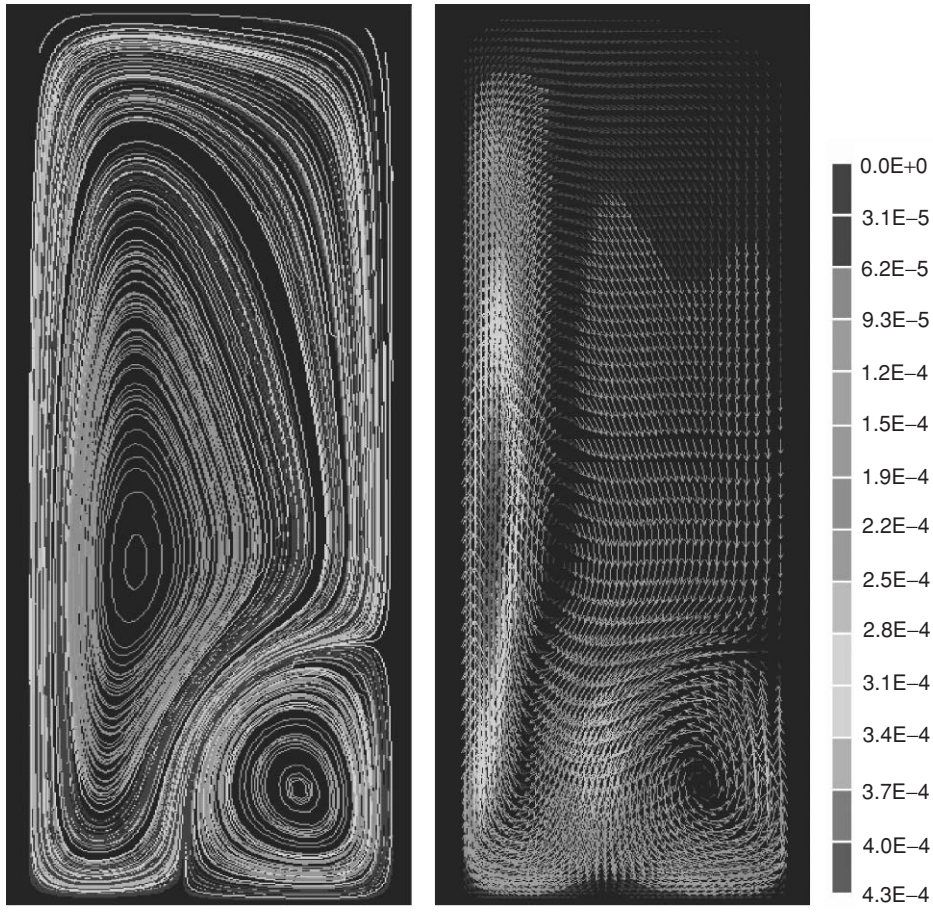

Figure 5.2. Velocity vector profile (m s^{-1}) and flow pattern of CMC in a cylindrical can heated by condensing steam after 1157 s. The right-hand side of each figure is the centerline.

5.2.2. Results of Simulation

5.2.2.1. Flow Pattern

Figures 5.2 and 5.3 show the velocity vector and the flow pattern of CMC and water in a can heated by steam condensing along its outside surface. Both figures show that the liquid adjacent to the wall, top, and bottom surfaces will receive heat from the condensing steam. As the liquid is heated, it expands and thus gets lighter. Liquid away from the sidewall stays at a much lower temperature. The buoyancy force created by the change in liquid density due to temperature variation (from the wall to the core) produces an upward flow near the sidewall. The hot liquid going up is deflected by the top wall and then travels radially toward the core. Being heavier, the liquid moves downward and then, toward the wall. Thus a recirculation flow is created (Figures 5.2 and 5.3).

These figures also show that the liquid at the wall is at rest because of the no-slip boundary conditions. For CMC, the magnitude of the maximum axial velocity at mid height near the can wall was 0.31 mm s^{-1} at $t = 1{,}157$ s, which was in good agreement with the results of Kumar and Bhattacharya (1991), who used the same viscous liquid (CMC) and the same heating conditions.

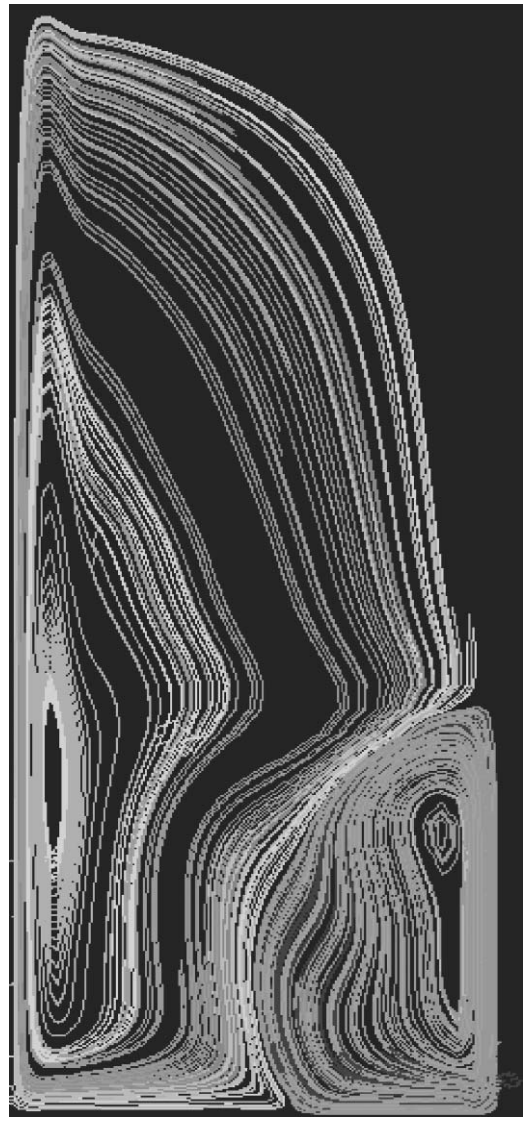

Figure 5.3. Flow patterns of water in a cylindrical can after 180 s of heating. The right-hand side of the figure is the centerline.

The velocity profiles of water contained in a can and heated under similar conditions have also been obtained. Typical velocities were 40 mm s^{-1} and 19 mm s^{-1} after 30 s and 240 s of heating respectively. This can be explained in terms of the Grashof number, which represents the ratio of the buoyancy force to viscous force. Because of these high velocities, the coldest region in the can filled with water reached 99°C after only 120 s of heating compared to 1,700 s for CMC. As heating progressed, a more uniform velocity was obtained, reducing buoyancy force in the liquid that led to a significant reduction in the velocity. The difference in the magnitude of the calculated velocities of water and the more viscous liquid (CMC) is expected due to the large difference in the viscosity of the two liquids.

Hiddink (1975) reported that for viscous fluids, the thickness of the ascending liquid region near the wall, which is the distance between the location of the stagnant region and the wall, was greater than that for water. This was attributed to the large difference in the values of viscosity of the two fluids. The reported thickness was 12–14 mm for the viscous liquid as compared to 6–7 mm for water. Kumar and Bhattacharya (1991) reported a thickness of 15–16 mm for the ascending CMC. Figure 5.2 shows that the thickness of the ascending viscous liquid (CMC) is in the range of 16–20 mm.

Datta and Teixeira (1987) reported the formation of a secondary flow (or eddies formation) at the bottom of the can near the centerline. The simulation done by Kumar and Bhattacharya (1991) for a viscous liquid (CMC) did not show any formation of secondary flow or eddies; however in our simulation, the secondary flow was evident in all the cases studied, which is expected whenever there is heating from the bottom. Figures 5.2 and 5.3 for both CMC and water show clear secondary flow formation at the bottom of the can.

5.2.2.2. Slowest Heating Zone and Temperature Profile

The temperature distribution during heating is presented in the form of isotherms in Figures 5.4 and 5.5 for CMC and water respectively and for different periods of heating. For CMC, the isotherms at $t = 54$ s are almost identical to those found in pure conduction heating, but over time, the isotherms are seen to be strongly influenced by convection. However for water, Figure 5.5 shows a strong influence of natural convection, even at the early stages of heating. After a short period of heating, the fluid near the bottom is heated by conduction only. However, instability results from the large difference between the can bottom temperature and the colder liquid coming in contact with the can bottom. This instability gives rise to bursts of convective cells (Benard convection cells). Figure 5.5 for water shows the irregular shape of the isotherms near the can bottom, which is caused by the random nature of Benard convective cell formations.

The SHZ in the can (i.e., the location of the lowest temperature at a given time) is not a stationary region in the liquid undergoing convection heating. Its location is not at the geometric center of the can, as it is in the case of conduction heating. Initially the content of the can is at uniform temperature. As heating begins, the mode of heat transfer changes from conduction to convection, and the SHZ moves from the geometric center to the heel of the can, as shown in Figure 5.4 for CMC. Figure 5.5 for water shows that the SHZ is not at the center of the can even during the initial period of heating. As heating progresses, the SHZ is pushed more toward the bottom of the can, as with CMC. It appears that the SHZ keeps moving during heating and eventually stays in a region that is about 10–15% of the can height from the bottom in both cases.

Figure 5.4 show that for CMC the SHZ develops a peculiar shape after only a short period of heating. The SHZ does not cover the whole bottom section of the can. However, for water, the SHZ fills the whole bottom section of the can, as shown in Figure 5.5. The temperature of the SHZ reaches about 100°C in 1,800 s in comparison to 150 s for water. Traditionally, the movement of the SHZ is a critical parameter in thermal process designs. Zechman and Pflug (1989) reported a location of the SHZ at about 10% of the height from the bottom, whereas Datta and Teixeira (1987) found it to migrate to slightly higher locations (15% from the bottom). These observations are in agreement with those found in our work and also with those reported by Kumar and Bhattacharya (1991). Our simulation shows for the first time the effect of secondary flow on the shape of the SHZ. The effect is to push the SHZ toward the wall, as is clearly seen in Figure 5.4 for CMC. According to this finding, careful consideration must be made in representing the coldest point by the measured temperature at the axis of the can, particularly at extreme locations close to the top and bottom (Figures 5.4 and 5.5).

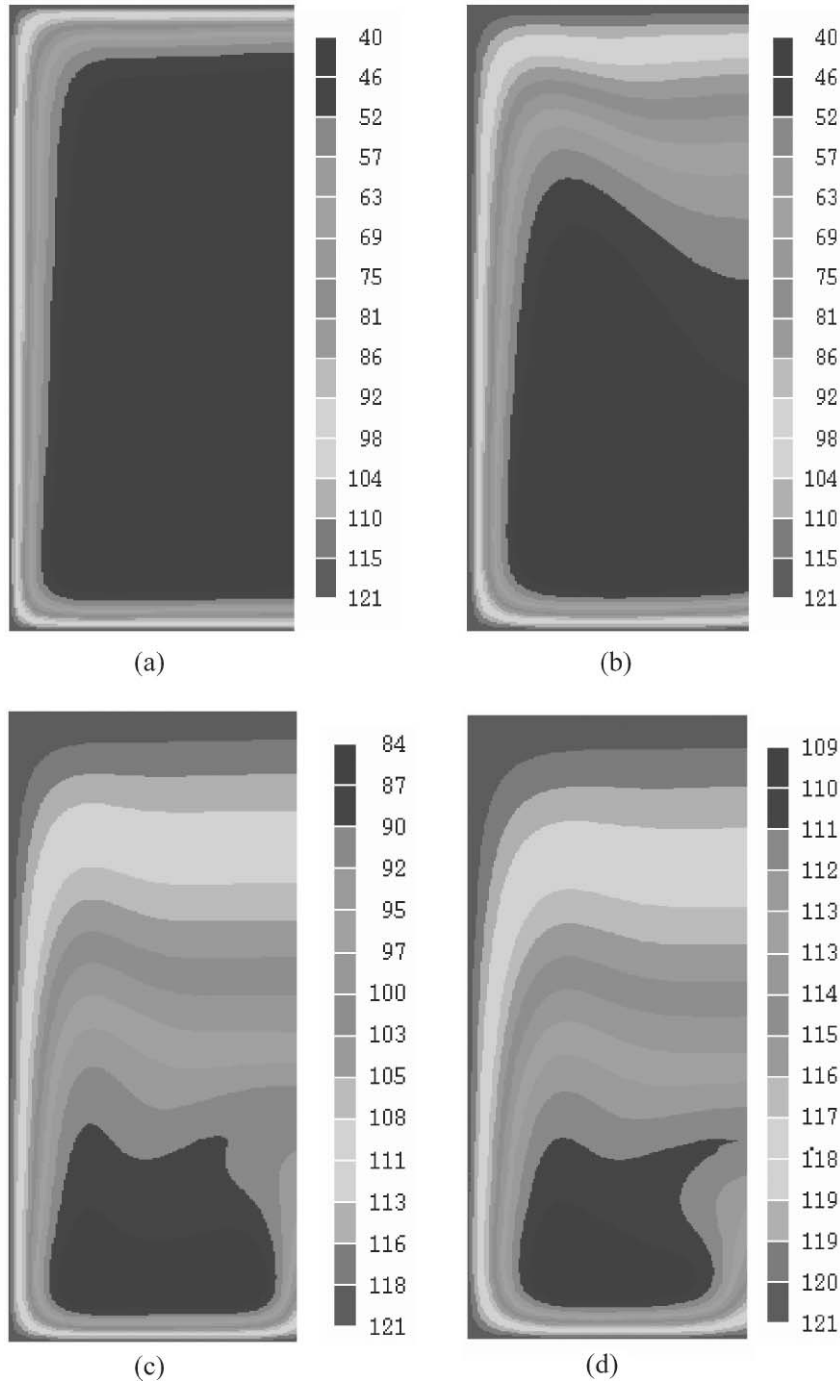

Figure 5.4. Temperature profiles in a can filled with CMC and heated by condensing steam after periods of (a) 54 s, (b) 180 s, (c) 1,157 s, and (d) 2,574 s. The right-hand side of each figure is the centerline.

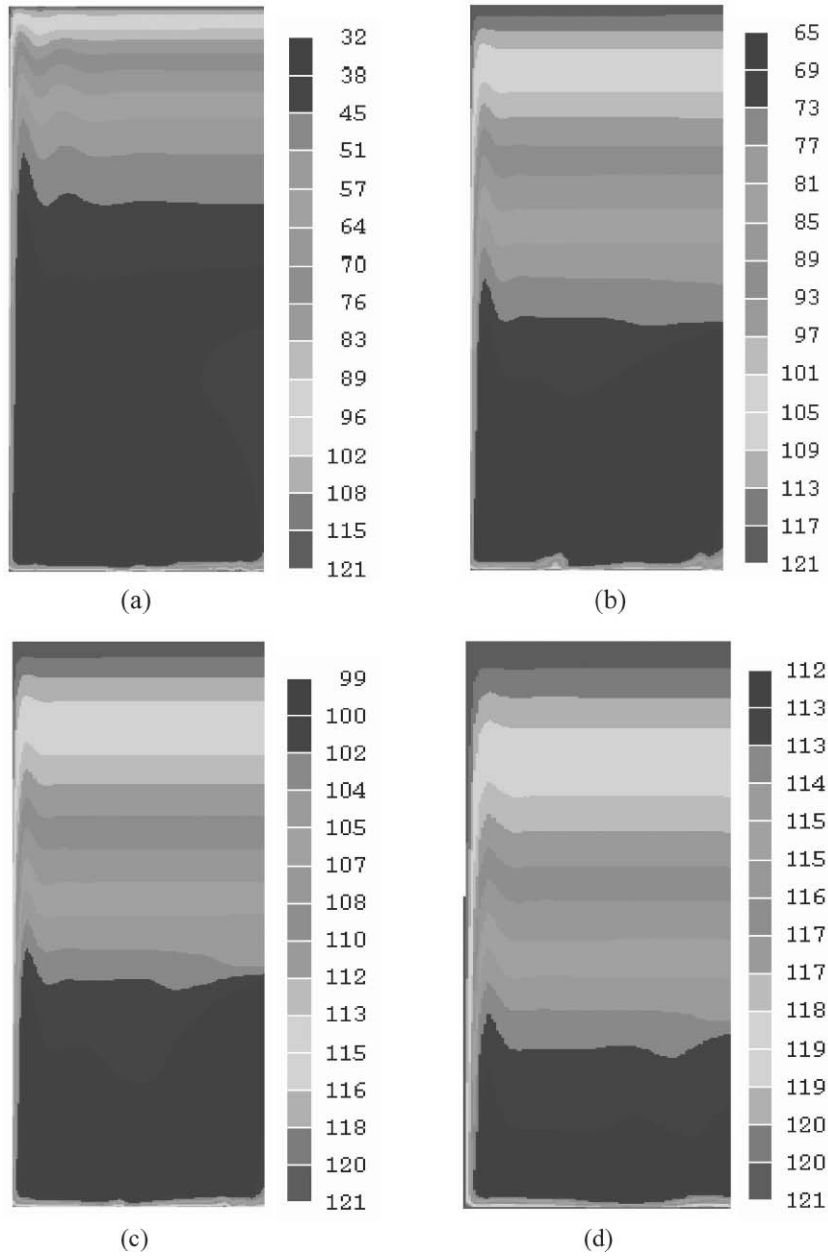

Figure 5.5. Temperature profiles in a can filled with water and heated by condensing steam after periods of (a) 20 s, (b) 60 s, (c) 120 s, and (d) 180 s. The right-hand side of each figure is centerline.

Figure 5.6 shows for water the change of temperature of the SHZ with heating time as predicted by the simulation based on both constant viscosity (measured at the film temperature) and temperature-dependent viscosity. This figure also includes the data obtained from the simulation reported by Datta and Teixeira (1987), based on constant viscosity. The result of our simulation, based on constant viscosity, is in good agreement with that of Datta and Teixeira. When the viscosity is

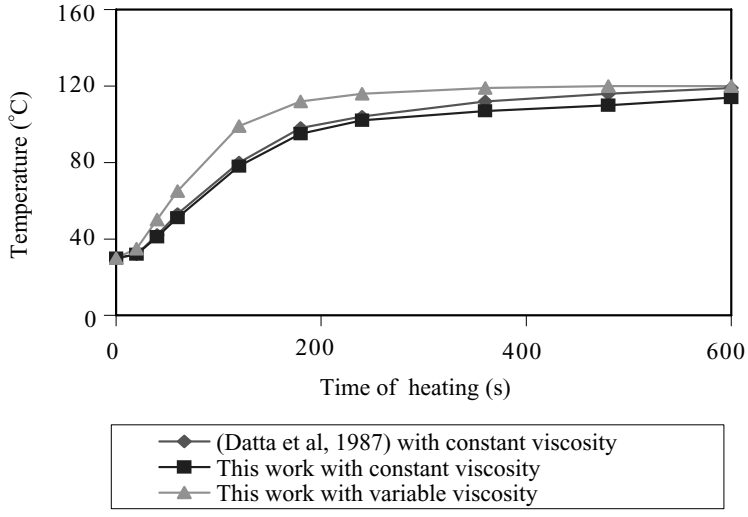

Figure 5.6. Transient temperature of water at the SHZ in a cylindrical can after 600 s of heating.

taken as a function of temperature, a much faster heating rate is observed, *illustrating the importance of taking into account the variation of viscosity with temperature, which has not been considered in previous simulations made reported in the literatures for water as a liquid food.* Similar observation may be deduced from Figure 5.7 for the temperature at the midpoint location in the can. The temperature at the geometric center of the can (Figure 5.7) is always higher than that at the SHZ (Figure 5.6), which supports the important practice of measuring the temperature at locations lower than the geometric center of the can. However, locating such a transient position experimentally is a very difficult task, leading to no choice other than following the moving location via computer simulations.

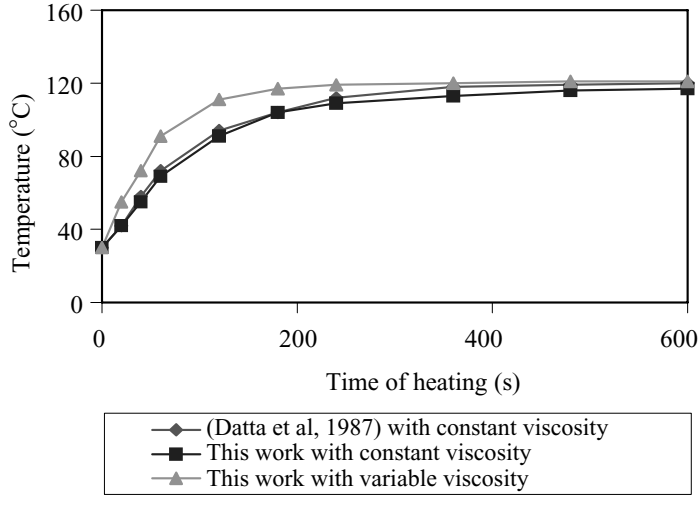

Figure 5.7. Transient temperature of water at the geometric center of the can after 600 s of heating.

5.3. TOP INSULATED CAN

In this section, the effect of the presence of an air gap (i.e., head space) at the top of the can on the heat transfer rate will be presented. This is important since it represents a real, practical situation.

The governing equations, physical properties, size of the can, and assumptions used to simplify the problem are the same as those used in the previous case. The boundary conditions used are the same as those used in Section 5.2.1.3 except for the top of the can, which is assumed insulated, as shown in Equation 5.13.

At the top of the can, $z = H$, which is assumed insulated (i.e., with an air gap):

$$\frac{\partial T}{\partial z} = 0, \qquad v_r = 0, \qquad v_z = 0 \quad \text{at } z = H(\text{can top}), \qquad 0 \le r \le R \tag{5.13}$$

The assumption of top insulation is used to represent the case of a can with a head space, which is the common situation for canned foods.

5.3.1. Results of Simulation

Figure 5.8 shows the velocity vector in a can filled with CMC and heated at 121°C from the bottom and sides only (i.e., top insulated) after 1,157 s. The velocity vector field shown in Figure 5.2 (for a

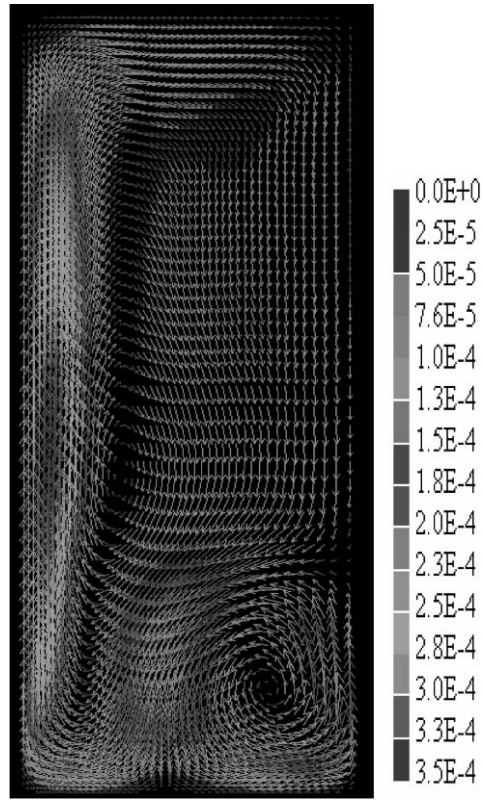

Figure 5.8. Velocity vector profile (m s^{-1}) in a top-insulated can filled with CMC and heated by condensing steam after 1157 s. The right-hand side of the figure is the centerline.

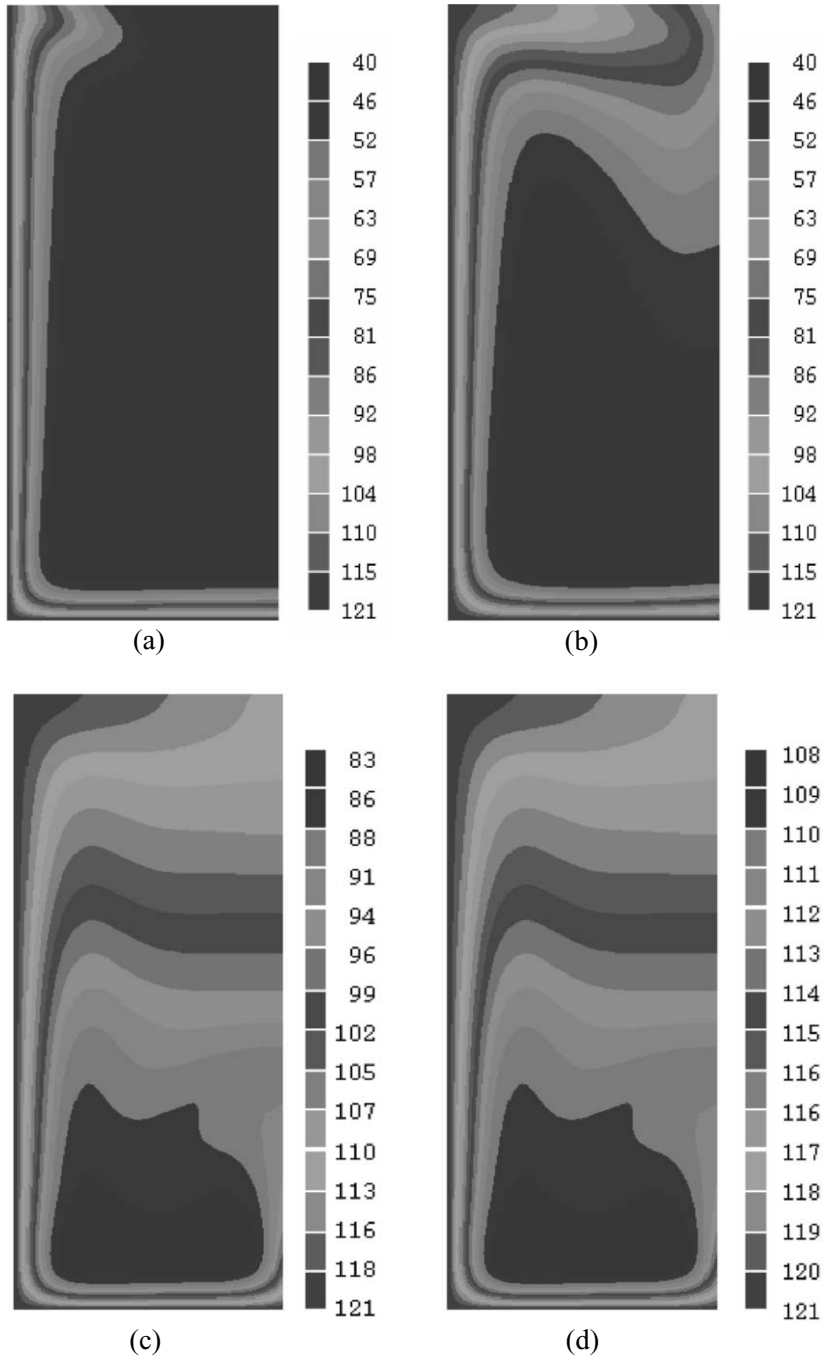

Figure 5.9. Temperature profiles in a can filled with CMC and heated by condensing steam (top insulated) after periods of (a) 54 s, (b) 180 s, (c) 1,157 s, and (d) 2,574 s. The right-hand side of each figure is the centerline.

can heated from all sides) is similar to that shown in Figure 5.8 (top insulated) with a slightly higher magnitude due to the more efficient heating in the former. The major difference between the heating in both cases is discussed in the next paragraph.

Figure 5.9 shows the temperature profiles in the top-insulated can filled with CMC and heated by condensing steam for different periods of time during thermal sterilization. This figure shows that the SHZ extends from the center of the can to the wall and tends to migrate to the bottom of the can as heating progresses. The results do not show any major difference from that shown for the can heated from all sides. Figures 5.4 and 5.9 show that the temperature difference from the top to the bottom of the can at the end of 2,574 s is almost the same. These two figures show that the location of the SHZ and its shape for both cases are similar. The observed difference in the temperature contour at the top of the can between the two cases is not sufficient to make a major change in the heating process. The convection currents are strong enough to minimize this difference even for such a viscous fluid as the one used in the current simulation.

5.4. EFFECT OF USING DIFFERENT RETORT TEMPERATURES ON BACTERIA AND VITAMIN C DESTRUCTION

The optimization of thermal processes such as sterilization relies on the accuracy of relevant kinetic data for bacterial inactivation and quality evolution. It is also dependent on the geometry and heating mechanism involved in the process. In this section, the effect of using different sterilization temperatures on bacteria deactivation and vitamins destruction is studied and analyzed. Profiles of temperature distribution, bacteria concentration, and of vitamin C (ascorbic acid) concentration in a can filled with concentrated cherry juice during thermal sterilization have been obtained through numerical simulations. Different heating medium temperatures of 121°C, 130°C, and 140°C are tested. In order to generate these profiles, the continuity, momentum, and energy equations are solved numerically, together with that of bacteria and vitamin concentration, using the CFD code PHOENICS, combined with reaction kinetics models. Natural convection that occurs during thermal sterilization of viscous liquid (concentrated cherry juice at 74 °Brix) in a cylindrical can heated from all sides is presented in this chapter. The simulations show clearly the dependency of the concentration of live bacteria and vitamin C on both the temperature distribution and the flow pattern as sterilization proceeds. The results also show that the best sterilization temperature may not be always 121°C, depending on the quality requirements imposed on individual food material of concern.

5.4.1. Numerical Approximation and Model Parameters

5.4.1.1. Computational Grid

The computations were performed for a can with a radius and height the same as those used in the two previous cases (Sections 5.2 and 5.3). A nonuniform grid system was used in the simulations with 3,500 nodal points: 70 in the axial direction and 50 in the radial direction, graded in both directions with a finer grid near the wall. The can outer surface temperature (top, bottom, and side) was assumed to rise instantaneously and remain constant (e.g., 121°C, 130°C, and 140°C) throughout the heating period. The natural convection heating of CMC was simulated for 2,600 s. It took 100 steps to achieve the first 200 s of heating, another 100 steps to reach 1000 s, and 300 steps for the total of 2,600 s of heating (Appendix B). This required 62 h of CPU time on the UNIX IBM RS6000 workstations at the University of Auckland.

5.4.1.2. Convection and Temporal Discretization

An important consideration in CFD is the discretization of the convection terms in the finite volume equations (FVEs). The accuracy and numerical stability of the solution depends on the numerical scheme used for these terms. The central issue is the specification of an appropriate relationship between the variables stored at the cell center and its value at each of the cell faces (Malin and Waterson, 1999). The convection discretization scheme used for all variables in our simulations is the hybrid-differencing scheme (HDS). The HDS of Spalding (1972) used in PHOENICS switches the discretization of the convective terms between the central differencing scheme (CDS) and the upwind differencing scheme (UDS) according to the local cell Peclet number Pe (ratio of convection to diffusion). Within PHOENICS the temporal discretization is fully explicit.

The cell Peclet number Pe for bacteria and vitamins within the flow domain in the z-direction is

$$\mathrm{Pe} = \frac{v_z \Delta z}{\alpha} \tag{5.14}$$

where v_z is a typical velocity (m s^{-1}), and Δz is a typical distance of the cell in the z-direction (mm). The thermal diffusivity α of the bacteria and the vitamins in the fluid is given by the Stokes–Einstein relation:

$$\alpha = \frac{K_\mathrm{B} T}{6\pi \mu a} \tag{5.15}$$

where K_B is the Boltzman constant, T is the temperature, μ is the apparent viscosity, and a is the radius of the particle (bacteria).

The calculated cell Peclet numbers within the flow domain in this study are of the order of 10^4, and hence the diffusion of bacteria and vitamins could be ignored. The effect of the diffusion of bacteria on the results of the simulation will be explained in detail in Chapter 7 (Section 7.1.1.3).

5.4.1.3. Physical Properties of Concentrated Cherry Juice

Concentrated fruit juice has important advantages over fresh juice because of its wider use as an ingredient in many food products such as ice creams, fruit syrups, jellies, and fruit juice beverages. It has higher stability than single-strength juices because of its low water activity, in addition to the reduced package, storage, and shipping cost (Luh et al., 1986). Cherry juice is one of the most popular juices because of its strong taste and attractive characteristics, such as agreeable color and pleasing flavor, besides its use to produce juice blends (Tressler et al., 1980). This is why cherry juice was the choice of liquid food for our next simulations. The properties of concentrated cherry juice used in the current simulations were $\rho = 1{,}052$ kg m^{-3}, $C_\mathrm{p} = 3{,}500$ J kg^{-1} K^{-1}, and $k = 0.554$ W m^{-1} K^{-1} (Hayes, 1987). The assumptions used were the same as those stated in Section 5.2.

Giner et al. (1996) measured the viscosity of concentrated cherry juice at different temperatures, concentrations, and shear rates and concluded that concentrated cherry juice (74 °Brix) may be assumed to behave as a Newtonian fluid. In the simulation presented here, the viscosity was assumed to be a function of temperature, following a second-order polynomial. Nonlinear curve fitting was used to fit the available data for concentrated cherry juice (74 °Brix) as reported by Giner et al. (1996). The values of a, b, and c in Equation 5.10 were found to be 1.472 Pa s, -4.26×10^{-2} Pa s K^{-1},

and 3.15×10^{-4} Pa s K^{-2} respectively. The variation of the density with temperature was governed by Boussinesq approximation as per the cases studied earlier.

5.4.1.4. Governing Equations for Mass Transfer of Bacteria and Vitamins

The PDEs governing natural convection of the fluid being heated are the Navier–Stokes equations in cylindrical coordinates (Bird et al., 1976) as in the previous Section 5.2. In addition to these equations, the following equations for concentrations of bacteria and vitamins are introduced:

Mass balance for bacteria:

$$\frac{\partial C_{\mathrm{rb}}}{\partial t} + v_r \frac{\partial C_{\mathrm{rb}}}{\partial r} + v_z \frac{\partial C_{\mathrm{rb}}}{\partial z} = D_{\mathrm{b}} \left[\frac{1}{r} \frac{\partial}{\partial r} \left(r \frac{\partial C_{\mathrm{rb}}}{\partial r} \right) + \frac{\partial^2 C_{\mathrm{rb}}}{\partial z^2} \right] - k_{\mathrm{b}} C_{\mathrm{rb}} \tag{5.16}$$

Mass balance for vitamins:

$$\frac{\partial C_{\mathrm{rv}}}{\partial t} + v_r \frac{\partial C_{\mathrm{rv}}}{\partial r} + v_z \frac{\partial C_{\mathrm{rv}}}{\partial z} = D_{\mathrm{v}} \left[\frac{1}{r} \frac{\partial}{\partial r} \left(r \frac{\partial C_{\mathrm{rv}}}{\partial r} \right) + \frac{\partial^2 C_{\mathrm{rv}}}{\partial z^2} \right] - k_{\mathrm{v}} C_{\mathrm{rv}} \tag{5.17}$$

The relative concentrations of bacteria and vitamin C (C_{rb} and C_{rv}) in Equations (5.16) and (5.17) are taken as a dimensionless species concentration, which are defined as the ratio of real-time concentrations (C_{b} and C_{v}) to the initial concentrations (C_{b0} and C_{v0}) multiplied by 100. The numerical approximations and the kinetics of bacteria deactivation and vitamin destruction are the same as those explained later in Chapters 7 and 8, except for the temperature of the wall (T_{w}), which was varied in each simulation studied.

The boundary conditions used for bacteria deactivation and vitamin C destruction are as follows:

$$\begin{aligned}
&\text{At the can boundary, } r = R, && \frac{\partial C_{\mathrm{rb}}}{\partial r} = 0 \quad \text{and} \quad \frac{\partial C_{\mathrm{rv}}}{\partial r} = 0 \\
&\text{At the bottom of the can, } z = 0, && \frac{\partial C_{\mathrm{rb}}}{\partial z} = 0 \quad \text{and} \quad \frac{\partial C_{\mathrm{rv}}}{\partial z} = 0 \\
&\text{At symmetry, } r = 0, && \frac{\partial C_{\mathrm{rb}}}{\partial r} = 0 \quad \text{and} \quad \frac{\partial C_{\mathrm{rv}}}{\partial r} = 0 \\
&\text{At the top of the can, } z = H, && \frac{\partial C_{\mathrm{rb}}}{\partial z} = 0 \quad \text{and} \quad \frac{\partial C_{\mathrm{rv}}}{\partial z} = 0
\end{aligned}$$

Other boundary conditions for temperature and velocities are the same as those used in Sections 5.2.1.3. The initial conditions used are $T = T_{\mathrm{ref}}$, $C_{\mathrm{rb}} = 100$, $C_{\mathrm{rv}} = 100$, $v_r = 0$, and $v_z = 0$. The model liquid is assumed to have constant properties except for viscosity (temperature dependent) and density (Boussinesq approximation). Density change with temperature is not significant when compared with the change in viscosity (Appendix B). The simplifications used in the simulation are the same as those used in Section 5.2.1.5. The additional assumption made for simplicity is that the effect of molecular diffusion of bacteria and vitamin C are neglected due to the relatively strong influence of the convection motion. This assumption has been verified by Ghani et al. (1999), allowing the simplifications of Equations (5.16) and (5.17) by omitting the diffusion term.

5.4.2. Results of Simulation

The effects of retort operating temperature on the rate of bacteria deactivation and vitamin C destruction were studied by introducing their kinetics based on information available in the literatures. Sterilization temperatures of 130°C and 140°C were tested in addition to the conventional sterilization temperature of 121°C usually used in the industry.

Figures 5.10 and 5.11 show the results of the simulations at two different times of 1,000 s and 1960 s for the different retort temperatures. The results at the early stages of heating showed that the process of heating is governed by conduction, and hence very limited bacteria deactivation may be seen. Figure 5.10a shows the change in the temperature and the concentrations of bacteria and vitamin C in the can after 1,000 s of heating at 121°C. Figures 5.10b and 5.10c show the corresponding results when the retort temperature is 130°C and 140°C. These figures show that the SHZ reaches 93°C when the retort temperature is 121°C, while it rises to 102°C when the retort temperature is 140°C. This causes the relative bacteria concentration in the SHZ to drop from 67% to 16.6% respectively (0.17 to 0.78 log reduction). As the retort temperature is increased from 121°C to 140°C, the relative concentration of vitamin C at locations near the wall drops from 86% to 54% respectively for the same reason explained earlier.

Figure 5.11 shows the result of the sterilization after 1960 s of heating for the three different sterilization temperatures. This is the time at which the bacteria concentration drops down to a low practical level, and hence it represents an important illustration of what is likely to occur in practice. The SHZ remains at the same location as the high bacteria concentration zone (HBCZ). For the same sterilization time, the relative concentration of bacteria in the HBCZ drops from $2.8 \times 10^{-3}\%$ to $1.2 \times 10^{-9}\%$ (4.6 to 10.9 log reduction) when the sterilization temperature is increased from 121°C to 140°C. The influence is very significant due to the exponential effect of temperature on the rate constant of bacteria deactivation, as represented by the Arrhenius equation. The corresponding relative vitamin C concentration at locations near the wall drops from 71% to 26% at the two sterilization temperatures.

Both concentrations of bacteria and vitamin C depend not only on the temperature but also on the flow pattern. This will be discussed in detail in Chapter 7 for bacteria and vitamin concentration. Figures 5.10 and 5.11 show that the SHZ and HBCZ occur at a similar location in the can. However, the HBCZ is clearly influenced by the flow pattern, as shown in Figure 5.12, which illustrates the existence of two stagnant regions. The influence of the flow pattern on vitamin C concentrations is even stronger as the locations of the high vitamin C concentration occur exactly at the stagnant zones.

The relative bacteria concentration in the SHZ is a good measure of the food sterility. However, in the analysis of vitamin destruction, it is more useful to calculate the average relative vitamin concentration in the whole can, which is calculated as the weighted average of the local concentrations (Appendix C):

$$C_{\text{ave}} = \frac{2}{R^2 L} \sum_{z=0}^{L} \sum_{r=0}^{R} rC \Delta z \Delta r \tag{5.18}$$

The calculated average vitamin C concentrations are plotted in Figure 5.13 for different retort temperatures. This figure shows that the average percentage destruction of vitamin C at the end of heating is about 25% of its initial concentration.

The relative bacteria concentrations at the HBCZ for different sterilization temperatures are shown in Figure 5.14. At the early stage of heating, the concentration of bacteria at HBCZ remains

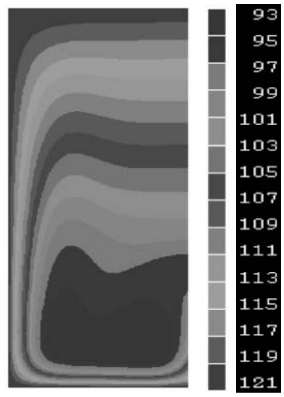

(a) Temperature (121°C)

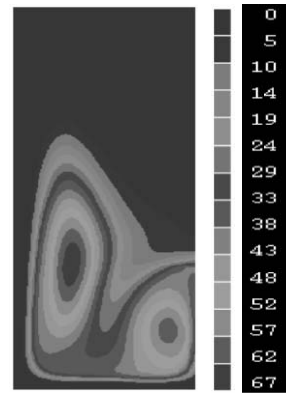

(a) Bacteria relative conc. (%)

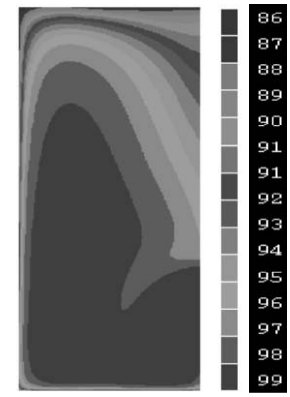

(a) Vitamin C relative conc. (%)

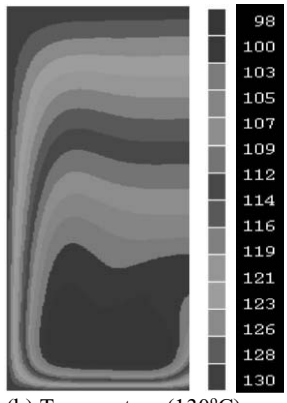

(b) Temperature (130°C)

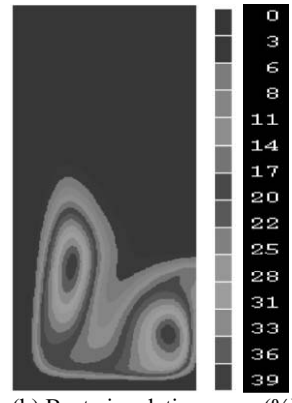

(b) Bacteria relative conc. (%)

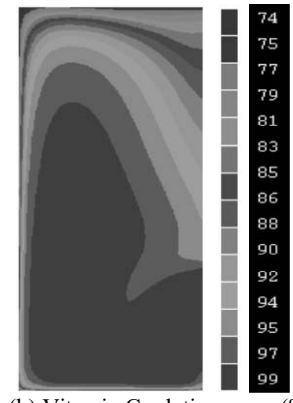

(b) Vitamin C relative conc. (%)

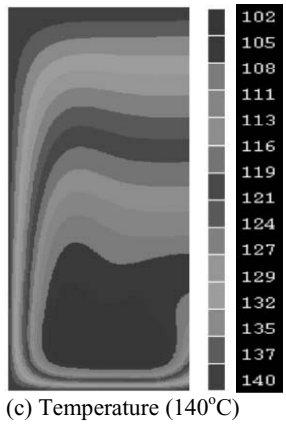

(c) Temperature (140°C)

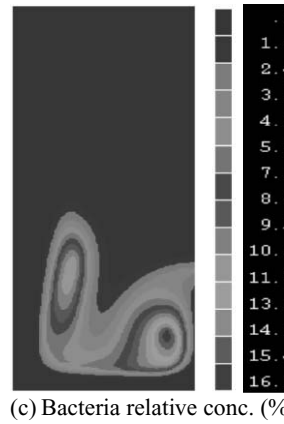

(c) Bacteria relative conc. (%)

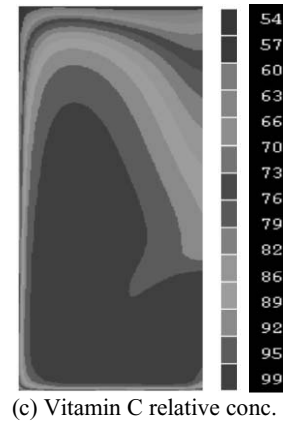

(c) Vitamin C relative conc. (%)

Figure 5.10. Temperature, bacteria deactivation, and vitamin C destruction profiles in a can filled with concentrated cherry juice and heated by condensing steam at (a) 121°C, (b) 130°C, and (c) 140°C after 1,000 s. The right-hand side of each figure is the centerline.

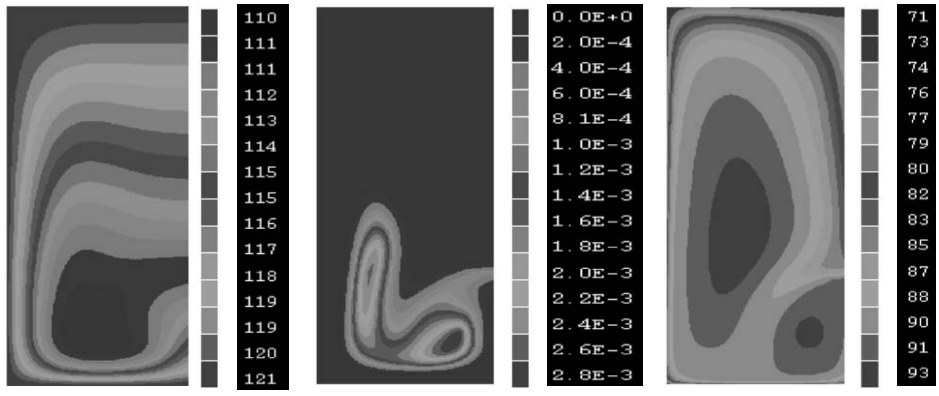

(a) Temperature (121°C) (a) Bacteria relative conc. (%) (a) Vitamin C relative conc. (%)

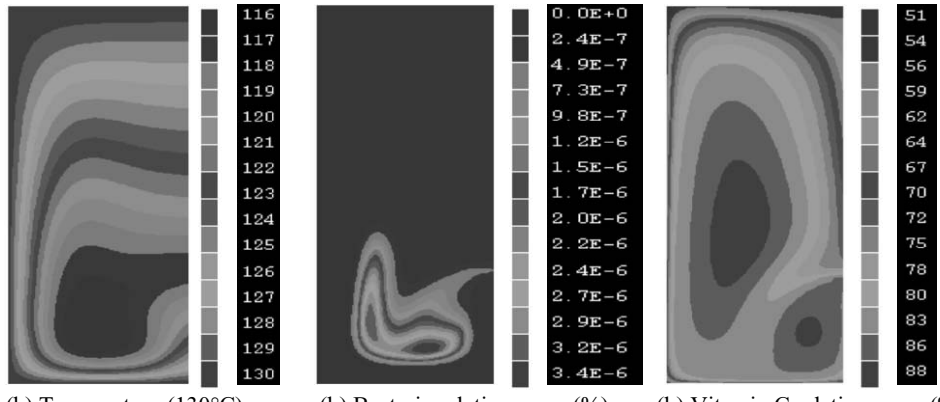

(b) Temperature (130°C) (b) Bacteria relative conc. (%) (b) Vitamin C relative conc. (%)

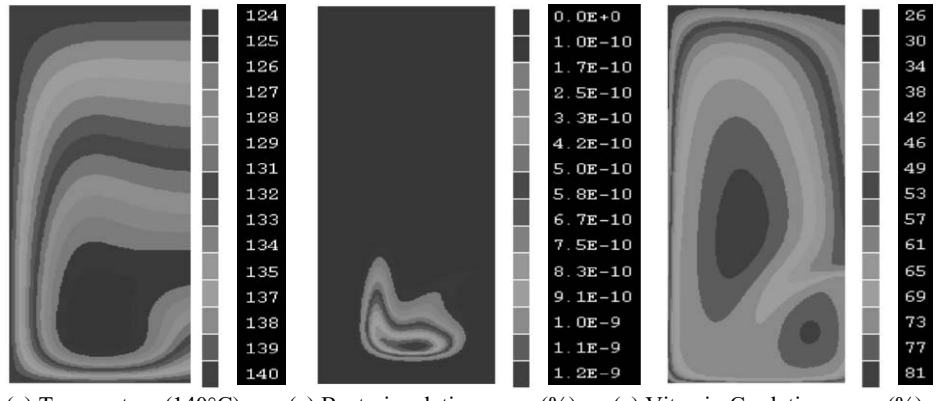

(c) Temperature (140°C) (c) Bacteria relative conc. (%) (c) Vitamin C relative conc. (%)

Figure 5.11. Temperature, bacteria deactivation, and vitamin C destruction profiles in a can filled with concentrated cherry juice and heated by condensing steam at (a) 121°C, (b) 130°C, and (c) 140°C after 1,960 s. The right-hand side of each figure is the centerline.

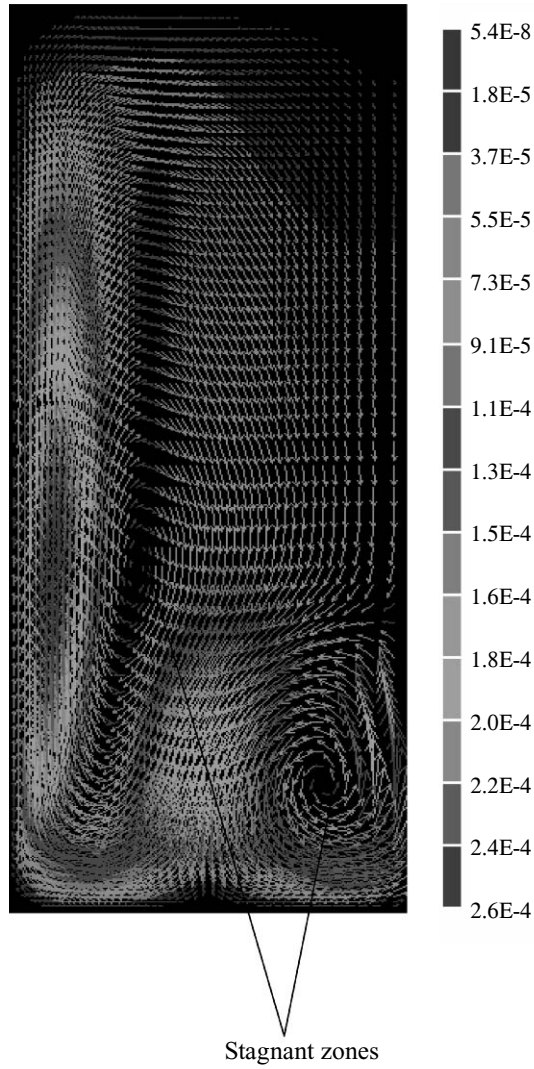

Figure 5.12. Velocity vector profile (m s^{-1}) in a can filled with concentrated cherry juice (74 °Brix) heated by condensing steam at 121°C after 2,450 s.

unchanged. As the heating progresses, the effect of temperature becomes very strong due to the exponential effect of temperature on the rate of bacteria inactivation. Assuming that a relative bacteria concentration of 10^{-7} (7 log reduction) at the HBCZ is acceptable, just for the purpose of comparison, Figure 5.14 shows that the time required for complete sterilization at 121°C, 130°C, and 140°C are 2,500 s, 2,100 s, and 1,800 s, respectively.

The effects of using different retort temperature on the rate of inactivation of bacteria and vitamins are different due to their different values of decimal reduction time (or activation energy). As expected, applying higher sterilization temperature will reduce sterilization time significantly. However the use of a higher temperature will also cause more destruction of vitamin C, as shown in Figure 5.13. Hence, it is likely that the best sterilization temperature may not be always 121°C, depending on the type of food material sterilized.

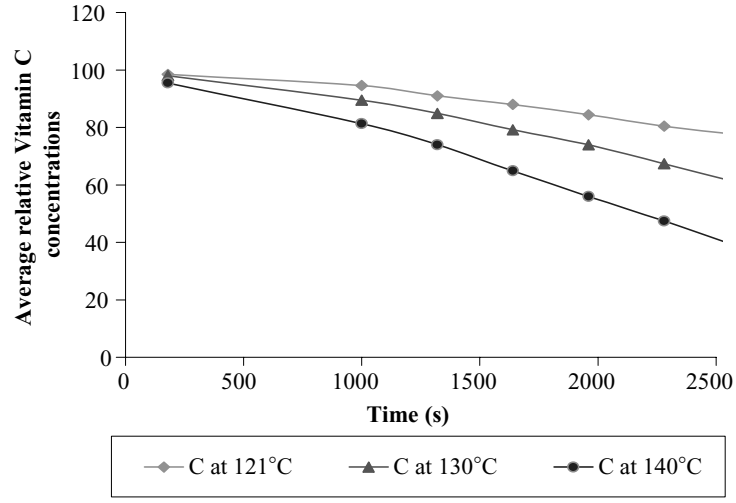

Figure 5.13. Average relative concentration of vitamin C versus time during sterilization of a can filled with concentrated cherry juice and heated by condensing steam at 121°C, 130°C, and 140°C after 2,600 s.

5.5. COMPARISON BETWEEN CONVECTION AND CONDUCTION HEATING

Determination of the unsteady-state temperature distribution in solid and liquid canned foods is necessary for accurate process control and for the design of sterilization systems. For this reason, the prediction of heat transfer in these widespread industrial processes has great significance (Akterian, 1994). Conduction-heated canned foods refer to sterilized foods in which heat is transferred mostly by thermal conduction, such as in very high-viscosity foods, meat and fish, as well as their derivatives and combinations.

The simulation of conduction-heated food (solid or very viscous liquid) does not require comprehensive CFD analysis. It is usually performed by solving the heat conduction equation, using the finite difference method (FDM), the finite element method (FEM), or the FVM of solution. However, for convenience the same CFD program was used in the analysis presented in this chapter. This exercise has been performed for the purpose of comparing conduction and convection heating.

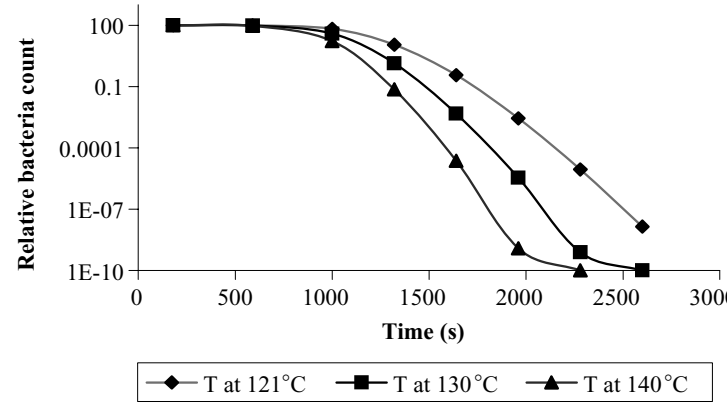

Figure 5.14. Relative bacteria concentration at the HBCZ versus time of sterilization of a can filled with concentrated cherry juice and heated by condensing steam at 121°C, 130°C, and 140°C after 2,600 s (Ghani et al., 2001).

Sterilization of canned liquid food in a metal can sitting in an upright position and heated at 121°C from all sides was predicted and studied for two cases. In the first case, the contents of the can were assumed to be heated by convection-dominated heating, while in the other case they were assumed to be heated by conduction only. A viscous liquid model (carrot-orange soup) was used as the model liquid food, which is one of the canned products of Heinz Watties Australasia located in Hastings, New Zealand.

5.5.1. Numerical Approximations and Model Parameters

For conduction heating, Equation (5.2) was simplified to the following:

$$\frac{\partial T}{\partial t} = \frac{k}{\rho C_p}\left[\frac{1}{r}\frac{\partial}{\partial r}\left(r\frac{\partial T}{\partial r}\right) + \frac{\partial^2 T}{\partial z^2}\right] \tag{5.19}$$

The boundary condition used was $T = T_w = 121°C$, and the initial condition was $T = T_{ref} = 19°C$. The reference temperature (T_{ref}) was chosen based on the actual temperature of the liquid food measured experimentally.

The properties of carrot-orange soup used in the current simulation were $\rho = 1{,}026$ kg m^{-3}, $C_p = 3{,}880$ J kg^{-1} K^{-1}, and $k = 0.596$ W m^{-1} K^{-1}. The properties were calculated from the values reported by Rahman (1995) and Hayes (1987) for all the food materials used in the soup, using their mass fractions. In the simulation presented here, the viscosity was assumed to be a function of temperature, following a second-order polynomial (Equation [5.10]). The viscosity of carrot-orange soup was measured at different temperatures, using Paar Physica Viscometer VT2. These values were 9.79 Pa s, 5.14 Pa s, and 2.82 Pa s at 30°C, 50°C, and 70°C respectively. A nonuniform grid system was used in these simulations. The heating of carrot-orange soup was simulated for 3,000 s as the total heating period. It took 10 steps to achieve the first 200 s of heating, another 10 steps to reach 1,000 s, and 30 steps for the total of 3,000 s of heating. The computations were performed for a can with a radius of 37 mm and height of 111 mm. This required 7 h of CPU time for the simulation of can heated by convection-dominated heating and 5 h by conduction heating.

5.5.2. Results of Simulations

The objective of this section is to show the major difference between conduction heating and convection-dominated heating of food in cans. Two simulations were performed to obtain the transient temperature profiles during heating of canned liquid food for the two cases explained above.

For convection-dominated heating, Figure 5.15 shows flow and velocity vector profiles of carrot-orange soup in a can heated by steam condensing along its outside surface. The magnitude of the maximum axial velocity at the midheight of the can near the wall was 0.35 mm s^{-1} at $t = 1{,}200$ s. As heating progressed, a more uniform temperature was obtained, reducing buoyancy force in the liquid that lead to a significant reduction in the magnitude of liquid velocity.

The temperature profiles shown in Figure 5.16 for different periods of heating are presented in the form of isotherms. The isotherms at $t = 60$ s are almost identical to pure conduction heating (Figure 5.17); but over time, the isotherms are seen to be strongly influenced by convection. As heating progressed, the temperature of the SHZ in the carrot-orange soup reached about 107°C in 3,000 s in comparison to only 83°C at the same time when heating was assumed to be dominated by conduction.

Figure 5.17 shows that the SHZ does not cover the bottom section of the can as in the case of convection-dominated heating (Figure 5.16), and it stays at the geometric center of the can during

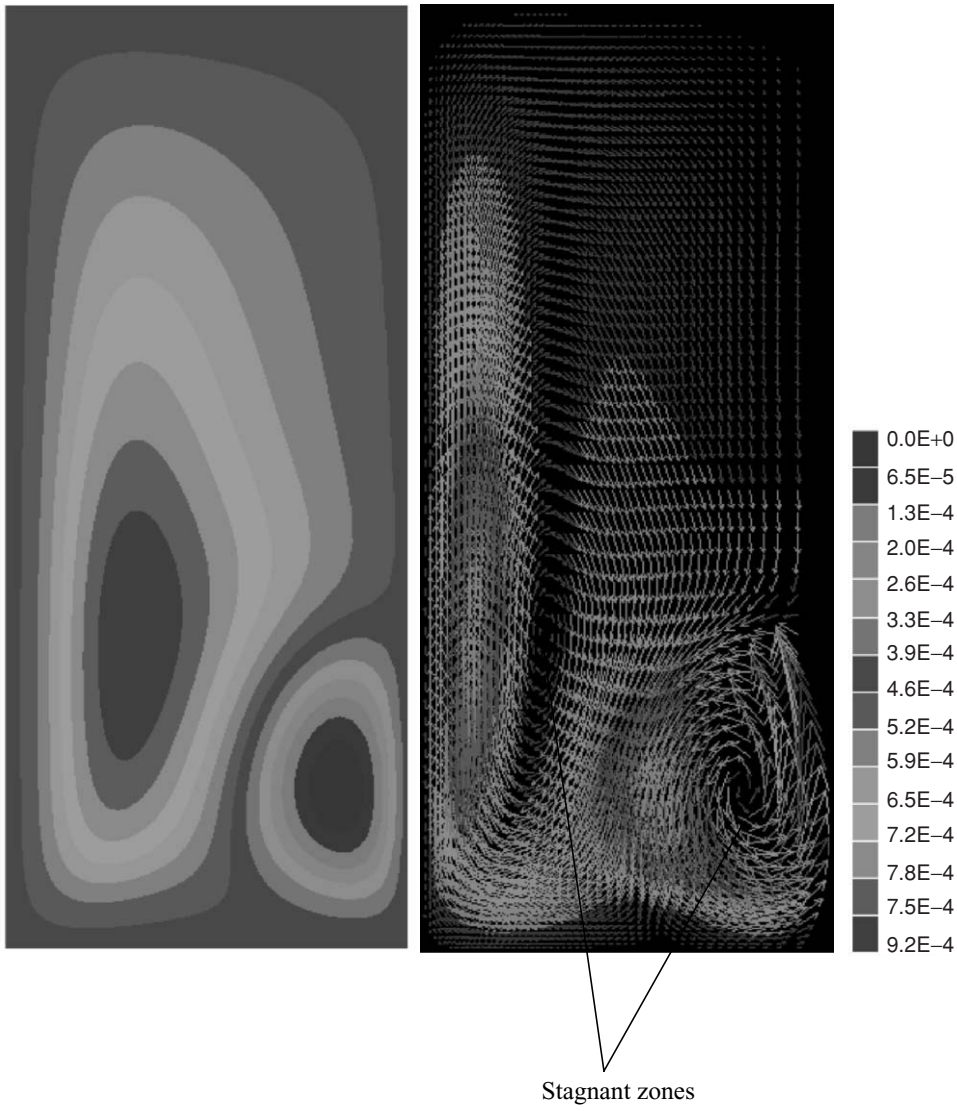

Figure 5.15. Streamline and velocity vector (m s^{-1}) profiles of carrot-orange soup in a can heated by condensing steam after 1,200 s. The right-hand side of each figure is the centerline. Ghani et al. (2000)

the whole period of heating as expected. The results presented in this section indicate that neglecting natural convection in the analysis of sterilization may lead to oversterilization and hence unnecessary excessive destruction of nutrients.

5.6. SIMULATION OF A HORIZONTAL CAN DURING STERILIZATION

In this simulation, natural convection heating in a 3-D can filled with carrot-orange soup, lying horizontally and heated by condensing steam at 121°C from all sides, is presented and analyzed.

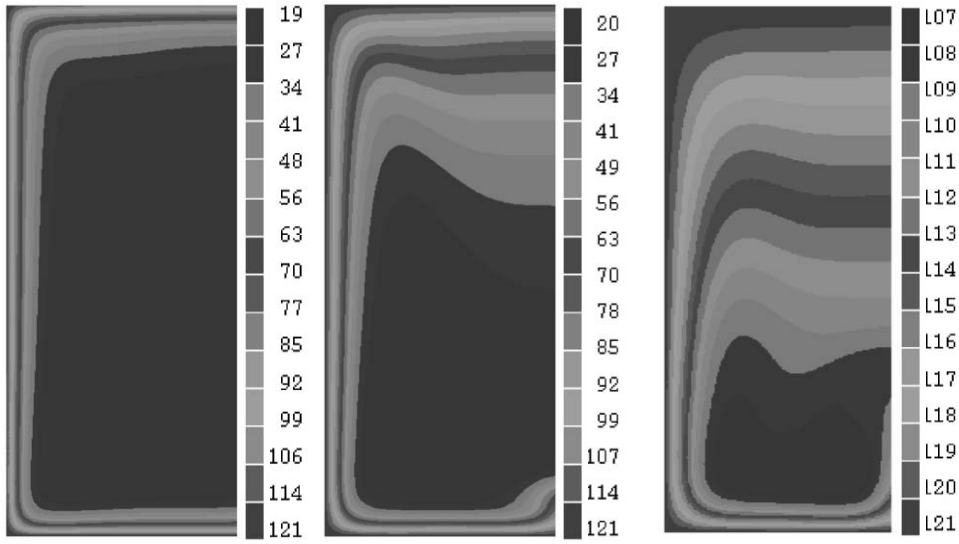

Figure 5.16. Temperature profiles in a can filled with carrot-orange soup and heated by condensing steam after periods of (a) 60 s, (b) 180 s, and (c) 3,000 s. The right-hand side of each figure is the centerline. Convection is the dominating mechanism of heat transfer inside the can.

The results of the simulation were compared with those for the can sitting in an upright position (vertical). In a vertical can, the analysis is based on two dimensions because of the axisymmetry, which reduces the problem from 3-D to 2-D. In the case of the can lying horizontally, this assumption is not valid, and 3-D analysis will be required.

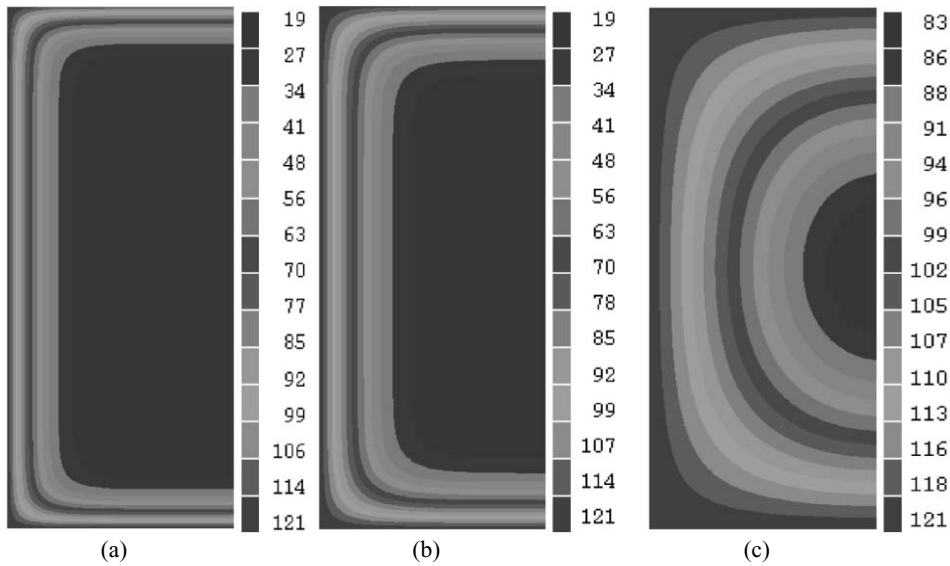

Figure 5.17. Temperature profiles in a can filled with carrot-orange soup and heated by only conduction after periods of (a) 60 s, (b) 180 s, and (c) 3,000 s. The right-hand side of each figure is the centerline.

5.6.1. Governing Equations and Boundary Conditions

The PDEs governing the natural convection heating of a fluid in a can lying horizontally are given below (Bird et al., 1976):

Energy conservation:

$$\frac{\partial T}{\partial t} + v_r \frac{\partial T}{\partial r} + \frac{v_\theta}{r}\frac{\partial T}{\partial \theta} + v_z \frac{\partial T}{\partial z} = \frac{k}{\rho C_p}\left[\frac{1}{r}\frac{\partial}{\partial r}\left(r\frac{\partial T}{\partial r}\right) + \frac{1}{r^2}\frac{\partial^2 T}{\partial \theta^2} + \frac{\partial^2 T}{\partial z^2}\right] \tag{5.20}$$

Momentum equation in the radial direction (r):

$$\rho\left(\frac{\partial v_r}{\partial t} + v_r\frac{\partial v_r}{\partial r} + \frac{v_\theta}{r}\frac{\partial v_r}{\partial \theta} - \frac{v_\theta^2}{r} + v_z\frac{\partial v_r}{\partial z}\right) =$$
$$-\frac{\partial p}{\partial r} + \mu\left[\frac{\partial}{\partial r}\left(\frac{1}{r}\frac{\partial}{\partial r}(rv_r)\right) + \frac{1}{r^2}\frac{\partial^2 v_r}{\partial \theta^2} - \frac{2}{r^2}\frac{\partial v_\theta}{\partial \theta} + \frac{\partial^2 v_r}{\partial z^2}\right] + \rho g \tag{5.21}$$

In order to simplify the analysis, the buoyancy force caused by density variation due to temperature is assumed to be governed by Boussinesq approximation (Equation [5.12]), which is used in the body force term of the momentum equation in the radial direction. The momentum equations in angular and vertical directions are as follows:

Momentum equation in the angular direction (θ):

$$\rho\left(\frac{\partial v_\theta}{\partial t} + v_r\frac{\partial v_\theta}{\partial r} + \frac{v_\theta}{r}\frac{\partial v_\theta}{\partial \theta} + \frac{v_r v_\theta}{r} + v_z\frac{\partial v_\theta}{\partial z}\right) =$$
$$-\frac{1}{r}\frac{\partial p}{\partial \theta} + \mu\left[\frac{\partial}{\partial r}\left(\frac{1}{r}\frac{\partial}{\partial r}(rv_\theta)\right) + \frac{1}{r^2}\frac{\partial^2 v_\theta}{\partial \theta^2} + \frac{2}{r^2}\frac{\partial v_r}{\partial \theta} + \frac{\partial^2 v_\theta}{\partial z^2}\right] \tag{5.22}$$

Momentum equation in the vertical direction (z):

$$\rho\left(\frac{\partial v_z}{\partial t} + v_r\frac{\partial v_z}{\partial r} + \frac{v_\theta}{r}\frac{\partial v_z}{\partial \theta} + v_z\frac{\partial v_z}{\partial z}\right) = -\frac{\partial p}{\partial z} + \mu\left[\frac{1}{r}\frac{\partial}{\partial r}\left(r\frac{\partial v_z}{\partial r}\right) + \frac{1}{r^2}\frac{\partial^2 v_z}{v\theta^2}\frac{\partial^2 v_z}{\partial z^2}\right] \tag{5.23}$$

The above equations are coupled with the continuity equation:

Continuity equation:

$$\frac{1}{r}\frac{\partial}{\partial r}(r\rho v_r) + \frac{1}{r}\frac{\partial}{\partial \theta}(\rho v_\theta) + \frac{\partial}{\partial z}(\rho v_z) = 0 \tag{5.24}$$

The *boundary conditions* used were as follows:

At the can surface ($r = R$, $z = 0$, and $z = L$),

$$T = T_w, \quad v_r = 0, \quad v_\theta = 0, \quad v_z = 0 \tag{5.25}$$

Initially the fluid is at rest and is at a uniform temperature:

$$T = T_{ref} = 19^\circ\text{C}, \quad v_r = 0, \quad v_\theta = 0, \quad v_z = 0 \quad \text{at} \quad 0 \le r \le R, \quad 0 \le z \le H \tag{5.26}$$

The properties of the liquid food material (carrot-orange soup) used in the current simulation were the same as those used in previous case (Section 5.5). A nonuniform grid system was used in the simulation with 105,000 cells: 50 in the radial direction, 70 in the vertical direction, and 30 in the angular direction, graded with a finer grid near the wall in both radial and vertical directions. For the purpose of comparison, the computations were performed for a can with a radius and height same as those used in Section 5.5. The can outer surface was heated from all sides at a constant temperature (121°C) throughout the heating period. The natural convection heating of carrot-orange soup was simulated for 3,000 s, and the time steps were the same as those used in Section 5.5. This required 18 h of CPU time on the UNIX IBM RS6000 workstations at the University of Auckland. Simulations were performed using four different meshes. The additional finer meshes showed no significant difference in the SHZ temperature versus time. Therefore, the mesh with 105,000 cells was used in the simulation.

5.6.2. Results of Simulation

Figure 5.18 shows the velocity vector of carrot-orange soup in a 3-D cylindrical can lying horizontally and heated by condensing steam for two different periods of heating: (a) 180 s and (b) 1,000 s. This figure shows that the vertical velocity of the fluid at 1,000 s ranged from 9.6×10^{-2} mm s^{-1} to 6.3×10^{-5} mm s^{-1}, which was lower than that observed in the vertical can (Figure 5.15) by a factor of 10. This was due to the lower Grashof number in the horizontal can since the characteristic dimension of the Grashof number in this case is equal to the can diameter, which is smaller than its height. The general behavior of the fluid motion in the horizontal can is similar to that in the vertical one (Section 5.2.2.1). The buoyancy force created by the change in liquid density due to temperature variation (from the wall to the core) produces an upward flow near the side walls. The hot liquid going up is deflected at the middle of the top wall and then travels radially toward the core. Being heavier, it then moves downward toward the wall. Thus a recirculating flow is created. Figure 5.18 also shows the secondary flow formation at the ends of the can, which affects the shape of the SHZ seen in Figure 5.19b. Figure 5.18b shows a stagnant region located at the middle height of the can, which is due to the largest area of the flow at this location.

Figure 5.19 shows the temperature profiles of the same can after 600 s at two different planes: (a) radial-angular plane and (b) radial-vertical plane. The can shown in this figure is in the horizontal position. The inclination shown is only to provide more clearly a 3-D image. This figure shows clearly the actual shape of the SHZ, which diminishes gradually as it descends from the middle of the can toward its bottom surface. The temperature profiles shown in Figure 5.20 for different periods of heating are presented in the form of isotherms. At $t = 60$ s, the isotherms are almost identical to pure conduction heating, as in Figure 5.16a. As heating progresses (at $t = 180$ s), the isotherms are seen to be influenced by convection but slower than that for the vertical can shown in Figure 5.16b. The shape of the SHZ seen in Figures 5.20b and 5.20c gradually takes the form of an ellipse, which settles down at the lower half of the can as natural convection develops.

Figure 5.21 shows the transient temperature of carrot-orange soup at the SHZ for horizontal and vertical cans heated by condensing steam at 121°C. This figure shows clearly the difference in the rate of heating between the two cases. It shows that faster rate of heating can be achieved by positioning the can in an upright position, which causes higher natural convection.

5.7. EFFECT OF CAN ROTATION ON STERILIZATION OF LIQUID FOOD

Determination of the temperature time history of processed food has practical and safety implications. Temperature time histories may be derived by using direct measurements or mathematical modeling

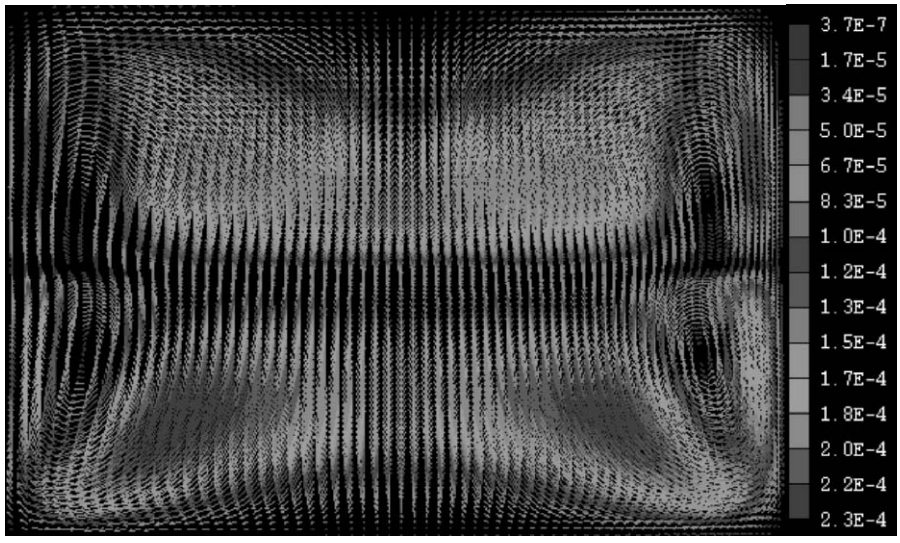

(a)

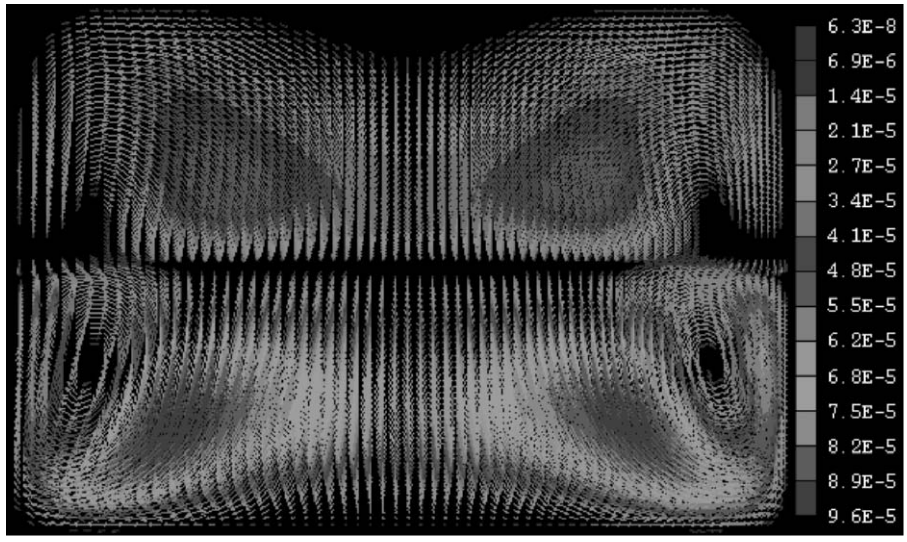

(b)

Figure 5.18. The $r-z$ plane velocity vector profile (m s^{-1}) of carrot-orange soup in a 3-D cylindrical can lying horizontally and heated by condensing steam after periods of (a) 180 s and (b) 1,200 s.

(Tucker and Holdsworth, 1991). Because of the complex nature of heat transfer in natural convection heating, the determination of the SHZ, which is defined as the location in the can receiving minimum heating, is a difficult task. The placement of thermocouple probes to record temperature during heating at various positions in the container disturbs the flow patterns. This is even more difficult for a can under rotation. Since the temperature field is very sensitive to the velocity field, the measurements of the temperature distribution in the can will be in error due to disturbance caused by the measuring probe (Kumar et al., 1990). Enzyme denaturation-based Temperature Time Integrators (TTI) used by Cox and Fryer (2001) offer an efficient method of validating the thermal processes associated with

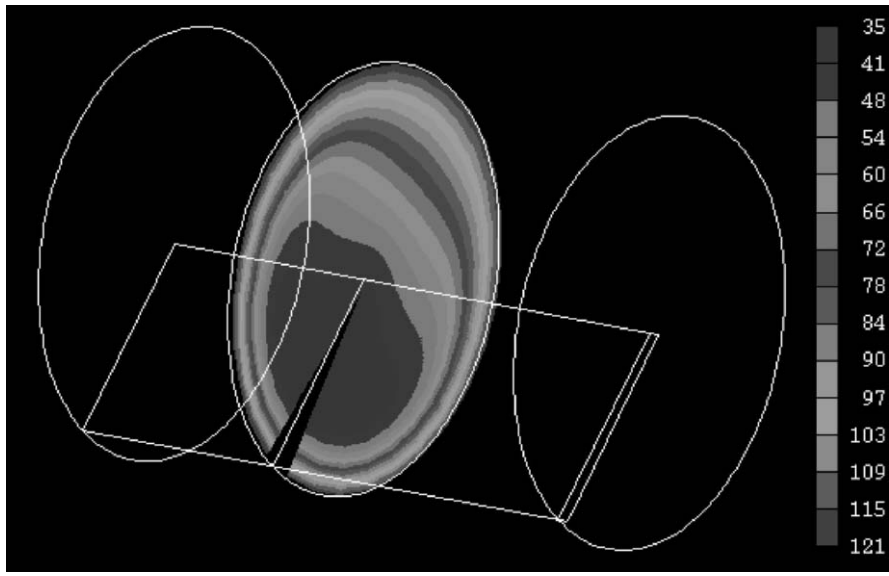

(a)

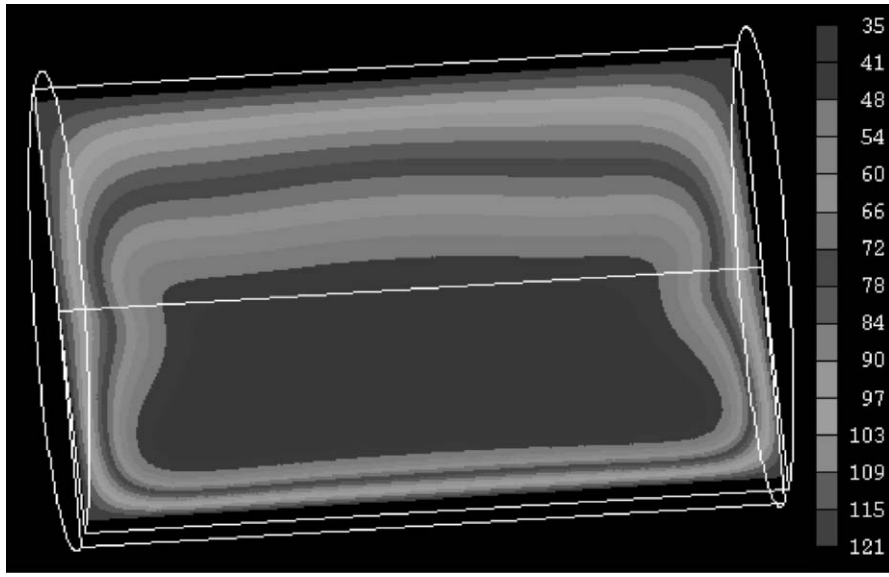

(b)

Figure 5.19. Temperature profiles of carrot-orange soup in a 3-D cylindrical can lying horizontally and heated by condensing steam after 600 s at two different planes: (a) radial-angular plane and (b) radial-vertical plane.

food manufacture and may be used to calculate process lethality. However, the use of TTI particles for the replacement thermocouples as a standard food industry practice requires verification, using accurate practical assessments and mathematical modeling. Cox and Fryer have also developed a new technique for measuring the flow field, food particle and liquid movement, as well as residence

(a)

(b)

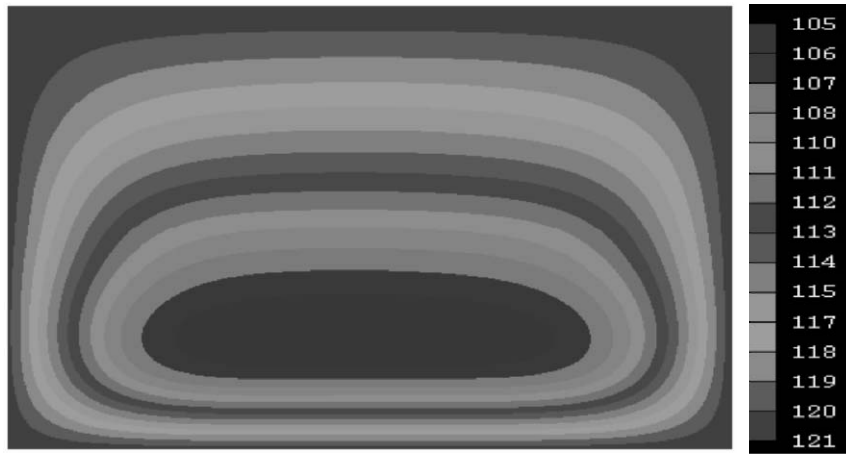

(c)

Figure 5.20. The $r-z$ plane temperature profiles of carrot-orange soup in a 3-D can lying horizontally and heated by condensing steam after periods of (a) 60 s, (b) 180 s, and (c) 3,000 s.

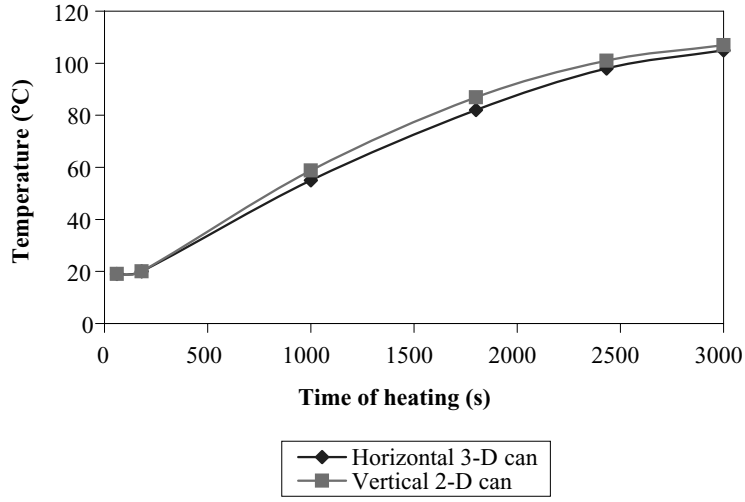

Figure 5.21. Transient temperature of carrot-orange soup at the SHZ in a cylindrical can heated by condensing steam after 3,000 s.

time, using Positron Emission Particle Tracking (PEPT), which can be used to measure flow patterns in opaque fluids in metal cans.

There are several factors that influence the heat penetration rate into the food particles in a container during sterilization. The most relevant factors include retort temperature, product viscosity, can head space, and rotation of the can (Ghani et al., 1999; Krishnamurthy et al., 2001). Cans are commonly processed in rotating retorts and warmed liquid food circulates within the can faster than that found in a stationary can (Kumar and Bhattacharya, 1991). Rotational processes may be applied to liquid or semifluid foods to increase the rate of heating within the container (Berry et al., 1979; Naveh and Kopelman, 1980; Van Loey et al., 1994). Assuming there is adequate heat supply, the can's rotation can lead to shorter process times with improved sensorial quality and reduce nutrient losses (Smout et al., 2000). The effect of rotation on the heat penetration parameters of canned white beans was investigated by Smout et al., who showed no clear relation between the nonuniformity of the heating parameters and the rotational speed.

The objective of this section of the book is to show the combined effect of natural and forced convection (rotation) on the temperature distribution and location of the SHZ in a 3-D can lying horizontally and filled with viscous liquid food. The effect of can rotation has not been previously analyzed using CFD. The 3-D geometry of the horizontal can and the effect of its rotation require efficient CFD analysis. In this work, sterilization of viscous liquid food (carrot-orange soup) in a metal can lying horizontally and rotated axially in a still retort was simulated. The can, which was rotating at 10 rpm, was assumed to be heated by steam at 121°C. The governing equations of mass, momentum, and energy conservation for the 3-D can were solved. Transient temperature and velocity profiles caused by natural and forced convection heating were presented and compared with those for a stationary can.

5.7.1. Formulation of a Model

In the simulation presented in this section, the viscosity of the liquid food used is assumed as a function of temperature, as used in the previous sections. The variation of the density with temperature was governed by Boussinesq approximation. Equation (5.26) for the momentum equation in the radial

direction (r) is used to describe its variation with temperature.

$$\rho\left(\frac{\partial v_r}{\partial t}+v_r\frac{\partial v_r}{\partial r}+\frac{v_\theta}{r}\frac{\partial v_r}{\partial \theta}-\frac{v_\theta^2}{r}+v_z\frac{\partial v_r}{\partial z}\right)=\frac{\partial p}{\partial r}+\mu\left[\frac{\partial}{\partial r}\left(\frac{1}{r}\frac{\partial}{\partial r}(rv_r)\right)\right.$$
$$\left.+\frac{1}{r^2}\frac{\partial^2 v_r}{\partial \theta^2}-\frac{2}{r^2}\frac{\partial v_\theta}{\partial \theta}+\frac{\partial^2 v_r}{\partial z^2}\right]+\rho_{\text{ref}}g[1-\beta(T-T_{\text{ref}})]$$

The properties of the liquid food material (carrot-orange soup) used in the current simulation are the same as those used in Section 5.5. The viscous heating is ignored as the liquid velocities due to can rotation and natural convection motion are expected to be low. At a constant pressure, the condensing steam maintains the outside can wall at a constant temperature of 121°C.

With the above-mentioned assumptions, the PDEs governing natural convection motion in a 3-D can are the Navier–Stokes equations in r, θ, and z coordinates (Bird et al., 1976).

The *boundary conditions* used are as follows:

The rotational speed of 10 rpm is employed as a system (operating) variable and is introduced to the boundary conditions as follows:

$$v_\theta = 2\pi\omega R \tag{5.27}$$

where ω is the rotational velocity (rad s^{-1}), and R is the radius of the can (m).

(a) Boundary condition at the can wall:
At the can wall, $r = R$,

$$T = T_w, \quad v_\theta = 2\pi\omega R, \quad v_R = 0, \text{ and } \quad v_z = 0, \text{ for } \quad 0 \le z \le H \tag{5.28}$$

(b) Boundary condition at the two ends (top and bottom) of the can:
At the two ends of the can, $z = 0$ and $z = L$,

$$T = T_w, \quad v_R = 0, \quad v_\theta = 0, \text{ and } v_z = 0, \text{ for } \quad 0 \le r \le R \tag{5.29}$$

Initially the fluid is at rest and is at a uniform temperature:

$$T = T_{\text{ref}} = 19^\circ\text{C}, \quad v_R = 0, \quad v_\theta = 0, \quad v_z = 0 \quad \text{at} \quad 0 \le r \le R, \quad 0 \le z \le H \tag{5.30}$$

5.7.2. Numerical Approach

5.7.2.1. Computational Grid

A nonuniform grid system in the radial and axial directions was used in the simulation with 105,000 cells: 50 in the radial direction, 70 in the axial direction, and 30 in the angular direction, graded with a finer grid near the wall in both radial and vertical directions. For the purpose of comparison, the computations were performed for a can with a radius and height the same as those used in Sections 5.5 and 5.6. The can's outer surface was heated from all sides at a constant temperature (121°C) throughout the heating period. The natural convection heating of carrot-orange soup was simulated for 3,000 s. This required about 19 h of CPU time on the UNIX IBM RS6000 workstations at the University of Auckland. For the purpose of comparison, all the computations were performed

for a can similar to that used in the previous case (Section 5.6). This included size of the can, number of divisions, heating time, and time steps used in the simulation.

5.7.3. Results of Simulation

The results of the simulations for can rotation were compared with those reported in the previous case (Section 5.6) for the same can containing the same soup but undergoing no rotation. Figure 5.22 shows the $r-z$ plane velocity vector of carrot-orange soup in the can heated by condensing steam for periods of 180 s, 1,000 s, and 3,000 s. Figure 5.22 also shows the formation of two high-velocity regions located close to the two ends of the can, but as time progresses, the two regions merge into one region covering the whole cross section of the can. The comparison between the velocity vector presented in Figures 5.22 and 5.23 shows the absence of secondary flow in the rotating can. This is expected due to the dominating effect of rotation when compared to the effect of natural convection only. The general behavior of the fluid motion in the nonrotated horizontal can was explained in detail in the previous case (Section 5.6).

The $r-z$ plane temperature profiles are presented in the form of isotherms, as shown in Figure 5.24. After 180 s of heating, the isotherms are almost identical to those usually obtained in pure conduction heating. As heating progresses (at $t = 600$ s, 1,000 s, 1,800 s, and 2,400 s), the isotherms are influenced by convection. The shape of the SHZ seen in Figures 5.24b–5.24f gradually takes the form of a distorted ellipse, which settles down at the lower half of the can, due to the effect of natural convection. In the stationary can, the SHZ covers the whole length of the can (Section 5.6), while it is found to lie at the center of the axis in the rotated can (Figures 5.24c–5.24f).

Figure 5.25 shows the r–θ plane temperature profiles of the same rotating can shown in Figure 5.24 (note that the can shown in this figure is in the horizontal position, and the inclination shown is only to provide a 3-D image). This figure shows the combined effect of natural convection and forced convection due to can rotation. As heating progresses, the SHZ splits into two distinct regions, which is unlike what has been observed previously in the stationary can when the SHZ remains as a single region settled at the bottom of the can. At the end of heating (3,000 s), the temperature of the SHZ reaches 109°C, while it is only 105°C in the stationary can. By taking the profiles of Figure 5.25f, it is found that the volume of the SHZ covers less than 5% of the total volume of the horizontal rotated can at the end of heating (3,000 s). The corresponding values for the stationary vertical and horizontal cans are about 20% and 10% respectively. The observed shrinkage of the SHZ in the rotating can is due to the significant mixing caused by can rotation.

Figure 5.26 shows the temperature profiles in the can at different z-planes. At the plane near the end of the can (Figure 5.26a), the temperature of the soup has reached 121°C almost at all the locations within that plane. However the z-plane near the center (Figure 5.26b) shows the two distinct SHZ regions with a temperature of only 109°C.

The variation in the temperature of the SHZ with time for both rotated and stationary cans is shown in Figure 5.27. The results indicate some improvement in the heating process due to a mild rotation of 10 rpm.

5.8. THERMAL STERILIZATION OF SOLID–LIQUID FOOD MIXTURE IN CANS

For solid food with conduction heating, the location of the SHZ can be determined experimentally (Pflug, 1975) since it lies always at the geometric center of the can. On the other hand, for liquid

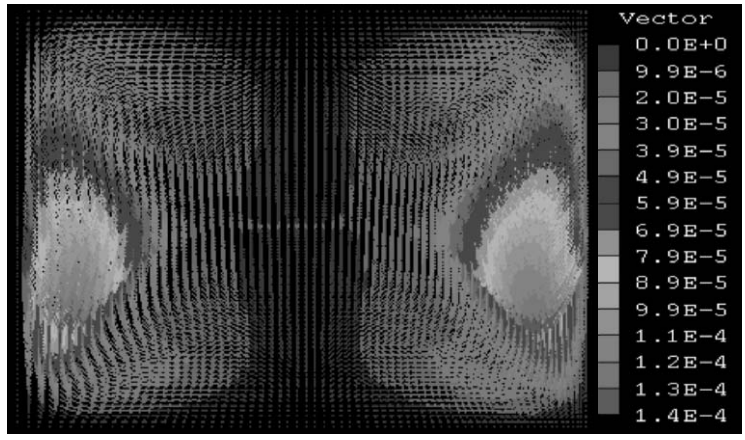

(a)

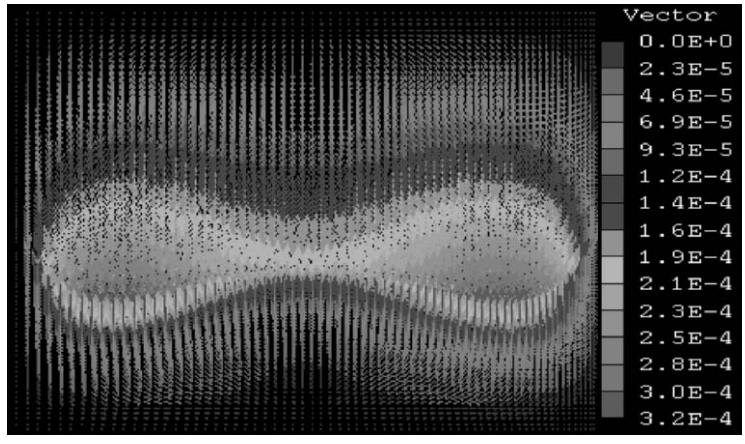

(b)

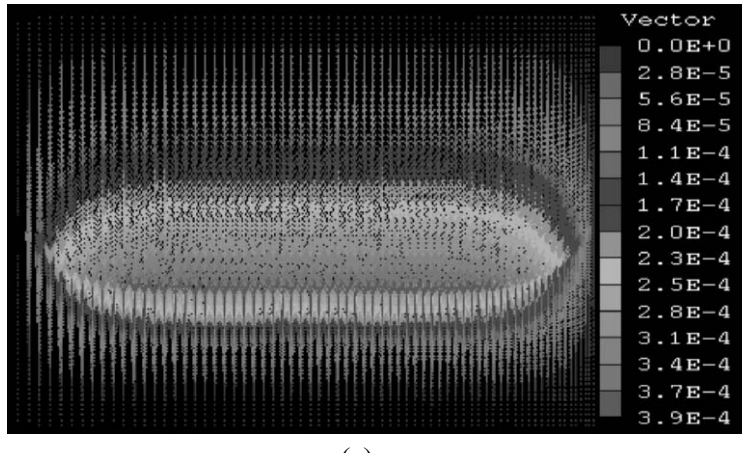

(c)

Figure 5.22. The $r-z$ plane velocity vector profiles (m s^{-1}) of carrot-orange soup in a 3-D cylindrical can rotated axially at 10 rpm and heated by condensing steam after periods of (a) 180 s, (b) 1,000 s, and (c) 3,000 s.

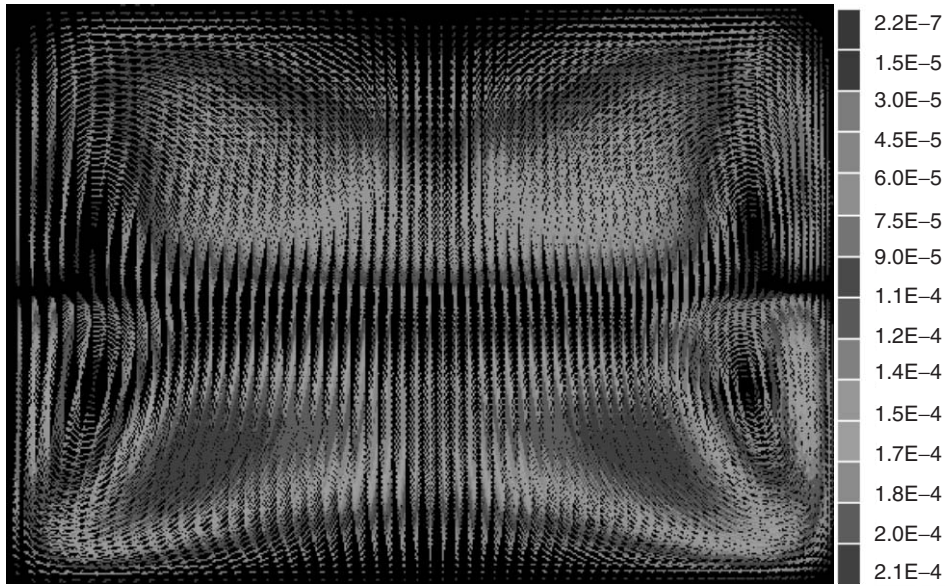

Figure 5.23. The $r-z$ plane velocity vector profile (m s^{-1}) of carrot-orange soup in a 3-D cylindrical can lying horizontally and heated by condensing steam (constant wall temperature, variable viscosity) after 1,000 s (Ghani et al., 2002).

food, the determination of the SHZ is a difficult task and requires numerical solutions of the PDEs describing fluid motion and heat transfer as discussed earlier.

The solid in a mixture of solid–liquid food, such as the one analyzed in this section, is heated by conduction, while heat transfer in the liquid is dominated by natural convection (Kumar et al., 1990). However, the heating time is usually calculated based on the assumption that the solid–liquid heats up by pure conduction. Ignoring the effect of natural convection in the liquid leads to heating times much longer than needed, which results in overprocessed products (Naveh et al., 1983).

The analysis presented in this section for solid food (pineapple slices) as impermeable and permeable to the flow of the syrup contained within the can has not been presented earlier. The study shows the action of the natural convection in the fluid, which plays an important role in the heating of the solid–liquid food mixture.

Flow pattern, temperature distribution, and shapes of the SHZ during heating of a solid–liquid food mixture (pineapple slices saturated with syrup) in a cylindrical can are predicted. The PDEs describing the conservation of mass, momentum, and energy are solved numerically using the same commercial CFDsoftware used in previous cases. Saturated steam at 121°C is used as a heating medium, where the metal can is heated from all sides. The model liquid is assumed to have constant properties except for the viscosity (temperature dependent) and density (Boussinesq approximation). Two methods of analysis are adopted in the simulation. In one of the methods, the pineapple slices are assumed permeable to syrup flow in their pores, while in the second method, the pineapple slices are assumed impermeable. The simulations also show the action of natural convection on the rate of heating, on the liquid flow pattern, and on the shape and movement of the SHZ.

5.8.1. Basic Model Equations and Solution Procedure

For the solid–liquid food mixture used in this study, the computations were performed for a can with a radius of 42 mm and height of 82 mm, as shown in Figure 5.28. The choice of the dimensions

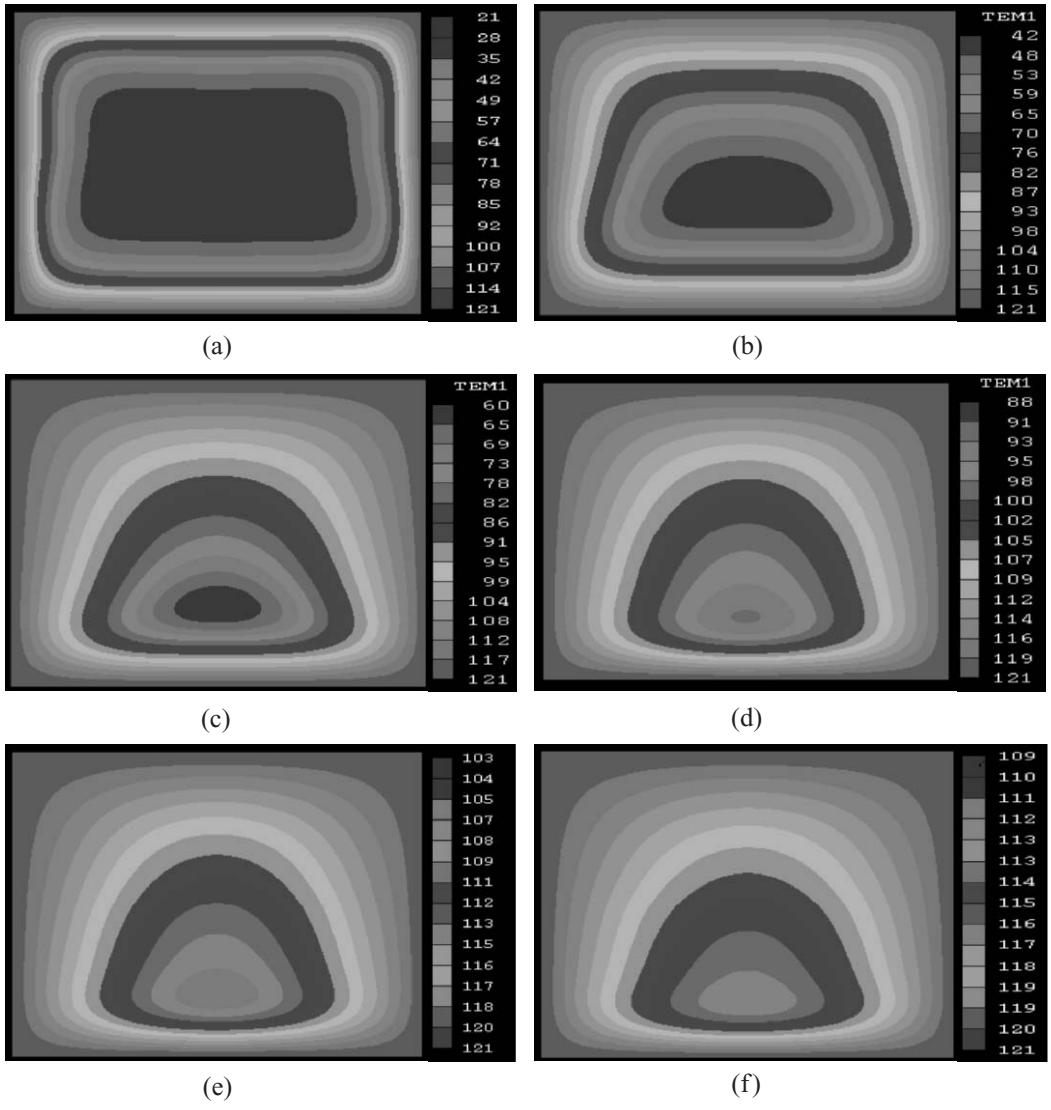

Figure 5.24. The $r-z$ plane temperature profiles of carrot-orange soup in a 3-D cylindrical can rotated axially at 10 rpm and heated by condensing steam after periods of (a) 180 s, (b) 600 s, (c) 1,000 s, (d) 1,800 s, (e) 2,400 s, and (f) 3,000 s.

of the can was similar to that usually used commercially. The can's outer surface temperature (top, bottom, and side) was assumed to rise instantaneously and be maintained at 121°C throughout the heating period. Two solid (pineapple slices) configurations were simulated. The first was with the assumption that pineapple slices are separated from the base of the can by the action of the fluid motion in the can. The second configuration was with the assumption that pineapple slices are sitting firmly on the base of the can (Figure 5.29). Most of the simulations conducted were based on the first assumed configuration, which is expected to be the most likely one.

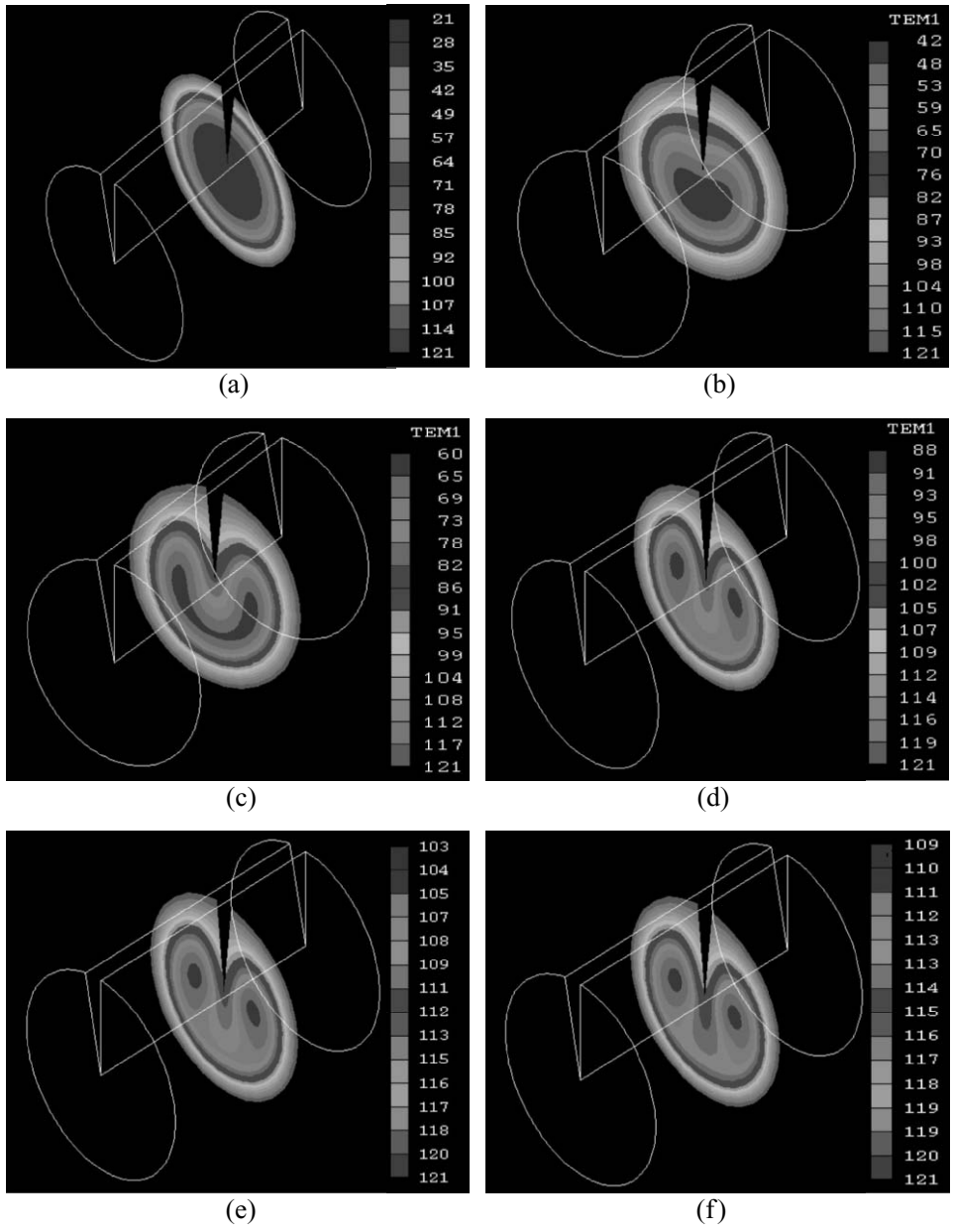

Figure 5.25. The $r-\theta$ plane temperature profiles of carrot-orange soup in a 3-D cylindrical can rotated axially at 10 rpm and heated by condensing steam after periods of (a) 180 s, (b) 600 s, (c) 1,000 s, (d) 1,800 s, (e) 2,400 s, and (f) 3,000 s.

5.8.1.1. Governing Equations and Boundary Conditions for the Pineapple Juice (Free Liquid)

The PDEs governing natural convection motion of the liquid food (pineapple syrup) contained with solid (pineapple slices) in a cylindrical space are the Navier–Stokes equations in cylindrical coordinates (Bird et al., 1976) and hence are the same as those given by Equations (5.1) to (5.4). The boundary conditions used are also the same as those given by Equations (5.5)–(5.8).

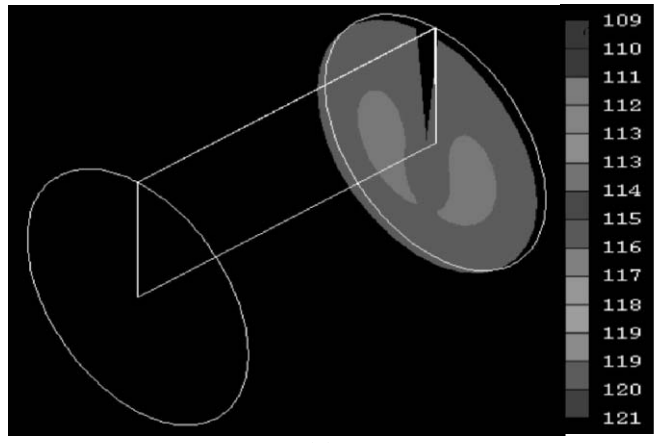

(a)

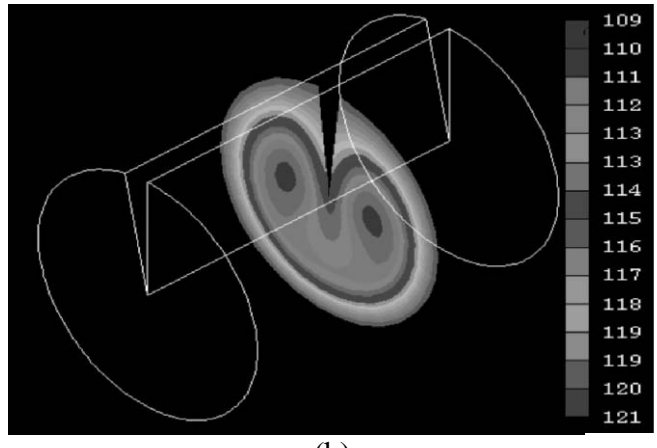

(b)

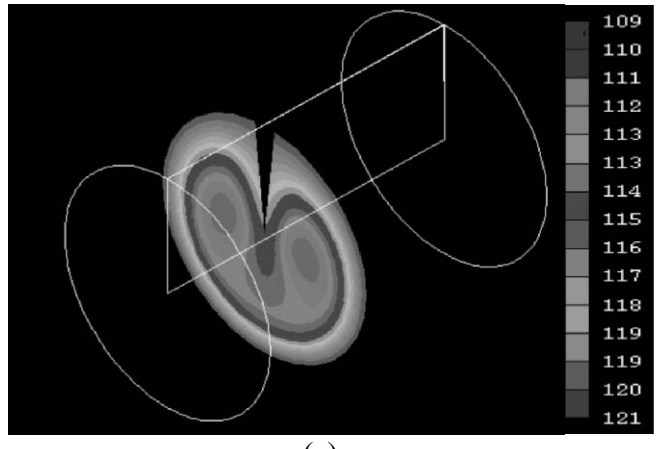

(c)

Figure 5.26. The $r-\theta$ plane temperature profiles of carrot-orange soup in a 3-D can rotated axially at 10 rpm and heated by condensing steam after a period of 3,000 s of heating and at different z-planes of (a) 0.0078 m, (b) 0.0055 m (center), and (c) 0.0780 m.

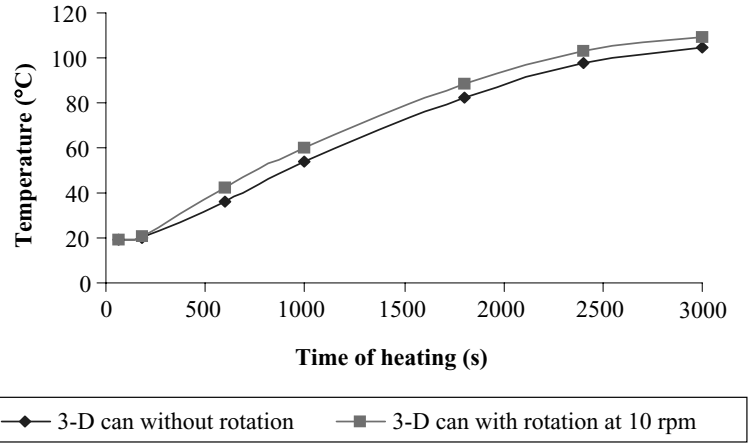

Figure 5.27. Transient temperature of carrot-orange soup at the SHZ in a 3-D can lying horizontally and heated by condensing steam with and without rotation during 3,000 s of heating.

5.8.1.2. Governing Equations for the Pineapple Slices (Solid)

Two different scenarios were investigated in the simulation of pineapple slices. In the first scenario the pineapple slices are modeled as an impermeable solid, where heat is transferred by conduction only. In this case, the two convection terms in the left-hand side of the energy Equation (5.2) can be omitted, reducing the governing equation to the well-known heat diffusion equation. In the second

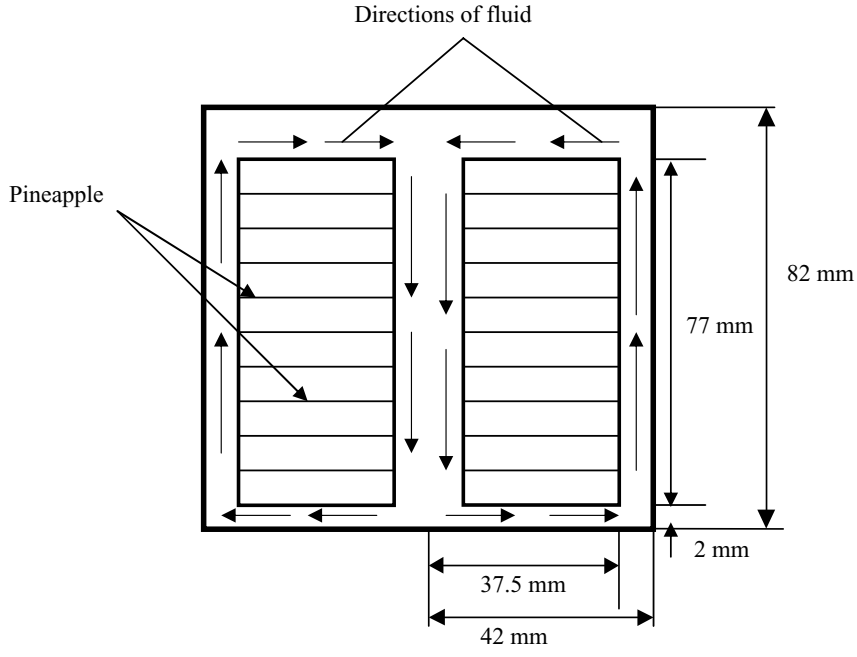

Figure 5.28. Sketch of the can containing syrup or pineapple slices.

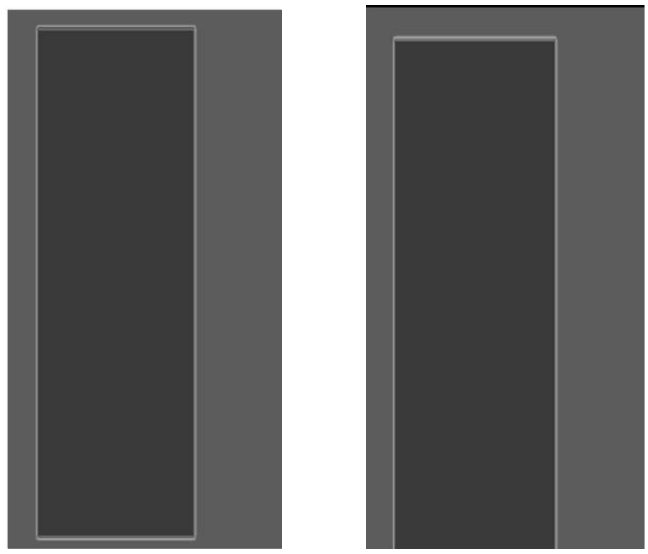

Figure 5.29. The two configurations assumed in the simulations: (a) the pineapple slices are floating in the syrup, and (b) the pineapple slices are sitting firmly on the base of the can. The right-hand side of each figure is the centerline.

scenario, the pineapple slices were modeled as a permeable porous solid, allowing the juice to flow through them, following Darcy's law.

Pineapple Slices as an Impermeable Solid

The effective thermal diffusivity of solid pineapple with the syrup contained in its pores is defined as follows:

$$\alpha_{\mathrm{m}} = \frac{k_{\mathrm{m}}}{(\rho C_{\mathrm{p}})_{\mathrm{m}}} \tag{5.31}$$

where k_{m} and $(\rho C_{\mathrm{p}})_{\mathrm{m}}$ are the weighted average values calculated from the known properties of solid pineapple and its juice (Nield and Bejan, 1992).

$$k_{\mathrm{m}} = k_{\mathrm{f}}\phi + k_{\mathrm{s}}(1-\phi) \tag{5.32}$$

$$(\rho C_{\mathrm{p}})_{\mathrm{m}} = (\rho C_{\mathrm{p}})_{\mathrm{f}}\phi + (\rho C_{\mathrm{p}})_{\mathrm{s}}(1-\phi) \tag{5.33}$$

where ϕ is the moisture content or porosity of the pineapple slices, and m, f, and s are the subscripts that refer to the porous medium, fluid, and solid, respectively.

A few pineapple slices were used for porosity (ϕ) measurements. These slices were placed in an oven at 80°C for a period of 36 h for complete drying. The average weights of the pineapple slices before and after drying were 32.01 g and 6.22 g respectively. These values gave an average moisture content of 80 wt%.

As discussed earlier, the energy conservation Equation (5.2) can be simplified to

$$\frac{\partial T}{\partial t} = \alpha_m \left[\frac{1}{r} \frac{\partial}{\partial r} \left(r \frac{\partial T}{\partial r} \right) + \frac{\partial^2 T}{\partial z^2} \right] \tag{5.34}$$

where α_m is the thermal diffusivity of the porous medium.

The physical properties used in the simulation were $\rho_s = 1{,}010$ kg m^{-3}, $(C_p)_s = 3{,}490$ J kg^{-1} K^{-1}, and $k_s = 0.549$ W m^{-1} K^{-1} for the pineapple slices. For the syrup (sucrose) used, these properties were $\rho_f = 988$ kg m^{-3}, $(C_p)_f = 3800$ J kg^{-1} K^{-1}, and $k_f = 0.434$ W m^{-1} K^{-1} (Hayes, 1987; Rahman, 1995). In the simulations presented here, the viscosity of the syrup (sucrose) was assumed to be a function of temperature, following a second-order polynomial (Equation [5.10]). Nonlinear curve fitting was used to fit the available measurements to obtain the constants of the polynomial.

Pineapple Slices as a Porous Solid

The pineapple slices used in this work can be assumed as a single consolidated porous solid. Darcy's law was implemented in the momentum equations, with permeability values of 10^{-8} m^2 and 10^{-7} m^2, as will be discussed in the following section.

The medium (i.e., pineapple slices) was generally modeled and assumed as an array of parallel fibers (rods) aligned perpendicular to the flow, which is the case relevant to the present work. Based on this assumption, the permeability (K) may be calculated as follows (Davis and James, 1996):

$$\frac{K}{a^2} = \frac{1}{8\phi} \left[\ln\left(\frac{1}{\phi} \right) - 1.476 + 2\phi \right] \tag{5.35}$$

where K is the permeability in the Darcy's law, ϕ is the porosity (volume of voids/total volume), and a is radius of the pineapple fiber.

For example, for a pore with fiber radii (a) of 1.0 mm and 0.5 mm, the permeability (K) values are 5.4×10^{-8} m^2 and 1.4×10^{-8} m^2 respectively for the square array. For the hexagonal array, the corresponding equation is the same except the constant being 1.490 instead of 1.476. This give values of permeability (K) of 5.2×10^{-8} m^2 and 1.3×10^{-8} m^2 for the two fiber sizes. These approximate values of permeability were obtained using a constant porosity of $\phi = 0.8$, as measured experimentally.

In porous media, the conservation equations for a radial geometry are as follows (Beck, 1972; Trivesan and Bejan, 1985):

Continuity equation:

$$\frac{1}{r} \frac{\partial}{\partial r} (r \rho v_{r_D}) + \frac{\partial}{\partial z} (\rho v_{z_D}) = 0 \tag{5.36}$$

Energy conservation:

$$(\rho C_p)_m \frac{\partial T}{\partial t} + (\rho C_p)_f \left(v_{r_D} \frac{\partial T}{\partial r} + v_{z_D} \frac{\partial T}{\partial z} \right) = k_m \left(\frac{1}{r} \frac{\partial}{\partial r} \left(r \frac{\partial T}{\partial r} \right) + \frac{\partial^2 T}{\partial z^2} \right) \tag{5.37}$$

Momentum equation in the vertical direction:

$$v_{z_D} = -\frac{K}{\mu} \frac{\partial P}{\partial z} + \rho_f g \tag{5.38}$$

Momentum equation in the radial direction:

$$v_{r_D} = -\frac{K}{\mu}\frac{\partial P}{\partial r} \tag{5.39}$$

By the use of the Depuit–Forchhiemer relationship, Darcy's velocities v_{r_D} and v_{z_D} can be written as follows (Nield and Bejan, 1992):

$$v_{r_D} = \phi V_r \tag{5.40}$$

$$v_{z_D} = \phi V_z \tag{5.41}$$

where v_{r_D} andv_{z_D} are Darcy's velocities in radial and axial directions respectively, and V_r and V_z are the intrinsic velocities in radial and axial directions. The boundary conditions used for the solid were the same as those used in Section 5.8.1.1.

5.8.1.3. Computational Grid

Through a mesh refinement study, a nonuniform grid system was used through the solid and liquid in the can. In the simulations, 3,444 nodal points were used: 42 in the radial direction and 82 in the axial direction, graded in both directions with a finer grid near the wall. The natural convection heating in the liquid and the conduction in the solid was simulated for 3,000 s, and the time steps were the same as those used in Section 5.5.

5.8.1.4. Assumptions Used in the Simulations

The simplifying assumptions used in the simulation were the same as those used in Section 5.2.1.5. Additional assumptions made are as follows:

1. The permeability of a periodic fibrous media is either a square or hexagonal array.
2. The permeability is homogenous and isotropic and remains constant throughout the heating process.
3. The pineapple slices are assumed either floating in the juice or sitting firmly in the can with no motion.

5.8.2. Results of Simulation

Figure 5.29a shows the most likely case of pineapple slices floating in juice, and Figures 5.30 and 5.31 show the results of the simulation (flow pattern and temperature profile) for a can heated by condensing steam from all sides in a still retort. Figure 5.32 shows the temperature profile for the same can but assuming the pineapple slices are sitting firmly on the base of the can.

5.8.2.1. Flow Pattern

The liquid and the solid adjacent to the wall, top, and bottom surfaces will receive heat from the condensing steam. As the liquid is heated, it expands and thus becomes lighter. The liquid away from the side wall (in the middle of the pineapple slices) stays at a much lower temperature. The buoyancy force created by the change in liquid density due to temperature variation (from the wall to

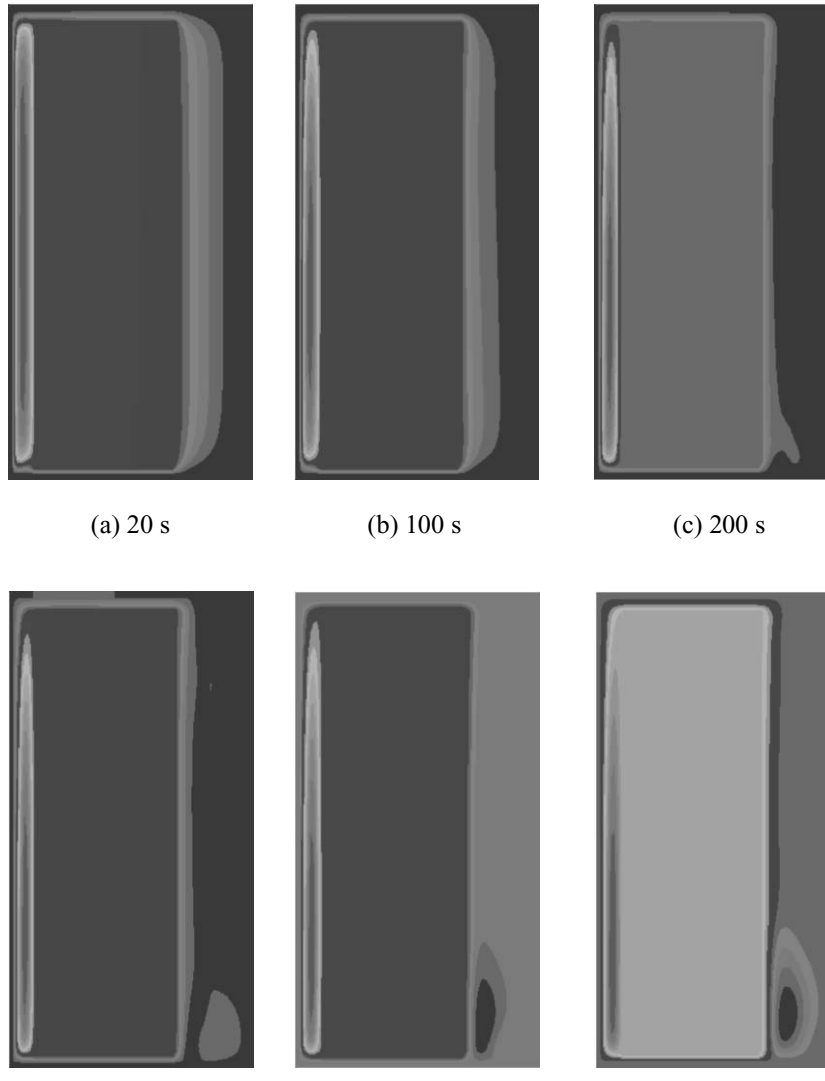

Figure 5.30. Streamlines of a solid–liquid food mixture (pineapple slices floating in the syrup) in a cylindrical can heated by condensing steam for periods of (a) 20 s, (b) 100 s, (c) 200 s, (d) 600 s, (e) 1,000 s, and (f) 2,000 s. The right-hand side of each figure is the centerline.

the core) produces an upward flow near the side wall. The hot liquid going up is deflected by the top wall and then travels radially toward the center of the pineapple slices. Being heavier, the liquid in the core moves downward and then radially toward the wall. Thus a recirculating flow is created. For the solid food (the pineapple slices), heat is transferred by conduction in the first scenario (Section Pineapple Slices as an Impermeable Solid) and by both conduction and convective flow through the pores in the second scenario (Section Pineapple Slices as a Porous Solid).

Figure Pineapple Slices as a Porous Solid shows that the liquid next to the wall is at rest because of the no-slip boundary conditions. It also shows different velocities within the rest of the can, shown

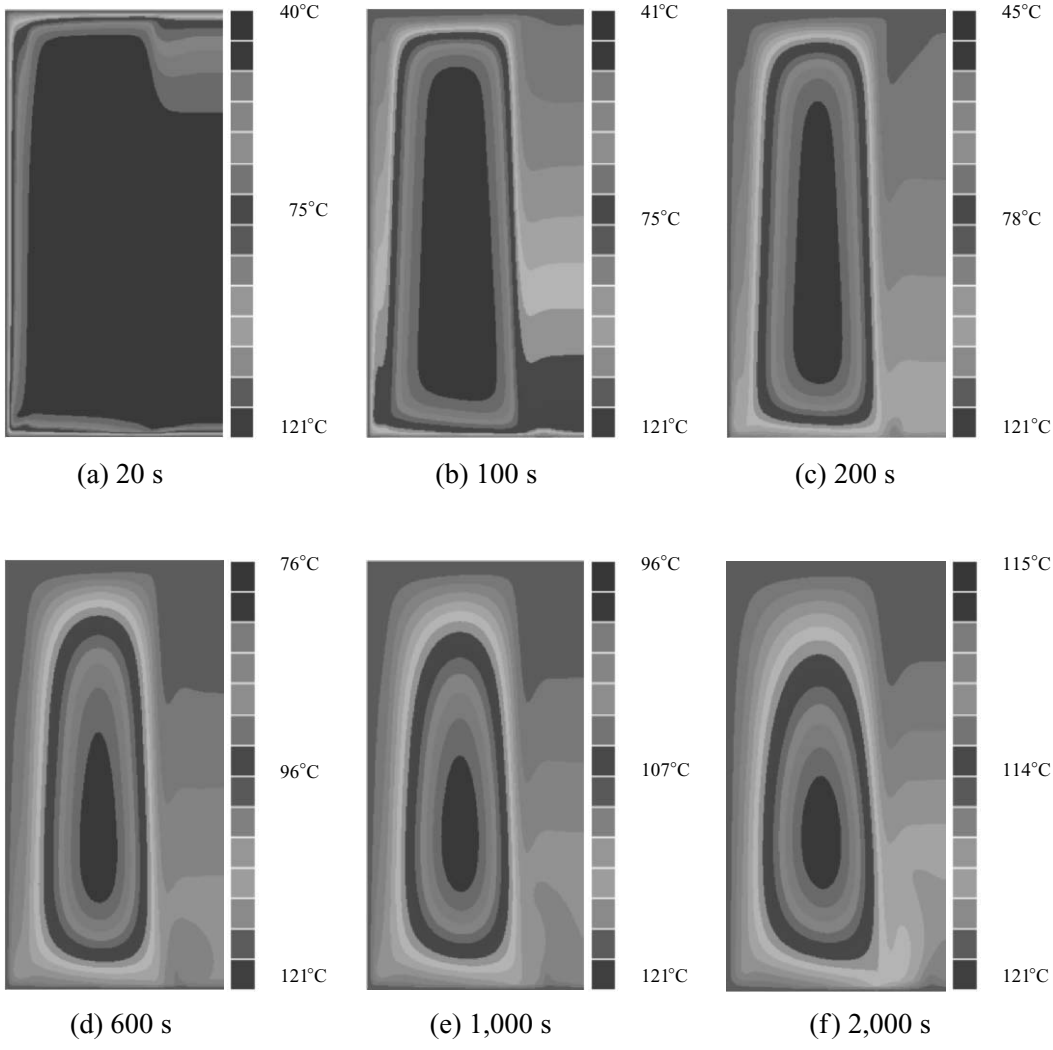

Figure 5.31. Temperature contours of a solid–liquid food mixture (pineapple slices floating in the syrup) in a cylindrical can heated by condensing steam for periods of (a) 20 s, (b) 100 s, (c) 200 s, (d) 600 s, (e) 1,000 s, and (f) 2,000 s. The right-hand side of each figure is the centerline.

by the stream functions. As heating is progressed, a more uniform velocity is obtained, reducing buoyancy force in the liquid that leads to significant reduction in the velocity. The simulation shows the formation of secondary flow or eddies, which is expected whenever there is heating from the bottom.

5.8.2.2. Temperature Distribution and the Slowest Heating Zone

The temperature distribution during heating is presented in the form of isotherms in Figure 5.31 for the case of pineapple slices floating in juice for different periods of heating. The isotherms at $t = 20$ s are almost identical to pure conduction heating for both solid and liquid food in the can, but over time, the isotherms in the liquid are seen to be influenced by convection. During the initial

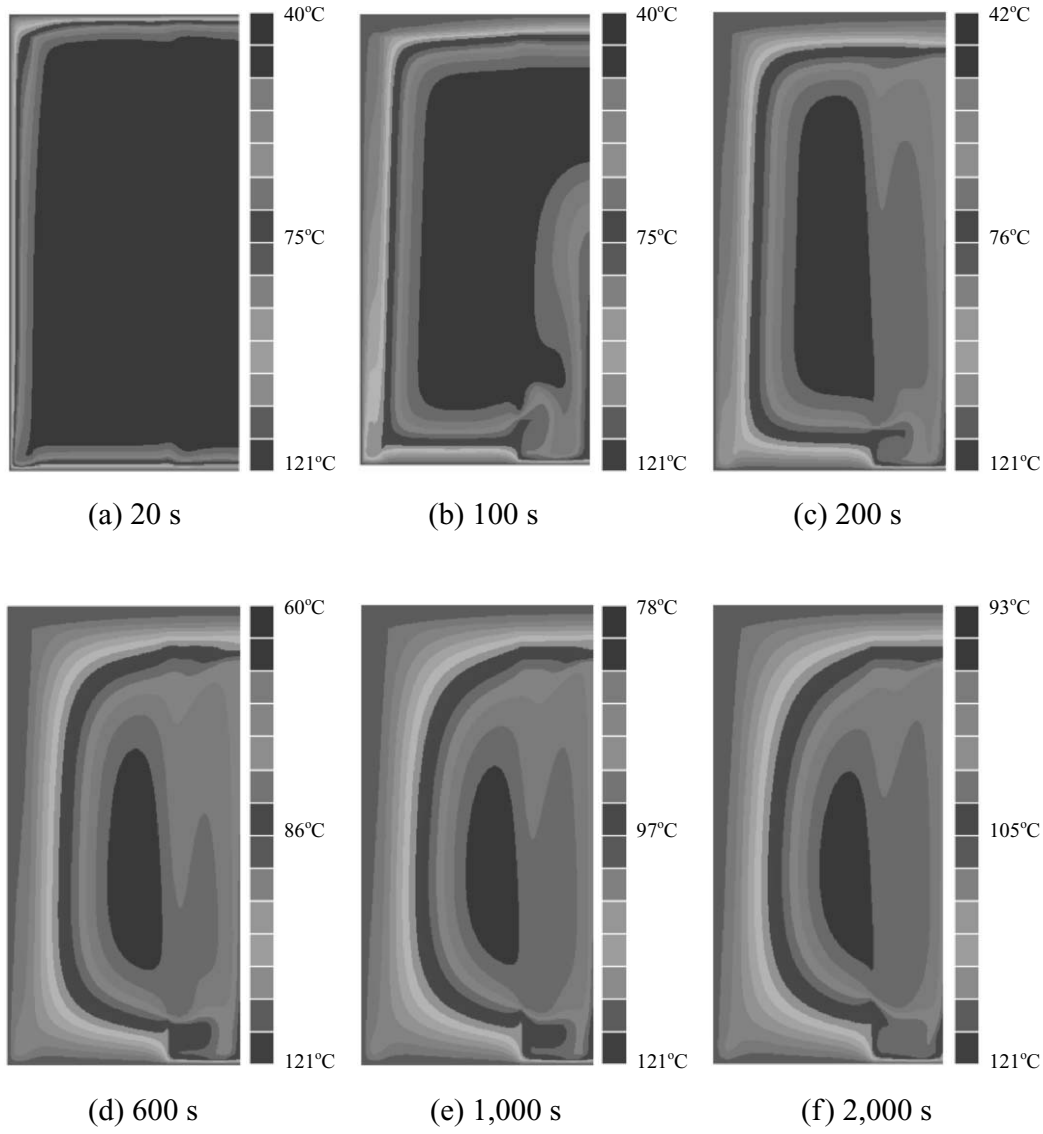

Figure 5.32. Temperature contours of a solid–liquid food mixture (pineapple slices sitting firmly on the base) in a cylindrical can heated by condensing steam for periods of (a) 20 s, (b) 100 s, (c) 200 s, (d) 600 s, (e) 1,000 s, and (f) 2,000 s. The right-hand side of each figure is the centerline.

heating period, the fluid near the bottom is heated by conduction. However, instability soon results from the large difference in the temperature between the heated bottom and the colder liquid coming in contact with it. This instability in the bottom layer gives rise to bursts of convective cells (i.e., the Benard convection cells). Figure 5.31 shows the irregular shape of the isotherms near the bottom, which is caused by the random nature of Benard convective cell formations.

Traditionally, the movement of the SHZ (i.e., the location of the lowest temperature at a given time) is a critical parameter in identifying food product sterility. As before, the SHZ in the can is not considered a stationary region lying in the middle of the solid food (pineapple slices) due to the

effect of liquid (syrup) undergoing convection heating. Initially the content of the can is at uniform temperature. As heating progresses (at $t = 100$ s), the temperature profiles become very different from those observed at the beginning of the heating (Figure 5.31a). The temperature profiles change as the mode of heat transfer in the liquid changes from conduction to convection. At this stage, the buoyancy force starts to be effective due to temperature variation of the liquid from the wall to the core. At later stages of heating, the flow of the hot liquid food coming from the side walls of the can will push the SHZ from the geometric center toward the bottom of the can, as shown clearly in Figures 5.31d–5.31f. The SHZ keeps moving during heating and eventually stays in a region that is about 30–35% of the can height from the bottom. The corresponding location of the SHZ for the can filled with only liquid was found to be at 10–12% of the can height from the bottom (Ghani et al., 1999a). Such an effect is expected, as the presence of solid reduces the effect of natural convection in the fluid causing the SHZ to move upward.

The temperature distribution during heating for the case of pineapple slices sitting firmly on the base of the can is presented in the form of isotherms in Figure 5.32, which shows much slower heating than that shown previously in Figure 5.31. This is due to the reduced effect of natural convection, caused by the presence of solid, which minimizes fluid circulation in the can. The assumption of the pineapple slices sitting at the base of the can (Figure 5.32) caused the SHZ to move closer toward the geometric center of the can. According to this finding, careful consideration must be made in estimating the thermal sterilization time of a solid-liquid food mixture. The temperature of the SHZ reached about 105°C in 2,000 s for the case of pineapple slices floating in the can, in comparison to 93°C for the case of pineapple slices sitting firmly on the base of the can.

NOMENCLATURE

a	radius of the particle, m
C	concentration of bacteria (number of bacteria m^{-3}) and vitamin (kg m^{-3})
C_p	specific heat of liquid food, J kg^{-1} K^{-1}
D	diffusion coefficient, m^2 s^{-1}
E	activation energy, kJ (kg mol)$^{-1}$
Gr	Grashof number, Gr $= \frac{d_v^3 \rho^2 g \beta \Delta T}{\mu^2}$, dimensionless
g	acceleration due to gravity, m s^{-2}
H	height of the geometry, m
K	permeability, m^2 (10^{-12} m^2 = Darcy)
k	thermal conductivity, W m^{-1} K^{-1}
K_B	Boltzman constant, dimensionless
L	length of the geometry, m
n	flow behavior index, 1
p	pressure, Pa
Pe	Peclet number, Pe $= \frac{v_z \Delta z}{\alpha}$, dimensionless
r	radial position from the centerline, m
R	radius of the can, m
R_g	gas constant, kJ (kg mol^{-1} K^{-1})
t	time, s
T	temperature, °C
V	Intrinsic velocity, m s^{-1}
v	velocity, m s^{-1}

α thermal diffusivity, $m^2\ s^{-1}$
β thermal expansion coefficient, K^{-1}
γ shear rate, s^{-1}
η_0 consistency index
μ viscosity, Pa s
ρ density, kg m^{-3}
ρ_{ref} reference density, kg m^{-3}
ϕ porosity, dimensionless
ω rotational velocity, rad s^{-1}

Subscripts

ave average
b bacteria
b_0 initial for bacteria
D Darcy's
f fluid
m mixed
R radius of the can
r radial direction
rb relative bacteria
ref reference
rv relative vitamin
s solid
v vitamin
v_0 initial for vitamin
w wall
z vertical or axial direction
x, y, z coordinates
θ angular direction

REFERENCES

Adrian, B. (1993). *Heat transfer* (pp. 339–340). New York: John Wiley & Sons.

Akterian, S.G. (1994). Numerical simulation of unsteady heat conduction in arbitrary shaped canned foods during sterilization processes. *Journal of Food Engineering, 21*, 343–354.

Beck, J.L. (1972). Convection in a box of porous material saturated with fluid. *The Physics of Fluids, 15*, 1377.

Berry, M.R., Savage, R.A., & Pflug, I.J. (1979). Heating characteristics of cream-style corn processed in a steritort: effects of headspace reel speed and consistency. *Journal of Food Science, 44*, 831–835.

Bird, R.B., Stewart, W.E., & Lightfoot, E.N. (1976). *Transport phenomena*. New York: John Wiley & Sons.

Cox, P.W., & Fryer, P.J. (2001). Food process analysis and modelling using novel flow and thermal history indicators. Sixth World Congress of Chemical Engineering, 23–27 September 2001, Melbourne, Australia.

Datta, A.K., & Teixeira, A.A. (1988). Numerically predicted transient temperature and velocity profiles during natural convection heating of canned liquid foods. *Journal of Food Science, 53*(1), 191–195.

Datta, A.K., & Teixeira, A.A. (1987). Numerical modeling of natural convection heating in canned liquid foods (Report No. 86-6516). St. Joseph, MI: Transaction of American Society of Agricultural Engineers.

Davis, A.M.J., & James, D.F. (1996). Slow flow through a model of fibrous porous medium. *International Journal of Multiphase Flow, 22*, 969.

Ghani, A.G., Farid, M.M., Chen, X.D., & Richards, P. (1999). Heat transfer and biochemical changes in liquid food during sterilization using computational fluid dynamics (CFD). CHEMICA 99 Conference, 26–29 September 1999, Newcastle, Australia.

Ghani, A.G., Farid, M.M., Chen, X. D., & Richards, P. (1999a). Numerical simulation of natural convection heating of canned food by computational fluid dynamics. *Journal of Food Engineering, 41*(1), 55.

Ghani, A.G., Farid, M.M., Chen, X.D., & Richards, P. (1999b). An investigation of deactivation of bacteria in canned liquid food during sterilization using computational fluid dynamics (CFD). *Journal of Food Engineering, 42*, 207.

Ghani, A.G., Farid, M.M., Chen, X.D., & Watson, C. (2000). Numerical simulation of transient two-dimensional profiles of temperature and flow velocity of canned food during sterilization. Eighth International Congress on Engineering and Food (ICEF8), April 2000, Pueblo, Mexico.

Ghani, A.G., Farid, M.M., Chen, X.D., & Richards, P. (2000a). Thermal sterilization of canned food in a 3-D pouch using computational fluid dynamics. *Journal of Food Engineering, 48*, 147–156.

Ghani, A.G., Farid, M.M., Chen, X.D., & Richards, P. (2001). A computational fluid dynamics study on the effect of sterilization temperatures on bacteria deactivation and vitamin destruction. *Journal of Process Mechanical Engineering, 215*, Part E, 1–9.

Ghani, A.G., Farid, M.M., & Chen, X.D. (2002a). Numerical simulation of transient temperature and velocity profiles in a horizontal can during sterilization using computational fluid dynamics, *Journal of Food Engineering, 51*, 77–83.

Ghani, A.G., Farid, M.M., & Chen, X.D. (2002b). Theoretical and experimental investigation of the thermal destruction of Vitamin C in food pouches. *Journal of computers and Electronics in Agriculture—special issue on "Applications of CFD in the Agri-food Industry," 34*, 129–143.

Giner, J., Ibarz, A., Garza, S., & Xhian-Quan (1996). Rheology of clarified cherry juices. *Journal of Food Engineering, 30*, 147–154.

Hayes, G.D. (1987). *Food engineering data handbook*. New York: John Wiley & Sons.

Hiddink, J. (1975). Natural convection heating of liquids, with reference to sterilization of canned food (Agricultural Research Report No. 839). Wageningen, The Netherlands: Center for Agricultural Publishing and Documentation.

Holman, J.P., & White, P.R.S. (1992). *Heat transfer*. U.K.: McGraw-Hill International.

Krishnamurthy, H., Ramaswamy, H.S., Sanchez, G., Sablani, S., & Pandey, P.K. (2001). Effect of guar gum concentration, rotation speed, particle concentration, retort temperature, and diameter of rotation on heat transfer rates during end-over-end processing of canned particulate non-Newtonian fluids. *Proceedings of the Eighth International Congress on Engineering and Food (ICEF8), Pueblo, Mexico, Volume 1*, 665–670, Lancaster, Pennsylvania 17604: Technomic.

Kumar, A., & Bhattacharya, M. (1991). Transient temperature and velocity profiles in a canned non-Newtonian liquid food during sterilization in a still—cook retort. *International Journal of Heat and Mass Transfer, 34*(4/5), 1083–1096.

Kumar, A., Bhattacharya, M., & Blaylock, J. (1990). Numerical simulation of natural convection heating of canned thick viscous liquid food products. *Journal of Food Science, 55*(5), 1403–1411.

Luh, B.S., Fienberg, B., Chung, J.I., & Woodroof, J.G. (1986). *Freezing fruits in commercial fruit processing* (pp. 263–351). Westport, CT: AVI.

Malin, M.R., & Waterson, N.P. (1999). Schemes for convection discretization on PHOENICS. *The PHOENICS Journal, 12*(2), 173–201.

Mills, A.F. (1995). *Basic heat and mass transfer*. Irwin. Upper Saddle River, N.J., Prentice Hall.

Naveh, D., & Kopelman, I.J. (1980). Effect of some processing parameters on the heat transfer coefficients in a rotating autoclave. *Journal of Food Processing and Preservation, 4*, 67–77.

Naveh, D., Kopelman, I.J., & Pflug, I.J. (1983). The finite element method in thermal processing of foods. *Journal of Food Science, 48*, 1086.

Nield, D.A., & Bejan, A. (1992). *Convection in porous media*. New York: Springer-Verlag.

Patankar, S.V., & Spalding, D.B. (1972). A calculation procedure for heat, mass and momentum transfer in three dimensional parabolic flows. *International Journal of Heat and Mass Transfer, 15*(10), 1787–1806.

Pflug, I.J. (1975). Procedures for carrying out a heat penetration test and analysis of the resulting data. Minneapolis, MN: Environmental Sterilization Lab.

Rahman, R. (1995). *Food properties handbook*. New York: CRC Press.

Smout, C., Avila, I., Van Loey, A.M.L., Hendrickx, M.E.G., & Silva, C. (2000). Influence of rotational speed on the statistical variability of heat penetration parameters and on non-uniformity of lethality in retort processing. *Journal of Food Engineering, 45*, 93–102.

Spalding, D.B. (1972). A novel finite-difference formulation for differential expressions involving both first and second derivatives. *International Journal of Numerical Methodology Engineering, 4*, 551.

Steffe, J.F., Mohamed, I.O., & Ford, E.W. (1986). Rheological properties of fluid foods: data compilation. In M.R. Okos (Ed.), *Physical and Chemical Properties of Foods*. St. Joseph, MI: Transaction of American Society of Agricultural Engineers.

Tressler, D.K., Charley, V.L.S., & Luh, B.S. (1980). Cherry, berry and other miscellaneous fruit juices. In P.E. Nelson & D.K. Tressler (Eds.), *Fruit and Vegetable Juice Processing Technology* (pp. 310–343). Westport, CT: AVI.

Trivesan, O.V., & Bejan, A. (1985). Natural convection with combined heat and mass transfer buoyancy effects in a porous medium. *International Journal of Heat and Mass Transfer,* 28, 1597.

Tucker, G.S., & Holdsworth, S.D. (1991). Mathematical modeling of sterilization and cooking processes for heat preserved foods-applications of a new heat transfer model. *Transaction of Institution of Chemical Engineers, 69*(3), 5.

Van Loey, A., Francis, A., Hendrickx, M., Maesmans, G., Noronha, J., & Tobback, P. (1994). Optimizing thermal process for canned white beans in water cascading retorts. *Journal of Food Science, 59*(4), 828–832.

Zechman, L.G., & Pflug, I.J. (1989). Location of the slowest heating zone for natural convection heating fluids in metal containers. *Journal of Food Science, 54*, 209–226.

CHAPTER 6

THEORETICAL ANALYSIS OF THERMAL STERILIZATION OF FOOD IN 3-D POUCHES

The objective of this chapter is to present the theoretical analysis of the process of thermal sterilization of canned liquid food in a three-dimensional (3-D) pouch. The prediction of temperature distribution and the migration of the slowest heating zone (SHZ) during natural convection heating in a pouch are presented for the first time in literature. Such information may be used to optimize the industrial sterilization process with respect to sterilization temperature and time. As a result of this investigation the companies involved in thermal retorting will be able to predict the necessary sterilization time required for any pouch containing any new liquid food products. This optimization process will save both energy and time, which are of great value for thermal retorting.

Sterilization of food in cans has been well studied both experimentally and theoretically, but little work has been done on sterilization of food in pouches, which has recently been introduced to the market. The two different liquid food materials used in this study (carrot-orange soup and broccoli-cheddar soup) were some of the products of Heinz Watties Australasia located at Hastings, New Zealand. The computational fluid dynamics (CFD) code PHOENICS used in the study of cans was also used here. Saturated steam at 121°C was assumed to be the heating medium. The partial differential equations (PDEs), describing the conservation of mass, momentum, and energy, were solved numerically together with bacteria and vitamin concentrations, using the finite volume method (FVM). The liquid foods used in the simulation were assumed to have temperature-dependent viscosity and density, while other physical properties were assumed constant.

In this chapter, the following cases are discussed:

1. Temperature distribution, velocity profiles, and the migration of the SHZ during sterilization of broccoli-cheddar soup
2. Temperature distribution, velocity profiles, and the migration of the SHZ during sterilization of carrot-orange soup
3. Simulation for the same pouch but on the assumption of pure conduction heating to illustrate the effect of natural convection heating in pouches
4. The effect of the cooling period of the pouch on the sterilization of carrot-orange soup

The results of these simulations are compared with the measurements of temperature distribution in Chapter 8.

The results of the simulations show that the velocity of the liquid food in the pouch is low due to the small height of the pouch and high viscosity of the soup. In all the simulations, the SHZ was found to migrate toward the bottom of the pouch into a region within 30–40% of the pouch height,

closest to its deepest end. Sterilization time was found to be shorter than that needed for cans, which is attributed to the large surface area per unit volume of the pouch.

6.1. THE PRINCIPLES OF POUCH MODELING

6.1.1. Basic Model Equations and Solution Procedure

The computations were performed for a 3-D pouch with a width (W) of 120 mm, the maximum height (H) of 40 mm, and a length (L) of 220 mm, which present the most probable dimensions of the selected pouch when lying horizontally. The pouch's outer surface temperature (top, bottom, and sides) was assumed to rise instantaneously and remain at 121°C throughout the heating period. The effect of the retort come-up time was studied in other simulations (Appendix D) and was found very small.

6.1.2. Computational Grid and Geometry Construction

The pouch volume was divided into 6,000 cells: 20 in the x-direction, 10 in the y-direction, and 30 in the z-direction, as described in Appendix E for the construction of the pouch geometry and shown in Figure 6.1. The natural convection heating of different types of soup such as broccoli-cheddar and carrot-orange was simulated for the total time of 3,000 s and was divided into 30 time steps. It took 10 steps to achieve the first 200 s of heating, another 10 steps to reach 1,000 s, and 30 steps for the total of 3,000 s of heating. Another simulation has been done for the heating and cooling cycles during sterilization of carrot-orange soup, which was simulated for a total time of 4,800 s (Appendix F).

In the construction of the pouch geometry, Equation (6.1) for an ellipse was used for the construction of the pouch grid in the x–y plane:

$$\left(\frac{x}{y}\right)^2 + \left(\frac{y}{b}\right)^2 = 1 \tag{6.1}$$

The height of the pouch, shown in Figure 6.2, can be written as

$$y = \pm b\sqrt{1 - \left(\frac{x}{a}\right)^2} \tag{6.2}$$

The 3-D grid was constructed by using a series of 2-D grids in the x–y plane with the height varying with the z-coordinate, as shown in Figure 6.2. The elliptical boundary created a distorted rectangle of cells. However, in order to minimize the distortion of grid cells in the corner, Equation (6.1) was rewritten in terms of θ, and the discontinuity between x and y grid lines was placed at x, which can be written in terms of a, b, and θ as (Appendix G):

$$x = \sqrt{\frac{\left(\frac{a^4}{b^2}\right)\tan^2\theta}{1 + \left(\frac{a^2}{b^2}\right)\tan^2\theta}} \tag{6.3}$$

where $\tan\theta$ is the gradient of the boundary at x, with $\theta = 45°$.

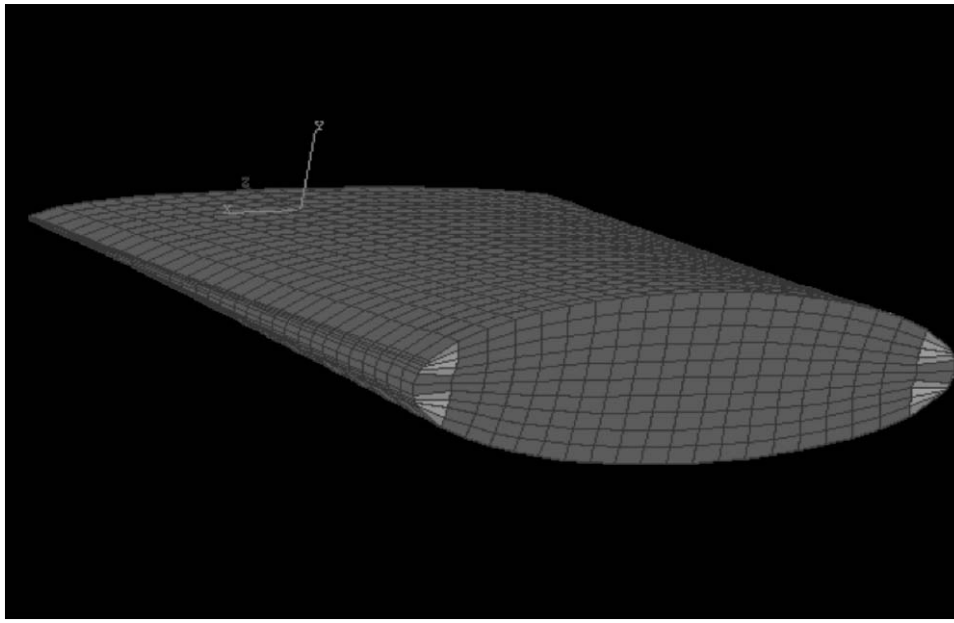

(a)

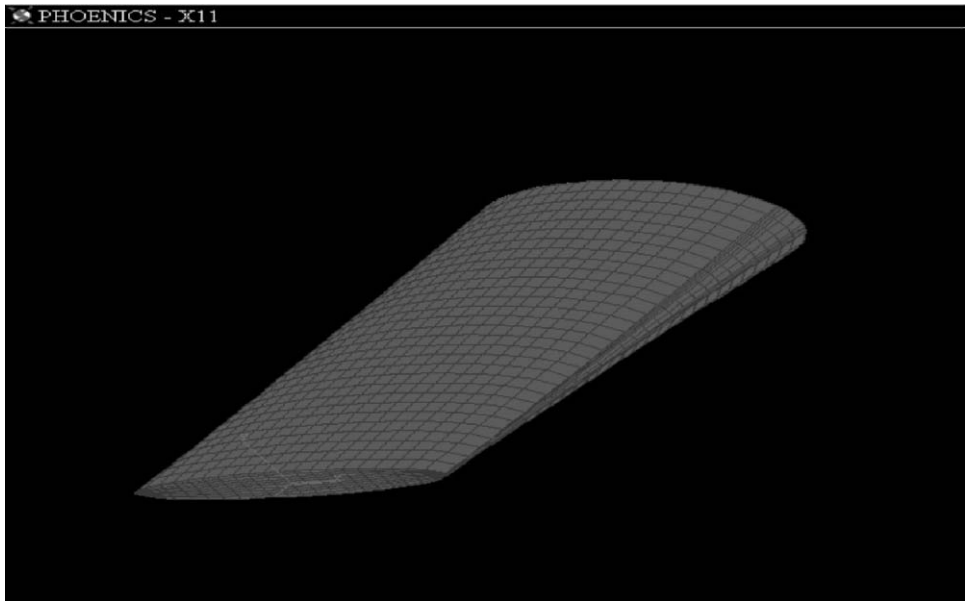

(b)

Figure 6.1. Pouch geometry and grid mesh showing (a) the widest end and (b) the narrowest end.

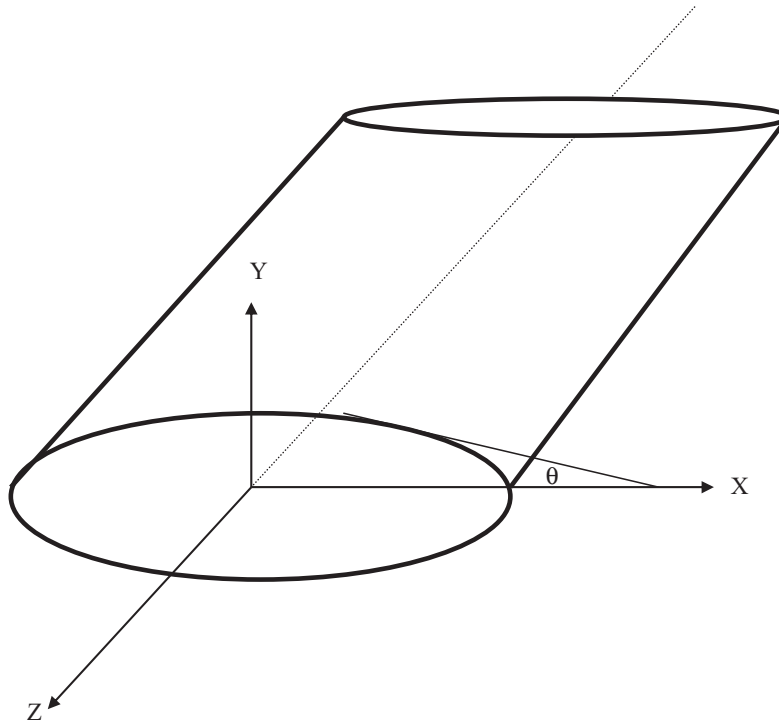

Figure 6.2. Geometry of the pouch.

The software used in the simulations was the same as the one used in the simulations of cans. The key characteristic of the method is the immediate dicretization of the integral equation of flow into the physical 3-D space (i.e., the computational domain covers the entire pouch, which was divided into a number of divisions in the three dimensions). The details of the code can be found in the PHOENICS manuals, especially the PHOENICS Input Language (PIL) manual.

In order to construct the geometry of the pouch, a body-fitted coordinate (BFC) approach was used. This was not required in the analysis of the can. For generating a curvilinear grid within the subdomain command, the option of solving PDEs for the corner coordinates within the currently active domain was used. This option involved the solution of Laplace equations for the Cartesian coordinates of the cell corners. The finite difference equations (FDE) solved for Cartesian coordinates were expressed in a linear form, so that they could be solved by means of linear equation solvers.

In the simulations, a variety of grid sizes (Figure 6.3) and time steps were used. Through mesh refinement study, it is clear from Figure 6.3 that the optimum mesh possible was the one used (20×10), which is due to the dominant orthogonal cells that lead to improve the stability of the solution. The results obtained showed that the solution reported in this study is almost time-step-independent and weakly dependent on grid size.

6.1.3. Governing Equations and Boundary Conditions

The PDEs governing natural convection motion in a pouch space are the Navier–Stokes equations in x, y, and z coordinates, as shown below (Bird et al., 1976):

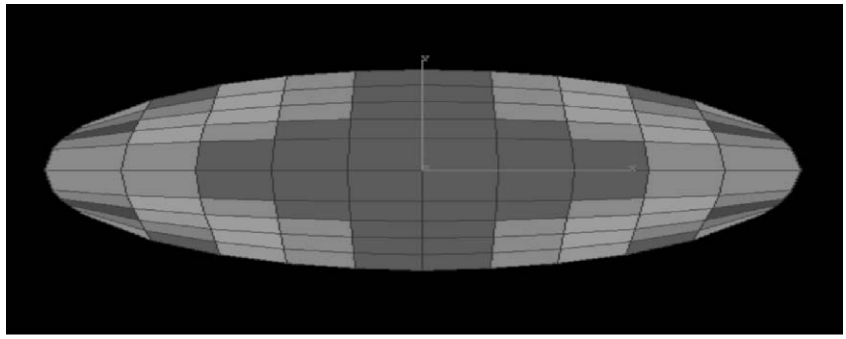

10×10

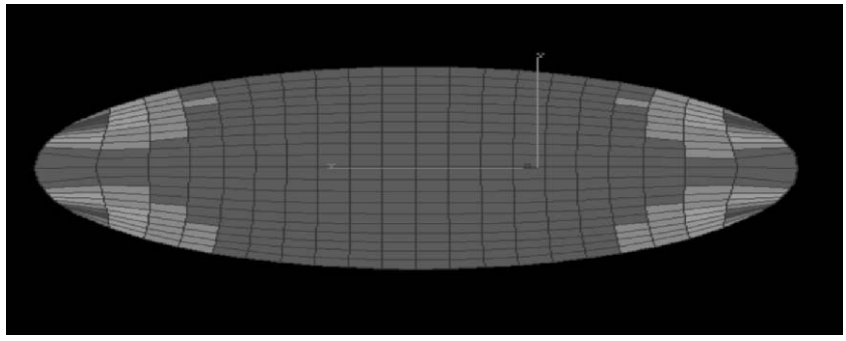

20×20

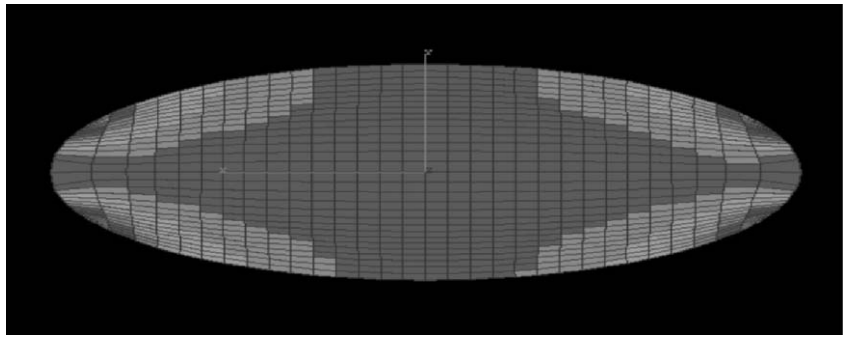

40×40

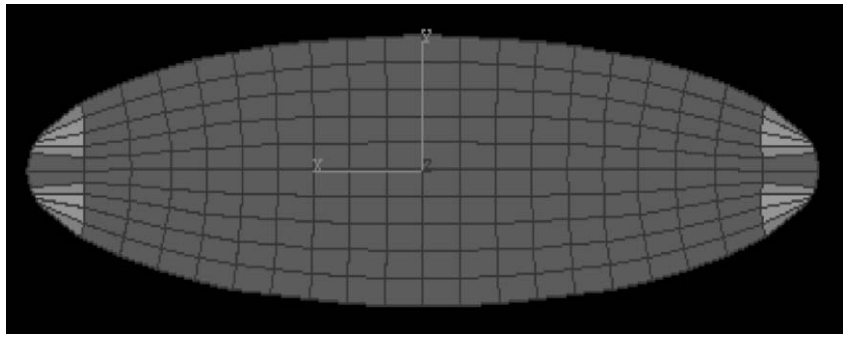

20×10

Figure 6.3. Different grid meshes used to test the cells of the pouch.

The continuity equation

$$\frac{\partial v_x}{\partial x} + \frac{\partial v_y}{\partial y} + \frac{\partial v_z}{\partial z} = 0 \tag{6.4}$$

The energy equation

$$\frac{\partial T}{\partial t} + v_x \frac{\partial T}{\partial x} + v_y \frac{\partial T}{\partial y} + v_z \frac{\partial T}{\partial z} = \frac{k}{\rho C_p}\left[\frac{\partial^2 T}{\partial x^2} + \frac{\partial^2 T}{\partial y^2} + \frac{\partial^2 T}{\partial z^2}\right] \tag{6.5}$$

The momentum equation in y-direction

$$\rho\left(\frac{\partial v_y}{\partial t} + v_x \frac{\partial v_y}{\partial x} + v_y \frac{\partial v_y}{\partial y} + v_z \frac{\partial v_y}{\partial z}\right) = -\frac{\partial P}{\partial y} + \frac{\partial}{\partial x}\left(\mu \frac{\partial v_y}{\partial x}\right) + \frac{\partial}{\partial y}\left(\mu \frac{\partial v_y}{\partial y}\right) + \frac{\partial}{\partial z}\left(\mu \frac{\partial v_y}{\partial z}\right) + \rho_{\text{ref}}\, g_x(1 - \beta(T - T_{\text{ref}}) \tag{6.6}$$

The momentum equation in x-direction

$$\rho\left(\frac{\partial v_x}{\partial t} + v_x \frac{\partial v_x}{\partial x} + v_y \frac{\partial v_x}{\partial y} + v_z \frac{\partial v_x}{\partial z}\right) = -\frac{\partial P}{\partial x} + \frac{\partial}{\partial x}\left(\mu \frac{\partial v_x}{\partial x}\right) + \frac{\partial}{\partial y}\left(\mu \frac{\partial v_x}{\partial y}\right) + \frac{\partial}{\partial z}\left(\mu \frac{\partial v_x}{\partial z}\right) + \rho g_x \tag{6.7}$$

The momentum equation in z-direction

$$\rho\left(\frac{\partial v_z}{\partial t} + v_x \frac{\partial v_z}{\partial x} + v_y \frac{\partial v_z}{\partial y} + v_z \frac{\partial v_z}{\partial z}\right) = -\frac{\partial P}{\partial z} + \frac{\partial}{\partial x}\left(\mu \frac{\partial v_z}{\partial x}\right) + \frac{\partial}{\partial y}\left(\mu \frac{\partial v_z}{\partial y}\right) + \frac{\partial}{\partial z}\left(\mu \frac{\partial v_z}{\partial z}\right) + \rho g_z \tag{6.8}$$

The *boundary conditions* used are as follows:

$T = T_w$, $v_x = 0$, $v_y = 0$, and $v_z = 0$ at the top surface, bottom surface, and side walls

The *initial conditions* used are as follows:

$$T = T_{\text{ref}} = 40^\circ\text{C}, \quad v_x = 0, \quad v_y = 0, \text{ and } v_z = 0$$

For conduction-dominated heating, Equations (6.4)–(6.8) reduce to a single equation:

$$\frac{\partial T}{\partial t} = \frac{k}{\rho C_p}\left(\frac{\partial^2 T}{\partial x^2} + \frac{\partial^2 T}{\partial y^2} + \frac{\partial^2 T}{\partial z^2}\right) \tag{6.9}$$

6.1.4. Physical Properties

The viscosity of broccoli-cheddar soup was measured at different temperatures and shear rates. In the simulations presented here, the viscosity (measured at low shear rate) was assumed to be a function of temperature. The viscosity was measured using a Paar Physica Viscometer VT2, located at the School of Engineering, University of Auckland. The values of the viscosities were taken at the extreme low shear rate, which closely simulates the situation in the pouch being sterilized. The

values of broccoli-cheddar soup viscosities at the low shear rate were 8.16 Pa s, 4.32 Pa s, and 2.65 Pa s at 30°C, 50°C, and 70°C respectively.

The properties of broccoli-cheddar soup used in the simulations were calculated from the values reported for the material used in the soup, using their mass fractions. These properties were $\rho = 1007$ kg m^{-3}, $C_p = 3520$ J kg^{-1} K^{-1}, and $k = 0.516$ W m^{-1} K^{-1} (Hayes, 1987; Rahman, 1995). The variation of the density with temperature was governed by Boussinesq approximation such as all the cases studied earlier, and Equation (5.12) was used to describe its variation with temperature.

The magnitude of the Grashof number in the pouch during sterilization was in the range of 10^{-1}–10^{1} (using the maximum temperature difference). This low Grashof number for the viscous liquid used in the simulations indicates that natural convection flow is laminar.

The assumptions used in the numerical simulations were similar to those reported in Section 5.2.1.4., except in one simulation in which the come-up time of the retort was taken into consideration and was implemented in the CFD code using Ground facility that allows user code to be incorporated (Appendix D).

6.2. RESULTS OF SIMULATION

6.2.1. Temperature Distribution and Flow Profile

The objective of this section is to analyze the calculated temperature distribution inside a 3-D pouch filled with liquid foods (broccoli-cheddar soup and carrot-orange soup) and sterilized by saturated steam heating at 121°C. The migration of the SHZ and the effect of the velocity profiles on its shape are also analyzed. In one of the simulations, the effect of cooling the pouch, following the heating process, is also presented and analyzed.

6.2.1.1. Temperature Distribution and Flow Profile of Broccoli-Cheddar Soup

Previous observations of thermal sterilization in a can (Chapter 5) showed that the SHZ (i.e., the location of the lowest temperature at a given time) is not a stationary region in the liquid undergoing convection heating. The same is found true for pouches in which the SHZ will not stay at the geometric center of the pouch as in conduction heating. As heating progresses, the SHZ is pushed more toward the bottom of the pouch and eventually stays in a region that is about 30% of the pouch height. Figure 6.4 shows the temperature distribution in different y-direction planes in a pouch filled with broccoli-cheddar soup at the end of heating (3,000 s). This figure clearly shows that the SHZ settles at 30% of the pouch height and at a location closer to the widest end of the pouch. The narrowest end of the pouch gets heated very quickly due to the large surface area per unit volume at that location.

Figure 6.5 shows the temperature distribution in a pouch at different periods of heating (60, 300, and 3,000 s, respectively). Initially the content of the pouch (broccoli-cheddar soup) is at uniform temperature. As heating progresses, the mode of heat transfer changes from conduction to convection. Figure 6.5a at $t = 60$ s is almost identical to pure conduction heating, but over time, the isotherms are seen to be influenced by convection as shown in Figure 6.5b.

The buoyancy force created by the change in liquid density due to temperature variation (from the walls, top, and bottom to the core) produces an upward flow. The hot liquid going up is deflected by the top wall and then travels toward the core. The liquid in the core moves downward and then toward the wall. Thus a circulating flow is created. As heating progresses, a more uniform velocity is obtained, reducing buoyancy forces in the liquid that leads to a significant reduction in the velocity. At the end of heating ($t = 3{,}000$ s), the circulation of the flow is reduced significantly due to low

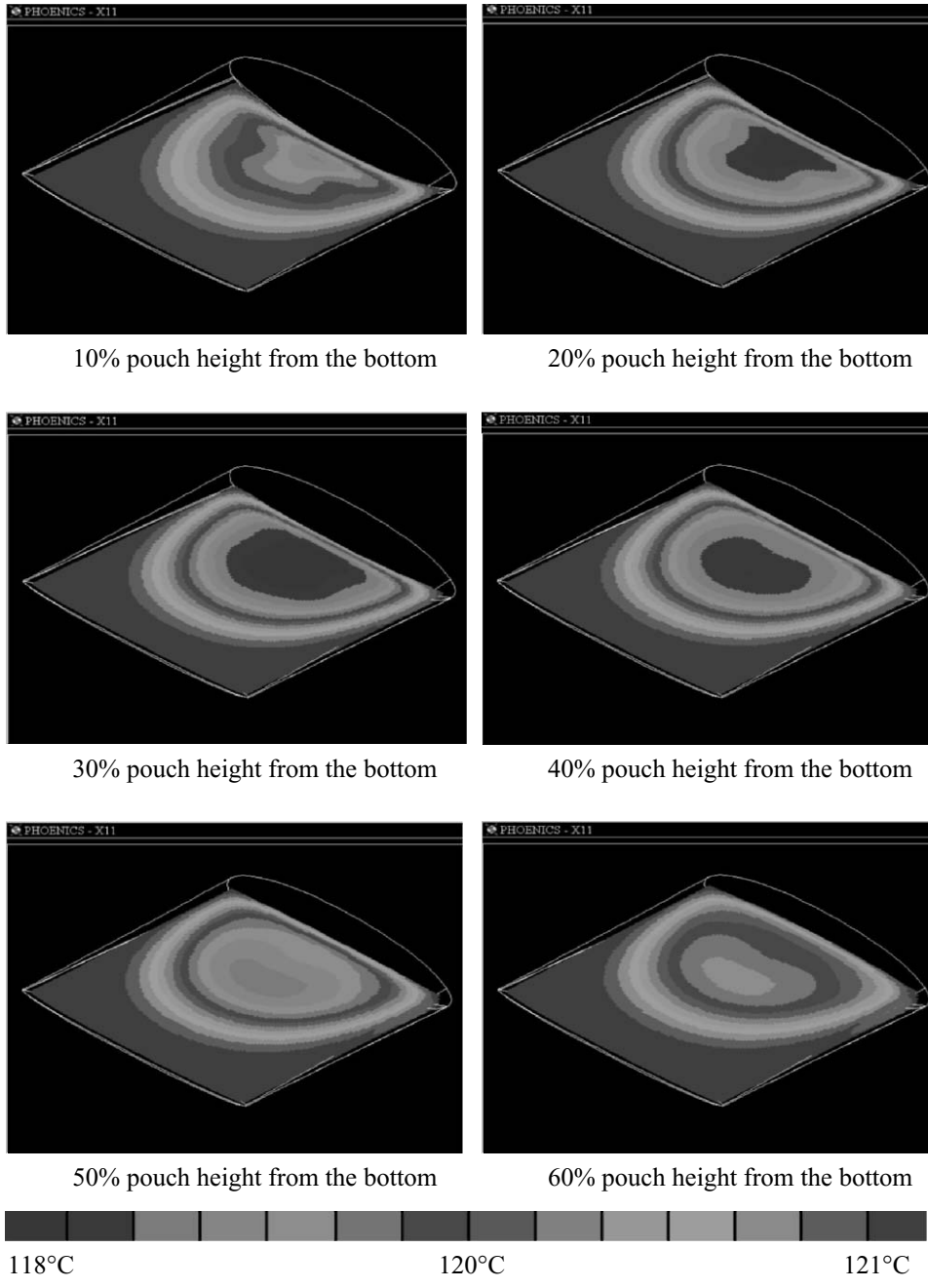

Figure 6.4. Temperature profiles at different *y*-planes in a pouch filled with broccoli-cheddar soup and heated by condensing steam after 3,000 s.

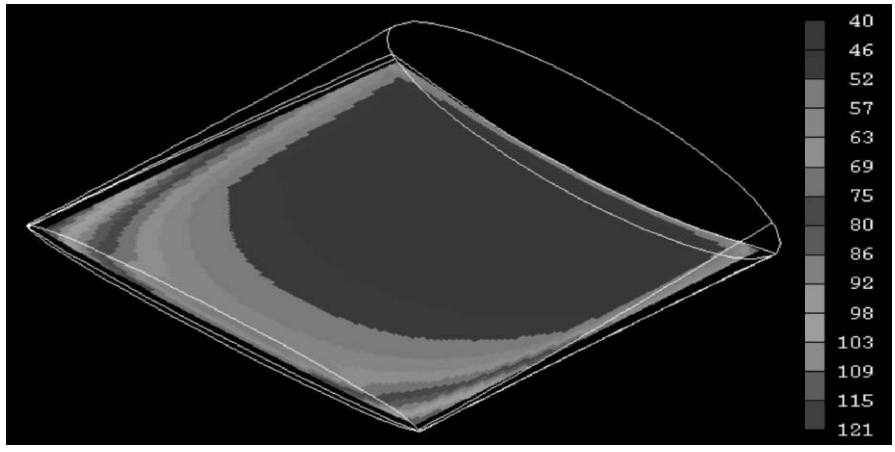

(a)

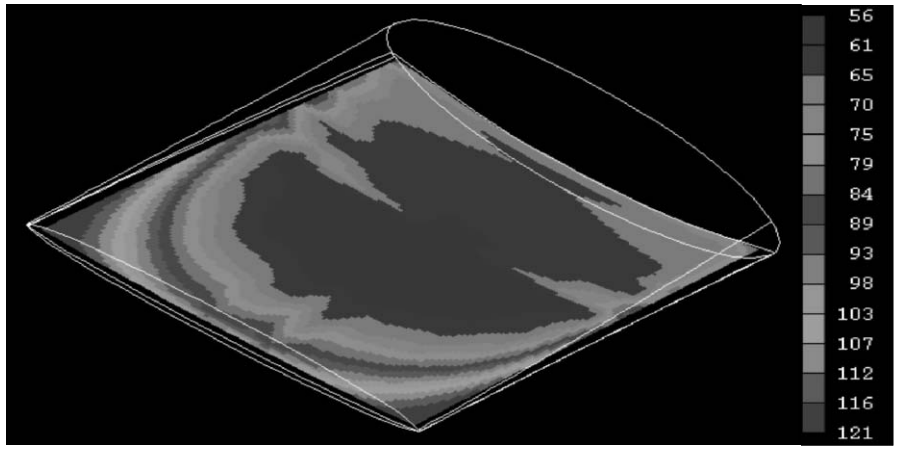

(b)

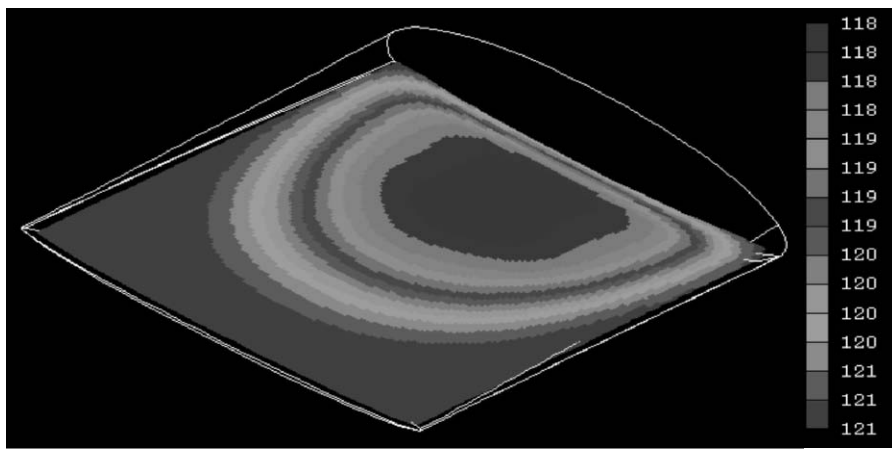

(c)

Figure 6.5. Temperature profile planes at 30% of the height from the bottom of a pouch filled with broccoli-cheddar soup and heated for different periods of (a) 60 s, (b) 300 s, and (c) 3,000 s.

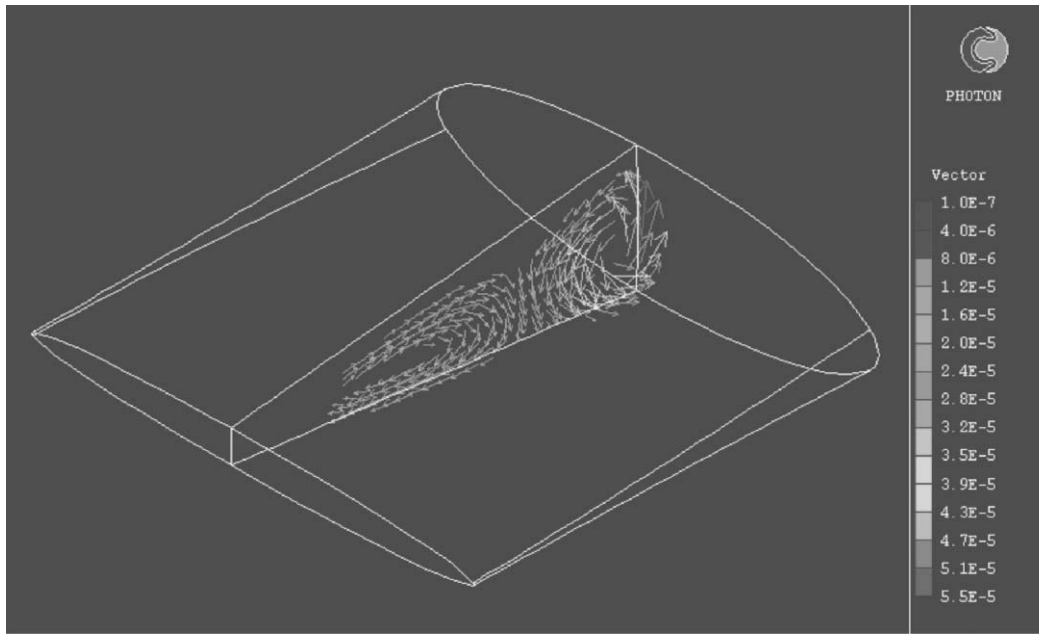

Figure 6.6. The x-plane velocity vector (m s^{-1}) of broccoli-cheddar soup in a pouch heated by condensing steam after 300 s.

temperature differences and the temperature distribution becoming similar to the conduction heating, as shown clearly in Figure 6.5c.

The convective circulation takes the form of a distorted torroid, with the flow rising up the pouch walls and descending in the center. However the circulation is strongest against the deepest end of the pouch, as shown in Figure 6.6. This strong circulation results in a cool band across the pouch, as seen in Figure 6.5b, at a distance about 35–40% of the length from the deepest end.

6.2.1.2. Temperature Distribution and Flow Profile of Carrot-Orange Soup

Two cases of carrot-orange soup have been simulated and studied. The first was for a pouch heated by a convection-dominating heating inside the pouch, while the second was for the pouch assumed to be heated by conduction only. The results of the temperature distribution and the migration of the SHZ for both cases were compared to illustrate the importance of natural convection heating in such a process.

Figures 6.7, 6.8, and 6.9 show the temperature distribution at different x, y, and z planes in a pouch filled with carrot-orange soup at the end of heating (3,000 s). The three figures, combined together, provide a detailed picture of the location of the SHZ at the end of the heating period. Such detailed information can be obtained at any time during sterilization. Figures 6.4 and 6.8 are very similar due to the similar physical properties of the broccoli-cheddar soup and carrot-orange soup. Figure 6.8 clearly shows the settlement of the SHZ at about 30% of the pouch height. This figure shows that the SHZ is not a stationary region, and its location is not at the geometric center of the pouch.

Figure 6.10 shows the temperature distribution in the pouch at different periods of heating (60, 200, 300, 1,000, 1,800, and 2,400 s). At time equal to 60 s, Figure 6.10 shows a temperature profile similar to that shown in Figure 6.11a for conduction heating, indicating that the heating process

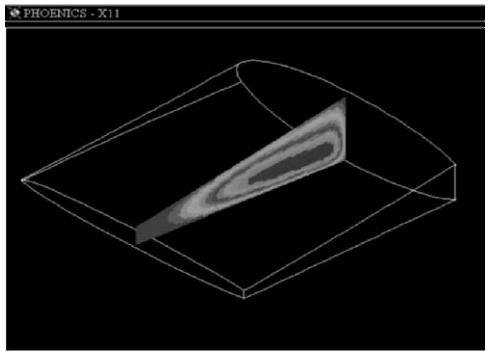

50% pouch distance from side wall

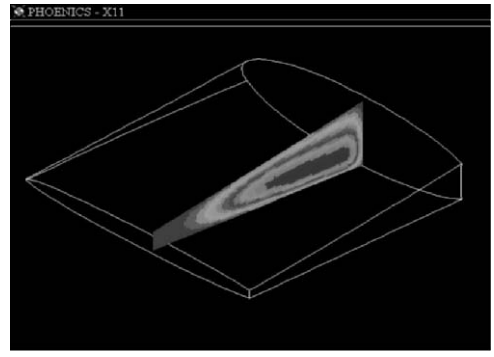

55% pouch distance from the right of side wall

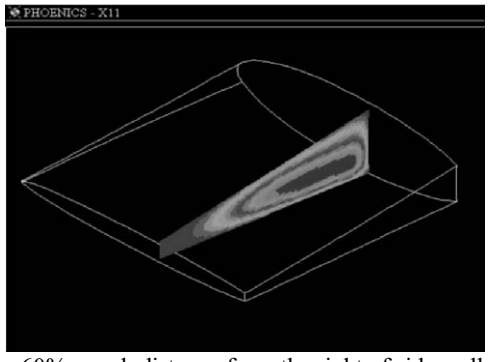

60% pouch distance from the right of side wall

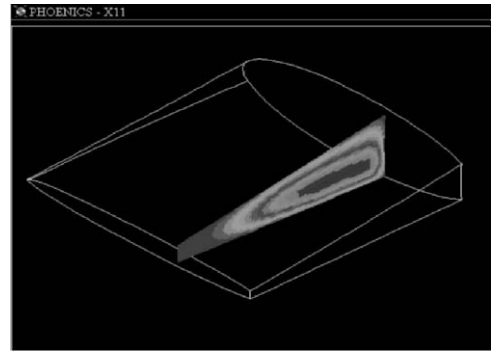

70% pouch distance from the right of side wall

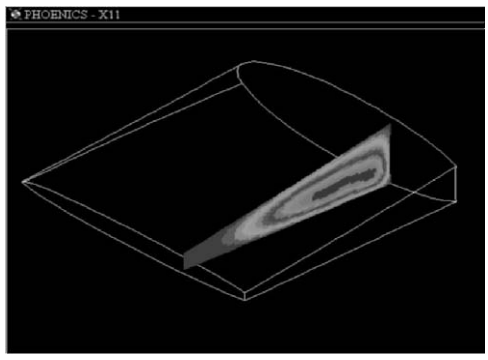

75% pouch distance from the right of side wall

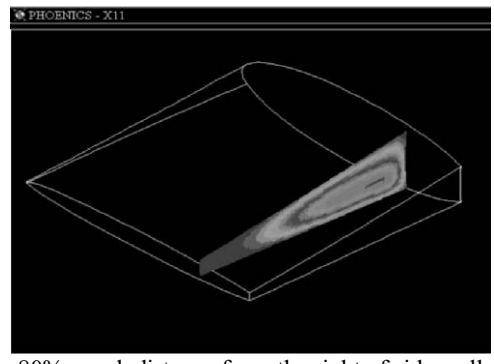

80% pouch distance from the right of side wall

Figure 6.7. Temperature profiles at different x-planes in a pouch filled with carrot-orange soup and heated by condensing steam after 3,000 s.

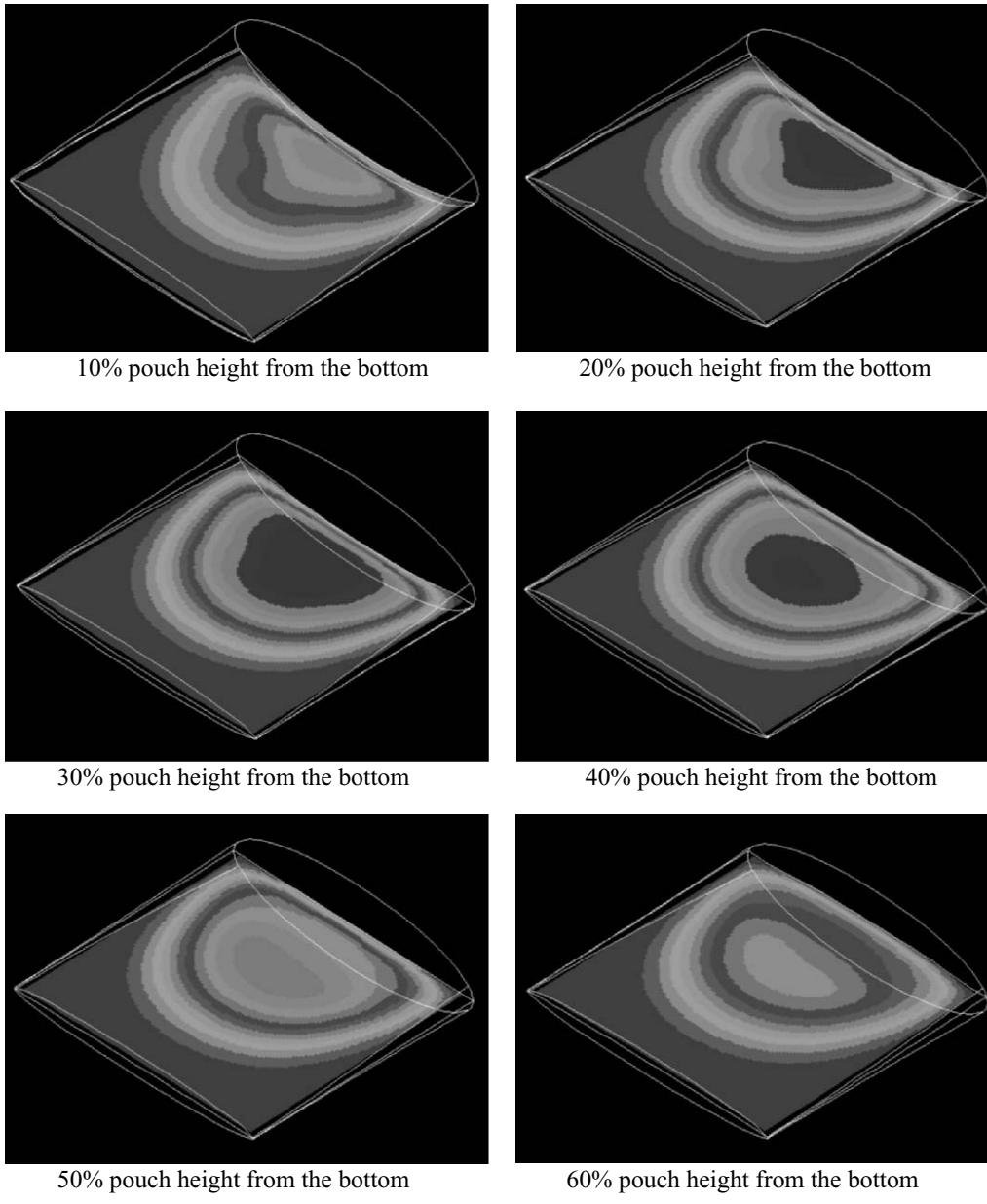

Figure 6.8. Temperature profiles at different *y*-planes in a pouch filled with carrot-orange soup and heated by condensing steam after 3,000 s.

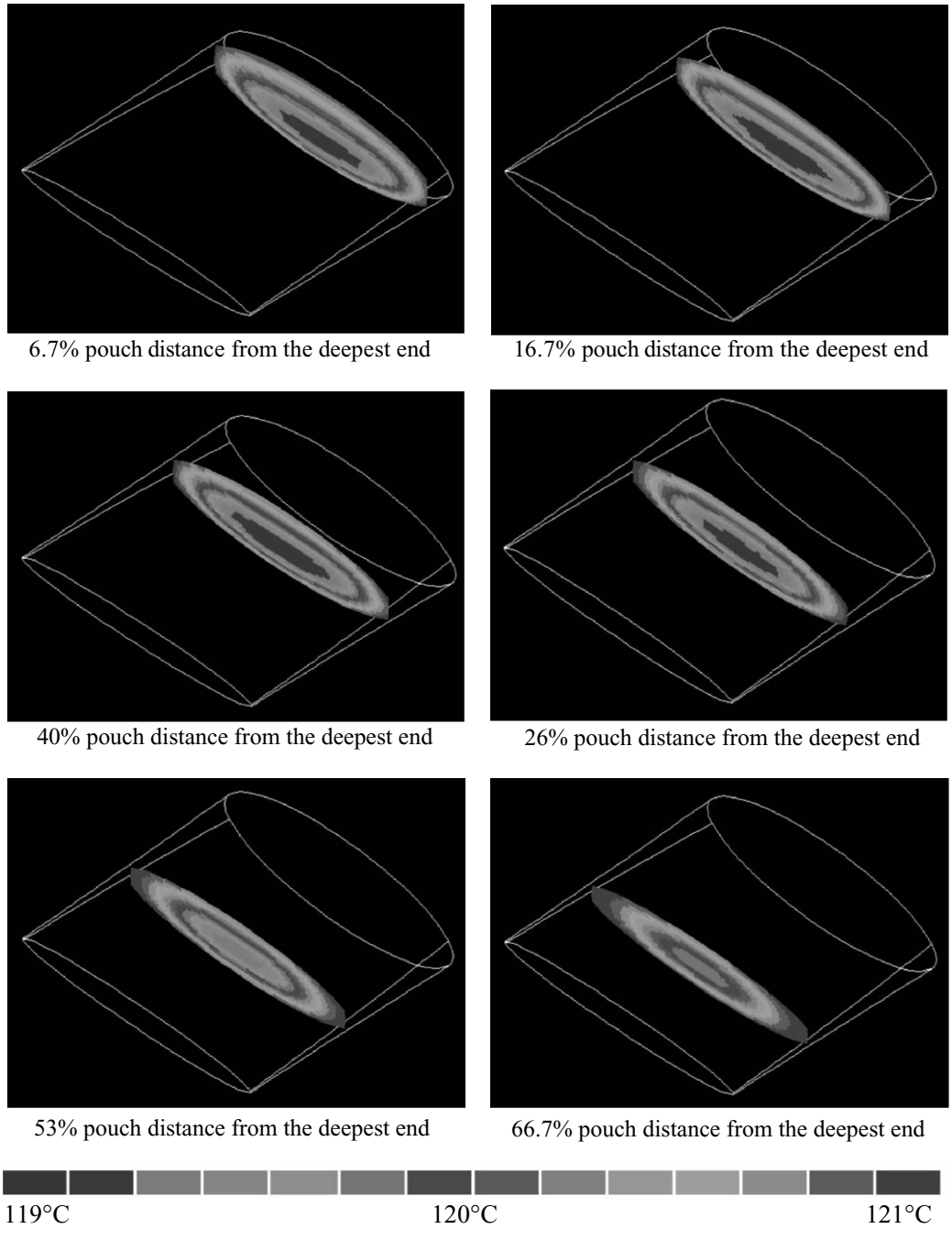

Figure 6.9. Temperature profiles at different z-planes in a pouch filled with carrot-orange soup and heated by condensing steam after 3,000 s.

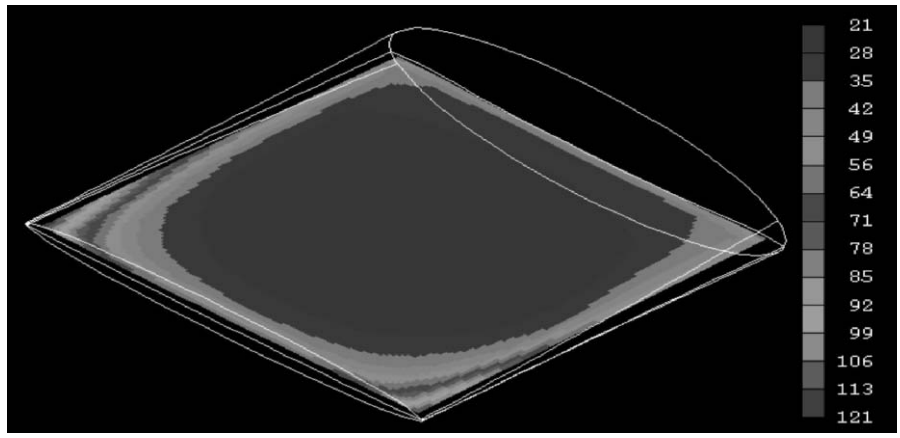

(a)

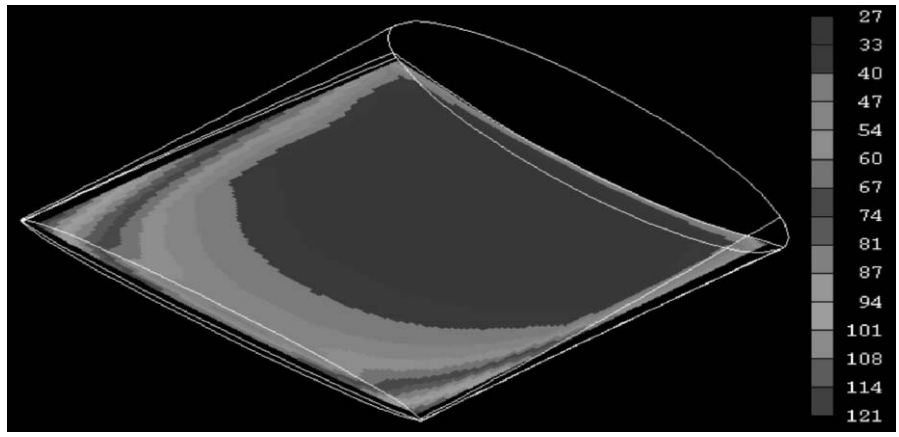

(b)

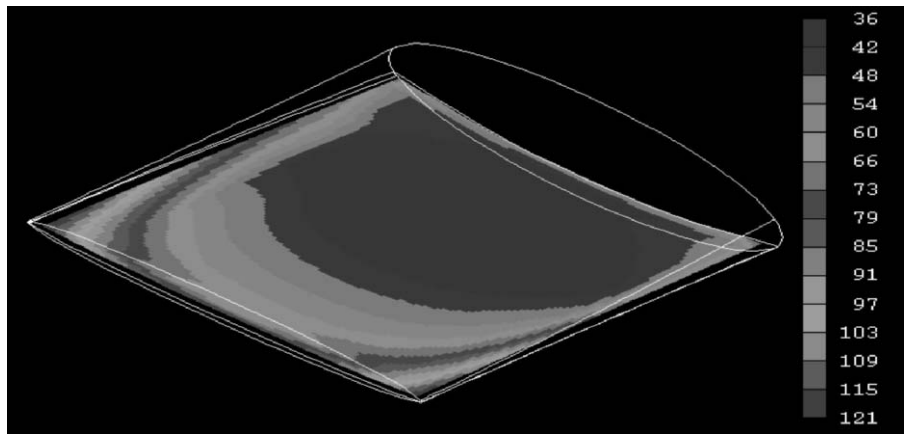

(c)

Figure 6.10. Temperature profile planes at 30% of the height from the bottom of a pouch filled with carrot-orange soup and heated for different periods of (a) 60 s; (b) 200 s; (c) 300 s, (d) 1,000 s, (e) 1,800 s, and (f) 3,000 s.

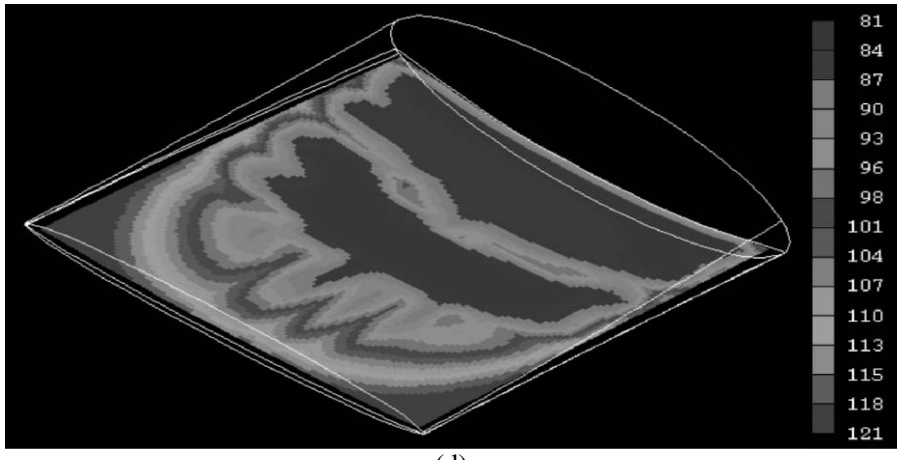

(d)

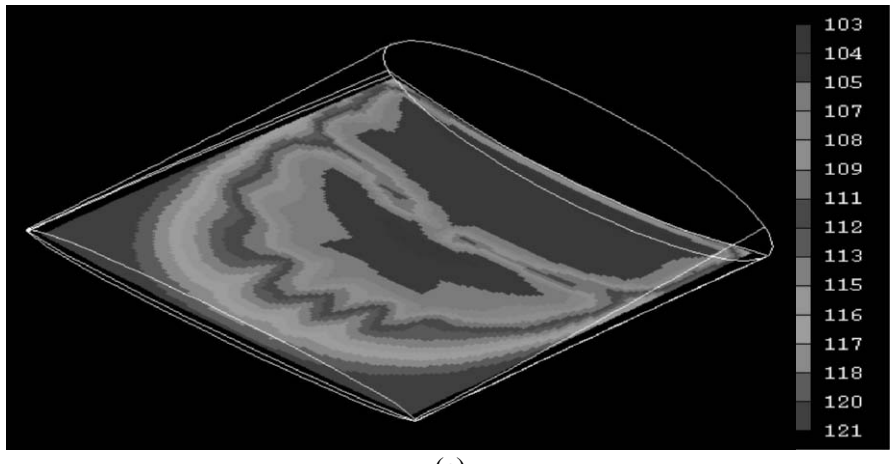

(e)

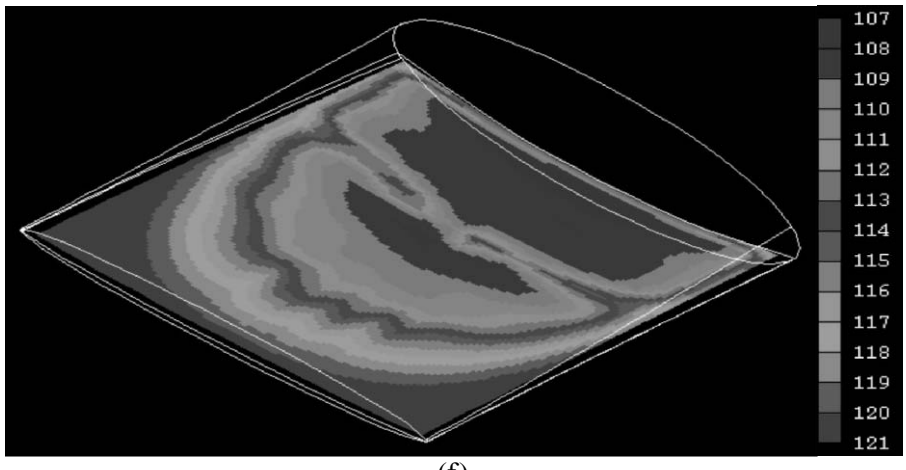

(f)

Figure 6.10. (*Continued*)

is controlled by conduction. At the later stage of heating (at $t = 300$ and 1,800 s), the isotherms are influenced by convection, as seen from the comparison of the isotherms shown in Figures 6.10c and 6.10e for convection heating with those of Figures 6.11b and 6.11c for conduction heating only. Figure 6.10d shows the temperature distribution in the pouch after 1,000 s of heating; this figure shows the presence of the SHZ at 30% of the height from the bottom, starting from the deepest end and extending to almost 60% of the pouch length. Within this region, Figure 6.10d shows the existence of a relatively hotter zone in the middle of the SHZ. These observations can be explained with reference to Figure 6.12 of the x-plane velocity vector, which shows a strong circulation. Although Figure 6.12 shows the existence of stagnant regions near both the deepest and the narrowest end of the pouch, the SHZ appears only in the deepest end because conduction dominates the heat transfer at the narrowest end of the pouch. The velocity of the liquid food at a position 8 cm from the widest end is found significantly higher due to the heat received from both ends of the pouch, as shown from the magnitude of the velocity in the same figure.

Figure 6.11 shows the result of the simulation for the same pouch described earlier but based on pure conduction heating. This figure shows that the SHZ remains at the geometric center of the pouch during the whole period of heating as expected. Figure 6.13 for the y-plane velocity vector clearly shows the effect of natural convection, which starts at the early stages of heating. Figure 6.13 also shows the axial velocity of the soup, which is found of the order of 10^{-2}–10^{-3}mm s^{-1}. The small velocity is due to the limited buoyancy caused in the shallow pouch containing viscous soup. The convective circulation takes the form of a distorted torroid, with the flow rising up the pouch walls and descending in the center (Figure 6.14). Figures 6.12 and 6.14 show that at the same time of heating ($t = 1{,}000$ s), the value of the velocity vector in the x-direction (Figure 6.12) is almost 10 times higher than the value of the velocity in the z-direction (Figure 6.14). This means that the velocity profiles in the x-direction have a clear dominant effect on the temperature distribution than those in the z-direction, as seen clearly from Figure 6.10d.

The simulation of a 3-D pouch filled with a carrot-orange soup shows that at the end of heating (3,000 s), the temperature at the SHZ is 119°C, as shown in Figures 6.7, 6.8, and 6.9. For the can studied in the previous chapter, at the same time of heating, the temperature of the SHZ was only 107°C for the can sitting in an upright position (Figure 5.16) and 105°C for the can lying horizontally (Figure 5.20). Although the can volume is smaller than the pouch volume and exhibits higher natural convection due to its height, the time needed to reach the required temperature is shorter. The reason is the large surface area per unit volume of the pouch (1.05 cm^2 cm^{-3}) compared to the surface area per unit volume of the can studied (0.68 cm^2 cm^{-3}).

6.3. HEATING AND COOLING CYCLES

During sterilization of food in a can and pouch, it is necessary to analyze the cooling process as well as the heating process as food in the core of the pouch may stay hot for a significant length of time, which will influence the degree of sterilization. In this section, the results of the temperature distribution and the migration of the SHZ and the slowest cooling zone (SCZ), during heating and cooling cycles, are compared and analyzed.

Transient temperature and the shape of the SCZ (i.e., the location of the hottest region) were simulated for a uniformly heated 3-D pouch containing carrot-orange soup. The simulation covered the whole heating and cooling cycles of 3,600 and 1,200 s duration respectively. Saturated steam at 121°C and water at 20°C were assumed to be the heating and cooling media respectively. The pouch used was the same as that used in all previous simulations. Governing equations, model parameters, and boundary conditions were the same as those explained in Sections 6.1.2 and 6.1.3.

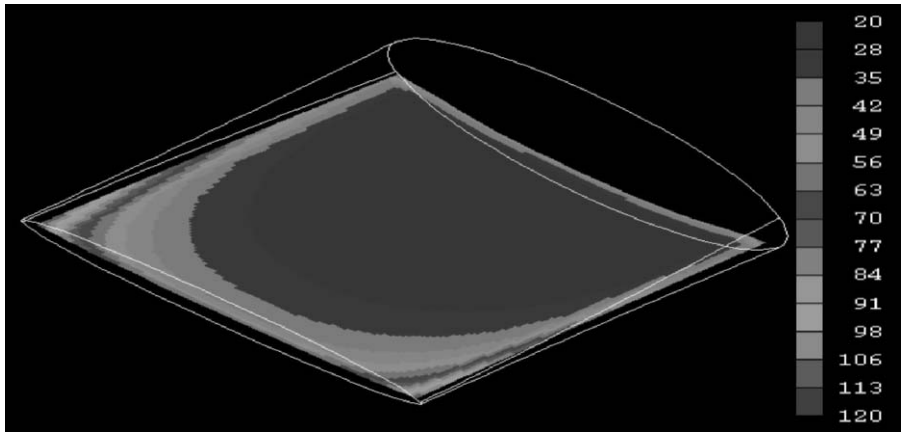

(a)

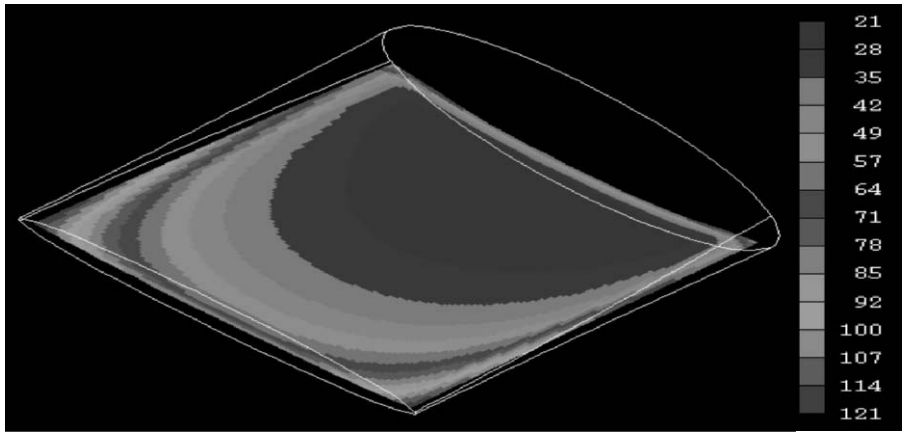

(b)

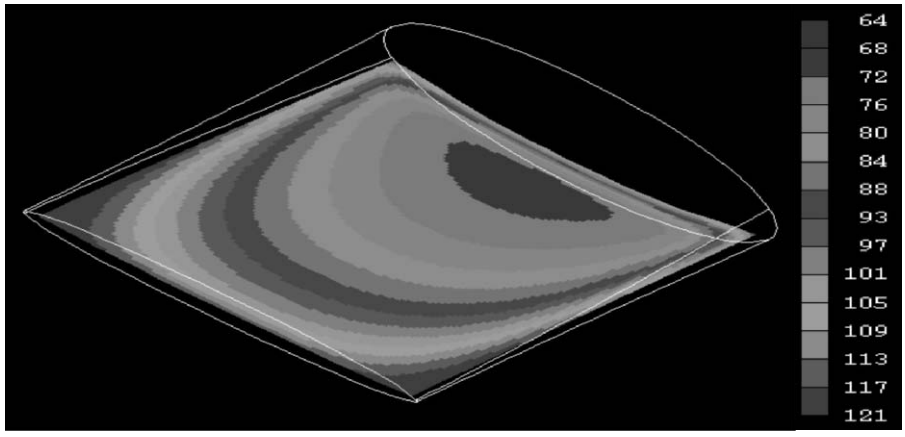

(c)

Figure 6.11. Temperature profile planes at 30% of the height from the bottom of a pouch filled with carrot-orange soup and heated by conduction only for different periods of (a) 60 s, (b) 300 s, and (c) 1,800 s.

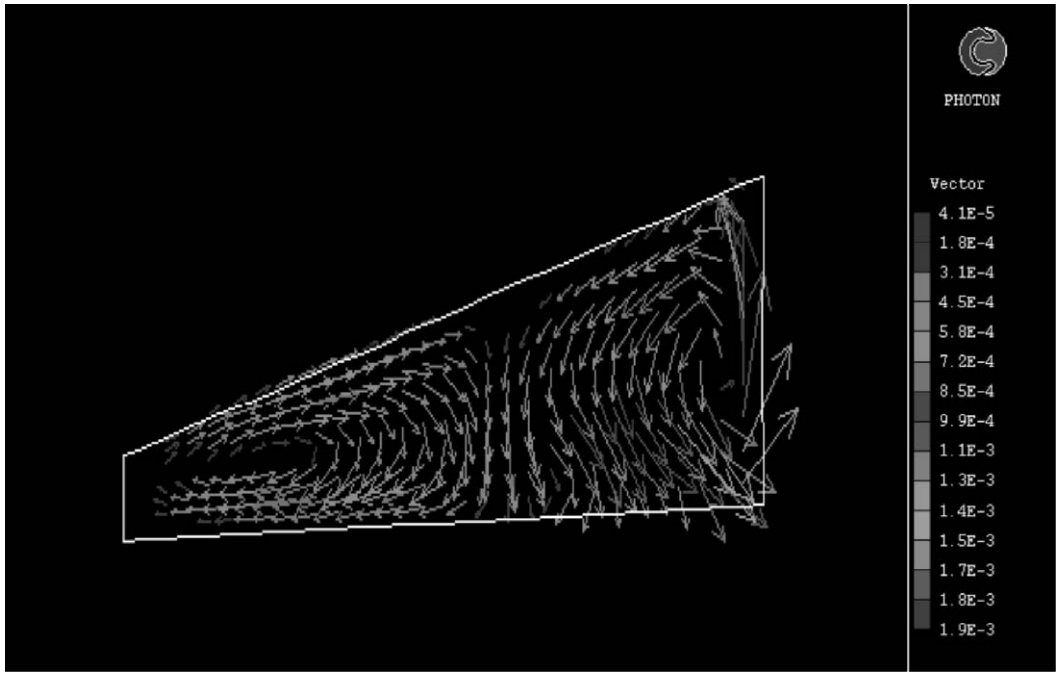

Figure 6.12. The center of the x-plane velocity vector (m s^{-1}) of carrot-orange soup in a pouch heated by condensing steam after 1,000 s, showing the effect of natural convection.

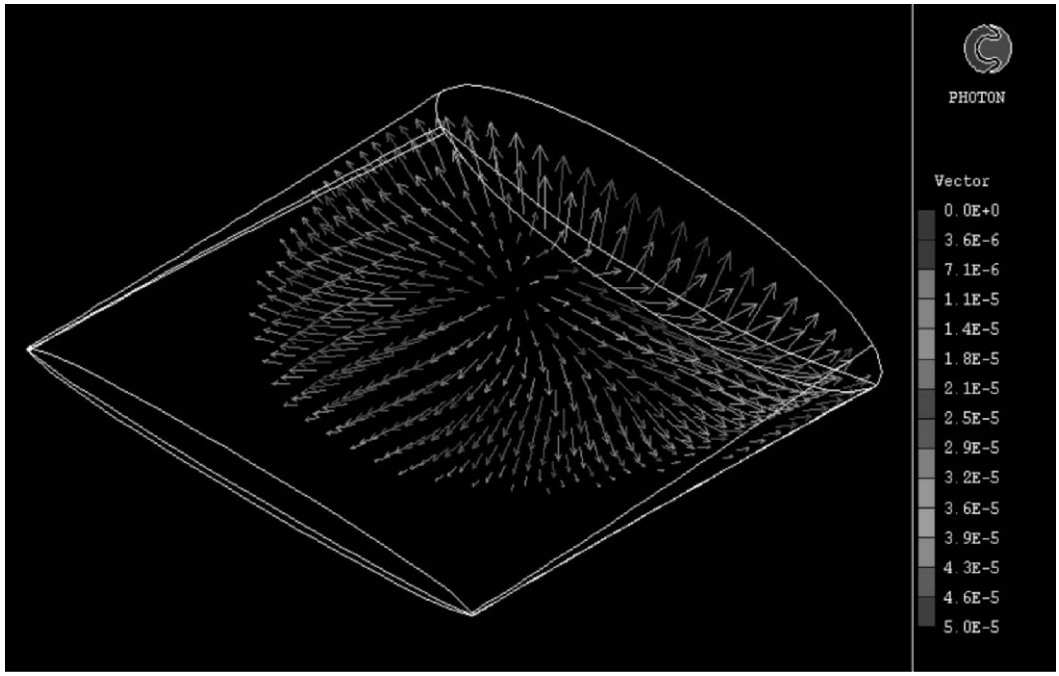

Figure 6.13. The y-plane velocity vector (m s^{-1}) of carrot-orange soup in a pouch heated by condensing steam after 300 s, showing the effect of natural convection.

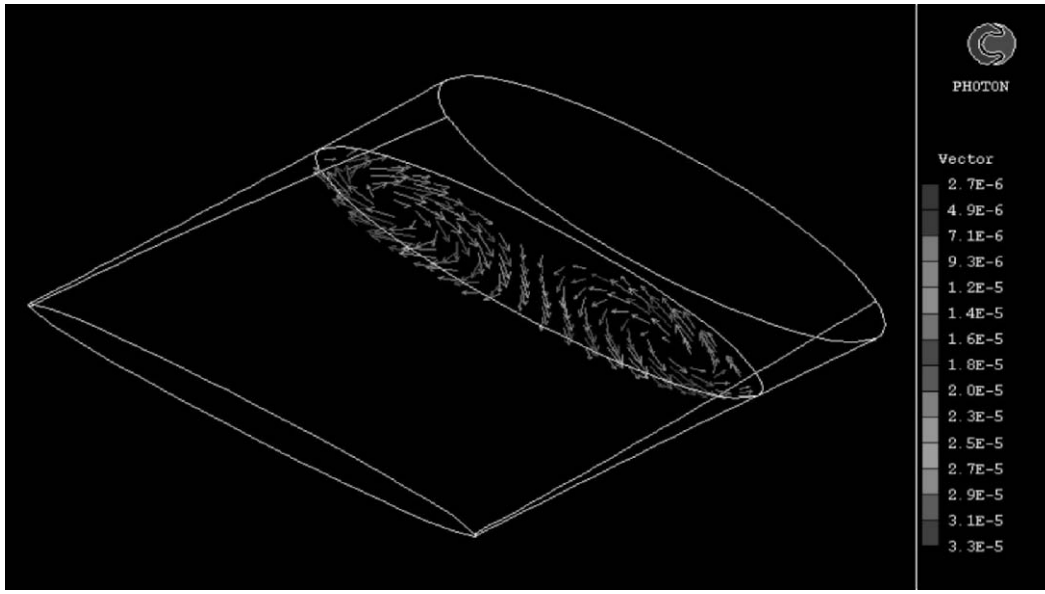

Figure 6.14. The z-plane velocity vector (m s^{-1}) of carrot-orange soup in a pouch heated by condensing steam after 1,000 s, showing the effect of natural convection.

Experimental validation has been performed for the same pouch, filled with the same liquid food, and heated under the same conditions, as discussed later in Chapter 8. The predicted results are in a good agreement with those measured experimentally.

6.3.1. Basic Model Equations and Solution Procedure

The computations were performed for a 3-D pouch with the same dimensions as those used in Section 6.1.1. The pouch outer surface temperature (top, bottom, and sides) was assumed to rise instantaneously to 121°C. The total simulation time for the heating and cooling cycles during sterilization of carrot-orange soup was 4,800 s. It took 60 time steps to achieve the total heating cycle (0–3,600 s), and 20 time steps for the cooling cycle (3,600–4,800 s). This required 12 h of CPU time on the UNIX IBM RS6000 workstations at the University of Auckland. The solution was obtained using a variety of grid sizes and time steps, and the results showed that the solutions are time-step independent and weakly dependent on grid variation.

During the cooling cycle following the heating, the temperature of the heating/cooling fluid at the wall switched from 121°C to 20°C (Appendix F). In cooling, the pouch surface temperature will not be the same as that of the water used in cooling. In the simulation, the surface heat transfer coefficient was incorporated into the model, with a value of 600 W m^{-2} K^{-1}. This value was chosen from literature and confirmed by calculations from the surface temperature measurements and a correlation of the form $\mathrm{Nu} = f(\mathrm{Gr} \times \mathrm{Pr})^n$, where Nu is the Nusselt number, dimensionless; Gr is the Grashof number, dimensionless; Pr is the Prandtl number, dimensionless; and f is the heating or cooling factor (Tucker, G.S. and Clark, P. 1990). In the heating cycle, the condensing steam is assumed to remain at a constant temperature at the pouch outer surface.

The properties of carrot-orange soup used in the current simulation were the same as those used in Section 5.5. These properties were calculated from the values reported for all the food materials used in the soup, using their mass fractions.

The shear rate calculated from our previous simulations for a can filled with a liquid having lower viscosity than the one used in this simulation (Ghani et al., 1998) was 0.01 s^{-1} only. The shear rate in the pouch will be even smaller due to the lower velocity of the liquid in the pouch. Because of the low shear rate the viscosity may be assumed independent of shear rate, and the fluid will behave as a Newtonian fluid. In the simulations presented here, the viscosity is assumed to be a function of temperature. The viscosity of carrot-orange soup used in the simulation is same as that used in Section 5.5.

6.3.2. Results of Simulation

6.3.2.1. Theoretical Predictions of the Heating Process

The result of the heating process period is analyzed and studied earlier (Section 6.2). The temperature profiles show that at the beginning of heating, the temperature profiles were similar to those heated by conduction only. As heating progresses, the mode of heat transfer changes from conduction to convection. At later stages of heating, the isotherms are mainly influenced by convection. At the end of heating, flow circulation is almost ceased due to the low temperature difference between the pouch wall and the bulk of the food. Hence, the temperature distribution becomes similar to conduction heating.

6.3.2.2. Theoretical Predictions of the Holding Time Period

During the holding time (60–70 min), the temperature of the pouch remains uniform at a temperature close to 121°C. The maximum variation in the temperature of the SHZ, during holding time, was 0.4°C. Although the holding time was only 10 min, it plays an important role in the sterilization, since the whole pouch remains at the maximum temperature of 121°C during this period.

6.3.2.3. Theoretical Predictions of the Cooling Process

In this section, the results of the temperature distribution and the migration of the SHZ during heating and the SCZ during cooling are compared and analyzed for the first time.

The results of the simulation are presented in Figures 6.15 and 6.16. In the lower section of the pouch, Figure 6.15 shows that the location of the SCZ remains at the center of the pouch. At higher locations, the SCZ tends to move toward the widest end of the pouch, which is probably due to the effect of natural convection currents influenced by the upper surface of the pouch. Figure 6.15 also shows that the SCZ covers a wider area at a location close to about 70% of the pouch height from the bottom unlike in heating, where the SHZ covered a wider area at 30% of the pouch height from the bottom.

The results of the simulation show that at the end of heating, the SHZ settled into a region within 30–40% of the pouch height above the bottom and at a distance of approximately 20–30% of the pouch length from its deepest end. In the cooling period, the SCZ was found to develop in the core of the pouch and gradually migrate toward the widest end. The vertical location of this SCZ was at about 60–70% of the pouch height.

During cooling, the lowest half of the pouch will be less influenced by convection compared to the upper half of the pouch, which is due to the variation of the density with temperature. This is reflected on the temperature profiles presented in Figure 6.15, which shows conduction-controlled heating at 30–40% of the pouch height from the bottom and convection-controlled heating at other heights, especially at 70% and 80% of the pouch height.

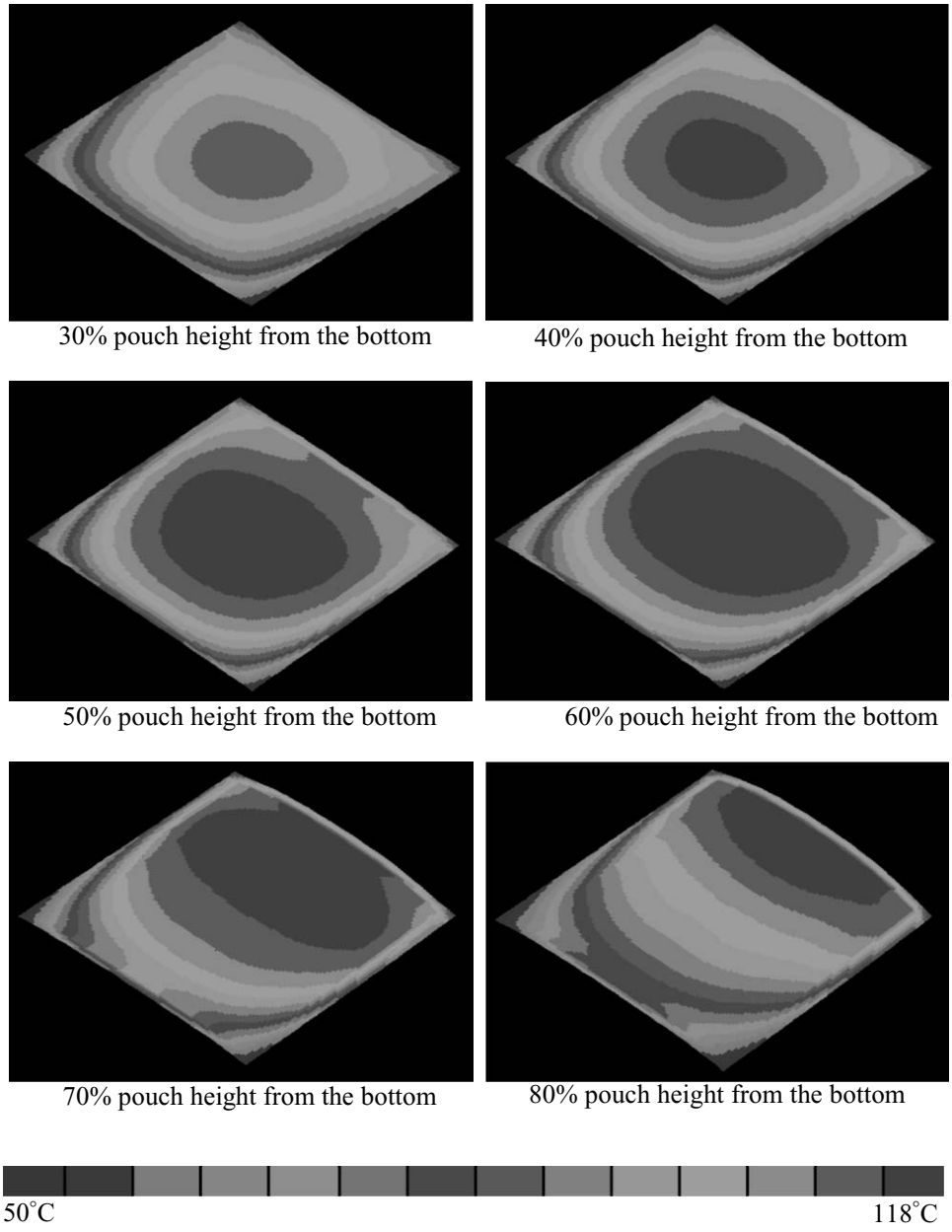

Figure 6.15. Temperature profiles at different y-planes in a pouch filled with carrot-orange soup after 600 s from the start of the cooling cycle.

Observations of temperature profiles at different y-planes and for different periods during the heating cycle show different results from the cooling cycle. During heating, the lowest half of the pouch is heated slower, while the upper half of the pouch is cooled slower in the case of cooling. This is why all of our results and profiles of temperature and velocity during the heating cycle are

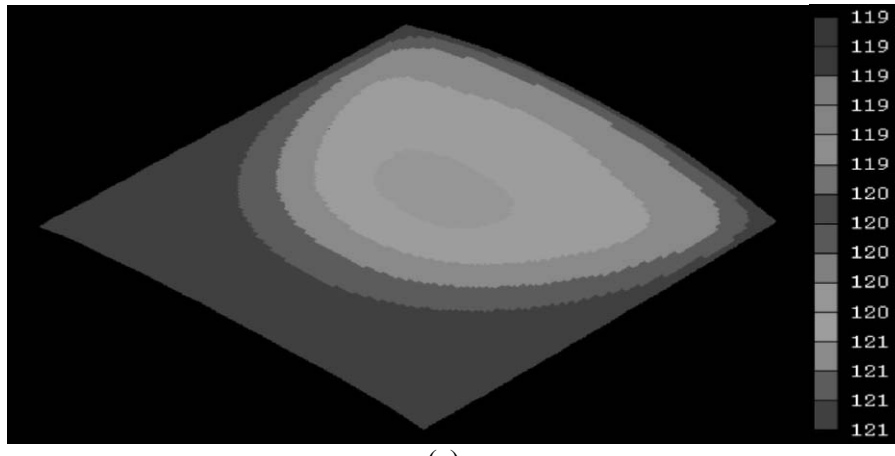

(a)

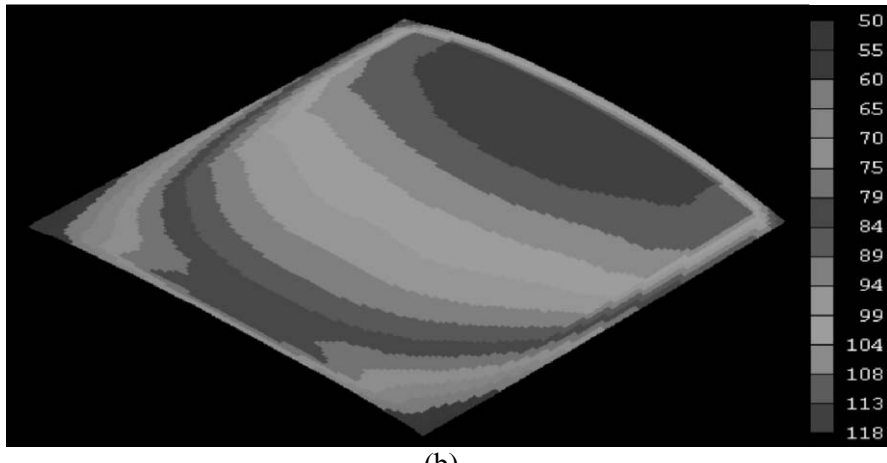

(b)

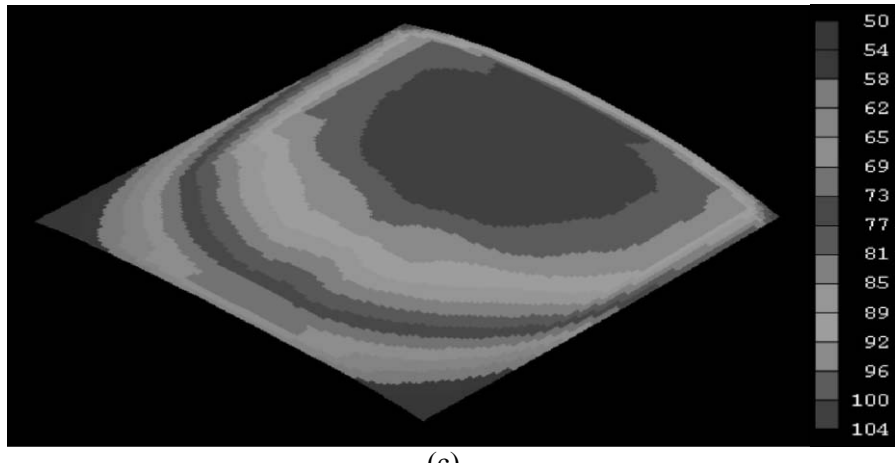

(c)

Figure 6.16. Temperature profile planes at 80% of the height from the bottom of a pouch filled with carrot-orange soup after (a) 3,000 s from the start of the heating cycle, (b) 600 s, and (c) 900 s from the start of the cooling cycle.

studied and presented in the lower part of the pouch, where the location of the SHZ and the effect of natural convection are dominant.

Figure 6.16 shows the temperature profile at 80% of the height from the bottom of the pouch filled with carrot-orange soup at different periods of heating and cooling. Cooling with water at 20°C starts at $t = 3{,}600$ s and continues until 4,800 s. In this figure, the temperature profiles during the cooling cycle show that the cooling process is influenced by convection as in the heating process.

NOMENCLATURE

C_p	specific heat of liquid food, J kg^{-1} K^{-1}
Gr	Grashof number, Gr $= \frac{d_v^3 \rho^2 g \beta \Delta T}{\mu^2}$, dimensionless
g	acceleration due to gravity, m s^{-2}
H	height of the geometry, m
h	heat transfer coefficient, W m^{-2} K^{-1}
k	thermal conductivity, W m^{-1} K^{-1}
L	length of the geometry, m
Nu	Nusselt number, Nu $= \frac{h_c d_v}{k}$, dimensionless
p	pressure, Pa
Pr	Prandtl number, Pr $= \frac{C_p \mu}{k}$, dimensionless
t	time, s
T	temperature, °C
W	width of the geometry, m
v	velocity, m s^{-1}
β	thermal expansion coefficient, K^{-1}
μ	viscosity, Pa s
ρ	density, kg m^{-3}

Subscripts

ref	reference
x,y,z	coordinates

REFERENCES

Bird, R.B., Stewart, W.E., & Lightfoot, E.N. (1976). *Transport phenomena*. New York: John Wiley & Sons.

Ghani, A.G., Farid, M.M., & Chen, X.D. (1998). A CFD simulation of the coldest point during sterilization of canned food. 26th Australian Chemical Engineering Conference (CHEMICA 98), 28–30 September 1998, Port Douglas, Queensland, No. 358.

Hayes, G.D. (1987). *Food engineering data handbook*. New York: Wiley.

PHOENICS Reference Manual, Part A: PIL. TR 200 A, Bakery House, London SW 19 5AU, U.K.: CHAM.

Rahman, R. (1995). *Food properties handbook*. USA: CRC Press.

Tucker, G.S., & Clark, P. (1990). Modeling the cooling phase of heat sterilization processes, using heat transfer coefficients. *International Journal of Food Science and Technology, 25*, 668–681.

CHAPTER 7

POUCH PRODUCT QUALITY

7.1. BACTERIA INACTIVATION IN FOOD POUCHES DURING THERMAL STERILIZATION

The analysis of inactivation of *Clostridium botulinum* during thermal sterilization of pouches (Ghani et al., 1999a) is extended to cover *Bacillus stearothermophilus*. *B. stearothermophilus* has greater heat resistance than other microorganisms encountered in foods, and its inactivation means that all other contaminants are inactivated also. The spore's viable count measured after different heating periods (Chapter 8) is compared with those predicted theoretically. Concentration profiles of *B. stearothermophilus* during natural convection heating of a food in a three-dimensional (3-D) pouch are also presented.

The death of microorganisms is expected to begin at an early stage of heating at locations near the wall, where the temperature approaches 121°C very quickly. While at other locations, the temperature may not rise until a much later time, experiencing a much lower rate of destruction. Hence it is necessary to solve the partial differential equation (PDE) governing the bacteria concentration, coupled with the equations of continuity, momentum, and energy in order to predict the overall destruction of microorganisms.

In the simulation presented in this chapter, natural convection heating of different viscous liquid foods in a 3-D pouch heated from all sides is presented. A computational procedure was developed for describing the changes in live bacteria concentration and its transient spatial distributions during sterilization processing of canned food. All liquid foods used were assumed to have constant physical properties except for the viscosity (temperature dependent) and density (Boussinesq approximation). The Arrhenius equation was used to describe the kinetics of bacteria death and the influence of temperature on the inactivation rate constant. It was introduced to the software package using FORTRAN code. The implementation of bacteria kinetics in computational fluid dynamics (CFD) code PHOENICS using *q1* and *Ground.f* coding is similar to those used for the can shown in Appendix B.

7.1.1. Fundamental Equations and Physiochemical Properties

7.1.1.1. Mathematical Model

The PDEs governing natural convection motion of fluid in a 3-D pouch are the Navier–Stokes equations in x, y, and z coordinates (Section 6.1.3). In addition to these equations, the following equation for the concentration of bacteria is introduced:

Mass balance for bacteria (concentration equation)

$$\frac{\partial C_{\mathrm{rb}}}{\partial t} + v_x \frac{\partial C_{\mathrm{rb}}}{\partial x} + v_y \frac{\partial C_{\mathrm{rb}}}{\partial y} + v_z \frac{\partial C_{\mathrm{rb}}}{\partial z} = D\left[\frac{\partial^2 C_{\mathrm{rb}}}{\partial x^2} + \frac{\partial^2 C_{\mathrm{rb}}}{\partial y^2} + \frac{\partial^2 C_{\mathrm{rb}}}{\partial z^2}\right] - k_{T_{\mathrm{b}}} C_{\mathrm{rb}} \qquad (7.1)$$

where C_{rb} represents the relative concentration of viable bacteria in the pouch at any time and location. It is taken as a dimensionless species concentration, which is defined as the ratio of real-time concentration C_b to the initial concentration C_{bo} multiplied by 100.

At the top surface, bottom surface, and side walls all the concentration gradients $\frac{\partial C_{rb}}{\partial x}$, $\frac{\partial C_{rb}}{\partial y}$, and $\frac{\partial C_{rb}}{\partial z}$ are set equal to zero.

Other *boundary conditions* for temperature and velocities were as follows:

$$T = T_w, \quad v_x = 0, \quad v_y = 0, \quad \text{and} \quad v_z = 0 \text{ at the top surface, bottom surface, and side walls}$$

Initially the fluid is at rest and is at a uniform temperature.

The *initial conditions* used in this case with the concentration were as follows:

$$T = T_0, \quad v_x = 0, \quad v_y = 0, \quad \text{and} \quad v_z = 0 \tag{7.2}$$

$$C_{rb} = C_{rb0} = 100, \quad v_x = 0, \quad v_y = 0, \quad \text{and} \quad v_z = 0 \tag{7.3}$$

where T is the temperature of the liquid food, T_w is the pouch wall temperature, T_0 is the food initial temperature, and C_{rb0} is the initial relative concentration of bacteria.

The assumptions used to simplify the problem were similar to those used in Section 5.2.1.4. The additional assumptions used were as follows:

1. The bacteria concentration can be assumed to be low, and hence, the effect of the interactions upon their diffusion can be ignored.
2. The diffusion coefficient of the live bacteria is assumed to be identical for live and dead bacteria.

At the early stages of this work, two simulations were performed for two cases in which the Brownian motion of bacteria was ignored in one of them. No significant differences were observed between the two cases. The calculated diffusion coefficient for bacteria was of order 10^{-12} m^2 s^{-1} (Chapter 5), which is low due to the high viscosity of most liquid food. The cell Peclet number, Pe (ratio of convection to diffusion), for bacteria within the flow domain in the z-direction was calculated and found to be of the order of 10^4, which allows the Brownian motion of bacteria to be ignored.

The computations were performed for a 3-D pouch with a width (W) of 120 mm, height (H) of 40 mm, and length (L) of 220 mm. The pouch outer surface temperature (top, bottom, and sides) was assumed to rise instantaneously and to be maintained at 121°C throughout the heating period. The pouch volume was divided into 6000 cells: 20 in the x-direction, 10 in the y-direction, and 30 in the z-direction, as described in Appendix E. The total simulation time used for the sterilization of carrot-orange soup was 3000 s as the total heating period, and it was divided into 30 time steps. The time steps used were same as those reported in Chapter 6 (Section 6.1.2). For beef-vegetable soup, the total simulation time used for the sterilization was 1800 s, with 18 equal time steps only.

7.1.1.2. Bacteria Inactivation Kinetics

The rate of bacteria inactivation is usually assumed to follow first-order kinetics (Reuter, 1993). The inactivation rate constant for bacteria k_{Tb} is a function of temperature and is usually described by

the Arrhenius equation as follows:

$$k_{T_b} = A_b e^{-E_b/R_g T} \tag{7.4}$$

where A is the preexponential factor, s^{-1}; E is the activation energy of bacteria inactivation, kJ (kg mol)$^{-1}$; R is the universal gas constant, kJ (kg mol)$^{-1}$ K^{-1}; and T is the temperature, K. In recent literature, the combined effect of temperature and pH on thermal inactivation of some types of bacteria and vitamins in a carrier liquid has been investigated using different approaches (Chiruta et al., 1997; Davey and Cerf, 1996; Davey et al., 1995). It is suggested that the description of the variation of reaction rates with temperature by an Arrhenius equation is a more accurate approach (Fryer, 1997). In a food process engineering context, the decimal reduction time (D_T), rather than Arrhenius equation, is often utilized to describe the same relationship. The relationship between the inactivation rate constant and the decimal reduction time is (Heldman and Hartel, 1997) as follows:

$$k_{T_b} = \frac{2.303}{D_{T_b}} \tag{7.5}$$

The inactivation rate constant k_{Tb} was then calculated using Equation (7.5). Equation (7.4) was used throughout the simulations after the preexponential factor A_b was determined from available data.

7.1.1.3. Brownian Motion of Bacteria

The effect of diffusion has not been thoroughly investigated in the literature. Bacteria studied in the past were usually assumed to undergo convective motion only (Datta, 1991), thus omitting the diffusion term in Equation (7.1).

The classical theory of Brownian motion applies to very dilute suspensions. This theory was developed by Einstein, concerning the random migration of isolated colloidal particles or large solute molecules due to interaction with the molecules of the suspending fluid (Batchelor, 1976). When the suspension is not very dilute, the interaction of various particles will affect one another's migration, thus often reducing the diffusivity. In the simulations presented here only the diffusion of noninteracting particles (i.e., the bacteria) was considered, which is described well by Batchelor.

The force required to move a spherical particle at velocity v relative to an infinite Newtonian fluid is given by Stokes' law (Bird et al., 1960):

$$F = 6\pi\mu\, av \tag{7.6}$$

where a is the radius of the rigid spherical particle (bacteria), and μ is the viscosity of the suspending fluid. Equation (7.6) is derived by solving the Navier–Stokes equations for the slow motion of a single sphere in an infinite fluid that is stationary far from the sphere. If a particle is immersed in a fluid in rotational (e.g., laminar) flow, forces are developed because the (solid) particle cannot exactly replace a stretching deforming fluid element. The ratio v/F is called the particle mobility (m) and is related to the diffusivity of the particles in the fluid by the Nernst–Einstein equation for diffusivity:

$$\alpha = K_B T \frac{v}{F} = K_B T m \tag{7.7}$$

The Nernst–Einstein equation is applicable to very dilute suspensions of uncharged particles. The diffusion coefficient will increase as the particle concentration is raised (Anderson et al., 1978;

Batchelor, 1976). Statistical mechanics has been used to deduce the Brownian diffusivities of particle in a fluid that is being deformed and when there is a particle concentration gradient. The presence of charge can also affect the diffusion (Buffham et al., 1995); however such an effect has not been included in our calculation for the diffusion coefficient. The combination of Equations (7.6) and (7.7) gives the Stokes–Einstein equation, and the diffusivity α value, reported in Chapter 5 (Equation [5.15]), is used in the present simulation.

In this chapter, the following cases have been studied:

1. Concentration profiles of bacteria (*C. botulinum*) in a pouch filled with carrot-orange soup and heated by condensing steam. The migration of the slowest heating zone (SHZ) during sterilization was also studied. The results of the simulations were compared with that for sterilization of a can.
2. Concentration profiles of bacteria (*B. stearothermophilus*) in a pouch filled with beef-vegetable soup, which has been performed for the purpose of comparison with our experimental results, discussed later in Chapter 9.

The properties of carrot-orange soup used in the current simulations were the same as those used in Section 5.5. The viscosity of beef-vegetable soup is measured at different temperatures and shear rates. In the simulations presented here, the viscosity is assumed to be a function of temperature (Equation [5.10]). The viscosity of beef-vegetable soup was measured using a Paar Physica Viscometer VT2, available at the Chemical Engineering Department at the University of Auckland. The values of the viscosity are taken at an extremely low shear rate, which closely simulate the situation in the pouch being sterilized. These values are 1.410 Pa s, 0.658 Pa s, and 0.417 Pa s at 30°C, 50°C, and 70°C respectively.

The properties of beef-vegetable soup, used in the current simulations, are calculated from the values reported (Hayes, 1987; Rahman, 1995) for the material used in the soup, using their known mass fractions. The calculated physical properties are $\rho = 1010\,\mathrm{kg\,m^{-3}}$, $C_P = 3120\,\mathrm{J\,kg^{-1}\,K^{-1}}$, and $k = 0.567\,\mathrm{W\,m^{-1}\,K^{-1}}$. The variation of the density with temperature was governed by Boussinesq approximation such as all the cases studied earlier. The calculated Grashof number in the pouch containing beef-vegetable soup used in the simulation was of the order of only 10, giving a good indication that the natural convection flow is laminar.

Clostridium botulinum

The inactivation of *C. botulinum* in a 3-D pouch filled with carrot-orange soup during thermal sterilization has been simulated. The results of the simulations were presented as concentration profiles. The choice of this type of bacteria was explained in detail in Chapter 3. The activation energy for bacteria inactivation was 30×10^4 J/mol, as reported by Reuter (1993) for the destruction of *C. botulinum*. The value of the decimal reduction time at 121°C (D_{121}) for *C. botulinum* is 0.1 s as reported by Heldman and Hartel (1997). The reaction rate constant K_{T_b} was then calculated using Equation (7.8), and Equation (7.7) was used to calculate the preexponential factor A_b, giving $A_b = 2.5 \times 10^{11}\,\mathrm{s^{-1}}$.

Bacillus stearothermophilus

The heat resistance of bacterial spores is of great importance for the thermal sterilization and preservation of foods. In low-acid foods, process operation can be based on inactivation of spores which are more heat resistant than *C. botulinum*. Spores of *B. stearothermophilus* are extremely heat resistant

(up to 20 times more resistant than *C. botulinum*). The D_{121} of *B. stearothermophilus* ranges from 4.0 to 5.0 min, with z values between 7.8 and 12.2°C (Stumbo, 1973). Growth of *B. stearothermophilus* spores results in "flat sour" spoilage because acid is produced but with little or no gas generated (Karel et al., 1975). Since flat sour spoilage does not develop unless the product is at temperatures above 43°C, controlled cooling after thermal processing is necessary.

Significant causes of food spoilage include under-processing, inadequate cooling, contamination of the product resulting from leakage through seams, and preprocess spoilage (Jay, 1996). Low-acid foods such as meat and seafood, milk, some vegetables (corn, lima, and beans), and meat and vegetable mixtures (such as the soup used in our simulation) are spoiled by the thermophilic flat-sour group (*B. stearothermophilus*, *B. coagulans*, *C. nigrificans*, *C. bifermentans*, and *Thermoanaerobacterium thermosaccharolyticum*). Typical thermophilic flat sour spoilage of low-acid canned food is caused by the growth of spore-forming, thermophilic facultative aerobes. *B. stearothermophilus* is the species typically responsible for this type of spoilage (Ayres et al., 1980; Gordon et al., 1973).

In this chapter, the analysis used to study the inactivation of *C. botulinum* during thermal sterilization was extended to cover the inactivation of *B. stearothermophilus* spores. The main objective was to validate the theoretical simulations, using experimental measurements. The reason for selecting this type of spore, besides its being not highly dangerous, is that these thermophilic spores have a greater heat resistance than most other organisms encountered in foods, as we have noted earlier. This characteristic is advantageous to the examination of foods and ingredients because it is possible to eliminate all organisms except the spores with which we are concerned. This is done prior to the sterilization process so that the deactivation process is related to a single type of microorganism (*B. stearothermophilus* only). It is difficult to study the deactivation of other types of bacteria, which are more sensitive to heat due to the fast killing rate. Further, activation is necessary to induce germination of the maximum number of spores in a population of many species in the sample used for the test (Cook and Gilbert, 1968; Stumbo, 1973).

The activation energy for the inactivation of *B. stearothermophilus* used in our simulation is calculated from the following equation (Fryer et al., 1997; Karel et al., 1975):

$$E_{\mathrm{b}} = \frac{2.303 R_g T^2}{Z} \tag{7.8}$$

Where E_{b} is the activation energy of bacteria inactivation, kJ (kg mol)$^{-1}$; R_g is the gas constant, kJ (kg mol)$^{-1}$ K^{-1}; T is the temperature, K; and Z is the temperature required to change the thermal death time (TDT) by a factor of 10. The values of D_T and Z at 121°C for *B. stearothermophilus*, used in the simulation, are 4.0 min and 10°C respectively. These values are obtained from the tables of kinetic data for some reaction processes in the food industry, which are available in the literature, such as those reported by Fellows, 1996, Hayes, 1987, Jay, 1996, Karel et al., 1975, Rahman, 1995, Stumbo, 1973. The inactivation rate constant $k_{T_{\mathrm{b}}}$ is then calculated using Equations (5.24) and (5.25), which are used to calculate the preexponential factor A_{b}.

7.2. RESULTS OF SIMULATION

7.2.1. *Clostridium botulinum*

Figure 7.1 shows the results of the simulation for a pouch filled with carrot-orange soup, steam-heated from all sides (at 121°C) in a still retort. The observations of bacteria (*C. botulinum*) deactivation profiles during thermal sterilization liquid food in a 3-D pouch show similar trends as those in

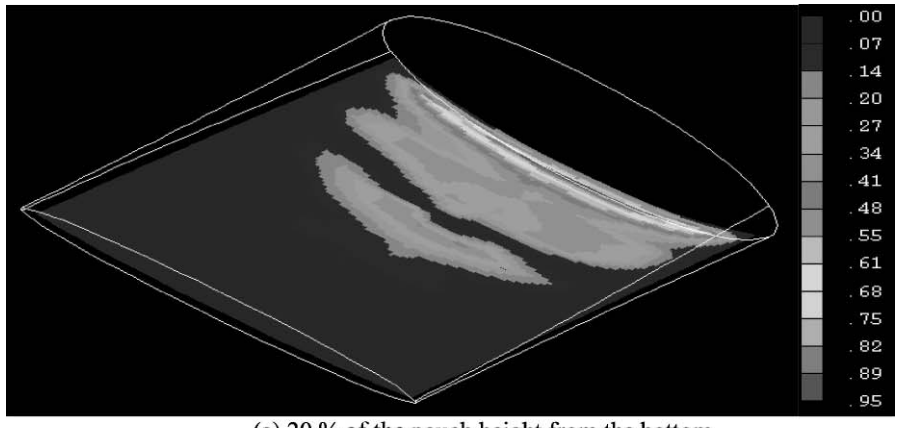

(a) 20 % of the pouch height from the bottom

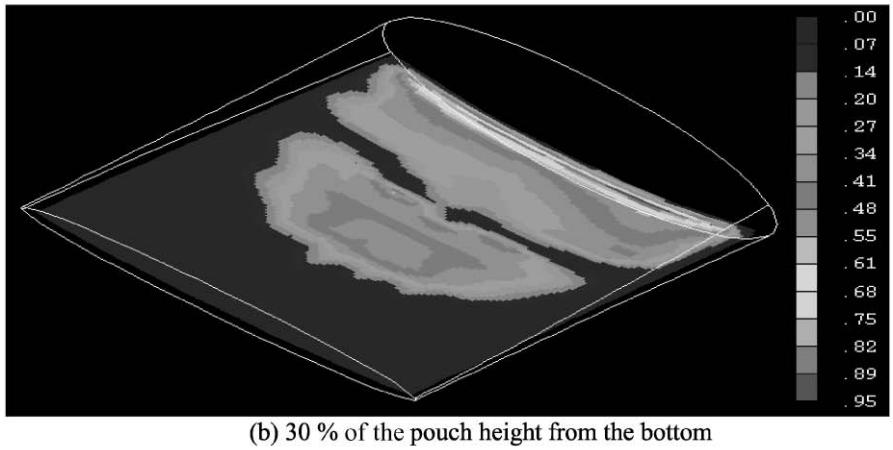

(b) 30 % of the pouch height from the bottom

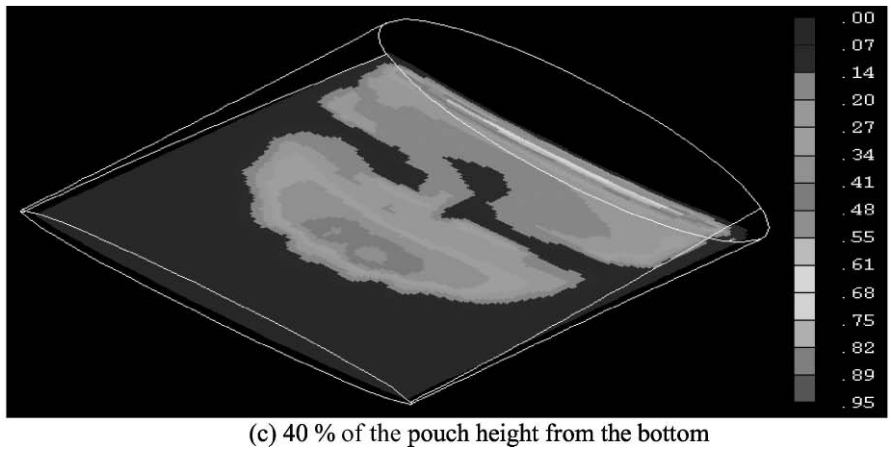

(c) 40 % of the pouch height from the bottom

Figure 7.1. Relative concentration profiles of *C. botulinum* at different y-planes in a pouch filled with carrot-orange soup and heated by condensing steam after 1000 s.

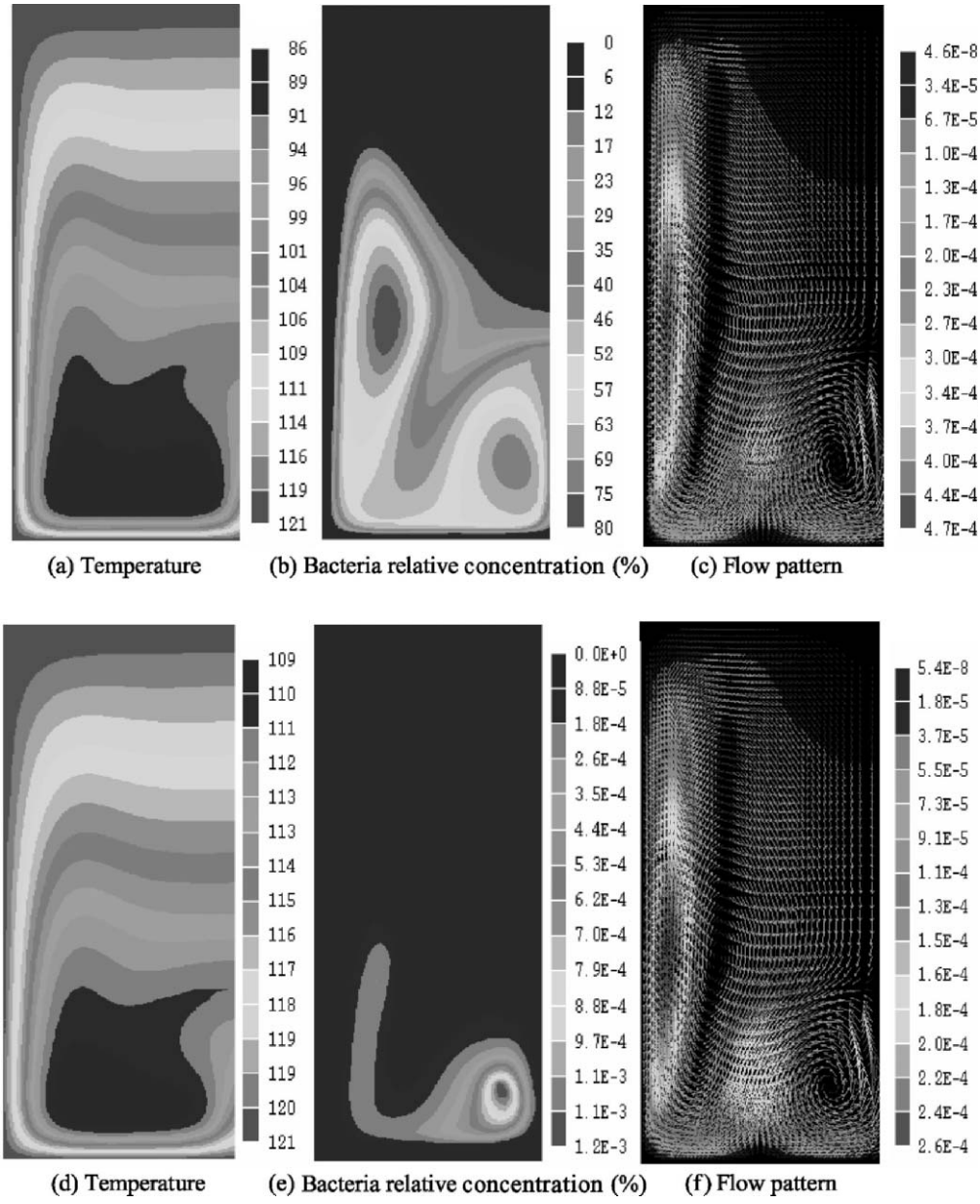

Figure 7.2. Temperature, bacteria deactivation, and velocity vector (ms^{-1}) profiles in a can filled with carboxyl methyl cellulose (CMC) and heated by condensing steam after 1157 s (a, b, and c) and 2574 s (d, e, and f) respectively. The right-hand side of each figure is the centerline (Ghani et al., 1999a).

the case of heating in cans shown in Figure 7.2. The appearance of a distinct SHZ was shown in Figures 7.2a and 7.2d. Figures 7.2c and 7.2f show the formation of a secondary flow at the bottom of the can. At the SHZ, the liquid and thus the bacteria carried with it are exposed to much less thermal treatment than the rest of the product. At the end of the heating, both the SHZ and the high bacteria concentration zone (HBCZ) remain at the same location.

The secondary flow influences the bacteria distribution significantly as can be seen from the two HBCZ shown in Figure 7.2b, which lie at the same location as the stagnant zones shown in Figure 7.2c. Figures 7.2b and 7.2e show that the bacteria deactivation is influenced significantly by both the temperature and the flow pattern. The highest concentration of bacteria shown in Figure 7.2b occurs at two locations. These locations belong to the minimum liquid velocity and low temperature zones. Similar observations are found at later stages of heating (Figure 7.2e).

Figure 7.1 shows, at the early stage of heating, the bacteria concentration profiles are almost identical to what is usually found in pure conduction heating, where bacteria are inactivated only at locations close to the wall of the pouch. At this early stage of heating, the bacteria concentration profile seems to be influenced mainly by the temperature profile and not by the flow pattern. This is evident from the higher rate of bacteria inactivation at the narrowest end of the pouch, where the temperature is higher, while the bulk of the pouch is little affected.

As heating progresses (at $t = 1000$ s), the temperature profiles are strongly influenced by convection currents (Figure 6.10d), as described earlier. Figure 7.1 shows the results of the simulation (the relative bacteria concentration profiles of *C. botulinum*) for a pouch filled with carrot-orange soup and heated by condensing steam after 1000 s. The temperature and bacteria concentration profiles shown in these figures (6.10d and 7.1) are very different from those observed at the beginning of the heating. The SHZ keeps moving during heating and eventually stays at 30% of the bottom of the pouch. The liquid and thus the bacteria carried with it at these locations are exposed to much less thermal treatment than the rest of the product. This can be shown clearly from the relative bacteria concentration profile shown in Figure 7.1b, at 30% of the pouch height from the bottom. After 1000 s of heating, the SHZ reaches 81°C (Figure 6.10d). In this zone (SHZ), the relative bacteria concentration ranges from 0.07 to 0.95 (3.2–2.0 log reduction) based on an initial value of 100, while almost complete inactivation of bacteria ($C_b/C_{b0} = 0$) occurs in most of the other locations (Figure 7.1).

Figure 7.1 also shows that the bacteria inactivation is influenced significantly by both the temperature (Figure 6.10d) and the flow pattern (Figures 6.12, 6.13, and 6.14), unlike those observed at the early stage of heating. The highest concentration of bacteria shown in Figure 7.1 occurs at two locations. These locations belong to the minimum liquid velocity and low temperature zones. Similar observations have been found at later stages of heating. At the end of the heating, the SHZ remains at the same location as the HBCZ. It is only after 3000 s of heating that most of the bacteria have been deactivated. This is true only for the high-viscosity liquid used in the simulation. A much shorter time would be required for the sterilization of liquid of low viscosity such as milk, orange juice, etc.

7.2.2. *Bacillus stearothermophilus*

In this simulation, natural convection currents of a viscous liquid food (beef-vegetable soup) in a 3-D pouch heated from all sides is presented and studied. A computational procedure is developed for describing the changes in the live bacteria spore (*B. stearothermophilus*) concentration and its spatial distribution during thermal sterilization processing. The main objective of this simulation is to compare the predictions with the experimental measurements.

Figures 7.3–7.5 show the results of the simulation. Results of *B. stearothermophilus* inactivation profiles during the thermal sterilization are similar to those of *C. botulinum*. At early stages of heating, the bacteria concentration profile seems to follow the temperature profile, which is due to pure conduction heating. As heating progresses (at $t = 300$ s), the temperature profile is strongly influenced by convection, and the bacteria concentration profile (Figure 7.3a) is influenced significantly by both the temperature distribution and the flow profile (Figure 7.5). At this stage, the buoyancy

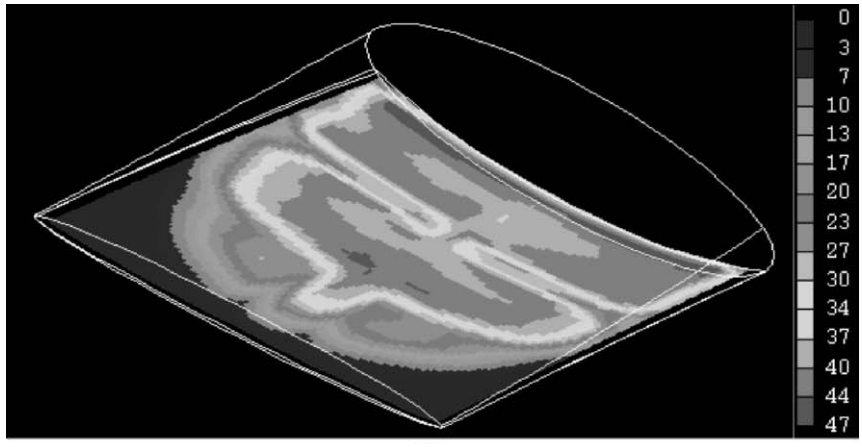

(a)

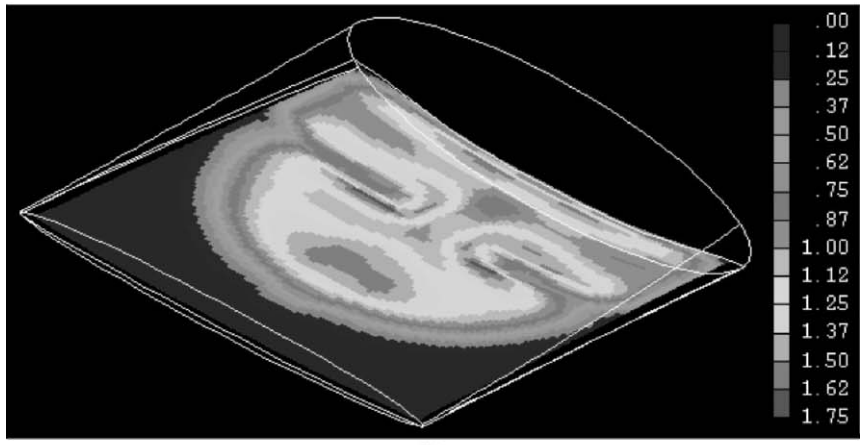

(b)

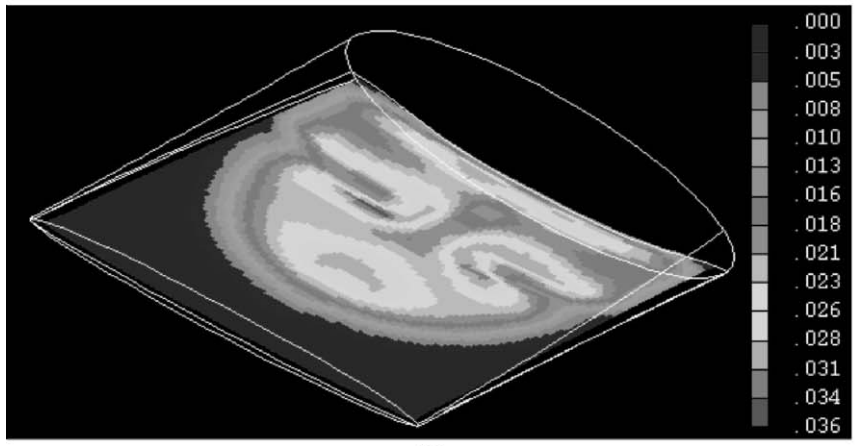

(c)

Figure 7.3. Relative concentration profiles of *B. stearothermophilus* spores at 30% of the height from the bottom of a pouch filled with beef-vegetable soup and heated by condensing steam after periods of (a) 300 s, (b) 900 s, and (c) 1500 s.

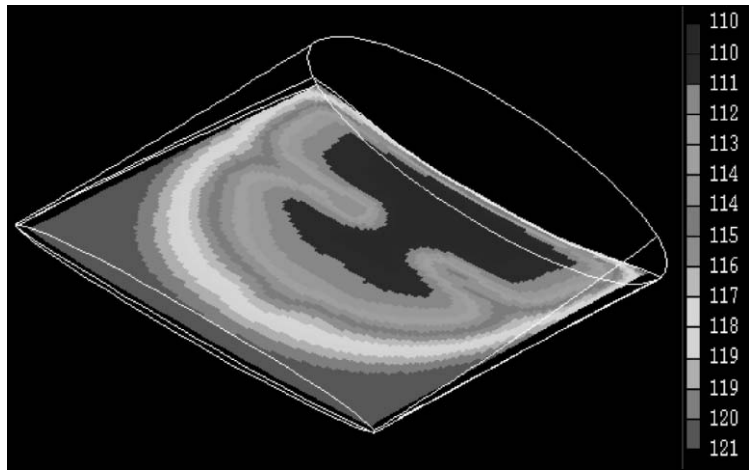

Figure 7.4. Temperature profiles of *B. stearothermophilus* at 30% of the height from the bottom of a pouch filled with beef-vegetable soup and heated by condensing steam after period of 1500 s.

force starts to be effective due to temperature variation from the wall to the core, and a recirculating flow pattern is created, as shown in Figure 7.5, for the x-plane velocity vector. The appearance of a distinct SHZ shown in Figure 7.4 has been discussed earlier. This can be shown clearly from the relative bacteria concentration profile presented in Figure 7.3. At the later stage of heating, the SHZ remains at the same location as the HBCZ, which can be clearly seen in Figures 7.3b and 7.3c.

Figure 7.4 shows that after 1500 s of heating, the SHZ in a pouch filled with beef-vegetable soup reaches 110°C using a sterilization temperature of 121°C. In this zone (SHZ), the relative bacteria concentration ranged from 0.036 to 0.003 (3.4–4.5 log reduction) based on the initial value of 100, while almost complete inactivation of bacteria ($C_b/C_{b0} = 0$) occurred in most of the other locations (Figure 7.3). At the same temperature (110°C) and after 1960 s, for a can filled with concentrated cherry soup and heated at a sterilization temperature of 121°C, Figure 7.6 shows that the relative

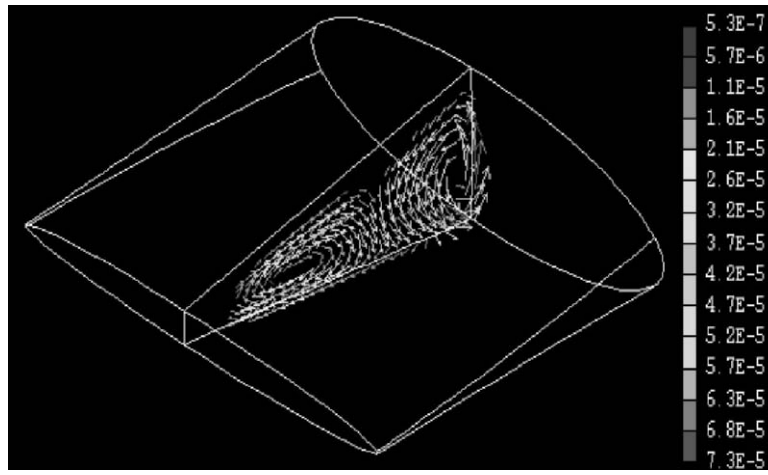

Figure 7.5. The x-plane velocity (ms^{-1}) of beef-vegetable soup in a pouch heated by condensing steam along outside surface after 300 s.

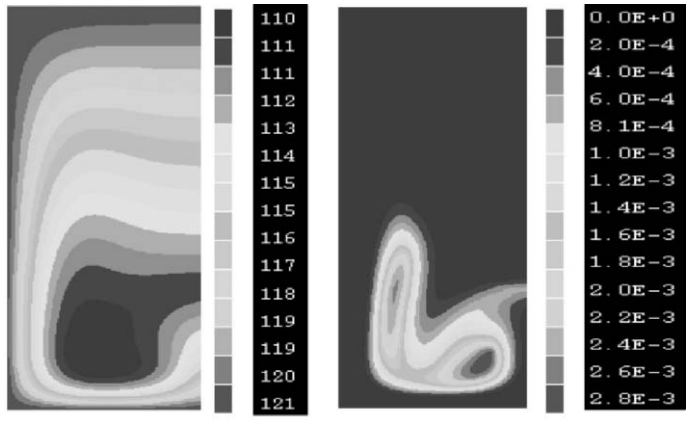

(a) Temperature (a) Bacteria relative conc. (%)

Figure 7.6. Temperature and bacteria deactivation profiles in a can filled with concentrated cherry juice and heated by condensing steam at 121°C after 1960 s. The right-hand side of each figure is the centerline (Ghani et al., 1999b).

bacteria concentration of *C. botulinum* ranged from 0.0028 to 0.0002 based on the initial value of 100 (4.5–5.7 log reduction) (Ghani et al., 1999b). This leads to the conclusion that at the same temperature, the inactivation of *C. botulinum* is 10–15 times faster than that for *B. stearothermophilus*.

The bacteria concentration in the SHZ (zone of minimum temperature) is a good measure of the food sterility. As mentioned earlier in Chapter 5, it is very difficult to measure local bacteria concentration in the pouch. Average value of the concentration can be measured by shaking the pouch after specified heating times. Hence, for the purpose of comparison with the theoretical predictions, it is necessary to calculate the mean viable bacteria concentration in the whole pouch. The weighted average concentration is defined as follows:

$$\overline{C} = \frac{1}{V_{\text{pouch}}} \sum_{i=1}^{n} \sum_{j=1}^{m} \sum_{k=1}^{l} C_{i,j,k} \Delta x \Delta y \Delta z \tag{7.9}$$

which is implemented in the software, using nested loops in a FORTRAN code.

The main purpose of these calculations was to validate the model against experimental measurements (Chapter 9). These calculations show that after heating periods of 300 s, 600 s, 900 s, 1200 s, 1500 s, and 1800 s, the average relative spore (*B. stearothermophilus*) concentrations drop to about 20.85%, 2.56%, 0.45%, 0.063%, 0.0076%, and 0.7×10^{-3}% (0.68, 1.6, 2.3, 3.2, 4.1, and 5.2 log reduction). The locations of high bacteria zones are usually at the SHZ, while complete inactivation of bacteria ($C_b/C_{b0} = 0$) occurred at most other locations.

7.3. DESTRUCTION OF VITAMINS IN FOOD POUCHES DURING THERMAL STERILIZATION

The destruction of vitamins follows a first-order reaction similar to microbial inactivation (Fellows, 1996). In general, the value of the decimal reduction time (D) for vitamins is higher than that of microorganisms and enzymes. The desired canning process of minimizing quality losses and achieving at the same time sufficient degree of sterility is possible because of the strong temperature dependence of spore inactivation as compared to quality destruction, sensorial as well as nutritional (Lund, 1977).

Several studies on computer simulations of sterilization of food have been done to investigate the effect of thermal sterilization on the retention of vitamins. Teixeira et al. (1969 and 1975) developed a numerical computer model to simulate the effect of a heat process on the destruction of thiamine in pea puree, which is usually relatively rich in thiamine. Saguy and Karel (1979) investigated and developed a method for calculating the optimum temperature profile as a function of the time needed to achieve a specified level of sterilization with maximum nutrient retention.

Fruits and vegetables are the most common food sources of vitamin C. Vitamin C exists naturally as two equally biologically active vitamins, L-ascorbic acid (AA) and dehydroascorbic acid (DHAA). These vitamins are often bound to protein in natural products. Vitamin C's most important chemical properties from an analytical perspective relate directly to its marked lack of stability. As one of the most liable vitamins, it is often used as an indicator of overall vitamin stability in foods.

Vitamin B_1 (thiamine) has been known as the vitamin whose deficiency produces some illness, especially to neurological function. Food sources of thiamine include meat, fish, whole cereal grains, fortified cereal, and bakery products, nuts, legumes, eggs, yeast, fruits, and vegetables. Endogenous vitamin B_2 (riboflavin) occurs in foods in three principal forms: riboflavin and its physiologically active coenzyme forms, flavin mononucleotide (FMN) and flavin adenine dinucleotide (FAD). The most important characteristic affecting vitamin B_2 is its photosensitivity. Degradation of vitamin B_2 by ultraviolet (UV) and visible light produces irreversible photo reduction as well as loss of vitamin activity (Nollet, 1996).

The objective of this chapter is to show how a computational fluid dynamics (CFD) modeling approach can be used to provide a rigorous analysis of sterilization in a 3-D pouch containing liquid foods, which has not been done previously. The theoretical analysis for the determination of vitamin concentration during thermal sterilization of a 3-D pouch filled with carrot-orange soup is presented. The analysis used to study the inactivation of bacteria earlier is extended to cover the destruction of different types of vitamins. The effect of the heating temperature on the biochemical changes during thermal sterilization of liquid food in a pouch similar to that used in the previous chapter is also presented.

The thermal destruction kinetics of the quality evolution was described by the concentration profiles. Profiles of concentrations of vitamins C (ascorbic acid [AA]), B_1 (thiamine), and B_2 (riboflavin) in a can filled with viscous liquid food (carrot-orange soup) during thermal sterilization were presented and studied. The governing equations of continuity, momentum, and energy were solved numerically together with vitamin concentrations equations, using the same software code used in all our previous work. The Arrhenius equation was used to describe the kinetics of these biochemical changes. It was introduced to the existing software package using a FORTRAN code. The details of this code can be found in the beginner's menu system user guide by Patankar and Spalding (1972), Radosavljevic and Wu (1990). The temperature dependence of the carrot-orange soup's viscosity and density was incorporated in the simulation. The simulation highlights the dependency of the concentration of vitamins on both temperature distribution and flow pattern as sterilization proceeds.

7.3.1. Numerical Approximations and Model Parameters

The concentration equation of the vitamins was introduced and solved together with the momentum and energy equations governing natural convection in a 3-D pouch (6.5–6.8):

Mass balance for vitamins (concentration equation)

$$\frac{\partial C_{\mathrm{rv}}}{\partial t} + v_x \frac{\partial C_{\mathrm{rv}}}{\partial x} + v_y \frac{\partial C_{\mathrm{rv}}}{\partial y} + v_z \frac{\partial C_{\mathrm{rv}}}{\partial z} = D\left[\frac{\partial^2 C_{\mathrm{rv}}}{\partial x^2} + \frac{\partial^2 C_{\mathrm{rv}}}{\partial y^2} + \frac{\partial^2 C_{\mathrm{rv}}}{\partial z^2}\right] - k_{T_{\mathrm{v}}} C_{\mathrm{rv}} \tag{7.10}$$

Table 7.1. Kinetic data for some chemical and biochemical reactions used in our simulations, as reported by Fryer et al. (1997).

Property for vitamins destruction	D_{121} (min)	E_v (kJ mol^{-1})
Ascorbic acid (C)	245	65–160
Thiamin (B_1)	38–380	90–125
Riboflavin (B_2)	2800	100

Where v_x, v_y, and v_z are the velocities in x, y, and z coordinates respectively (ms^{-1}), k_T is the destruction rate constant of vitamins C, B_1, or B_2, and C_{rv} is the relative concentration (%) of vitamins C, B_1, or B_2 in the pouch at any time and location. The concentration is taken as a dimensionless species concentration, which is defined as the ratio of real-time concentration (C) (kg m^{-3}) to the initial concentration (C_0) (kg m^{-3}) multiplied by 100. The boundary conditions used were similar to those used for bacteria explained earlier in this chapter.

The properties of carrot-orange soup were $\rho = 1{,}026$ kg m^{-3}, $C_P = 3880$ J kg^{-1} K^{-1}, and $k = 0.596$ W m^{-1} K^{-1}. The properties were calculated from the values reported by Rahman (1995) and Hayes (1987) for all the food materials used in the soup, using their mass fractions. The simplifying assumptions used in the current simulation were the same as those used in the simulation of the bacteria inactivation mentioned earlier in this chapter. The effect of molecular diffusion of vitamins was also tested and found small due to the process being convection dominated. The variation of the density with temperature was governed by Boussinesq approximation such as all the cases studied earlier.

7.3.2. Vitamin Destruction Kinetics

The kinetics of vitamin destruction is similar to that used for bacteria inactivation. The reaction rate constants for vitamins are a function of temperature as described by Arrhenius equation:

$$k_{T_v} = A_v e^{-E_v/R_g T} \tag{7.11}$$

The kinetic data for the destruction of vitamins used in our simulations are given in Table 7.1. The values of the preexponential factor (A_v) were calculated using the reported values of activation energy shown in Table 7.1. These values are 2.85×10^9 s^{-1}, 8.5×10^8 s^{-1}, and 2.48×10^8 s^{-1} for vitamins C, B_1, and B_2 respectively.

The calculated Grashof number for the viscous liquid used in the simulation gives a good indication that natural convection flow is laminar. The computations were performed for a 3-D pouch with a width (W) of 120 mm, height (H) of 40 mm, and length (L) of 220 mm. The pouch outer surface temperature (top, bottom, and sides) was assumed to rise instantaneously and to be maintained at 121°C throughout the heating period.

7.4. RESULTS OF SIMULATION

The effect of sterilization temperature on the rate of destruction of different types of vitamins is presented here. Figures 7.7, 7.8, and 7.9 show the results of the simulation at times of 200 s, 1000 s, and 3000 s for vitamins C, B_1, and B_2 respectively. At the early stage of heating ($t = 200$ s), heat transfer is solely controlled by conduction as shown by the comparison between the convection heating (Figure 6.10a) and conduction heating (Figure 6.11a) discussed earlier. The destruction of

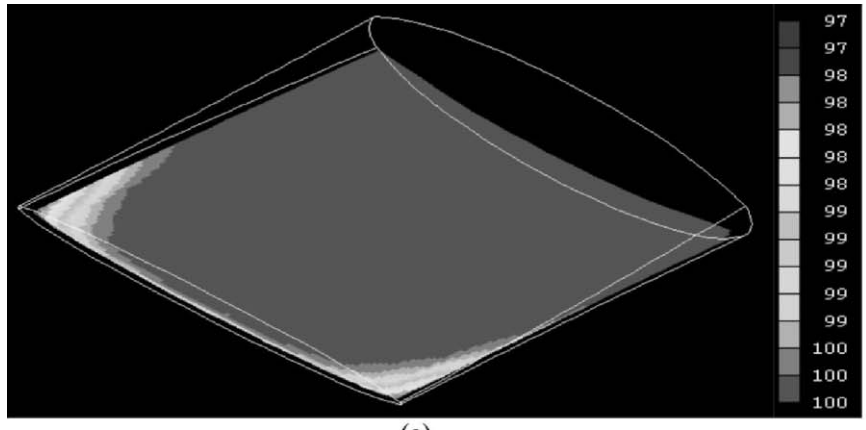

(a)

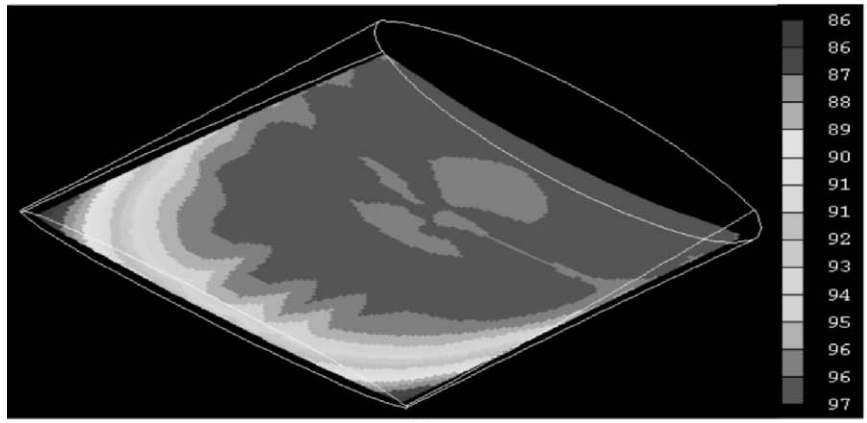

(b)

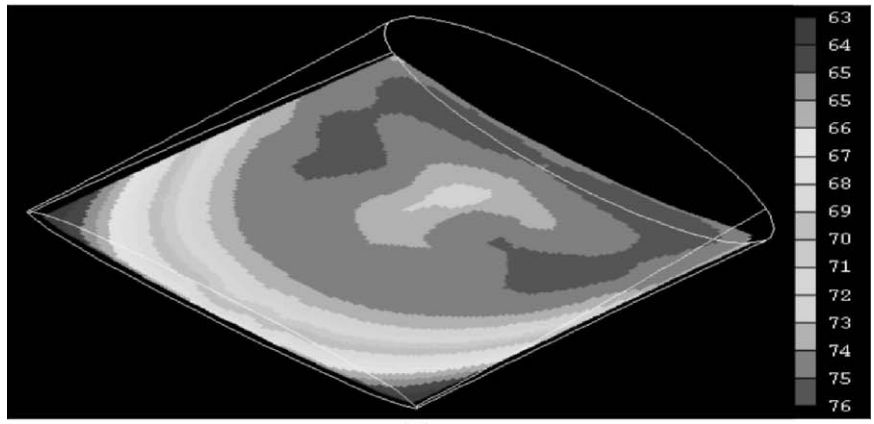

(c)

Figure 7.7. Relative concentration profiles of vitamin C at 30% of the height from the bottom of a pouch filled with carrot-orange soup and heated by condensing steam after periods of (a) 200 s, (b) 1000 s, and (c) 3000 s.

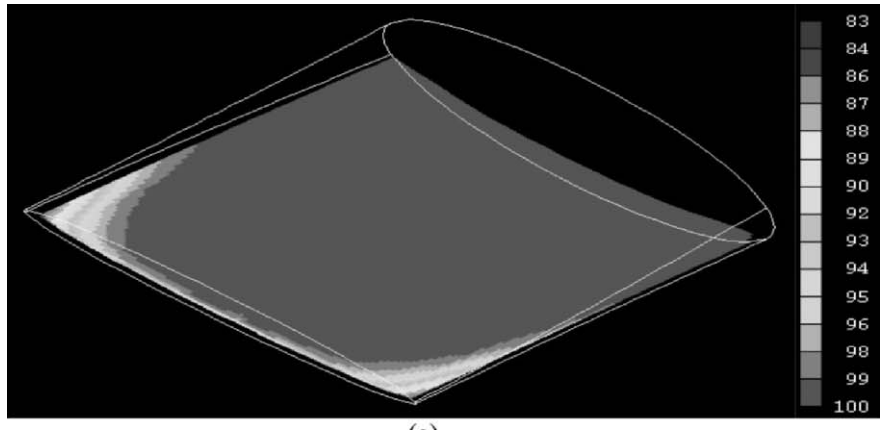

(a)

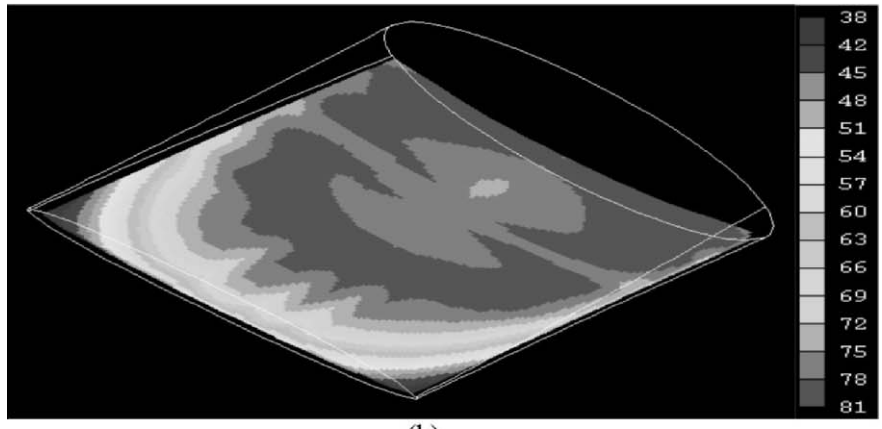

(b)

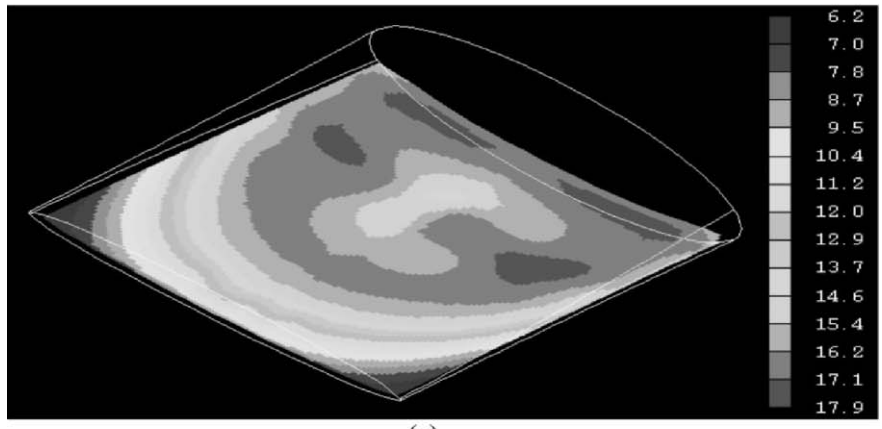

(c)

Figure 7.8. Relative concentration profiles of vitamin B_1 at 30% of the height from the bottom of a pouch filled with carrot-orange soup and heated by condensing steam after periods of (a) 200 s, (b) 1000 s, and (c) 3000 s.

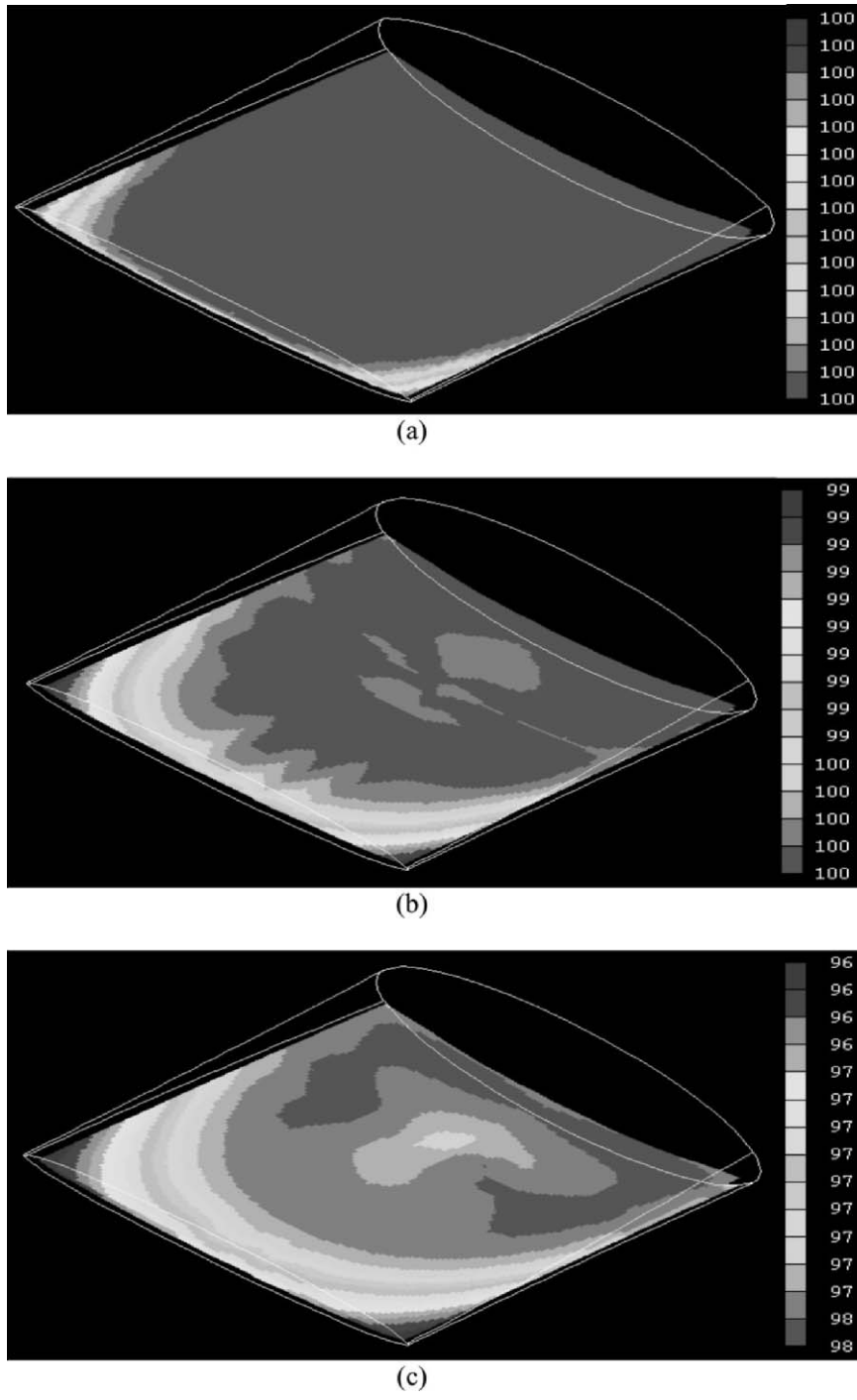

Figure 7.9. Relative concentration profiles of vitamin B_2 at 30% of the height from the bottom of a pouch filled with carrot-orange soup and heated by condensing steam after periods of (a) 200 s, (b) 1000 s, and (c) 3000 s.

vitamins C, B_1, and B_2 shown in Figures 7.7a, 7.8a, and 7.9a follows similar trends but with varying degree.

As time progresses, heating is dominated by natural convection, as shown in Figure 6.10d. Figures 7.7b, 7.8b, and 7.9b show the results of the simulation after relatively longer periods of 1000 s. These figures show that most vitamin (C, B_1, and B_2) destruction occurs at locations near the wall and especially at the narrowest end of the pouch, which are the locations of high temperature. The figures also show that the vitamins are concentrated at the SHZ, and the destruction of vitamins has occurred mostly in other locations. The liquid and thus the vitamins carried with it are exposed to much less thermal treatment at the SHZ than the rest of the product. Figures 7.7b, 7.8b, and 7.9b show clearly the combined effects of the temperature distribution (Figure 6.10d) and velocity profile (Figures 6.12, 6.13, and 6.14) on the shape and location of the high vitamin concentration zone (HVCZ). Figure 6.14 for the z-plane velocity vector, at 8 cm from the widest end, shows the effect of fluid circulation that leads to two stagnant zones, which affect the HVCZ, shown by Figures 7.7b and 7.8b. These results lead to the conclusion that the vitamin profiles depend not only on temperature distribution but also on velocity profiles in the pouch. The locations of the HVCZ occur almost within the stagnant zones, which belong to minimum liquid velocity.

Figure 7.10 shows the relative concentration profiles of vitamins C, B_1, and B_2 in the x-plane of the center of the pouch filled with carrot orange-soup and heated by condensing steam at the end of heating (3,000 s). This figure shows the locations of the HVCZ at the two stagnant zones, which can be explained clearly in terms of the x-plane velocity vector shown in Figure 6.12b (Chapter 6).

Figure 7.11 shows the locations of high vitamin C concentration zones at different z-planes in the pouch after 1000 s of heating. Figures 7.11a and 7.11b show that the HVCZ occurs at the lower half of the pouch, which is due to the effect of natural convection currents, such as that shown in Figure 6.14. At locations close to the narrowest end, Figures 7.11c and 7.11d show that the HVCZ stays at the mid-height of the plane. This is due to the influence of conduction dominating heating in the locations at the narrowest end of the pouch.

It is very difficult to measure local vitamin concentration in the pouch. Average values of the concentration can be measured by shaking the pouch at the end of different sterilization times, same as those used in bacteria measurements explained earlier in this chapter. Hence, for the purpose of comparison with the theoretical predictions, it is necessary to calculate the mean vitamin concentration in the whole pouch. The calculation was based on the weighted average of the local vitamin concentrations, and the equation used is the same as those used earlier for bacteria concentration (Equation [7.9]). These calculations show that at the end of heating (at $t = 3000$ s), the average relative vitamin concentrations drop to about 71%, 12%, and 97% for the vitamins C, B_1, and B_2 respectively.

Observations of relative bacteria and vitamins concentration profiles during natural convection heating show that concentrations of both bacteria and vitamins depend on both the temperature and the flow pattern. The locations of low destruction zones belong to minimum liquid velocity and low temperature zones. It was also found from Figures 6.10d, 6.12, 6.14, 7.7b, 7.8b, 7.9b, and 7.1 that at the same time (at $t = 1000$ s), the relative bacteria concentration profile (Figure 7.1) seems to be influenced mainly by temperature profiles (Figure 6.10d). The influence of the flow pattern (Figures 6.12 and 6.14) on vitamin concentration profiles (Figures 7.7b, 7.8b, and 7.9b) is even stronger than those on bacteria, as the location of the high vitamin concentration occurs almost within the stagnant zone. The rate of bacteria inactivation is higher than that of vitamin destruction, which is due to the low value of the decimal reduction time of bacteria compared to that of vitamins, which makes the bacteria inactivation more sensitive to temperature. This explains why the bacteria profile follows exactly the temperature profile.

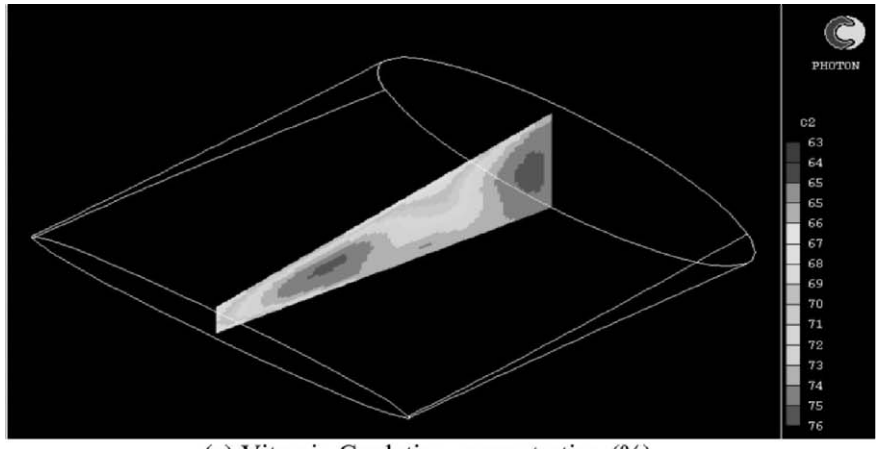

(a) Vitamin C relative concentration (%)

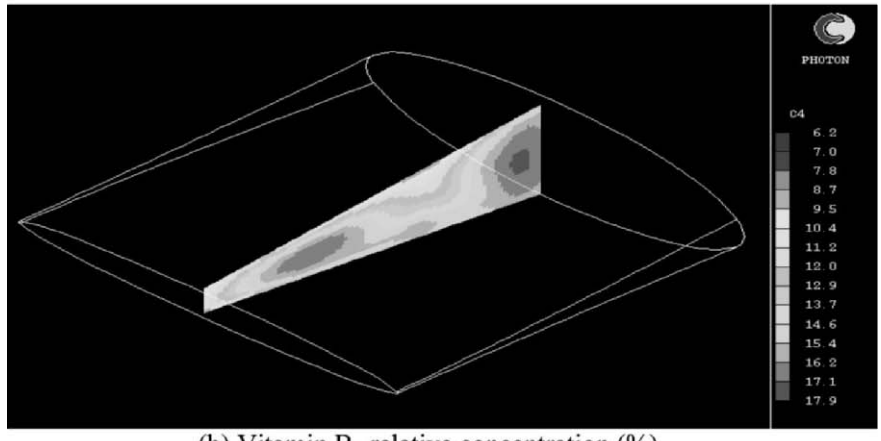

(b) Vitamin B_1 relative concentration (%)

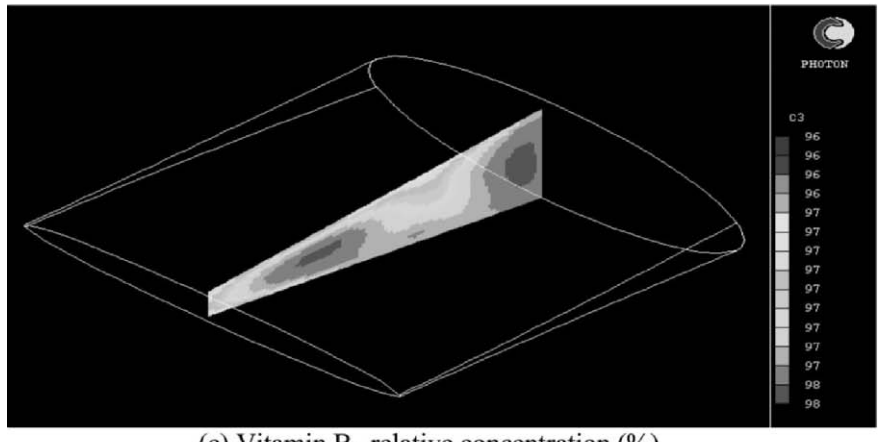

(c) Vitamin B_2 relative concentration (%)

Figure 7.10. Relative concentration profiles of vitamins C, B_1, and B_2 at 50% of the x-plane of a pouch filled with carrot-orange soup and heated by condensing steam after 3,000 s.

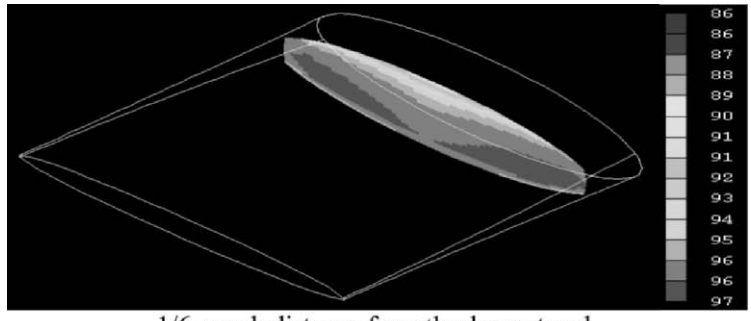

1/6 pouch distance from the deepest end

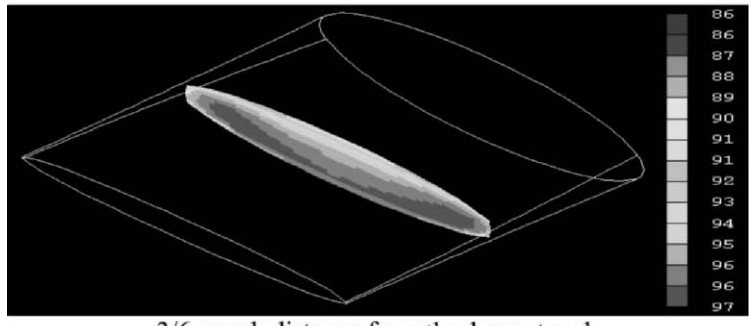

3/6 pouch distance from the deepest end

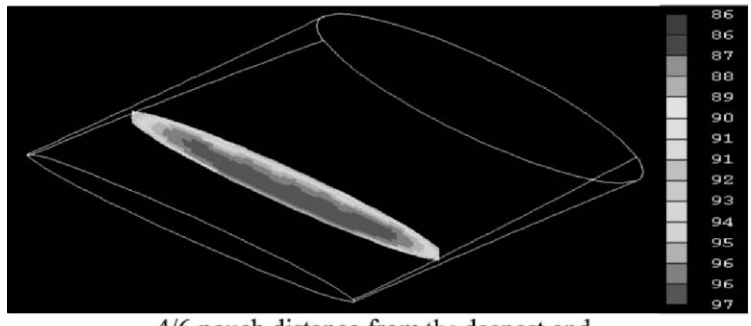

4/6 pouch distance from the deepest end

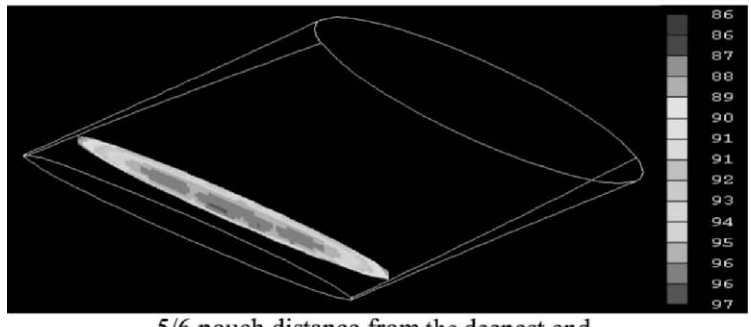

5/6 pouch distance from the deepest end

Figure 7.11. Relative concentration profiles of vitamin C at different y-planes in a pouch filled with carrot-orange soup and heated by condensing steam after 1000 s.

NOMENCLATURE

a	area, m^2
A	preexponential factor, s^{-1}
C	concentration of bacteria (number of bacteria m^{-3}) and vitamin (kg m^{-3})
d_v	vertical dimension, m
D_T	decimal reduction time, min
E	activation energy, kJ (kg mol)$^{-1}$
Gr	Grashof number, Gr $= \frac{d_v^3 \rho^2 g \beta \Delta T}{\mu^2}$, dimensionless
g	acceleration due to gravity, m s^{-2}
H	height of the geometry, m
k_T	reaction rate constant, s^{-1}
L	length of the geometry, m
m	particle mobility (v/F)
Pe	Peclet number, Pe $= \frac{v_z \Delta z}{\alpha}$, dimensionless
R_g	gas constant, kJ (kg mol)$^{-1}$ K^{-1}
t	time, s
T	temperature, °C
W	width of the geometry, m
v	velocity, m s^{-1}
V	volume, m^{-3}
Z	temperature required to change the thermal death time (TDT) by a factor of 10, °C
β	thermal expansion coefficient, K^{-1}
μ	viscosity, Pa s
ρ	density, kg m^{-3}
α	diffusion coefficient, m^2 s^{-1}

Subscripts

b	bacteria
b_{0o}	initial for bacteria
0	initial
rb	relative bacteria
rv	relative vitamin
v	vitamin
v_0	initial for vitamin
w	wall
x, y, z	coordinates

REFERENCES

Anderson, J.L., Rauh, R., & Moroles, A. (1978). Particle diffusion as a function of concentration of ionic strength. *Journal of Physics Chemistry, 82*, 608–616.

Ayres, J.C., Mundt, J.O., & Sandine, W.E. (1980). *Microbiology of foods*. San Francisco, CA: W. M. Freeman and Co..

Batchelor, G.K. (1976). Brownian diffusion of particles with hydrodynamic interaction. *Journal of Fluid Mechanics, 74*, 1–29.

Bird, R.B., Stewart, W.E., & Lightfoot, E.N. (1960). *Transport Phenomena*. New York: John Wiley & Sons.

Buffham, B.A., & Cumming, I.W. (1995). Prevention of particle deposition in crossflow microfiltration. *Transactions of the Institution of Chemical Engineers*, Part A, 445–449.

Chiruta, J., Davey, K.R., & Thomas, C.J. (1997). Thermal inactivation kinetics of three vegetative bacteria as influenced by combined temperature and pH in a liquid medium. *Transactions of the Institution of Chemical Engineers*, Part C, Bio products and Food Processing, *75*, 174–180.

Cook, A.M., & Gilbert, R.J. (1968). Factors affecting the heat resistance of *Bacillus stearothermophilus* spores. *Food Technology, 3*, 285.

Datta, A.K. (1991). Mathematical modeling of biochemical changes during processing of liquid foods and solutions. *Biotechnology Progress, 7*, 397–402.

Davey, K.R., & Cerf, O. (1996). Predicting the concomitant denaturation of vitamins as influenced by combined process temperature and pH in batch and continuos flow sterilization. *Transactions of the Institution of Chemical Engineers*, Part C, Bio products and Food Processing, *74*, 200–206.

Davey, K.R., Hall, R.F., & Thomas, C.J. (1995). Experimental and model studies of the combined effect of temperature and pH on the thermal sterilization of vegetative bacteria in liquid. *Transactions of the Institution of Chemical Engineers*, Part C, Bio products and Food Processing, *73*, 127–132.

Fellows, P.J. (1996). *Food processing technology, principles and practice*. U.K.: Woodhead Publishing Series in Food Science and Technology.

Fryer, J.P., Pyle, D.L., & Rielly, C.D. (1997). *Chemical engineering for the food industry*. Blackie Academic & Professional.

Ghani, A.G., Farid, M.M., Chen, X.D., & Richards, P. (1999a). An investigation of deactivation of bacteria in canned liquid food during sterilization using computational fluid dynamics (CFD). *Journal of Food Engineering, 42*, 207–214.

Ghani, A.G., Mohammed, M.F., Chen, X.D., & Richards, P. (1999b). Heat transfer and biochemical changes in liquid food during sterilization using computational fluid dynamics (CFD). CHEMICA 99 Conference, 26–29 September 1999, Newcastle, Australia.

Gordon, R.E., Haynes, W.C., & Pang, C. (1973). *The genus Bacillus* (Agriculture Handbook No. 427). Washington, DC: U.S. Department of Agriculture.

Hayes, G.D. (1987). *Food engineering data handbook*. New York, NY 10158: John Wiley & Sons.

Heldman, D.R., & Hartel R.W. (1997). *Principles of food processing*. New York: Chapman & Hall.

Jay, J. M. (1996). *Modern food microbiology*. New York: Chapman & Hall.

Karel, M., Fennema, O.R., & Lund, D.B. (1975). *Principles of food science*, Part II. New York: Marcel Dekker.

Lund, D.B. (1977). Maximizing nutrient retention. *Food Technology, 31*(2), 71–80.

Nollet, M.L. Leo (1996). *Handbook of food analysis, physical characterization and nutrient analysis*. New York: Marcel Dekker.

Patankar, S.V., & Spalding, D.B. (1972). A calculation procedure for heat, mass and momentum transfer in three-dimensional parabolic flows. *International Journal of Heat and Mass Transfer, 15*(10), 1787–1806.

PHOENICS Reference Manual, Part A: PIL. TR 200 A, Bakery House, London SW 19 5AU, U.K.: CHAM.

Radosavljevic, D., & Wu, J.Z. (1990). *The PHOENICS beginner's menu system user guide*. TR 217 A, Bakery House, London SW 19 5AU, U.K.: CHAM.

Rahman, R. (1995). *Food properties handbook*. USA: CRC Press.

Reuter H. (1993). *Aseptic processing of foods*. Lancaster, USA: Technomic Publishing.

Saguy, I., & Karel, M. (1979). Optimal retort temperature profile in optimizing thiamin retention in conduction-type heating of canned foods. *Journal of Food Science, 44*, 1485–1490.

Stumbo, C.R. (1973). *Thermo bacteriology in food processing* (2nd ed.). New York: Academic Press.

Teixeira, A.A., Dixon, J.R., Zahradnik, J.W., & Zinsmeister, G.E. (1969). Computer optimization of nutrient retention in thermal processing of conduction-heated foods. *Food Technology, 23*(6), 134–140.

Teixeira, A.A., Stumbo, C.R., & Zahradnik, J.W. (1975). Experimental evaluation of mathematical and computer models for thermal process evaluation. *Journal of Food Science, 40*, 653–655.

CHAPTER 8

EXPERIMENTAL MEASUREMENTS OF THERMAL STERILIZATION OF FOOD IN 3-D POUCHES

The objective of this chapter is to validate the theoretical predictions of temperature distribution, vitamin C destruction, and bacteria (*Bacillus stearothermophilus*) inactivation during sterilization of food in a pouch.

8.1. TEMPERATURE MEASUREMENTS IN POUCHES

The measurements of temperature distribution in a pouch were conducted at Heinz Watties Australasia Research and Development Laboratories located at Hastings, New Zealand. Temperature at different locations in a pouch filled with carrot-orange soup was measured throughout the whole period of sterilization. The equipment and materials used in the measurements were as follows:

1. Pouches filled with carrot-orange soup, produced by Heinz Watties Australasia
2. Easteel Pilot Plant Retort-Full Immersion Process
3. Thermocouple probe with "G" Jack Plugs, length 7 m, needle 80 $\times$ 1.2 mm^2
4. Process validation and monitoring system (ELLAB), with E-Val software
5. IBM ThinkPad 600 Pentium II Laptop
6. Power supplies 110–240 V, 50/60 Hz
7. Plastic pieces (glands) of lengths 15 mm, 35 mm, and 40 mm, used to hold the thermocouple in the pouches
8. Slipring contact with 12 channels, complete with connection cables
9. Temperature data logger with 16 channels
10. "T" plugs and termination plugs interface and coax cables

A single pouch filled with the soup was placed in a newly developed retort, with validation and monitoring system software run on an IBM ThinkPad 600 Pentium laptop, to analyze all measurements. The retort operates using saturated steam at 121°C. The measurements were performed for a single pouch having a width of 120 mm, height of 40 mm, and length of 220 mm, same as those used in the simulations (Section 6.1). The pouch was sitting on a tray in a horizontal position and heated for 50 min for complete sterilization. The total time for the whole sterilization process of carrot-orange soup was 5,400 s. The first 3,600 s were for the heating cycle, another 600 s were used for holding time, and the remaining 1,200 s were used for the cooling cycle to complete the sterilization process.

Thermocouple probes were placed at different locations in the pouch to measure the temperature distribution inside the pouch. The thermocouple probes were connected to a temperature data logger

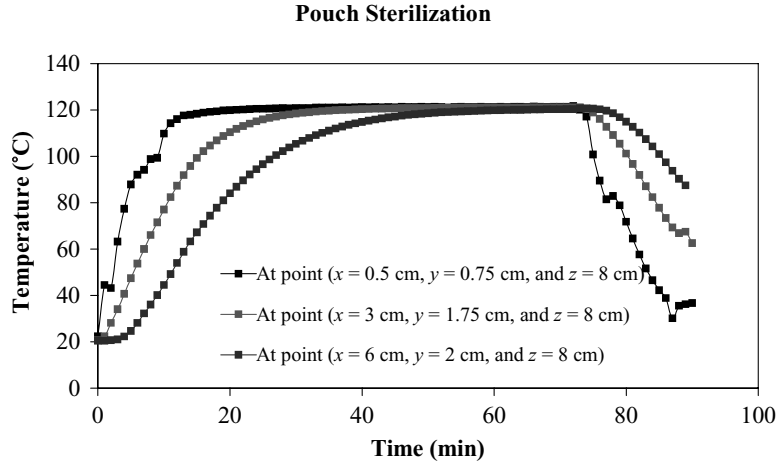

Figure 8.1. Experimental measurements of temperature at different locations in a pouch filled with carrot-orange soup during heating, holding time, and cooling cycles of the sterilization process.

with 16 channels to carry out the measurements. The temperatures were measured at the z-plane (Figure 6.2), which was 8 cm apart from the widest end of the pouch and at x–y positions of (0.50 cm, 0.75 cm), (3.00 cm, 1.75 cm), and (6 cm, 2 cm). The conduit pieces used to hold the thermocouple probes in place had different heights of 15 mm, 35 mm, and 40 mm. The results of the measurement for the complete sterilization (i.e., the heating cycle, holding time, and cooling cycle) were plotted, as shown in Figure 8.1. Heating and cooling curves are usually used to describe the temperature history of canned food during sterilization; they are used to determine the proper heat processes for canned food (Hayakawa and Ball, 1969).

In saturated steam retorts, the temperature and the pressure are controlled to remove air that may be in the system (i.e., ventilation). Air that is not removed can cause localized lowering of the temperature inside the retort. This can be seen clearly in Figure 8.1 at the measured point ($x = 0.50$ cm, $y = 0.75$ cm, and $z = 8.00$ cm) close to the wall, which is more sensitive than points measured at other locations.

8.1.1. Temperature Measurements During the Heating Cycle

Figure 8.1, for the period from 0 to 60 min, shows the measured temperature at different locations in a pouch filled with carrot-orange soup and heated by condensing steam. It shows a significant temperature distribution in the pouch throughout the whole period of heating. Such results indicate that a single temperature measurement is not sufficient to define the degree of sterility of the food. Figure 8.2 shows a good agreement between the measured and calculated temperatures near the wall, whether the calculation is based on conduction heating or combined convection/conduction heating. Figures 8.3 and 8.4 show a comparison between the measured temperatures at two locations far from the wall of the pouch and those obtained from the computer simulations. Both of these figures show a far better agreement between the measurements and predictions when based on convection/conduction heating compared to pure conduction heating. Figure 8.3 shows that the predicted temperature is higher than that measured. This might be due to the distorted torroid caused by convective circulation such as that appears clearly in Figures 6.10d–6.10f, which occurs at the same location of the thermocouple used in the measurement. Figure 8.4 shows a comparison between the measured temperature at the slowest heating zone (SHZ) of the pouch and that obtained from

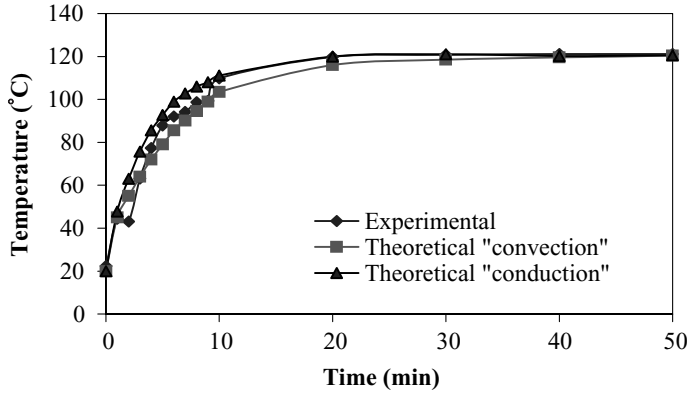

Figure 8.2. Experimental measurements and theoretical predictions of temperature of a pouch heated in a retort by condensing steam at 121°C (at $x = 0.50$ cm from the wall, $y = 0.75$ cm from the bottom, and $z = 8.00$ cm from the widest end of the pouch).

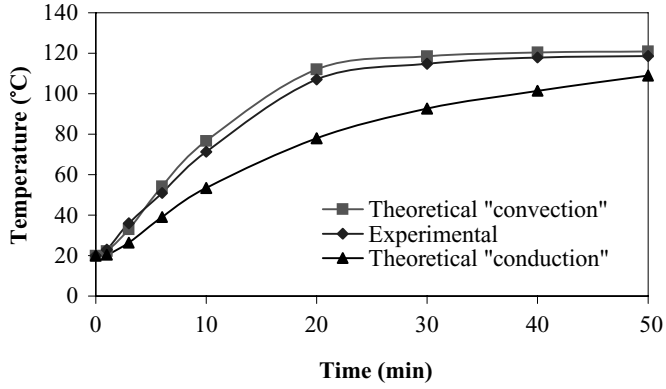

Figure 8.3. Experimental measurements and theoretical predictions of temperature of a pouch heated in a retort by condensing steam at 121°C (at $x = 3.00$ cm from the wall, $y = 1.75$ cm from the bottom, and $z = 8.00$ cm from the widest end of the pouch).

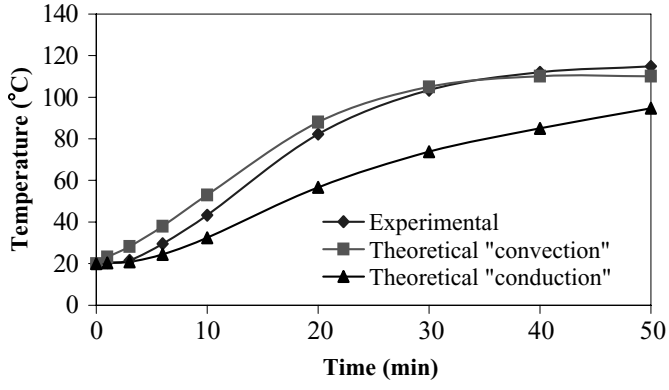

Figure 8.4. Experimental measurements and theoretical predictions of temperature at the SHZ of a pouch heated in a retort by condensing steam at 121°C (at $x = 6$ cm from the wall, $y = 2$ cm from the bottom, and $z = 8$ cm from the widest end of the pouch).

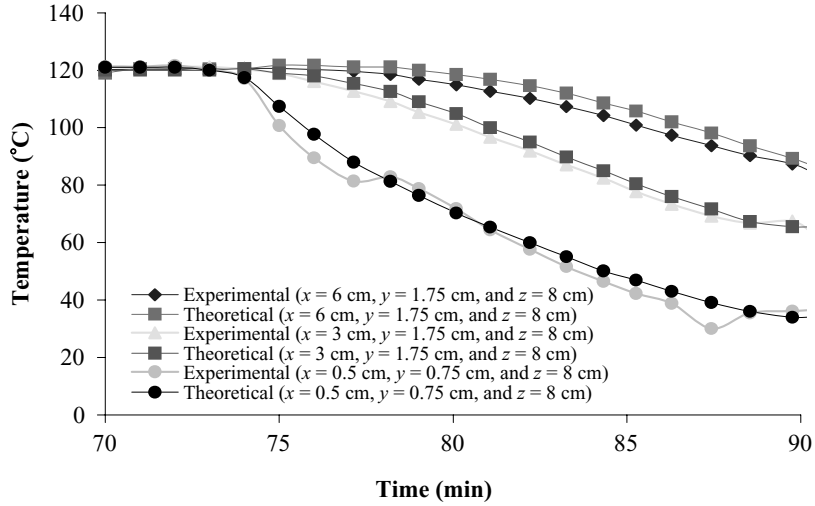

Figure 8.5. Experimental measurements and theoretical predictions of temperature at different locations in a pouch filled with carrot-orange soup during the cooling cycle of the sterilization process.

the computer simulations at another location. This figure as well as Figure 8.3 shows clearly that the predicted temperature in the can is higher than that measured experimentally. This is probably due to the influence of the large-size temperature probes used, which tends to reduce the natural convection motion during the heating process. Based on this finding, we conclude that the measurements usually done in the industry with such a big probe can lead to an inaccurate estimate of sterilization time.

8.1.2. Temperature Measurements During the Cooling Cycle

Figure 8.5 shows the measured temperature distributions at different locations (same locations used in the heating cycle) in a pouch filled with carrot-orange soup during the cooling cycle. Water at 20°C was used for cooling. The figure shows significant temperature distributions in the pouch throughout the whole period of cooling.

During the holding time (60–70 min), there was no significant change in the temperature of the pouch, as shown in Figure 8.1. The maximum change in the temperature of the SHZ was only 0.4°C during the holding time. Accordingly the temperature at the end of the heating period was used as the initial temperature in the cooling period of the simulation. The effect of the holding time on the bacteria inactivation is important, as mentioned earlier in Section 6.3.2.2.

During cooling following the thermal processing, the container surface temperature will not be the same as the measured temperature of the water used in cooling. Several trials were performed by Richardson et al. (1988), who attached surface thermocouples to the can surface in addition to other locations, in an effort to improve the measurements so that they could be used to assess the simulation results. In their simulations, the surface heat transfer coefficient was incorporated into the model, with a value of 600 W m^{-2} K^{-1}. This value was chosen from literature and confirmed by calculations from the surface temperature measurements and available correlation of the form $\mathrm{Nu} = f(\mathrm{Gr} \times \mathrm{Pr})^n$, where Nu is the Nusselt number, dimensionless; Gr is the Grashof number, dimensionless; Pr is the Prandtl number, dimensionless; and f is the heating or cooling factors (Tucker, G.S. and Clark, P. 1990).

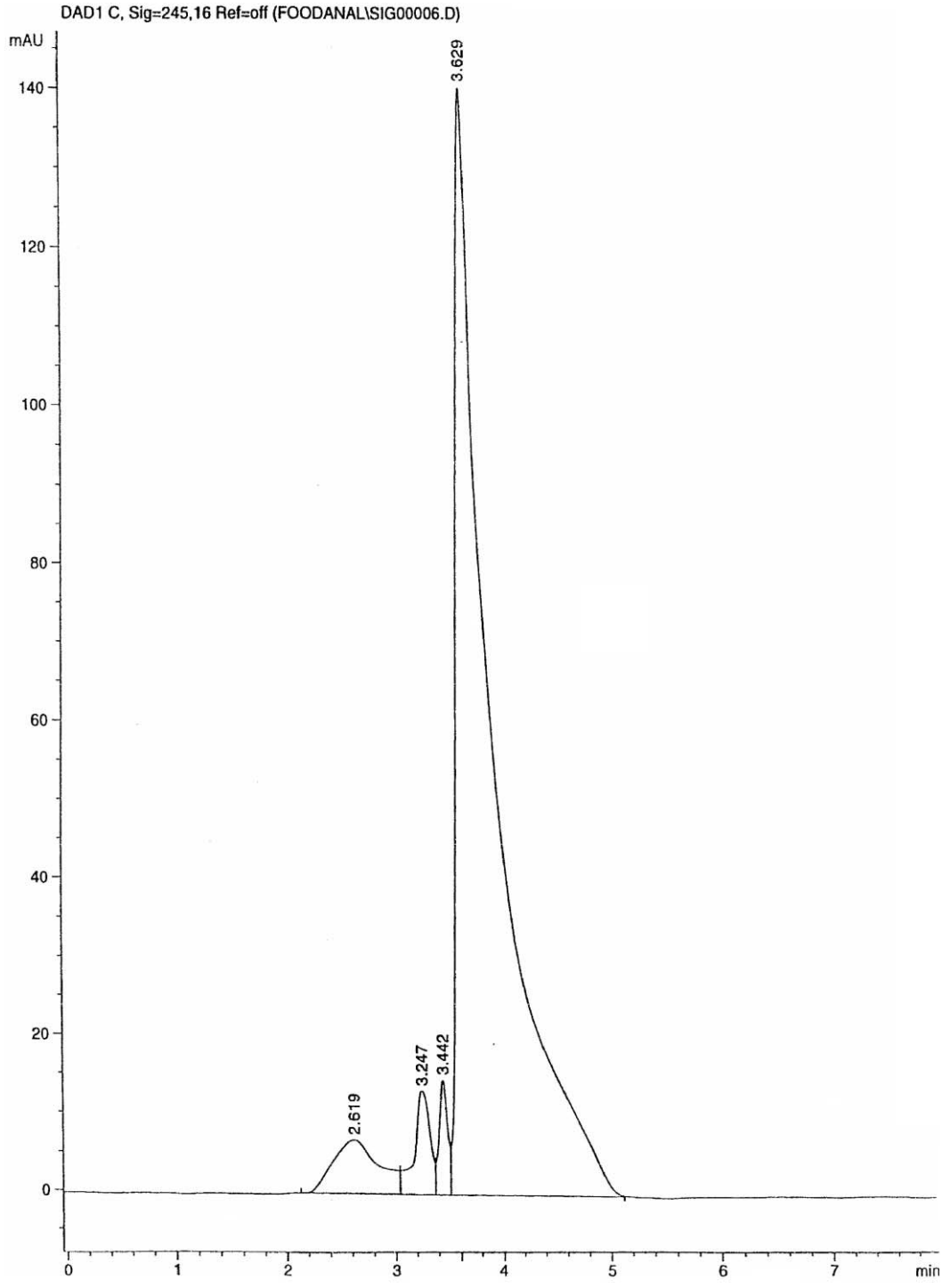

Figure 8.6. HPLC run for the standard sample of ascorbic acid of value 0.067 mg/ml.

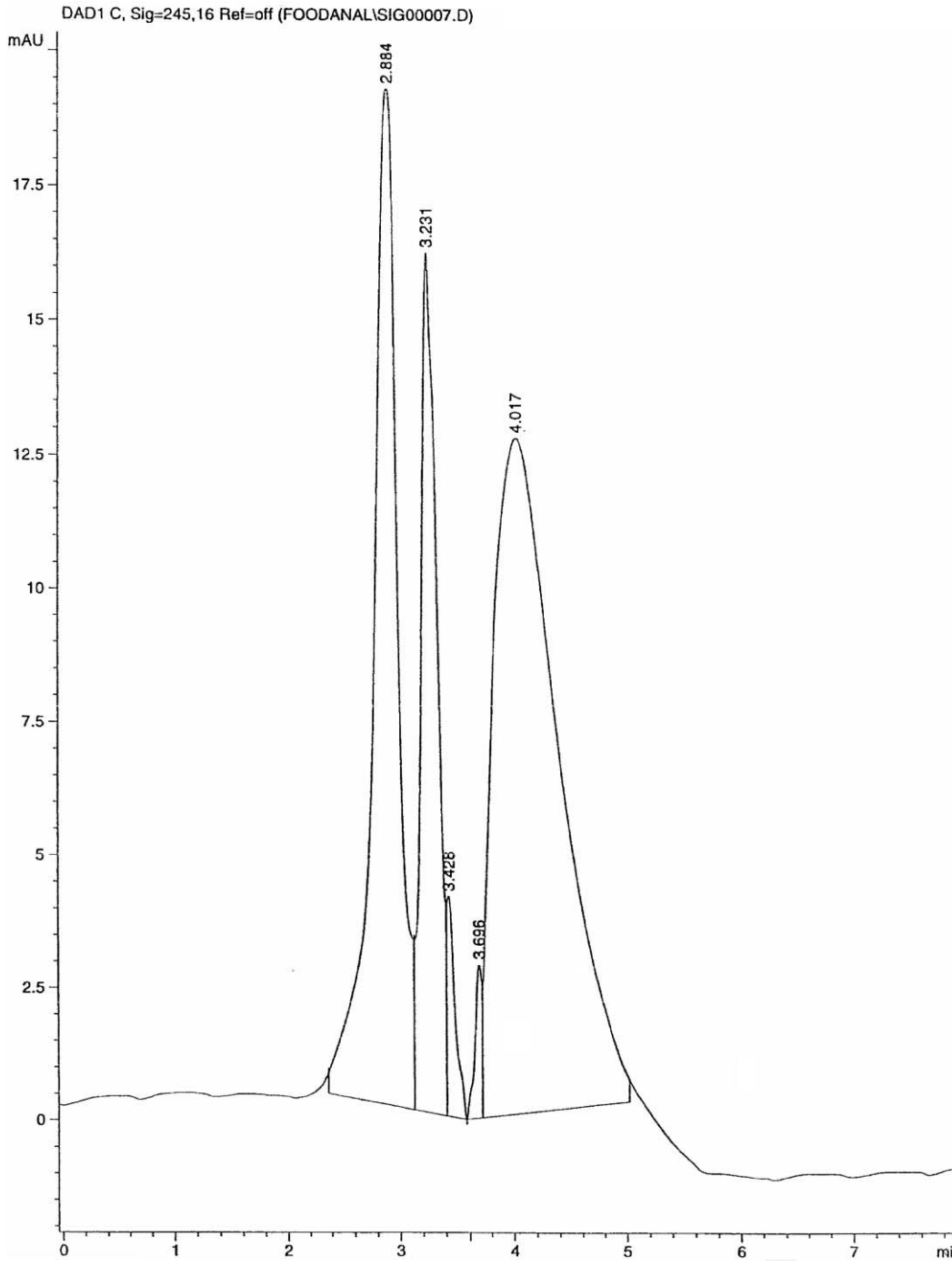

Figure 8.7. HPLC run for the standard sample of ascorbic acid of value 0.013 mg/ml.

Experimental thermal processing data has also been subject to three well-documented problems arising during cooling (Tucker and Cfdra):

1. Ebullition can be caused by the retort pressure falling too early during the cooling phase while center temperatures are still in excess of 100°C. This results in partial boiling of the contents and a consequent temperature fall and product movement, with the cooler surface layers moved toward the bulk of the can. Therefore a greater drop in the temperature of this zone is recorded than would be the case with better control of pressure release (Teixeira et al., 1985). Figure 8.1 shows a drop in the temperature at locations near the wall, which consequently causes more rapid cooling as observed at all other locations. This may explain the higher rates of cooling observed experimentally compared to those predicted.
2. Pressurized cooling water can be forced into thermocouple housing (Cleland and Gesterkamp, 1983) if the screw fitting is slightly loose. Conduction along the stainless steel probe will subsequently occur, artificially lowering the temperature. This problem was not expected in the system used in our experiments, due to the tightness of the thermocouple probes and the advanced equipment used.
3. Conduction along the stainless steel probe itself may cause the measured temperature to drop faster inside the container (i.e., the pouch). This problem was not expected in our experiments, due to the thin thermocouple wire used.

8.2. ANALYSIS OF VITAMIN C (ASCORBIC ACID) DESTRUCTION

The measurements of vitamin C destruction were divided into two stages. The first stage was to sterilize five pouches filled with carrot-orange soup at different heating periods of 0 min, 10 min, 20 min, 30 min, 40 min, and 50 min respectively. The sterilization of pouches was conducted at Heinz Watties Australasia Research and Development Laboratories. The equipment and materials used were the same as those described in Section 8.1. After each sample had been sterilized for a specific period, duplicate samples were taken from each of the five pouches in addition to the samples taken from a nonsterilized pouch. The contained samples were sealed and kept in a refrigerator with sufficient light protection. The second part of the work, comprising the analysis of vitamin C, was conducted at the Food Science Department, University of Auckland.

8.2.1. Equipment and Materials Used in the Analysis

Samples of carrot-orange soup provided for different periods of sterilization were tested. The equipment and materials used in the analysis of vitamin C were as follows:

High-performance liquid chromatography (HPLC) and HP Chem Station with Data Acquisition, Rev.A.06.01 [403], running on HP1100 system, which consists of the following:

- HP1100 degasser
- HP1100 autosampler
- HP1100 quaternary pump
- HP1100 column thermostat
- HP1100 diode array detector (DAD)
- The C18 column (PHENOMENUX Type LUNA 5U C [18], 250 × 460 mm)
- Metaphosphoric acid in 0.01 N H_2SO_4
- 2,6-dichloroindophenol

- Standard samples of pure ascorbic acid
- Analytical balance (METTLER Toledo Ag204, $d = 0.1$ mg)
- Mixer (IKA MSI minishaker)
- Centrifuge (SORVALL RC 28S)
- Blenders (WARING 8010S, 8,000–12,000 rpm)
- Homogenizer (IKA LABORTECHNIK T2S, 8,000–24,000 rpm)
- Measuring cylinder, Burette (50 ml), Buchner funnel and glasses such as beakers and volumetric flask
- Filter paper

8.2.2. Experimental Procedures

Two methods were used for the determination of vitamin C concentration, an HPLC method and the 2,6-diclorophenolindophenol titrimetric method.

8.2.2.1. HPLC Method

A number of samples, blank and standard runs, were tested using the HPLC method—using the HP1100 System—available at the Food Science Department, University of Auckland. In this method, the HPLC operating conditions were a flow rate of 0.7 ml per minute, an ultraviolet (UV) detector (set at 245 nm), a 20 μl injection, a mobile phase of 55:45 methanol to water, and a C18 column.

Two standards of ascorbic acid were made up in the extracting solution of 0.067 and 0.013 mg/ml. A peak, due to vitamin C, was seen at 3.6 to 4.0 min, as shown in Figures 9.6 and 9.7, following peaks due to the carrier solvent (metaphosphoric acid). The areas of the vitamin C peaks in the initial runs were used to estimate the concentration of vitamin C in the soups. The peak was quite broad in the standard runs but was generally sharper in the soup samples.

In the HPLC analysis, full UV-visible spectra were taken for each peak, and the areas and heights of the peaks were recorded. It was found that up to 12 separate peaks could be seen in the soup samples, as shown in Figure 8.8. This was due to the complex nature of the soup tested. Based on these results, it was decided not to use the HPLC method for analysis.

8.2.2.2. 2,6-Dichlorophenolindophenol Titrimetric Method

Measurement of ascorbic acid by direct titration with 2,6-dichloroindophenol dye is the most commonly used method because it is simple and rapid (Albrecht and Schafer, 1990). The International Standard ISO 6557/2 (1984) and AOAC (1980) specify two routine methods for the determination of ascorbic acid content of fruits and vegetables:

1. 2,6-diclorophenolindophenol titrimetric method
2. 2,6-diclorophenolindophenol spectrometric method after extraction with xylene

In this study, the 2,6-diclorophenolindophenol titrimetric method was used. The principle is extraction of the ascorbic acid from the test sample, using either oxalic acid solution or metaphosphoric acid-acetic acid solution, followed by titration with 2,6-diclorophenolindophenol dyestuff until a salmon pink color is obtained.

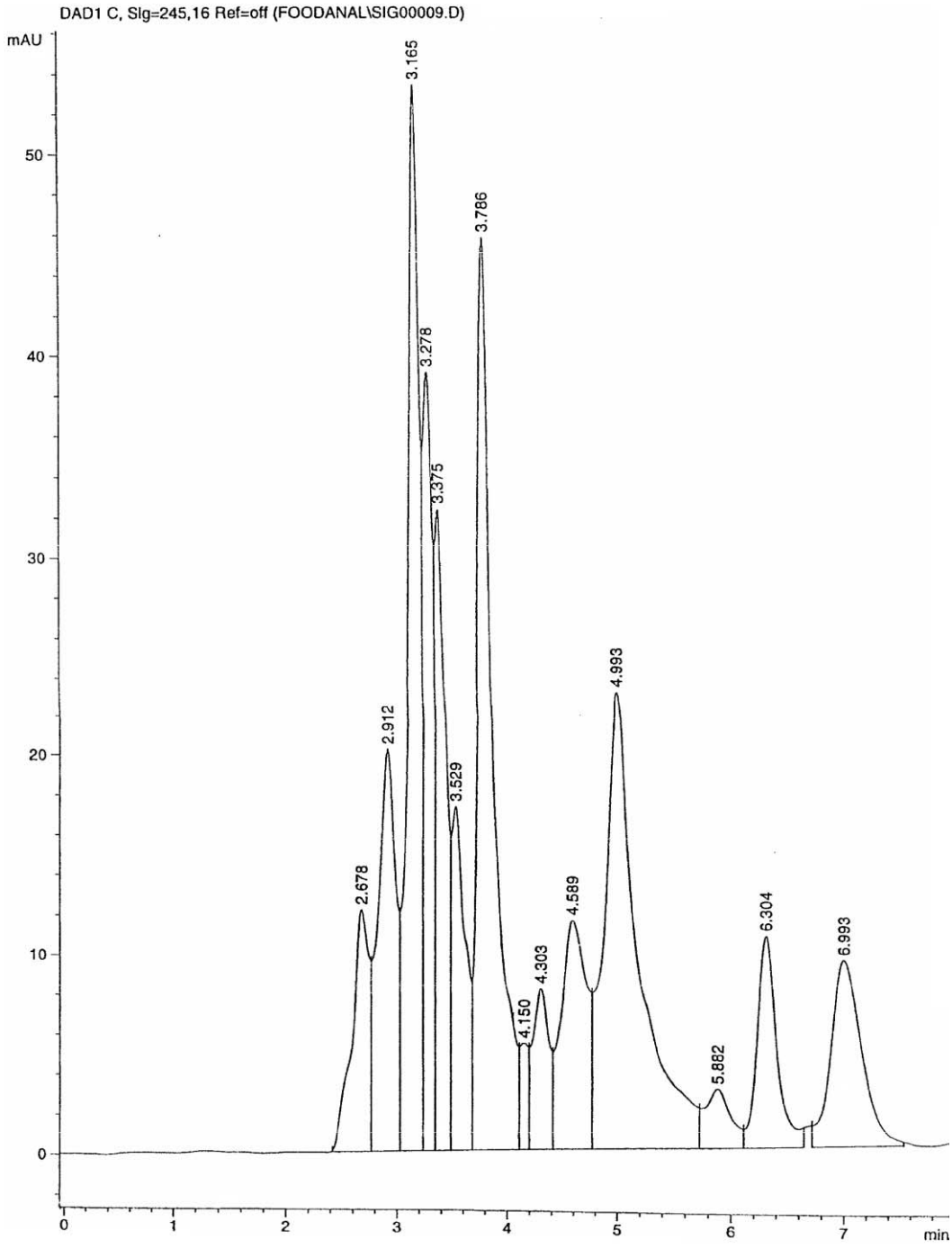

Figure 8.8. HPLC run for the soup sample.

Prepare the Extraction Solution

The extracting solution used is 0.3% metaphosphoric acid in 0.01 N H_2SO_4. The preparation of the solution is as follows:

1. Weigh out 0.6 g of metaphosphoric acid.
2. Add it to 200 ml of 0.01 N H_2SO_4 in a volumetric flask.
3. Homogenize the result by using a magnetic stirrer for 5–6 min or more until the metaphosphoric acid is dissolved completely.

Extract Ascorbic Acid from the Soup Samples

The method used to extract ascorbic acid from the soup samples is as follows:

1. Weigh out 10 g of soup into a blender.
2. Add 40 ml of the supplied extracting solution (0.3% metaphosphoric acid in 0.01 N H_2SO_4).
3. Homogenize the solution by blending for at least 2–3 min.
4. Centrifuge the homogenate for 4–5 min at 3000 rpm. This is due to the complex mixture of the viscous liquid food.
5. Filter the resulting homogenate through a Buchner funnel under vacuum.
6. Use a further 5 ml of extracting solution to rinse out the blender.
7. Transfer the solution into a 50 ml volumetric flask, and make up to the mark using the extracting solution. Take 10 ml aliquots for indophenol titration.

Prepare Ascorbic Acid Solution for Standardization

Three standards samples of ascorbic acid are used in the extracting solution (0.3% metaphosphoric acid in 0.01 N H_2SO_4) in order to construct its calibration curve. These are 0.067 mg/ml, 0.050 mg/ml, and 0.013 mg/ml. A 100-ml sample is prepared from which only 10 ml is required for the titration.

Prepare the 2,6-Diclorophenolindophenol Dyestuff Solution

On the basis of an official AOAC method, the following steps are used:

1. Dissolve 42 mg of sodium hydrogen carbonate ($NaHCO_3$) into 50 ml of distilled water in a 200 ml volumetric flask.
2. Add 50 mg of 2,6-diclorophenolindophenol.
3. Shake vigorously until the dye (2,6-diclorophenolindophenol) has dissolved.
4. Dilute to 200 ml with distilled water.
5. Mix the solution, and transfer it into a 50-ml burette as required, ready for the titration.

8.2.2.3. Titration

Take three aliquot portions from each sample, and titrate 10 ml of each sample with the dyestuff solution until a salmon pink coloration, persisting for at least 5 s, is obtained. Carry out three determinations on test portions taken from the same test sample. Record the volume of the dyestuff solution used each time. The volumes of the indophenol solution required in the titration of the three standard samples of ascorbic acid (see Section 8.2.2.2.3) were 11.0 ml, 8.2 ml, and 2.0 ml

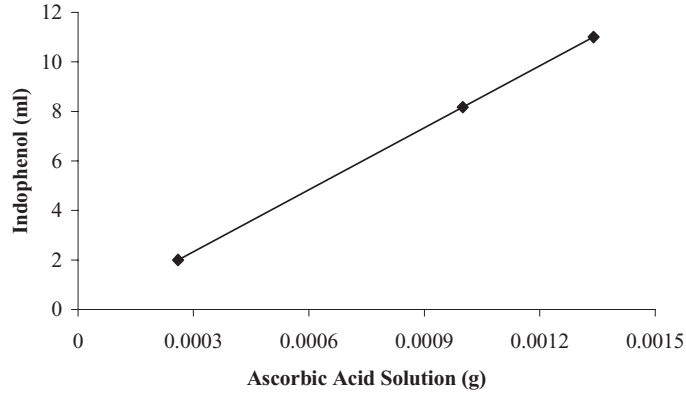

Figure 8.9. Calibration curve of ascorbic acid for the standard samples of 0.067 mg/ml, 0.050 mg/ml, 0.013 mg/ml, based on a 10-ml sample.

respectively. These values were plotted to construct the calibration curves of ascorbic acid, which are shown in Figure 8.9.

The soup samples, heated at different periods of 0, 10, 20, 30, 40, and 50 min, prepared as described in Section 8.2.2.2.2, were used in the titration method. The arithmetic mean volumes of dyestuff solution (2,6-diclorophenolindophenol) required for these samples were 5.9, 5.7, 5.5, 5.2, 4.7, and 4.3 ml respectively. From the ascorbic acid calibration curve (Figure 8.9), these volumes are equivalent to 0.72, 0.71, 0.68, 0.64, 0.60, and 0.55 mg of ascorbic acid respectively, corresponding to concentrations of 0.072, 0.071, 0.068, 0.064, 0.060, and 0.055 mg/ml respectively (Figure 8.10). By dividing each value obtained from the calibration curve to the initial one, we have the relative concentrations of 100%, 96.8%, 91.15%, 84.64%, 78.44%, 70.85%. These values were plotted and compared with the predicted values in Figure 8.11, which shows a good agreement between the prediction and the experimental measurements.

8.3. ENUMERATION OF SPORES AFTER HEAT TREATMENT

The experimental measurements for the enumeration of *B. stearothermophilus* spores following the heat treatment of pouches filled with beef-vegetable soup were conducted at the Biotechnology

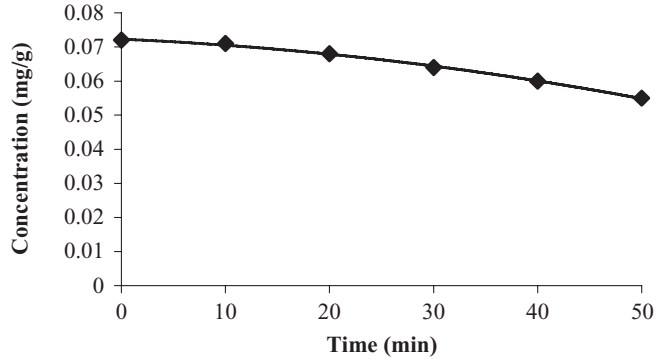

Figure 8.10. Experimental destruction of ascorbic acid concentration with time.

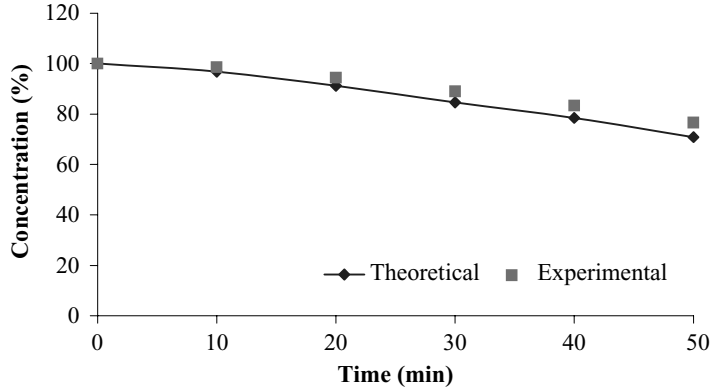

Figure 8.11. Experimental and theoretical destruction of relative ascorbic acid concentration (%) with time.

Laboratory at the Chemical Engineering Department, University of Auckland. Pouches of the same size as those used in the theoretical analysis were used in the measurements. The purpose was to validate the theoretical predictions of the inactivation of *B. stearothermophilus* spores conducted in Chapter 7.

The following is a summary of the methods and procedures involved in the enumeration of the spores of *B. stereothermophillus* that were harvested and subsequently injected into the pouches. A validation procedure was developed and performed to ensure that both the media and the bacteria species used would cope with the heat treatment. The validation procedure also allowed for the determination of methods by which spore suspensions could be produced to enable their injection into the soup pouches.

8.3.1. Equipment and Materials Used in the Measurements

The materials and equipment used in the measurements were as follows:

1. Stock culture of *B. stereothermophillus*.
2. Spore agar (nutrient sporulation medium), which is the media used to promote the germination of *Bacillus* spores that survived the heat treatment procedure. This media contains metal salts, yeast extract, and a nutrient agar base, as follows:
   Compositions (ingredients per liter)
   - Nutrient agar (Difco dehydrated) 23.0 g
   - Salt solution 5.0 ml
   - Yeast extract 0.5 g

   Salt solution (ingredients per liter)
   - $CaCl_2$ 15.54 g
   - $MnCl_2 \cdot 4H_2O$ 1.98 g
   - $MgCl_2 \cdot 6H_2O$ 40.66 g

The method of preparation of this media is as follows:

1. Prepare an adequate amount of salt solution, and set it aside.
2. Separately rehydrate nutrient agar using distilled water (23 g per liter), and add yeast extract (0.5 g per liter).

3. Add the salt solution (5 ml per liter), and sterilize in the autoclave for 15 minutes at 121°C.
4. Pouches filled with beef-vegetable soup, produced by Heinz Watties Australasia, Hastings, New Zealand.
5. Petri dishes used to house the growth media.
6. Stomacher bags used to dilute and mix the soup after heat treatment.
7. Loops used to streak the spore-producing culture on the spore agar to allow the future use of the culture.
8. Syringes used to inject the spores into the soup pouches.
9. Pipettes and pipette tips used in the serial dilution of the spore suspension and the diluted soup.
10. Scale (SARTORIUS BP1105, Biolab Scientific Limited, Max 110 g, d = 0.1 mg).
11. Gas-heating elements used to heat the pressure cooker to provide the test conditions (saturated steam at 121°C).
12. A pressure cooker (TTK Prestige Ltd, 12-l volume).
13. A mixer (Auto Vortex Mixer Mt 19, CHILTERN Scientific), which was used to homogenized the suspensions filled in tubes.
14. Autoclaves (TOMY Auto calve SS-325) used to sterilize the equipment and melt the agar at 121°C for 15 min.
15. Two water baths (GRANT W28, Grant Instrument Cambridge Limited, England), were used, the first set at 100°C to prepare the spores, while the second set at 45°C to hold the agar at this temperature, to prevent it from gelatinization.
16. An incubator (GALLENKAMP, Economy Incubator with fan size 2, Watson Victor Ltd, New Zealand) used to incubate the petri dishes at 55°C.
17. A sterilization tape used to seal the pouches after spore injection.

8.3.2. Validation Procedure

The original culture of *B. stereothermophillus* spores was further subcultured on spore agar to ensure that the bacterial cells would grow on this media. These cultures were then placed in a refrigerator to promote the generation of spores within the bacterial cells, which could later be harvested and injected into the soup pouches.

8.3.2.1. Spore Culture/Media Method Validation

The first protocol to be developed for this practical series was one to assess the efficiency and the viability of the media (nutrient sporulation medium) to be used and the bacterial culture's (stock culture for *B. stereothermophillus*) ability to produce a spore. This would also enable us to determine a method by which the spores could be harvested. In this work, the spores were not separated from the dead cells to produce pure spore suspension, because this would require several centrifugation and filtration steps. It was assumed that heat treatment of the vegetative cells of the stock culture would release the spores and destroy vegetative cells, thus providing us with a usable spore suspension (Balows et al., 1991; Starr et al., 1981).

The following protocol was used in the validation of spore culture and media method:

1. Melt agar at 121°C for 15 min.
2. Transfer bacterial cells from the stock culture to several test tubes that contain sterile water, using a plastic loop, to provide a cell suspension, which will later be heat treated to give us a suspension of spore.

3. Heat the cell suspension produced in step 2 at 100°C for 10 min to kill vegetative cells and release the spores. The time (10 min) was chosen based on the heat treatment time that was used in the reported method of spore enumeration (Balows et al., 1991; Starr et al., 1981).
4. Prepare 9 ml volumes of sterile water to allow for serial dilutions. It is expected that the number of spores present would be very high, so sufficient numbers of these 9 ml volume are required to allow us to dilute up to 10^9. A serial dilution involves transferring of 1 ml of a suspension to 9 ml of water. This in turn dilutes the original suspension 10-fold. From this 10-fold dilution, 1 ml is transferred into another 9 ml of water, giving a total 100-fold dilution of the original suspension. This process is repeated (serial dilutions) until the original spore suspension has been diluted 10^9-fold.
5. Pipette 1 ml volumes from each of the dilutions on to sterile petri dishes (one dish/dilution). After all of the dilutions had been dispensed, pour 10–15 ml of nutrient sporulation agar (NSA) on these plates. Shake the plates gently to ensure that the spores are distributed throughout the agar in order to allow easy counting.
6. Place the petri dishes obtained from step 5 in plastic bags/sleeves, and incubate at 55°C for 3 days. The petri dishes are placed in bags to prevent the agar dehydrating at this temperature.
7. After 3 days, examine the plates for the growth of spore colonies. Each colony that is formed on a petri dish is assumed to have developed from a single spore or colony-forming unit. Therefore counting the number of bacterial colonies and multiplying this number by the dilution factor will allow us to estimate the number of spores or colony forming units present within the original spore suspension.

This initial trial was set up to ensure that both the media and the bacterial culture to be used were compatible. For this reason the number of cells present on the plates was not important. The key here was to ensure that the media and *B. stereothermophillus* were compatible.

8.3.2.2. Validation of Heat Treatment Time

The protocol used in this work was developed to examine the reproducibility of the results using the same method as above. This also determined an optimum heat treatment time for the "harvesting" of spores from the stock culture. The purpose was to duplicate different exposure times at 100°C, thus providing us with a basis for comparison and a means by which we could assess the viability of our method. It was decided to use three time intervals at 100°C, which were 10, 20, and 30 min, respectively. The validation procedure for this protocol was as follows:

1. Melt agar at 121°C for 15 min.
2. Prepare spore inoculums/suspensions (heavy in the sense that a large number of the cells are transferred from the stock culture on a petri dish to a volume of sterile water), and then distribute them over six tubes (5 ml into each tube).
3. Set up 9 ml water test tubes for serial dilutions, as described in step 4 of the previous section. Set up petri dishes for the different serial dilutions.
4. Heat two tubes of the stock solution at 100°C for different periods of 10 min, 20 min, and 30 min, as described above.
5. Cool the tubes in ice water immediately after heat treatment. This is to prevent the germination of spores before they are placed in the NSA. If this occurs, then division of live cells is possible and may obtain a result that does not reflect the actual number of spores present in the suspension.
6. Perform serial dilutions on each stock sample after heat treatment in order to obtain a countable number of spores.

Table 8.1. Spore heat treatment validation

DILUTION	10 min	20 min	30 min
10^1	TN	TN	TN
10^2	TN	TN	TN
10^3	TN	TN	TN
10^4	69	96	99
10^5	11	10	11
10^6	1	<1	1
10^7	<1	<1	<1
STOCK	TN	TN	TN

7. Pour the NSA in plates (petri dishes) and shake the plates, as in step 4 of the previous section.
8. Incubate the plates at 55°C for three days. After incubation count the number of colony forming units on each plate to determine the number of spores present in each of the heat-treated stock solutions.

The results shown in Table 8.1 are the average values for each time interval tested. Each number represents the number of colony forming units counted on each plate (petri dish) at different dilutions.

A value of <1 indicates that no colonies were counted, but due to the small volume of sample being tested, zero number of colonies cannot be ascertained. A "TN" indicates that the number of colony forming units was too numerous to count.

From the results above we can see that the method is very reproducible and that the spores have the ability to survive at 100°C for at least 30 min. Accordingly, it was decided to use 100°C for 30 min to prepare the spores for the rest of this practical work because this time would ensure that no vegetative cells at all remained after heat treatment. It should be noted that at the time of this trial, the stock culture itself was plated on petri dishes to allow for the comparison of the number of cells before and after heat treatment.

8.3.3. Pouch Testing

Spore counts were performed for the following:

a. The spore stock solution, to give the initial number of spores that were injected into the soup pouches
b. Soup pouches filled with beef-vegetable soup and heated for different periods of 5, 10, 15, 20, 25, and 30 min
c. A blank soup pouch filled with soup only for each of the above testing intervals, to ensure that the soup had no spores

The following protocol was the method used in the enumeration of *B. stearothermophilus* spores that were injected into pouches filled with beef-vegetable soup and heated at different periods:

1. Dispense 9 ml of sterile water into test tubes for the serial dilution of all samples to be tested, and set up and label the petri dishes to allow pipetting the serial dilutions that were produced.
2. Create a spore/cell stock solution in 300 ml of water. Mix this using agitation, and then store on ice until ready to use.
3. Prepare the spore suspension, which involves the division of the cell suspension into six test tubes. Heat these test tubes at 100°C for 30 min to kill all the live cells and leave only the

Table 8.2. Spore count at different sterilization periods and dilutions

Dilution	5 min	5 min	10 min	10 min	15 min	15 min	20 min	20 min	25 min	25 min
	WS	WOS	WS	WOS	WS	WOS	WS	WOS	WS	WOS
(10^2)	TN	<1	TN	<1	53	<1	9	<1	<1	<1
(10^2)	TN	<1	TN	<1	45	<1	5	<1	2	<1
(10^3)	280	<1	35	<1	6	<1	<1	<1	<1	<1
(10^3)	240	<1	33	<1	5	<1	<1	<1	<1	<1
(10^4)	26	<1	4	<1	<1	<1	<1	<1	<1	<1
(10^5)	3		<1		<1		<1		<1	
(10^6)	<1		<1		<1		<1		<1	
(10^7)	<1		<1		<1		<1		<1	

WS = pouches injected with spores
WOS = pouches without spores

spores to be used in this trial. After the heat treatment has been completed, place the test tubes on ice to prevent the vegetation/growth of the spores.

4. Use two pouches for each time interval. Inoculate/inject the first pouch with 5 ml of spore suspension that was produced in step 3, while keeping the second pouch intact (no spores injected). After that shake the pouches thoroughly, and place them in the pressure cooker. Heat the water in the pressure cooker to generate saturated steam at a temperature of 121°C. Place the pouches on a metal base raised above the water level in the pressure cooker. This is done to ensure uniform heating of the pouches by the condensing steam and not by the boiling water.
5. At the completion of the heat treatment process, place the pouches on ice to prevent sporulation (spore germination). After they are cooled, shake the pouches, and dilute the contents of the pouches 10-fold using sterile water. To do this pour 25 g of soup from the pouch into a stomacher bag, and add it to 225 g of water to give a 10-fold dilution.
6. After this initial dilution, perform a serial dilution, and place 1 ml from each dilution on a sterile petri dish poured with agar. For the infected soup pouches, perform dilutions from 10^2 to 10^7, while for the noninfected soup perform dilutions from 10^2 to 10^4. At the same time, plate out a sample of the spores only (SO) that were produced in the initial heat treatment step to give a count of the number of spores that were present in the initial inoculums.
7. Then incubate the petri dishes at 55°C for 72 h. After incubation count the number of colony forming units on each plate to determine the number of spores present in each sample. With the serial dilution used, no spore count was found after 30 min of sterilization, so it was not possible to obtain a spore count at that time. The following results were obtained (Table 8.2).

Five milliliters of the liquid containing the spores were injected into the pouch of 500 ml volume to give the dilution factor of 100. This factor was multiplied by the serial dilution factor to give us the final number of spores that remained in the soup after the test conditions were applied. Based on the above, the following results (Table 8.3) were obtained for the spore count.

Table 8.3. Measured spore concentration (%) after different sterilization periods

	SO	5 min	10 min	15 min	20 min	25 min
Final Spore Count	15×10^7	2.7×10^7	3.6×10^6	5.2×10^5	7×10^4	1×10^4
Relative Spore Concentration (%)	100	18	2.4	0.35	0.047	0.0067
Log Reduction	0	0.74	1.6	2.5	3.3	4.2

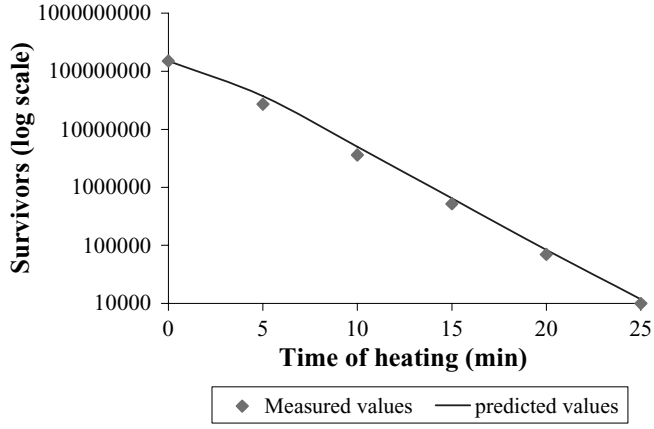

Figure 8.12. Rate of destruction curve of predicted and measured counts of *B. stearothermophilus* spores heated at 121°C in a 3-D pouch filled with beef-vegetable soup.

The average relative bacteria (*B. stearothermophilus* spores) concentrations in the whole pouch obtained from the computer simulation dropped down to 24.85%, 3.34%, 0.43%, 0.056%, 0.0079%, and 0.7×10^{-3}% (0.61, 1.48, 2.37, 3.25, 4.10, and 5.15 log reduction) after heating periods of 300, 600, 900, 1,200, 1,500, and 1,800 s respectively. These values are plotted in Figure 8.12 for the purpose of comparison, which shows very good agreement between the experimental and the theoretical prediction of the degree of sterilization.

REFERENCES

Albrecht, J.A., & Schafer, H.W. (1990). Comparison of two methods of ascorbic acid determination in vegetables. *Journal of Liquid Chromatography, 13*(13), 2633–2641.

AOAC (1980). *Official Methods of Analysis* (13th ed.). Washington, DC: Association of Official Analytical Chemists.

Balows, A., Truper, H.G., Dworkin, M., Harder, W., & Heinz Schleifer, K. (1991). *The prokaryotes*, *a hand book on the biology of bacteria ecophysiology, isolation, identification, applications* (Vol. 2). Springer-Verlag.

Cleland, A.C., & Gesterkamp, M.F. (1983). The effect of irregular cooling phenomena on the lethality of thermal process. *Food Technology, 18*, 411–425.

Hayakawa, K., & Ball, C.O. (1969). A note on theoretical cooling curve of a cylindrical can of thermally conductive food. *Journal of Canadian Institute of Food Technology, 2*(3), 115–119.

ISO 6557/2 (1984). Fruits, vegetables and derived products: -Determination of ascorbic acid content, Part 2—Routine methods.

Richardson, P.S., Kelly, P.T., & Holdsworth, S.D. (1988). *Computer modelling for the control of sterilization processes* (Technical memorandum 518). Chipping Campden, UK.

Starr, M.P., Stolp, H., Truper, H.G., Balows, A., & Schlegel, H.G. (1981). *The prokaryotes, A hand book on habitats, isolation, and identification of bacteria* (Vol. 2). Springer-Verlag.

Teixeira, A.A., Dolan, K., Datta, A.K., & Adams, J.P. (1985). Retort depressurization effect on cooling rates in conduction-heating canned foods. *Transaction of the American Society of Agricultureal Engineering, 28*, 645–648, 656.

Tucker, G.S., & Clark, P. (1990). Modeling the cooling phase of heat sterilization processes, using heat transfer coefficients. *International Journal of Food Science and Technology, 25*, 668–681.

CHAPTER 9

A NEW COMPUTATIONAL TECHNIQUE FOR THE ESTIMATION OF STERILIZATION TIME IN CANNED FOOD

As we have illustrated in the previous chapters, sterilization of liquid food in pouches is complicated by the influence of natural convection currents induced by the hot walls of the can. In order to predict the temperature variation of the slowest heating zone (SHZ) with time, it is necessary to use computational fluid dynamics (CFD) analysis, which can be accomplished using any of a number of available commercial software packages. However the required computational time is usually of the order of hours, as reported in Chapter 5.

In this chapter, a simple method of calculation was developed to predict the SHZ without the requirement of sophisticated computations. A new correlation was developed for the prediction of the sterilization time of liquid food in vertical and horizontal cans. The correlation was developed by analogy with the analytical solution available for heat conduction in a solid cylinder. The results of a large number of computer simulations, some of which have been presented in previous chapters, were used to generate the data required for building the correlation. Liquid foods with a large variation in viscosity, and cans of different sizes, were used in these simulations.

The correlations developed in this chapter were limited to sterilization of food in cans. A similar approach may be followed in the future to develop correlations, which may be used to predict sterilization of food in pouches.

9.1. INTRODUCTION

The study of in-can sterilization has been experimental for a long time. In industrial retorts, heat is transferred from the heating media (usually steam) to the wall of the can with a very high condensation heat transfer coefficient. Heat is then transferred to the liquid food in the can by conduction through the metal wall with negligible resistance. Both of these thermal resistances can be ignored in most of the applications as they have negligible effect on the overall heat transfer rate. Heat is transferred from the wall of the can to the liquid inside it by both conduction and natural convection induced by the hot wall of the can. It is this internal heat transfer that controls the heat transfer rate in the can. The analysis of the internal heat transfer requires the solution of the Navier–Stokes equations, which was not possible until the recent development of high-speed computers. This was the subject of the previous chapters of this book in which CFD analysis was used to describe sterilization of high- and low-viscosity liquid foods in pouches and vertical and horizontal cans.

The geometric configuration of the horizontal can required a three-dimensional analysis due to the loss of axisymmetry associated with the vertical can, which caused further complication in the analysis and increased computational time (Ghani et al., 2002). Although the effect of natural convection currents in the horizontal can was less than in the vertical can due to the smaller vertical dimension (diameter), it was strong enough to push the SHZ toward the lower half of the horizontal can.

CFD is a powerful tool for the analysis of in-can sterilization; however, the computational time can be as high as 50 h using high-speed computers. This time depends on several factors such as the mesh, time steps, and iteration number and whether the physical properties of the canned food are taken as a constant or as a function of temperature. The CFD simulation can be conducted for any new can dimensions introduced by the canning industry and for any new product. However, the canning industry may not always have the facilities or the expertise required to run such comprehensive simulations. The other alternative is to conduct experimental measurements for any new product or can size introduced. The temperature probes used by the industry are relatively large in size, influencing the fluid motion and hence the temperature distribution in the can. Until a precise temperature-measuring technique is developed (which does not influence the fluid motion in the can), the computational technique remains to be the most powerful one.

The objective of this chapter is to utilize the vast information available from the CFD analysis of sterilization of different liquid foods contained in vertical and horizontal cans of different sizes to develop a simple computational technique that can be used for fast calculation of the required sterilization time, without the need for large computers or high computational skills. The method can be used by the industry to estimate the sterilization time for any new product and any can size to be introduced.

9.2. THEORETICAL APPROACH

Unsteady-state heat conduction through a solid cylindrical geometry, subjected to external convection heating, is usually analyzed using numerical methods. However for long cylinders ($H/r_0 \geq 10$), a one-dimensional analysis may be used to provide an analytical solution to the heat transfer problem (Incropera and DeWitt, 1996). Such analytical solutions have been available since 1955 for an infinite cylinder with a uniform initial temperature distribution and a convection boundary (Schneider, 1955). The exact solution is given by the following series (Incropera and DeWitt, 1996):

$$\theta^* = \sum_{n=1}^{\infty} C_n \exp\left(-\xi_n^2 \mathrm{Fo}\right) J_0\left(\xi_n r^*\right) \tag{9.1}$$

where

$$\theta^* \equiv \frac{\theta}{\theta_i} = \frac{T_\infty - T}{T_\infty - T_i} \tag{9.2}$$

$$r^* \equiv \frac{r}{r_0} \tag{9.3}$$

$$\mathrm{Fo} = \frac{\alpha t}{r_0^2} \tag{9.4}$$

$$C_n = \frac{2}{\xi_n} \frac{J_1 \xi_n}{J_0^2(\xi_n) + J_1^2(\xi_n)} \tag{9.5}$$

The discrete values of ξ_n are positive roots of the transcendental equation

$$\xi_n \frac{J_1(\xi_n)}{J_0(\xi_n)} = Bi \tag{9.6}$$

J_1 and J_0 are Bessel functions of the first kind, and their values are tabulated in most heat transfer textbooks. The roots of the above transcendental equation are tabulated by Schneider (1955).

For cases with Fo > 0.2, the above solution can be approximated by a single term as follows:

$$\theta^* = \theta_0^* J_0(\xi_1 r^*) \tag{9.7}$$

On the basis of the above equation, the center temperature may be expressed by

$$\theta_0^* = C_1 \exp\left(-\xi_1^2 \mathrm{Fo}\right) \tag{9.8}$$

Values of the coefficients C_1 and ξ_1 are usually listed for a range of Biot numbers (Incropera and DeWitt, 1996). Equation (9.8) provides a rapid calculation for the center temperature of an infinite cylinder subjected to convection heating or cooling. It is this equation and Equation (9.7), for the temperature at any radial position, which were used to generate what is known as Heisler charts, given by most heat transfer textbooks.

The assumption of an infinite cylinder ($L/r_0 \geq 10$) is not met in most of the can sizes used in the canning industry, so Equation (9.8) cannot be used in its existing form to describe heat transfer in such geometries. In order to minimize such error, the radius of the can (r_0) in Equation (9.4), is replaced by the ratio $2V/A$, which will account for the heat transfer from all sides of the can. The ratio $2V/A$ is a shape factor (characteristic dimension) that can be used for any geometry, including spheres and slabs. However, in the canning industry, a cylindrical can is commonly used, and we will limit our discussion to such geometry. The characteristic dimension ($2V/A$) for a cylinder is

$$\frac{2V}{A} = \frac{r_0 L}{r_0 + L} \tag{9.9}$$

The value of the characteristic dimension given by Equation (9.9) is r_0 for an infinite cylinder, which satisfies the definition of Fo used in Equation (9.8). For a finite cylinder such as a can with a height equal to its diameter, Equation (9.8) gives a characteristic length of 2/3 r_0. The 33% reduction in the characteristic length is due to the heat transfer contribution of the top and bottom of the can. Equation (9.8) gives a characteristic length of $L/2$ for a short can with a height equal to its radius. It does not provide a correct characteristic dimension for extremely short cans, but such geometry is of no practical interest.

It is postulated in this work that if the natural convection effect in the liquid food contained in a can during sterilization can be accounted for by using an effective thermal conductivity, then the solution given by Equation (9.8) can be used to predict the SHZ temperature. However, the center of the can here is defined as the thermal center and not the geometric center of the can. This is to simplify the analysis since the SHZ is not a stationary point but rather a continuously moving and shrinking region. The required condition of Fo > 0.2 is well met in all practical can dimensions.

Natural convection heating in enclosures has been widely studied, and some empirical correlations have been developed to predict the natural convection effect in rectangular cavities, concentric cylinders, and spheres. However, such a correlation is not available for liquids contained in vertical

and horizontal cans. All available correlations have been developed for cases were the two surfaces are at different temperatures, unlike the case of the can, which has an isothermal surface. For a rectangular cavity composed of two walls having height H and separated by a distance δ, the following correlation has been developed for a small aspect ratio (Catton, 1978):

$$\overline{\mathrm{Nu}_\delta} = 0.22\left(\frac{\mathrm{Pr}}{0.2+\mathrm{Pr}}\mathrm{Ra}_\delta\right)^{0.28}\left(\frac{H}{\delta}\right)^{n} \quad \begin{bmatrix} 2 < \dfrac{H}{\delta} < 10 \\ \mathrm{Pr} < 10^5 \\ 10^3 < Ra_\delta < 10^{10} \end{bmatrix} \tag{9.10}$$

where $\delta = L$ and $n = -0.25$.

$$\mathrm{Pr} = \frac{C_\mathrm{p}\mu_\mathrm{film}}{k} \tag{9.11}$$

and

$$\mathrm{Ra}_\delta = \mathrm{Gr}_\delta\,\mathrm{Pr} \tag{9.12}$$

All the physical properties of the liquid foods used in the simulations were measured at the liquid film temperature (T_f).

$$T_\mathrm{f} = \frac{121 + T_\mathrm{SHZ}}{2} \tag{9.13}$$

In order to follow up the same concept for the vertical can, the distance separating the two walls (δ) in Equation (9.10) was replaced by the radius of the can (r_0), keeping H as the height of the can (Figure 9.1a). The reason for such choice is clear from the expected cellular flow in both cavities as shown in Figures 9.1a and 9.1b. The convection currents shown in Figure 9.1b for vertical cans have been reported by a number of investigators (Ghani et al., 1998; Ghani et al., 2003; Kumar et al., 1990; Kumar and Bhattacharya, 1991).

For a vertical can, the exponent of n was found to be 0.25 and not -0.25, which is probably due to the major difference between the geometry of the parallel walls and that of the can. The value of the coefficient $n = -0.25$ was found from the best fit of the developed model to all the CFD simulations conducted, as will be discussed later.

For a horizontal can, the convection currents shown in Figure 9.1c are supported by the velocity vectors shown in Figure 9.2, which indicate clearly the existence of the two stagnant zones. The selection of the characteristic dimension for natural convection to be used in the calculation of Nusselt number and Rayleigh number lies between the can diameter and its half-length, as suggested by the convection current shown in Figure 9.1c. In the horizontal can used in the simulation, the half-length of the can was smaller than its diameter, so it was decided to use $H/2$ in Equation (9.10) as a characteristic dimension (δ). The height of the can (H) in Equation (9.10) was replaced by the can diameter ($2r_0$). These characteristic dimensions are used to define the natural convection in the vertical and horizontal cans. They are different from the characteristic dimension ($2V/A$) used to define the conduction path.

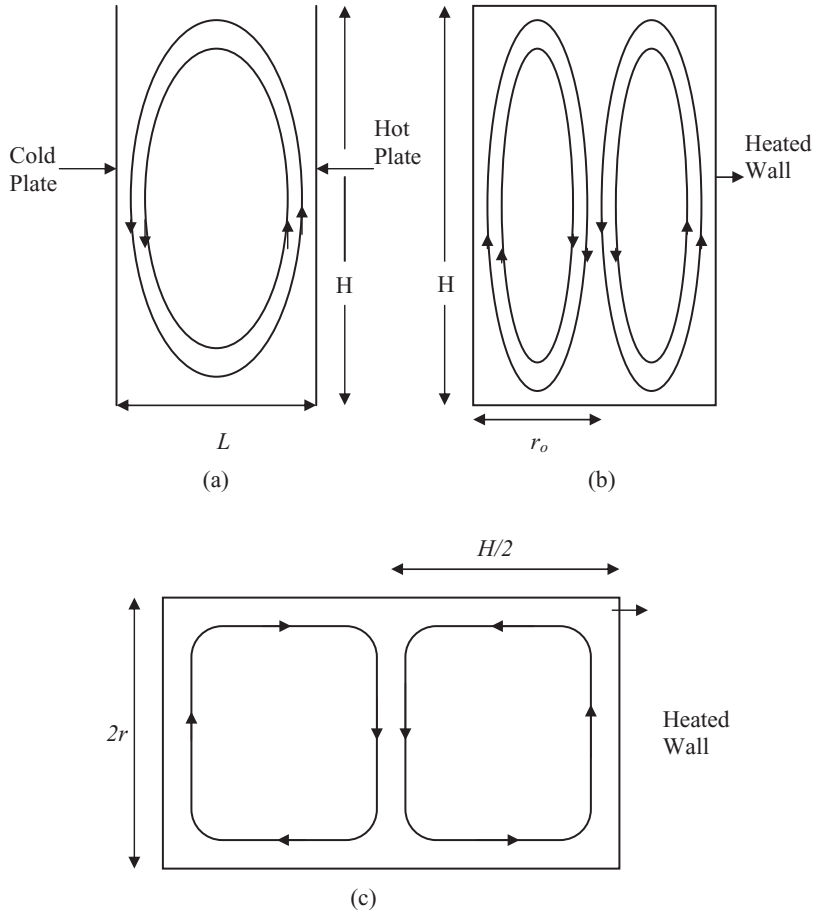

Figure 9.1. Natural convection current cavities filled with liquid in (a) parallel vertical plates, (b) a vertical can heated from the surface, and (c) a horizontal can heated from the surface.

Steam is usually used for in-can sterilization. The steam condensation heat transfer coefficient is very high. Hence the can wall may be assumed to remain at the condensing steam temperature during the whole period of heating. This is a realistic assumption, which will make the right-hand side of Equation (9.10) a function of the Fourier number only. This is equivalent to the first straight line in the semilog plot of the Heisler chart mentioned earlier. As we have noted, the can radius was not used in the definition of Fo as is usual in conduction analysis for an infinite cylinder. Instead, in order to account for the heat transfer from the top and bottom sides of the can, the ratio $(2V/A)$ of the can was used in the definition of Fo given below:

$$\mathrm{Fo} = \frac{\alpha_e t}{(2V/A)^2} \tag{9.14}$$

This is not the usual Fo because it contains an effective thermal diffusivity of the liquid, which is a function of Nu:

$$\alpha_e = \frac{ke}{\rho C_p} = \frac{k\mathrm{Nu}_\delta}{\rho C_p} \tag{9.15}$$

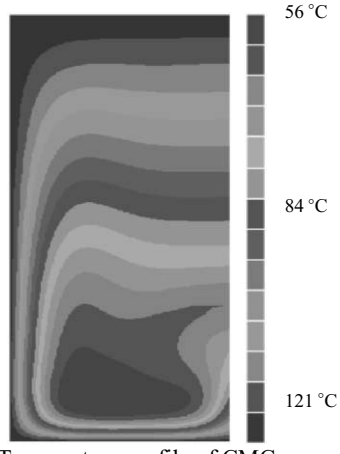

Temperature profile of CMC in a vertical can, 600 s

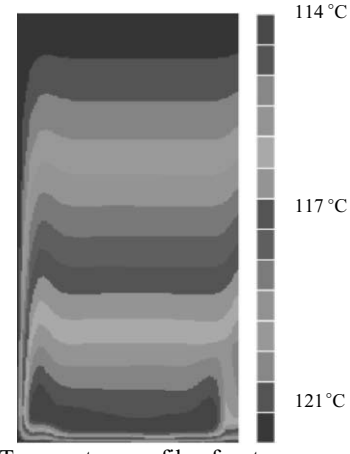

Temperature profile of water in a vertical can 600 s

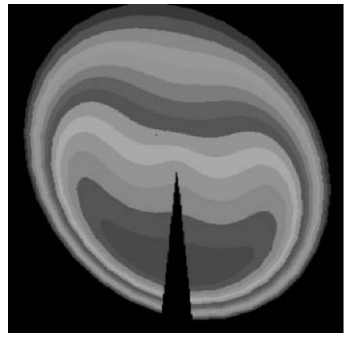

Radial-angular plane temperature profile of carrot-orange soup in a horizontal can, 600 s

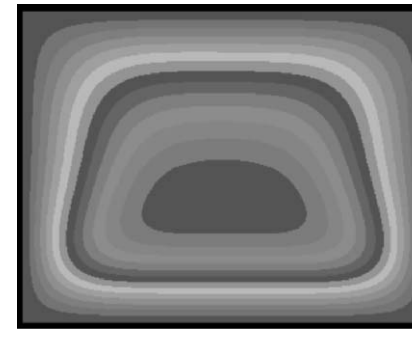

Radial-vertical plane temperature profile of carrot-orange soup in a horizontal can, 600 s

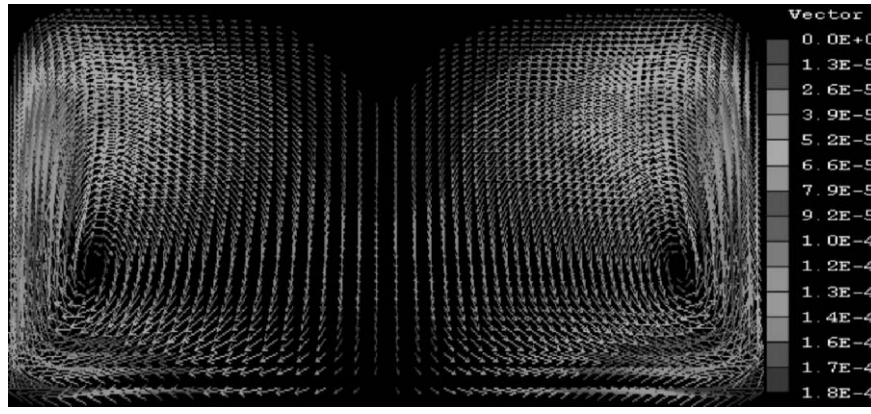

Velocity vectors profile of carrot-orange soup in a horizontal can, 600 s

Figure 9.2. Temperature and velocity profiles during sterilization of different liquid foods in vertical and horizontal cans of the same size, after 600 s of heating.

Table 9.1. Geometry of cans and types of liquid used in the seven CFD simulations.

Case Study	Can Dimensions	Position	Fluid Used	Heating Time
1	$r = 4.08$ cm, $L = 11$ cm	Vertical	CMC	4,600 s
2	$r = 3.5$ cm, $L = 15$ cm	Vertical	CMC	4,600 s
3	$r = 7$ cm, $L = 30$ cm	Vertical	CMC	8,100 s
4	$r = 4.08$ cm, $L = 11$ cm	Vertical	Fluid with viscosity 10 times than that of CMC	8,820 s
5	$r = 4.08$ cm, $L = 11$ cm	Vertical	Fluid with viscosity one tenth than that of CMC	2,170 s
6	$r = 4.08$ cm, $L = 11$ cm	Vertical	Water	600 s
7	$r = 4.08$ cm, $L = 11$ cm	Horizontal	Carrot-orange soup	4,600 s

The effective thermal conductivity of the liquid in the above equation accounts for the effect of natural convection currents developed during heating. The dimensionless temperature (θ_0^*) is written in term of the temperature of the SHZ rather than the temperature of the geometric center of the can as discussed earlier:

$$\theta_0^* = \frac{T_\infty - T_{\text{SHZ}}}{T_\infty - T_i} \tag{9.16}$$

Based on Equation (9.8), a single relationship should exist between this dimensionless SHZ temperature (θ_0^*) and Fo, which must be independent of the can geometry, the type of liquid used, and the sterilization temperature. This is the main objective of this analysis, and in order to achieve this, a number of CFD simulations were carried out for cans of different geometries containing water, viscous liquid foods, and very viscous liquid foods in addition to the simulations presented in Chapter 5. The variation of the viscosity provided full coverage of the effect of natural convection.

The CFD analysis covers seven main cases, as shown in Table 9.1.

9.3. APPLICATION OF THE NEW COMPUTATIONAL APPROACH

Figure 9.3 shows the temperature of the SHZ against sterilization time for all the cases analyzed using CFD analysis. It shows that sterilization time may vary from 600 s for water as a liquid food contained

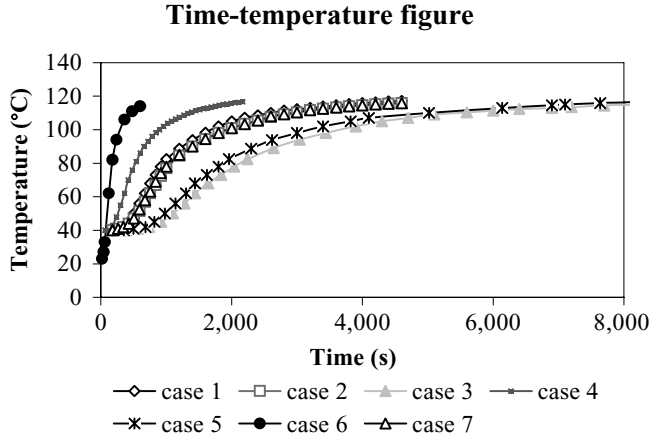

Figure 9.3. Variation of the temperature of the SHZ for the seven CFD simulations.

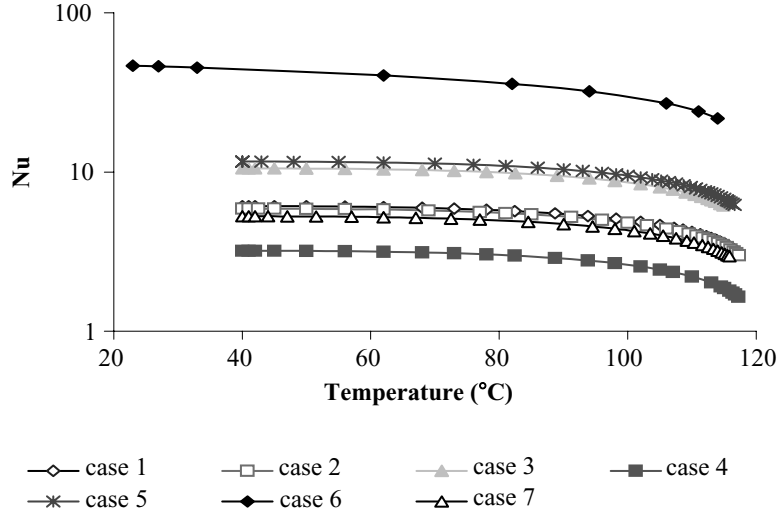

Figure 9.4. Variation of the Nusselt number with time for the seven cases studied.

in a small can to more than 8,000 s for a viscous liquid contained in a relatively large can (Table 9.1). The effect of natural convection on sterilization time due to the use of different viscous liquids can be seen clearly from the comparison between the two graphs defined by Cases 4 and 6. The effect of using different can sizes on sterilization time can be seen from the comparison between Cases 1 and 3.

Figure 9.4 shows how Nu changes as heating progresses for the different cases studied. No significant change in Nu occurs at the early stages of heating since the decrease in liquid viscosity is counterbalanced by the slight decrease in the driving temperature ($121^\circ C - T_{SHZ}$). As heating progresses, the decrease in the driving temperature becomes more than the decrease in liquid viscosity, leading to a continuous drop in the values of Nu. At the end of heating, Nu drops to 1.6 for the high-viscosity liquid, approaching conduction control process (Nu = 1). For water (low-viscosity fluid), the final values of Nu remain high (of the order of 20), indicating that heat transfer is still controlled by natural convection.

Figure 9.5 shows a plot of the dimensionless SHZ temperature (θ_0^*) against liquid Fo. It is important to note that all the seven graphs of Figure 9.3 lie on a single line even though they belong to simulations for liquids with viscosity varying by five orders of magnitude and for a wide range of can sizes. Such an excellent agreement is a strong support to the new method of analysis presented here.

Figure 9.5 can be used to determine the sterilization time needed for any liquid food contained in a can of any size, within the range tested, as follows:

1. Using the desired final SHZ temperature, the dimensionless SHZ temperature (θ_0^*) can be calculated from Equation (9.16).

   Figure 9.5 can be used to determine the value of Fo, which corresponds to the desired SHZ temperature. Alternatively, the following equation may be used, which is obtained from nonlinear curve fitting of the data of Figure 9.5:

$$\begin{aligned} \theta_0^* &= 1.96\, e^{-1.2\mathrm{Fo}} \quad \text{for} \quad \mathrm{Fo} > 2.1 \\ \theta_0^* &= 1.0 \quad \text{for} \quad \mathrm{Fo} < 2.1 \end{aligned} \tag{9.17}$$

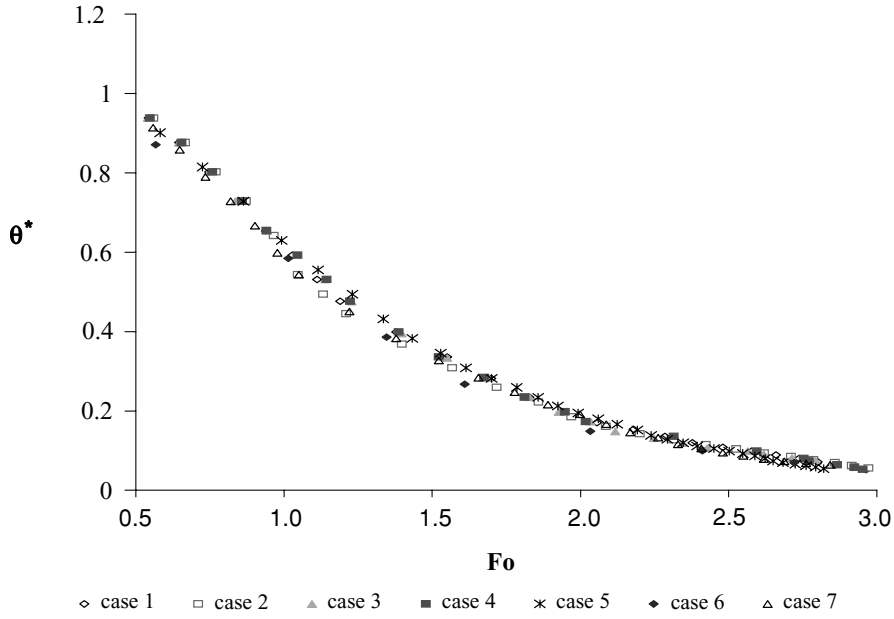

Figure 9.5. Generalized correlation for the dimensionless SHZ temperature as a function of the Fourier number.

2. The effective thermal diffusivity ($\alpha_e = \alpha$ Nu) varies during the sterilization procedure due to the variation in the value of Nu. In order to avoid stepwise calculation, an average $\overline{\text{Nu}}$ may be used to calculate the average value of α_e over the whole period of heating.
3. Sterilization time may be obtained from the calculated values of Fo and α_e as in the following equation:

$$t = \frac{\text{Fo}\left(2V/A\right)^2}{\overline{\alpha}_e} \tag{9.18}$$

Where $\overline{\alpha}_e$ is the average value of α_e over the whole period of heating.

NOMENCLATURE

A	surface area of the can (m^2)
B_i	Biot number, $Bi = \frac{hr_o}{k}$ (dimensionless)
C_n	coefficient defined by equation (2)
C_P	specific heat of liquid food (J $kg^{-1}K^{-1}$)
F_o	Fourier number, $F_o = \frac{\alpha_t}{r_o^2}$ *or* $\frac{\alpha_e t}{(2V/A)^2}$ (dimensionless)
Gr_δ	Grashof number based on L, $Gr_\delta = \frac{g\beta\Delta T\delta^3\rho^2}{\mu^2}$ (dimensionless)
H	height of the can (m)
h	external convection heat transfer coefficient (J $s^{-1}m^{-2}$ K)
J_1, J_0	Bessel functions of the first kind (equations 1–7)
k	thermal conductivity of the liquid food (J m^{-1} $K^{-1}s^{-1}$)
k_e	effective thermal conductivity of the liquid food (J m^{-1} $K^{-1}s^{-1}$)

L distance between two vertical walls (m)
n exponent of (H/δ) in equation (9)
Nu_δ Nusselt number based on δ, $Nu = \frac{h_c \delta}{k}$ (dimensionless)
$\overline{Nu}$ average Nusselt number (dimensionless)
Pr Prandtl number, $\Pr = \frac{C_p \mu}{k}$ (dimensionless)
Ra_δ Rayleigh number based on δ, $Ra_\delta = Gr_\delta \Pr$ (dimensionless)
r,θ,z radial, angular and vertical direction of the can
r_o radius of the can (m)
r^* radial coordinate, $r^* \equiv \frac{r}{r_o}$ (dimensionless)
t heating time (s)
T temperature (°C)
T_i initial temperature (°C)
T_w wall temperature (°C)
T_∞ steam temperature (°C)
V volume of the can (m^3)
v_r velocity in radial direction (ms^{-1})
v_θ velocity in angular direction (ms^{-1})
v_z velocity in axial direction (ms^{-1})
θ temperature difference, $\theta = T - T_\infty$ (°C)
θ_i maximum possible temperature difference, $\theta_i = T_i - T_\infty$ (°C)
θ^* temperature, $\theta^* \equiv \frac{\theta}{\theta_i} = \frac{T_\infty - T}{T_\infty - T_i}$(dimensionless)
θ_o^* slowest heating zone temperature, $\theta_o^* = \frac{T_\infty - T_{SHZ}}{T_\infty - T_i}$(dimensionless)
α thermal diffusivity of the liquid food, $\alpha = \frac{k}{\rho C_p}$ ($m^2\ s^{-1}$)
α_e effective thermal diffusivity of the liquid food, $\alpha_e = \alpha\ Nu$ ($m^2\ s^{-1}$)
$\overline{\alpha}_e$ average effective thermal diffusivity, ($m^2\ s^{-1}$)
β thermal expansion coefficient (K^{-1})
δ characteristic dimension for natural convection, $\delta = r_o$ for vertical can and $\delta = H/2$ for horizontal can (m)
μ viscosity (Pa.s)
ρ density (kg m^{-3})
ρ_i density at initial temperature (kg m^{-3})
ξ_n coefficient defined in equation (6)

REFERENCES

Adrian, B. (1993). *Heat transfer* (pp. 339–340). New York: Wiley.

Catton, I. (1978). Natural convection in enclosures. *Proceeding of the Sixth International Heat Transfer Conference, Toronto, Canada,* Volume 6, 13–31.

Ghani, A.G., Farid, M.M. & Chen, X.D. (1998). A CFD simulation of the coldest point during sterilization of canned food, 26th Australian Chemical Engineering Conference, 28–30 September, 1998, Port Douglas, Queensland, No. 358.

Ghani, A.G., Farid, M.M. & Chen, X.D. (2002). Numerical simulation of transient temperature and velocity profiles in a horizontal can during sterilization using computational fluid dynamics. *Journal of Food Engineering, 51*, 77–83.

Ghani, A.G., Farid, M.M. & Chen, X.D. (2003). Numerical simulation of transient two-dimensional profiles of temperature, concentration and flow of liquid food in a can during sterilization. In Welti-Chanes, J., velez, J., & Barbosa-Canovas, G. (Eds.). *Transport phenomena in food processing* (pp. 463–482). Boca Raton, USA: CRC Press.

Incropera, F.B. & DeWitt, D.B. (1996). *Fundamentals of heat & mass transfer*. New York: Wiley.
Kumar, A., & Bhattacharya, M. (1991). Transient temperature and velocity profiles in a canned non-Newtonian liquid food during sterilization in a still—cook retort. *International Journal of Heat and Mass Transfer, 34*(4/5), 1083–1096.
Kumar, A., Bhattacharya, M., & Blaylock, J. (1990). Numerical simulation of natural convection heating of canned thick viscous liquid food products. *Journal of Food Science, 55*(5), 1403–1411.
Schneider, P.J. (1955). *Conduction heat transfer*. Reading, MA: Addison Wesley.

APPENDIX A

Program input file (q1) of PHOENICS

Thermal sterilization of a can filled with carboxyl methyl cellulose (CMC) and heated by condensing steam at 121°C from all sides.

```
TALK=T;RUN( 1, 1);VDU=X11-TERM
IRUNN    =       1 ;LIBREF =    166
************************************************************
   Group 1. Run Title
TEXT (Thermal sterilization of can filled with CMC)
************************************************************
   Group 2. Transience
STEADY=F
      * Set overall time and no. of steps
RSET(U,0.000E+00,2.574E+03,300)
      * Cut regions
RSET(T,L,0,1.800E+02)
RSET(T,L,0,1.000E+03)
      * Modify regions
RSET(T,1,100,1.000E+00)
RSET(T,2,100,1.000E+00)
RSET(T,3,100,1.000E+00)
************************************************************
   * Groups 3, 4, 5 Grid Information
      * Overall number of cells, RSET(M,NX,NY,NZ,tolerance)
RSET(M,1,51,69)
      * Set overall domain extent:
      *       xulast  yvlast  zwlast   name
XSI= 6.283E+00;YSI= 4.05E-02;ZSI= 1.11E-01;RSET(D,CAN    )
      * Set objects: x0       y0       z0
      *              dx       dy       dz       name
XPO= 0.000E+00;YPO= 0.000E+00;ZPO= 1.11E-01
XSI= 6.283E+00;YSI= 4.05E-02;ZSI= 0.000E+00;RSET(B,UP    )
XPO= 0.000E+00;YPO= 0.000E+00;ZPO= 0.000E+00
XSI= 6.283E+00;YSI= 4.05E-02;ZSI= 0.000E+00;RSET(B,DOWN    )
XPO= 0.000E+00;YPO= 0.000E+00;ZPO= 5.55E-02
XSI= 6.283E+00;YSI= 4.05E-02;ZSI= 0.000E+00;RSET(B,PLATE    )
XPO= 0.000E+00;YPO= 4.05E-02;ZPO= 0.000E+00
XSI= 6.283E+00;YSI= 0.000E+00;ZSI= 1.11E-01;RSET(B,SIDE    )
```

```
      * Modify default grid
RSET(Y,1,51,7.000E−01)
RSET(Z,1,34,1.600E+00)
RSET(Z,2,35,8.000E−01)
************************************************************
   Group 6. Body-Fitted coordinates
************************************************************
   Group 7. Variables: STOREd,SOLVEd,NAMEd
ONEPHS =    T
      * Non-default variable names
NAME( 46) =BLOK ; NAME( 47) =SPH1
NAME( 48) =TEM1 ; NAME( 49) =DEN1
NAME( 50) =PRPS
      * Solved variables list
SOLVE(P1    ,V1    ,W1    ,TEM1)
      * Stored variables list
STORE(PRPS,DEN1,SPH1,BLOK)
      * Additional solver options
SOLUTN(P1 ,Y,Y,Y,N,N,Y)
SOLUTN(V1 ,Y,Y,Y,N,N,Y)
SOLUTN(W1 ,Y,Y,Y,N,N,Y)
SOLUTN(TEM1,Y,Y,Y,N,N,Y)
************************************************************
   Group 8. Terms & Devices
TERMS (P1 ,Y,Y,Y,Y,Y,N)
TERMS (V1 ,Y,Y,Y,Y,Y,N)
TERMS (W1 ,Y,Y,Y,Y,Y,N)
TERMS (TEM1,Y,Y,Y,Y,Y,N)
NEWRH1 =    T
NEWENL =    T
************************************************************
   Group 9. Properties
RHO1    = GRND10
CP1     = GRND10
ENULA=4.35E−03
ENULB=-6.55E−05
ENULC=2.72E−07

ENUL    = GRND2    ;ENUT    = 0.000E+00
PRNDTL(TEM1) = −GRND10
        * List of user-defined materials to be read by EARTH
        MATFLG=T;IMAT=1
        * Name
        *Ind. Dens. Viscos. Spec.heat Conduct. Expans. Compr.
        * <CMC>
        90 950 1.4284E−02 4100 7.0000E−01 2.0000E−04 0.0
************************************************************
   Group 10. Inter-Phase Transfer Processes
************************************************************
```

```
   Group 11. Initialise Var/Porosity Fields
FIINIT(BLOK) = 1.000E+00 ;FIINIT(PRPS) = 9.000E+01
PATCH (TIMI    ,INIVAL,#1,#1,#1,#1,#1,#2,#1,#1)

INIT(TIMI ,TEM1, 0.000E+00, 4.000E+01)

RSTGRD = F

INIADD = F
************************************************************
   Group 12. Convection and diffusion adjustments
************************************************************
   Group 13. Boundary & Special Sources
PATCH (BUOYANCY,PHASEM,1,1,1,51,1,69,1,300)
COVAL (BUOYANCY,V1    , FIXFLU    , GRND3    )
COVAL (BUOYANCY,W1    , FIXFLU    , GRND3    )

PATCH (UP    ,HIGH    ,#1,#1,#1,#1,#2,#2,#1,#3)
COVAL (UP    ,V1    , FIXVAL    , 0.000E+00)
COVAL (UP    ,W1    , FIXVAL    , 0.000E+00)
COVAL (UP    ,TEM1, FIXVAL    , 1.210E+02)

PATCH (SIDE    ,NORTH    ,#1,#1,#1,#1,#1,#2,#1,#3)
COVAL (SIDE    ,V1    , FIXVAL    , 0.000E+00)
COVAL (SIDE    ,W1    , FIXVAL    , 0.000E+00)
COVAL (SIDE    ,TEM1, FIXVAL    , 1.210E+02)

PATCH (DOWN    ,LOW    ,#1,#1,#1,#1,#1,#1,#1,#3)
COVAL (DOWN    ,V1    , FIXVAL    , 0.000E+00)
COVAL (DOWN    ,W1    , FIXVAL    , 0.000E+00)
COVAL (DOWN    ,TEM1, FIXVAL    , 1.210E+02)

BUOYA = 0.000E+00 ; BUOYB = 0.000E+00 ; BUOYC =−9.810E+00
BUOYD = GRND10
BUOYE = 4.000E+01
EGWF = T
************************************************************
   Group 14. Downstream Pressure For PARAB
************************************************************
   Group 15. Terminate Sweeps
LSWEEP =    400
LITHYD =    2
SELREF =   T
RESFAC = 1.000E−03
************************************************************
   Group 16. Terminate Iterations
************************************************************
   Group 17. Relaxation
RELAX(V1    ,FALSDT, 1.103E−05)
RELAX(W1    ,FALSDT, 1.103E−05)
RELAX(TEM1,FALSDT, 4.411E−02)
```

```
*****************************************************************
   Group 18. Limits
*****************************************************************
   Group 19. EARTH Calls To GROUND Station
GENK   =   T
CSG10  =Q1
*****************************************************************
   Group 20. Preliminary Printout
ECHO   =   T
*****************************************************************
   Group 21. Print-out of Variables
INIFLD   =   T
OUTPUT(BLOK,Y,N,Y,N,N,N)
OUTPUT(SPH1,N,N,Y,Y,N,N)
OUTPUT(DEN1,Y,N,Y,N,N,N)
OUTPUT(PRPS,Y,N,Y,N,N,N)
*****************************************************************
   Group 22. Monitor Print-Out
IXMON =   1 ;IYMON =   20 ;IZMON =   30
TSTSWP =   −1
UWATCH =   T
USTEER =   T
*****************************************************************
   Group 23. Field Print-Out & Plot Control
NTPRIN =   10 ;ISTPRF =   1 ;ISTPRL =   10000
   No PATCHes used for this Group
*****************************************************************
   Group 24. Dumps For Restarts
IDISPA =   10
CSG1   =M
*****************************************************************
STOP
```

APPENDIX B

Program input file (q1) and the modification of ground.f subroutine in PHOENICS

Bacteria deactivation and vitamin destruction during thermal sterilization of a can filled with concentrated cherry juice and heated by condensing steam at 121°C from all sides.

```
TALK=T;RUN( 1, 1);VDU=X11-TERM
IRUNN    =       1 ;LIBREF =    166
************************************************************
   Group 1. Run Title
TEXT (Bacteria deactivation and vitamin destruction in concentrated cherry juice during sterilization)
************************************************************
   Group 2. Transience
STEADY=F
   * Set overall time and no. of steps
RSET(U,0.000E+00,2.60E+03,30)
   * Cut regions
RSET(T,L,0,2.000E+02)
RSET(T,L,0,1.000E+03)
   * Modify regions
RSET(T,1,10,1.000E+00)
RSET(T,2,10,1.000E+00)
RSET(T,3,10,1.000E+00)
************************************************************
Groups 3, 4, 5 Grid Information
   * Overall number of cells, RSET(M,NX,NY,NZ,tolerance)
RSET(M,1,50,70)
   * Set overall domain extent:
   *       xulast     yvlast     zwlast     name
XSI= 6.283E+00;YSI= 4.05E-02;ZSI= 1.100E-01;RSET(D,CAN       )
   * Set objects: x0    y0    z0
   *          dx     dy     dz     name
XPO= 0.000E+00;YPO= 0.000E+00;ZPO= 1.100E-01
XSI= 6.283E+00;YSI= 4.05E-02;ZSI= 0.000E+00;RSET(B,UP        )
XPO= 0.000E+00;YPO= 0.000E+00;ZPO= 0.000E+00
XSI= 6.283E+00;YSI= 4.05E-02;ZSI= 0.000E+00;RSET(B,DOWN      )
XPO= 0.000E+00;YPO= 0.000E+00;ZPO= 5.5E-02
XSI= 6.283E+00;YSI= 4.05E-02;ZSI= 0.000E+00;RSET(B,PLATE     )
XPO= 0.000E+00;YPO= 4.05E-02;ZPO= 0.000E+00
XSI= 6.283E+00;YSI= 0.000E+00;ZSI= 1.100E-01;RSET(B,SIDE      )
```

```
* Modify default grid
RSET(Y,1,50,7.000E−01)
RSET(Z,1,35,1.600E+00)
RSET(Z,2,35,8.000E−01)
************************************************************
   Group 6. Body-Fitted coordinates
************************************************************
   Group 7. Variables: STOREd,SOLVEd,NAMEd
ONEPHS =   T
   * Non-default variable names
NAME( 46) =BLOK ; NAME( 47) =SPH1
NAME( 48) =TEM1 ; NAME( 49) =DEN1
NAME( 50) =PRPS
   * Solved variables list
SOLVE(P1   , V1    , W1    , TEM1    , C1    , C2    , C3    , C4)
   * Stored variables list
STORE(PRPS,DEN1,SPH1,BLOK   )
   * Additional solver options
SOLUTN(P1   ,Y,Y,Y,N,N,Y)
SOLUTN(V1   ,Y,Y,Y,N,N,Y)
SOLUTN(W1   ,Y,Y,Y,N,N,Y)
SOLUTN(TEM1,Y,Y,Y,N,N,Y)
************************************************************
   Group 8. Terms & Devices
TERMS (P1   ,Y,Y,Y,Y,Y,N)
TERMS (V1   ,Y,Y,Y,Y,Y,N)
TERMS (W1   ,Y,Y,Y,Y,Y,N)
TERMS (TEM1,Y,Y,Y,Y,Y,N)
TERMS (C1   ,Y,Y,Y,Y,Y,N)
TERMS (C2   ,Y,Y,Y,Y,Y,N)
TERMS (C3   ,Y,Y,Y,Y,Y,N)
TERMS (C4   ,Y,Y,Y,Y,Y,N)
NEWRH1   =   T
NEWENL   =   T
************************************************************
   Group 9. Properties
RHO1   = GRND10
CP1   = GRND10
ENULA   = 1.40E−03  ; ENULB   =−4.05E−05 ; ENULC   = 2.99E−07
ENUL   = GRND10   ;ENUT   = 0.000E+00
PRNDTL(TEM1) = −GRND10
PRNDTL(C1) = 0.0
PRNDTL(C2) = 0.0
PRNDTL(C3) = 0.0
PRNDTL(C4) = 0.0
   * List of user-defined materials to be read by EARTH
   MATFLG=T;IMAT=1
   * Name
```

```
   *Ind. Dens. Viscos. Spec.heat Conduct. Expans. Compr.
   * <CHERY>
   92 1052 1.476E−01 3500 5.540E−01 2.0000E−04 0.0
************************************************************
   Group 10. Inter-Phase Transfer Processes
************************************************************
   Group 11. Initialise Var/Porosity Fields
FIINIT(BLOK) = 1.000E+00 ;FIINIT(PRPS) = 9.200E+01
PATCH (TIMI    ,INIVAL,#1,#1,#1,#1,#1,#2,#1,#1)
INIT(TIMI    ,TEM1, 0.000E+00, 4.00E+01)
INIT(TIMI    ,C1    , 0.000E+00, 1.000E+02)
INIT(TIMI    ,C2    , 0.000E+00, 1.000E+02)
INIT(TIMI    ,C3    , 0.000E+00, 1.000E+02)
INIT(TIMI    ,C4    , 0.000E+00, 1.000E+02)
RSTGRD   =   F
INIADD   =   F
************************************************************
   Group 12. Convection and diffusion adjustments
************************************************************
   Group 13. Boundary & Special Sources

PATCH (BUOYANCY,PHASEM,1,1,1,50,1,70,1,30)
COVAL (BUOYANCY,V1    , FIXFLU    , GRND3    )
COVAL (BUOYANCY,W1    , FIXFLU    , GRND3    )

PATCH (BACTERIA,PHASEM,1,1,1,50,1,70,1,30)
COVAL (BACTERIA,C1    , GRND1    , 0.000E+00    )

PATCH (VITAMINC,PHASEM,1,1,1,50,1,70,1,30)
COVAL (VITAMINC,C2    , GRND2    , 0.000E+00    )

PATCH (RIBOFLA,PHASEM,1,1,1,50,1,70,1,30)
COVAL (RIBOFLA,C3    , GRND3    , 0.000E+00    )

PATCH (THIAMIN,PHASEM,1,1,1,50,1,70,1,30)
COVAL (THIAMIN,C4    , GRND4    , 0.000E+00    )

PATCH (UP    ,HWALL    ,#1,#1,#1,#1,#2,#2,#1,#3)
COVAL (UP    ,V1    , FIXVAL    , 0.000E+00)
COVAL (UP    ,W1    , FIXVAL    , 0.000E+00)
COVAL (UP    ,TEM1, FIXVAL    , 1.21E+02)

PATCH (SIDE    ,NWALL    ,#1,#1,#1,#1,#1,#2,#1,#3)
COVAL (SIDE    ,V1    , FIXVAL    , 0.000E+00)
COVAL (SIDE    ,W1    , FIXVAL    , 0.000E+00)
COVAL (SIDE    ,TEM1, FIXVAL    , 1.21E+02)

PATCH (DOWN    ,LWALL    ,#1,#1,#1,#1,#1,#1,#1,#3)
COVAL (DOWN    ,V1    , FIXVAL    , 0.000E+00)
```

```
COVAL (DOWN    ,W1    , FIXVAL    , 0.000E+00)
COVAL (DOWN    ,TEM1, FIXVAL    , 1.210E+02)


BUOYA    = 0.000E+00 ; BUOYB = 0.000E+00 ; BUOYC =−9.810E+00
BUOYD    = GRND10
BUOYE    = 4.000E+01
EGWF    =    T
************************************************************
   Group 14. Downstream Pressure For PARAB
************************************************************
   Group 15. Terminate Sweeps
LSWEEP =    40
LITHYD =      2
SELREF =    T
RESFAC = 1.000E−03
************************************************************
   Group 16. Terminate Iterations
************************************************************
   Group 17. Relaxation
RELAX(V1    ,FALSDT, 1.103E−03)
RELAX(W1    ,FALSDT, 1.103E−03)
RELAX(TEM1,FALSDT, 4.411E+00)
************************************************************
   Group 18. Limits
************************************************************
   Group 19. EARTH Calls To GROUND Station
GENK    =    T
CSG10  =Q1
************************************************************
   Group 20. Preliminary Printout
ECHO    =    T
************************************************************
   Group 21. Print-out of Variables
INIFLD  =    T
OUTPUT(BLOK,Y,N,Y,N,N,N)
OUTPUT(SPH1,N,N,Y,Y,N,N)
OUTPUT(DEN1,Y,N,Y,N,N,N)
OUTPUT(PRPS,Y,N,Y,N,N,N)
************************************************************
   Group 22. Monitor Print-Out
IXMON  =       1 ;IYMON  = 20 ;IZMON =       30
TSTSWP =       −1
UWATCH =       T
USTEER =       T
************************************************************
   Group 23. Field Print-Out & Plot Control
NTPRIN =       1 ;ISTPRF =       1 ;ISTPRL =    10000
NYPRIN =       1 ;IYPRF =       25 ;IYPRL = 25
```

```
NZPRIN =       1 ;IZPRF =       35 ;IZPRL = 35
ITABL =      1
   No PATCHes used for this Group
************************************************************
   Group 24. Dumps For Restarts
IDISPA =      1
CSG1      =M
************************************************************
STOP
```

Modification of group 13 of ground.f subroutine in PHOENICS

To measure the concentrations of the bacteria and the vitamins

```
C FILE NAME GROUND.FTN- - - - - - - - - - - - - - - - - - - - - -130995
   SUBROUTINE GROUND
   INCLUDE 'lp21/d_includ/satear'
   INCLUDE 'lp21/d_includ/grdloc'
   INCLUDE 'lp21/d_includ/grdear'
   INCLUDE 'lp21/d_includ/grdbfc'
   COMMON/GENI/NXNY,IGFIL1(30),IPRL,IBTAU,ILTLS,IGFIL(15),ITEM1,
   1 ITEM2,ISPH1,ISPH2,ICON1,ICON2,IPRPS,IRADX,IRADY,IRADZ,IVFOL
   COMMON/DRHODP/ITEMP,IDEN
CXXXXXXXXXXXXXXXXXXXXXXXXXXXXXXXXXXXXXXXXXX USER
SECTION STARTS:
C
C 1   Set dimensions of data-for-GROUND arrays here. WARNING: the
C     corresponding arrays in the MAIN program of the satellite
C     and EARTH must have the same dimensions.
     PARAMETER (NLG=100, NIG=200, NRG=200, NCG=100)
C
COMMON/LGRND/LG(NLG)/IGRND/IG(NIG)/RGRND/RG(NRG)/CGRND/CG(NCG)
   LOGICAL LG
   CHARACTER*4 CG
C
C 2   User dimensions own arrays here, for example:
C    DIMENSION GUH(10,10),GUC(10,10),GUX(10,10),GUZ(10)
C
C 3   User places his data statements here, for example:
C    DATA NXDIM,NYDIM/10,10/
C
C 4   Insert own coding below as desired, guided by GREX examples.
C     Note that the satellite-to-GREX special data in the labelled
C     COMMONs /RSG/, /ISG/, /LSG/ and /CSG/ can be included and
C     used below but the user must check GREX for any conflicting
C     uses. The same comment applies to the EARTH-spare working
C     arrays EASP1, EASP2,....EASP20. In addition to the EASPs,
C     there are 10 GRound-earth SPare arrays, GRSP1,...,GRSP10,
```

```
C     supplied solely for the user, which are not used by GREX. If
C     the call to GREX has been deactivated then all of the arrays
C     may be used without reservation.
C
c**********************************************************************
***
    IXL=IABS(IXL)
    IF(IGR.EQ.13) GO TO 13
    IF(IGR.EQ.19) GO TO 19
    GO TO (1,2,3,4,5,6,25,8,9,10,11,12,13,14,25,25,25,25,19,20,25,
    125,23,24),IGR
  25 CONTINUE
    RETURN
C*********************************************************************
C- - - GROUP 1. Run title and other preliminaries
C
    1 GO TO (1001,1002,1003),ISC
C * - - - - - - - - - -GROUP 1 SECTION 3 - - - - - - - - - - - - - -
C- - - Use this group to create storage via GXMAKE which it is not
C     necessary to dump to PHI for restarts
C
1003 CONTINUE
    GO TO 25
C
  1001 CONTINUE
C
C     User may here change message transmitted to the VDU screen
    IF(.NOT.NULLPR)
    1 CALL WRYT40('GROUND file is GROUND.F of:    130995 ')
C
    RETURN
    1002 CONTINUE
    RETURN
C*********************************************************************
C
C- - - GROUP 2. Transience; time-step specification
C
    2 CONTINUE
      RETURN
C*********************************************************************
C
C- - - GROUP 3. X-direction grid specification
C
    3 CONTINUE
      RETURN
C*********************************************************************
C
C- - - GROUP 4. Y-direction grid specification
```

```
C
   4 CONTINUE
     RETURN
C*************************************************************
C
C- - - GROUP 5. Z-direction grid specification
C
   5 CONTINUE
     RETURN
C*************************************************************
C
C- - - GROUP 6. Body-fitted coordinates or grid distortion
C
   6 CONTINUE
     RETURN
C*************************************************************
C    * Make changes for this group only in group 19.
C- - - GROUP 7. Variables stored, solved & named
C*************************************************************
C
C- - - GROUP 8. Terms (in differential equations) & devices
C
      8 GO TO (81,82,83,84,85,86,87,88,89,810,811,812,813,814,815,816)
     1,ISC
   81 CONTINUE
C    * - - - - - - - - - SECTION 1 - - - - - - - - - - - - - - - - - -
C    For U1AD.LE.GRND- - - phase 1 additional velocity. Index VELAD
      RETURN
   82 CONTINUE
C    * - - - - - - - - - SECTION 2 - - - - - - - - - - - - - - - - - -
C    For U2AD.LE.GRND- - - phase 2 additional velocity. Index VELAD
      RETURN
   83 CONTINUE
C    * - - - - - - - - - SECTION 3 - - - - - - - - - - - - - - - - - -
C    For V1AD.LE.GRND- - - phase 1 additional velocity. Index VELAD
      RETURN
   84 CONTINUE
C    * - - - - - - - - - SECTION 4 - - - - - - - - - - - - - - - - - -
C    For V2AD.LE.GRND- - - phase 2 additional velocity. Index VELAD
      RETURN
   85 CONTINUE
C    * - - - - - - - - - SECTION 5 - - - - - - - - - - - - - - - - - -
C    For W1AD.LE.GRND- - - phase 1 additional velocity. Index VELAD
      RETURN
   86 CONTINUE
C    * - - - - - - - - - SECTION 6 - - - - - - - - - - - - - - - - - -
C    For W2AD.LE.GRND- - - phase 2 additional velocity. Index VELAD
      RETURN
```

```
   87 CONTINUE
C    * - - - - - - - - - SECTION 7 - - - - Volumetric source for gala
      RETURN
   88 CONTINUE
C    * - - - - - - - - - SECTION 8 - - - - Convection fluxes
C- - - Entered when UCONV =.TRUE.; block-location indices are:
C    LD11 for east and north (accessible at the same time),
C    LD12 for west and south (accessible at the same time),
C    LD2 for high (which becomes low for the next slab).
C    User should provide INDVAR and NDIREC IF's as appropriate.
      RETURN
   89 CONTINUE
C    * - - - - - - - - - SECTION 9 - - - - Diffusion coefficients
C- - - Entered when UDIFF =.TRUE.; block-location indices are LAE
C    for east, LAW for west, LAN for north, LAS for
C    south, LD11 for high, and LD11 for low.
C    User should provide INDVAR and NDIREC IF's as above.
C    EARTH will apply the DIFCUT and GP12 modifications after the user
C    has made his settings.
C
      RETURN
   810 CONTINUE
C    * - - - - - - - - - SECTION 10 - - - Convection neighbours
      RETURN
   811 CONTINUE
C    * - - - - - - - - - SECTION 11 - - - Diffusion neighbours
      RETURN
   812 CONTINUE
C    * - - - - - - - - - SECTION 12 - - - Linearised sources
      RETURN
   813 CONTINUE
C    * - - - - - - - - - SECTION 13 - - - Correction coefficients
      RETURN
   814 CONTINUE
C    * - - - - - - - - - SECTION 14 - - - User's own solver
      RETURN
   815 CONTINUE
C    * - - - - - - - - - SECTION 15 - - - Change solution
      RETURN
   816 CONTINUE
C    * - - - - - - - - - SECTION 16 - - - Change DVEL/DPs
      RETURN
C
C    * See the equivalent section in GREX for the indices to be
C    used in sections 7 - 16
C
C    * Make all other group-8 changes in GROUP 19.
C*****************************************************************
```

```
C
C - - - GROUP 9. Properties of the medium (or media)
C
C     The sections in this group are arranged sequentially in their
C     order of calling from EARTH. Thus, as can be seen from below,
C     the temperature sections (10 and 11) precede the density
C     sections (1 and 3); so, density formulae can refer to
C     temperature stores already set.
    9 GO TO (91,92,93,94,95,96,97,98,99,900,901,902,903,904,905),ISC
C*****************************************************************
900 CONTINUE
C     * - - - - - - - - - SECTION 10 - - - - - - - - - - - - - - - - -
C     For TMP1.LE.GRND- - - - - - phase-1 temperature Index TEMP1
      RETURN
  901 CONTINUE
C     * - - - - - - - - - SECTION 11 - - - - - - - - - - - - - - - - -
C     For TMP2.LE.GRND- - - - - - phase-2 temperature Index TEMP2
      RETURN
  902 CONTINUE
C * - - - - - - - - - SECTION 12 - - - - - - - - - - - - - - - - - -
C     For EL1.LE.GRND- - - - - - phase-1 length scale Index LEN1
      RETURN
  903 CONTINUE
C     * - - - - - - - - - SECTION 13 - - - - - - - - - - - - - - - - -
C     For EL2.LE.GRND- - - - - - phase-2 length scale Index LEN2
      RETURN
  904 CONTINUE
C     * - - - - - - - - - SECTION 14 - - - - - - - - - - - - - - - - -
C     For SOLVE(TEM1)- - - - - - phase-1 specific heat
      RETURN
  905 CONTINUE
C     * - - - - - - - - - SECTION 15 - - - - - - - - - - - - - - - - -
C     For SOLVE(TEM2)- - - - - - phase-2 specific heat
      RETURN
   91 CONTINUE
C     * - - - - - - - - - SECTION 1 - - - - - - - - - - - - - - - - - -
C     For RHO1.LE.GRND- - - density for phase 1     Index DEN1
      RETURN
   92 CONTINUE
C     * - - - - - - - - - SECTION 2 - - - - - - - - - - - - - - - - - -
C     For DRH1DP.LE.GRND- - - D(LN(DEN))/DP for phase 1
C               Index D1DP
      RETURN
   93 CONTINUE
C     * - - - - - - - - - SECTION 3 - - - - - - - - - - - - - - - - - -
C     For RHO2.LE.GRND- - - density for phase 2     Index DEN2
      RETURN
   94 CONTINUE
```

```
C    * - - - - - - - - - SECTION 4 - - - - - - - - - - - - - - - - - -
C    For DRH2DP.LE.GRND- - - D(LN(DEN))/DP for phase 2
C                                        Index D2DP
      RETURN
   95 CONTINUE
C    * - - - - - - - - - SECTION 5 - - - - - - - - - - - - - - - - - -
C    For ENUT.LE.GRND- - - reference turbulent kinematic viscosity
C                                        Index VIST
      RETURN
   96 CONTINUE
C    * - - - - - - - - - SECTION 6 - - - - - - - - - - - - - - - - - -
C    For ENUL.LE.GRND- - - reference laminar kinematic viscosity
C                                  Index VISL
      RETURN
   97 CONTINUE
C    * - - - - - - - - - SECTION 7 - - - - - - - - - - - - - - - - - -
C    For PRNDTL( ).LE.GRND- - - laminar PRANDTL nos., or diffusivity
C                                        Index LAMPR
      RETURN
   98 CONTINUE
C    * - - - - - - - - - SECTION 8 - - - - - - - - - - - - - - - - - -
C    For PHINT( ).LE.GRND- - - interface value of first phase
C                                       Index FII1
      RETURN
   99 CONTINUE
C    * - - - - - - - - - SECTION 9 - - - - - - - - - - - - - - - - - -
C    For PHINT( ).LE.GRND- - - interface value of second phase
C                                        Index FII2
      RETURN
C*****************************************************************
C
C- - - GROUP 10. Inter-phase-transfer processes and properties
C
    10 GO TO (101,102,103,104),ISC
   101 CONTINUE
C    * - - - - - - - - - SECTION 1 - - - - - - - - - - - - - - - - - -
C    For CFIPS.LE.GRND- - - inter-phase friction coeff.
C                                       Index INTFRC
      RETURN
   102 CONTINUE
C    * - - - - - - - - - SECTION 2 - - - - - - - - - - - - - - - - - -
C    For CMDOT.EQ.GRND- inter-phase mass transfer Index INTMDT
      RETURN
   103 CONTINUE
C    * - - - - - - - - - SECTION 3 - - - - - - - - - - - - - - - - - -
C    For CINT( ).EQ.GRND- - - phase1-to-interface transfer coefficients
C                                       Index COI1
      RETURN
```

```
  104 CONTINUE
C    * - - - - - - - - SECTION 4 - - - - - - - - - - - - - - - - -
C    For CINT( ).EQ.GRND- - - phase2-to-interface transfer coefficients
C                                  Index COI2
      RETURN
C*****************************************************************
C
C- - - GROUP 11. Initialization of variable or porosity fields
C                                  Index VAL
  11 CONTINUE
     RETURN
C*****************************************************************
C
C- - - GROUP 12. Convection and diffusion adjustments
C
  12 CONTINUE
    RETURN
C*****************************************************************
C
C- - - GROUP 13. Boundary conditions and special sources
C                                  Index for Coefficient - CO
C                                  Index for Value    - VAL
  13 CONTINUE
    GO TO (130,131,132,133,134,135,136,137,138,139,1310,
    11311,1312,1313,1314,1315,1316,1317,1318,1319,1320,1321),ISC
  130 CONTINUE
C- - - - - - - - - SECTION 1 - - - - - - - - - - - - - coefficient = GRND
      RETURN
  131 CONTINUE
C- - - - - - - - - SECTION 2 - - - - - - - - - - - - - coefficient = GRND1
  IF ( INDVAR . EQ . C1 ) THEN
  CALL FN1 ( CO    , 2.50E+11    )
  LTMP=LBNAME('TEM1')
  CALL FN32(CO,LTMP,−31873.95,273.15)

  ENDIF
  RETURN
  132 CONTINUE
C- - - - - - - - - SECTION 3 - - - - - - - - - - - - - coefficient = GRND2
  IF ( INDVAR . EQ . C2 ) THEN
  CALL FN1 ( CO    , 2.850E+9    )
  LTMP=LBNAME('TEM1')
  CALL FN32(CO,LTMP,−12027.9,273.15)

  ENDIF
  RETURN
  133 CONTINUE
C- - - - - - - - - SECTION 4 - - - - - - - - - - - - - coefficient = GRND3
```

```
   IF ( INDVAR . EQ . C3 ) THEN
   CALL FN1 ( CO , 2.480E+8    )
   LTMP=LBNAME('TEM1')
   CALL FN32(CO,LTMP,−12027.9,273.15)

   ENDIF
   RETURN
   134 CONTINUE
C- - - - - - - - - SECTION 5 - - - - - - - - - - - - - coefficient = GRND4
   IF ( INDVAR . EQ . C4 ) THEN
   CALL FN1 ( CO , 8.5E+08    )
   LTMP=LBNAME('TEM1')
   CALL FN32(CO,LTMP,−10825.11,273.15)

   ENDIF
   RETURN
   135 CONTINUE
C- - - - - - - - - SECTION 6 - - - - - - - - - - - - - coefficient = GRND5
   RETURN
   136 CONTINUE
C- - - - - - - - - SECTION 7 - - - - - - - - - - - - - coefficient = GRND6
   RETURN
   137 CONTINUE
C- - - - - - - - - SECTION 8 - - - - - - - - - - - - - coefficient = GRND7
   RETURN
   138 CONTINUE
C- - - - - - - - - SECTION 9 - - - - - - - - - - - - - coefficient = GRND8
   RETURN
   139 CONTINUE
C- - - - - - - - - SECTION 10 - - - - - - - - - - - - - coefficient = GRND9
   RETURN
   1310 CONTINUE
C- - - - - - - - - SECTION 11 - - - - - - - - - - - - - coefficient = GRND10
   RETURN
   1311 CONTINUE
C- - - - - - - - - SECTION 12 - - - - - - - - - value = GRND
   RETURN
   1312 CONTINUE
C- - - - - - - - - SECTION 13 - - - - - - - - - value = GRND1
   RETURN
   1313 CONTINUE
C- - - - - - - - - SECTION 14 - - - - - - - - - value = GRND2
   RETURN
   1314 CONTINUE
C- - - - - - - - - SECTION 15 - - - - - - - - - value = GRND3
   RETURN
   1315 CONTINUE
C- - - - - - - - - SECTION 16 - - - - - - - - - value = GRND4
```

```
   RETURN
   1316 CONTINUE
C- - - - - - - - - SECTION 17 - - - - - - - - - value = GRND5
   RETURN
   1317 CONTINUE
C- - - - - - - - - SECTION 18 - - - - - - - - - value = GRND6
   RETURN
   1318 CONTINUE
C- - - - - - - - - SECTION 19 - - - - - - - - - value = GRND7
   RETURN
   1319 CONTINUE
C- - - - - - - - - SECTION 20 - - - - - - - - - value = GRND8
   RETURN
   1320 CONTINUE
C- - - - - - - - - SECTION 21 - - - - - - - - - value = GRND9
   RETURN
   1321 CONTINUE
C- - - - - - - - - SECTION 22 - - - - - - - - - value = GRND10
   RETURN
C*****************************************************************
C
C- - - GROUP 14. Downstream pressure for PARAB=.TRUE.
C
   14 CONTINUE
   RETURN
C*****************************************************************
C* Make changes to data for GROUPS 15, 16, 17, 18 GROUP 19.
C*****************************************************************
C
C- - - GROUP 19. Special calls to GROUND from EARTH
C
    19 GO TO (191,192,193,194,195,196,197,198,199,1910,1911),ISC
   191 CONTINUE
C    * - - - - - - - - - SECTION 1 - - - Start of time step.
   RETURN
   192 CONTINUE
C    * - - - - - - - - - SECTION 2 - - - Start of sweep.
   RETURN
   193 CONTINUE
C    * - - - - - - - - - SECTION 3 - - - Start of iz slab.
   RETURN
   194 CONTINUE
C    * - - - - - - - - - SECTION 4 - - - Start of iterations over slab.
   RETURN
   1911 CONTINUE
C    * - - - - - - - - - SECTION 11- - - After calculation of convection
C                            fluxes for scalars, and of volume
C                            fractions, but before calculation of
```

```
C                              scalars or velocities
   RETURN
   199 CONTINUE
C    * - - - - - - - - - SECTION 9 - - - Start of solution sequence for
C                                        a variable
   RETURN
   1910 CONTINUE
C    * - - - - - - - - - SECTION 10- - - Finish of solution sequence for
C                                         a variable
   RETURN
   195 CONTINUE
C    * - - - - - - - - - SECTION 5 - - - Finish of iterations over slab.
   RETURN
   196 CONTINUE
C    * - - - - - - - - - SECTION 6 - - - Finish of iz slab.
   RETURN
   197 CONTINUE
C    * - - - - - - - - - SECTION 7 - - - Finish of sweep.
   RETURN
   198 CONTINUE
C * - - - - - - - - - SECTION 8 - - - Finish of time step.
C
   RETURN
C*************************************************************
C
C- - - GROUP 20. Preliminary print-out
C
   20 CONTINUE
   RETURN
C*************************************************************
C* Make changes to data for GROUPS 21 and 22 only in GROUP 19.
C*************************************************************
C
C- - - GROUP 23. Field print-out and plot control
   23 CONTINUE
   RETURN
C*************************************************************
C- - - GROUP 24. Dumps for restarts
C
   24 CONTINUE
END
```

APPENDIX C

Modification of Group 19 of ground.f subroutine in PHOENICS

To calculate the average concentrations of bacteria and vitamins in cans.

```
C*************************************************************
C* Make changes to data for GROUPS 15, 16, 17, 18 GROUP 19.
C*************************************************************
C
C- - - GROUP 19. Special calls to GROUND from EARTH
C
   19 GO TO (191,192,193,194,195,196,197,198,199,1910,1911),ISC
   191 CONTINUE

C    * - - - - - - - - - - - - - - - - - - SECTION 1 - - - - Start of time step.
      RETURN
   192 CONTINUE
C    * - - - - - - - - - - - - - - - - - - SECTION 2 - - - - Start of sweep.
        SUMCON2=0.0
        SUMCON3=0.0
        SUMCON4=0.0
        SUMVOL=0.0
   RETURN
193 CONTINUE
        LFCON2=L0F(C2)
        LFCON3=L0F(C3)
        LFCON4=L0F(C4)
C           C2, C3 and C4 is the Vitamins C, B1 and B2 concentration
     LFVOL=L0F(VOL)
     DO 3335 IX=1,NX
     DO 3335 IY=1,NY
        L2=LFCON2+IY+NY*(IX-1)
        L3=LFCON3+IY+NY*(IX-1)
        L4=LFCON4+IY+NY*(IX-1)
        L1=LFVOL+IY+NY*(IX-1)

        SUMCON2=SUMCON2+F(L1)*F(L2)
        SUMCON3=SUMCON3+F(L1)*F(L3)
        SUMCON4=SUMCON4+F(L1)*F(L4)
        SUMVOL=SUMVOL+F(L1)
```

```
3335 CONTINUE
C    * - - - - - - - - - - - - - - - - - - SECTION 3 - - - - Start of iz slab.
      RETURN
   194 CONTINUE
C    * - - - - - - - - - - - - - - - - - - SECTION 4 - - - - Start of iterations over slab.
      RETURN
   1911 CONTINUE
C    * - - - - - - - - - - - - - - - - - - SECTION 11 - - - - After calculation of convection
C                                          fluxes for scalars, and of volume
C                                          fractions, but before calculation of
C                                          scalars or velocities
      RETURN
   199 CONTINUE
C    * - - - - - - - - - - - - - - - - - - SECTION 9 - - - - Start of solution sequence for a variable
C
      RETURN
   1910 CONTINUE
C    * - - - - - - - - - - - - - - - - - - SECTION 10 - - - - Finish of solution sequence for a variable
C
      RETURN
   195 CONTINUE
C    * - - - - - - - - - - - - - - - - - - SECTION 5 - - - - Finish of iterations over slab.
      RETURN
   196 CONTINUE
C    * - - - - - - - - - - - - - - - - - - SECTION 6 - - - - Finish of iz slab.
      RETURN
   197 CONTINUE
C    * - - - - - - - - - - - - - - - - - - SECTION 7 - - - - Finish of sweep.
      RETURN
   198 CONTINUE

      WRITE(14,*)'/***AVERAGE CONCENTRATION AT TIME STEP **/'
      WRITE(14,3333)SUMCON2/SUMVOL,SUMCON3/SUMVOL,
                    SUMCON4/SUMVOL,ISTEP

3333 FORMAT(4(F10.6),I5)
C * - - - - - - - - - - - - - - - - - - SECTION 8 - - - - Finish of time step.
C
    RETURN
```

APPENDIX D

Modification of Group 13 of program input file (q1) and Group 13 (section 15) of ground.f subroutine in PHOENICS

To measure the retort response time (i.e., the retort come-up time).

Group 13 of program input file (q1)

```
************************************************************
Group 13. Boundary & Special Sources

PATCH (BUOYANCY, PHASEM,1,NX,1,NY,1,NZ,1,LSTEP)
COVAL (BUOYANCY, U1    ,  FIXFLU    , GRND3)
COVAL (BUOYANCY, V1    ,  FIXFLU    , GRND3)
COVAL (BUOYANCY, W1    ,  FIXFLU    , GRND3)

PATCH (BACTERIA,PHASEM,1,NX,1,NY,1,NZ,1,LSTEP)
COVAL (BACTERIA,C1 ,    GRND1    , 0.000E+00 )

PATCH (VITAMINC,PHASEM,1,NX,1,NY,1,NZ,1,LSTEP)
COVAL (VITAMINC,C2    ,    GRND2    , 0.000E+00 )

PATCH (RIBOFLA,PHASEM,1,NX,1,NY,1,NZ,1,LSTEP)
COVAL (RIBOFLA,C3    ,    GRND3    , 0.000E+00 )

PATCH (THIAMIN,PHASEM,1,NX,1,NY,1,NZ,1,LSTEP)
COVAL (THIAMIN,C4    ,    GRND4    , 0.000E+00 )

PATCH (UP       ,HWALL ,1,NX,1,NY,NZ,NZ,1, LSTEP)
COVAL (UP       ,U1  , FIXVAL , 0.000E+00)
COVAL (UP       ,V1  , FIXVAL , 0.000E+00)
COVAL (UP       ,TEM1, FIXVAL , GRND3)

PATCH (SIDE    ,NWALL ,1,NX,NY,NY,1,NZ,1, LSTEP)
COVAL (SIDE    ,U1  , FIXVAL , 0.000E+00)
COVAL (SIDE    ,W1  , FIXVAL , 0.000E+00)
COVAL (SIDE    ,TEM1, FIXVAL , GRND3)

PATCH (SIDS    ,SWALL ,1,NX,1,1,1,NZ,1, LSTEP)
COVAL (SIDS    ,U1  , FIXVAL , 0.000E+00)
COVAL (SIDS    ,W1  , FIXVAL , 0.000E+00)
COVAL (SIDS    ,TEM1, FIXVAL , GRND3)
```

```
PATCH (DOWN    ,LWALL ,1,NX,1,NY,1,1,1, LSTEP)
COVAL (DOWN    ,U1  , FIXVAL , 0.000E+00)
COVAL (DOWN    ,V1  , FIXVAL , 0.000E+00)
COVAL (DOWN    ,TEM1,   FIXVAL , GRND3)

PATCH (WATTIE   ,EWALL ,NX,NX,1,NY,1,NZ,1, LSTEP)
COVAL (WATTIE   ,V1  , FIXVAL , 0.000E+00)
COVAL (WATTIE   ,W1  , FIXVAL , 0.000E+00)
COVAL (WATTIE  ,TEM1,   FIXVAL , GRND3)

PATCH (WATTIES ,WWALL ,1,1,1,NY,1,NZ,1, LSTEP)
COVAL (WATTIES ,V1  , FIXVAL , 0.000E+00)
COVAL (WATTIES ,W1  , FIXVAL , 0.000E+00)
COVAL (WATTIES ,TEM1, FIXVAL , GRND3)

BUOYA  = 0.000E+00 ; BUOYB =−9.810E+00 ; BUOYC = 0.000E+00
BUOYD  = GRND10
BUOYE  = 4.000E+01
EGWF  =  T
************************************************************
```

Group 13 of ground.f subroutine

```
************************************************************************
C
C- - - GROUP 13. Boundary conditions and special sources
C                              Index for Coefficient - CO
C                              Index for Value - VAL
   13 CONTINUE
      GO TO (130,131,132,133,134,135,136,137,138,139,1310,
      11311,1312,1313,1314,1315,1316,1317,1318,1319,1320,1321),ISC
   130 CONTINUE
C- - - - - - - - - - - - - - - - - - SECTION 1 - - - - - - - - - - - - - coefficient = GRND
      RETURN
   131 CONTINUE
C- - - - - - - - - - - - - - - - - - SECTION 2 - - - - - - - - - - - - - coefficient = GRND1
      IF ( INDVAR . EQ . C1 ) THEN
      CALL FN1 ( CO , 2.500E+11 )
      LTMP=LBNAME('TEM1')
      CALL FN32(CO,LTMP,−31873.95,273.15)

      ENDIF
      RETURN
   132 CONTINUE
C- - - - - - - - - - - - - - - - - - SECTION 3 - - - - - - - - - - - - - coefficient = GRND2
      IF ( INDVAR . EQ . C2 ) THEN
      CALL FN1 ( CO , 2.850E+9 )
      LTMP=LBNAME('TEM1')
      CALL FN32(CO,LTMP,−12027.9,273.15)
```

```
      ENDIF
      RETURN
   133 CONTINUE
C- - - - - - - - - - - - - - - - - - SECTION 4 - - - - - - - - - - - - - coefficient = GRND3
      IF ( INDVAR . EQ . C3 ) THEN
      CALL FN1 ( CO , 2.480E+8 )
      LTMP=LBNAME('TEM1')
      CALL FN32(CO,LTMP,−12027.9,273.15)

      ENDIF
      RETURN
   134 CONTINUE
C- - - - - - - - - - - - - - - - - - SECTION 5 - - - - - - - - - - - - - coefficient = GRND4
      IF ( INDVAR . EQ . C4 ) THEN
      CALL FN1 ( CO , 8.5E+08 )
      LTMP=LBNAME('TEM1')
      CALL FN32(CO,LTMP,−10825.11,273.15)

      ENDIF
      RETURN
   135 CONTINUE
C- - - - - - - - - - - - - - - - - - SECTION 6 - - - - - - - - - - - - - coefficient = GRND5
      RETURN
   136 CONTINUE
C- - - - - - - - - - - - - - - - - - SECTION 7 - - - - - - - - - - - - - coefficient = GRND6
      RETURN
   137 CONTINUE
C- - - - - - - - - - - - - - - - - - SECTION 8 - - - - - - - - - - - - - coefficient = GRND7
      RETURN
   138 CONTINUE
C- - - - - - - - - - - - - - - - - - SECTION 9 - - - - - - - - - - - - - coefficient = GRND8
      RETURN
   139 CONTINUE
C- - - - - - - - - - - - - - - - - - SECTION 10 - - - - - - - - - - - - - coefficient = GRND9
      RETURN
   1310 CONTINUE
C- - - - - - - - - - - - - - - - - - SECTION 11 - - - - - - - - - - - - - coefficient = GRND10
      RETURN
   1311 CONTINUE
C- - - - - - - - - - - - - - - - - - SECTION 12 - - - - - - - - - - - - - - - - - - - value = GRND
      RETURN
   1312 CONTINUE
C- - - - - - - - - - - - - - - - - - SECTION 13 - - - - - - - - - - - - - - - - - - - value = GRND1
      RETURN
   1313 CONTINUE
C- - - - - - - - - - - - - - - - - - SECTION 14 - - - - - - - - - - - - - - - - - - - value = GRND2
      RETURN
   1314 CONTINUE
```

```
C- - - - - - - - - - - - - - - - - - - SECTION 15 - - - - - - - - - - - - - - - - - - - value = GRND3
      TC=60.0
      WALTEM=97.0+24.0*(1-EXP(-TIM/TC))
      CALL FN1 (VAL,WALTEM)
      RETURN
   1315 CONTINUE
C- - - - - - - - - - - - - - - - - - - SECTION 16 - - - - - - - - - - - - - - - - - - - value = GRND4
      RETURN
   1316 CONTINUE
C- - - - - - - - - - - - - - - - - - - SECTION 17 - - - - - - - - - - - - - - - - - - - value = GRND5
      RETURN
   1317 CONTINUE
C- - - - - - - - - - - - - - - - - - - SECTION 18 - - - - - - - - - - - - - - - - - - - value = GRND6
      RETURN
   1318 CONTINUE
C- - - - - - - - - - - - - - - - - - - SECTION 19 - - - - - - - - - - - - - - - - - - - value = GRND7
      RETURN
   1319 CONTINUE
C- - - - - - - - - - - - - - - - - - - SECTION 20 - - - - - - - - - - - - - - - - - - - value = GRND8
      RETURN
   1320 CONTINUE
C- - - - - - - - - - - - - - - - - - - SECTION 21 - - - - - - - - - - - - - - - - - - - value = GRND9
      RETURN
   1321 CONTINUE
C- - - - - - - - - - - - - - - - - - - SECTION 22 - - - - - - - - - - - - - - - - - - - value = GRND10
      RETURN
C*************************************************************
C
```

APPENDIX E

Groups 1–6 of program input file (q1) of PHOENICS

The construction of the pouch geometry.

```
TALK=T;RUN( 1, 1);VDU=X11-TERM

   GROUP 1. Run title and other preliminaries
TEXT(Pouch sterilization)

INTEGER(NXA,NYB,NZC,COUNTI,COUNTJ,COUNTK)
REAL(A,BB,B,C,PI,TA,COEF,COEF2,COEFI,COEFJ,COEFK)

A=0.12
B=0.04
C=0.22
PI=4.0*ATAN(1.0 )

 CELLS
NXA=10;NYB=5;NZC=30

   GROUP 2. Transience; time-step specification
STEADY= F
   * Set overall time and no. of steps
RSET(U,0.000E+00,3.00E+03,30)
   * Cut regions
RSET(T,L,0,2.00E+02)
RSET(T,L,0,1.000E+03)
   * Modify regions
RSET(T,1,10,1.000E+00)
RSET(T,2,10,1.000E+00)
RSET(T,3,10,1.000E+00)

   GROUP 3. X-direction grid specification
NX=2*NXA
XULAST=2*A

   GROUP 4. Y-direction grid specification
NY=2*NYB
YVLAST=2*B
```

```
   GROUP 5. Z-direction grid specification
NZ=NZC
ZWLAST=C

   GROUP 6. Body-fitted coordinates or grid distortion
BFC=T;NONORT=T

NX
NY
NZ

 Set all coordinates to zero
DOMAIN(1,NX+1,1,NY+1,1,NZ+1)
SETLIN(XC,0)
SETLIN(YC,0)
SETLIN(ZC,0)

MESG( Begining Grid Generation
TA=45.*PI/180

BB=B
COUNTK=1
DO KK=1,NZC+1
B=BB-(BB-0.009)*(COUNTK-1)/NZC
COEFK=C*(((COUNTK-1)/NZ)-1)

 Ellipse tangent at 45degs
COEF=(((A**4/B**2)*TAN(TA)**2)/(1+(A**2/B**2)*TAN(TA)**2))**0.5
COEF2=A-COEF

 Vertical Ends
COUNTJ=1
DO JJ=1,NYB+1
COEFI=A-COEF2*(COUNTJ-1)/NYB
COEFJ=((1-(COEFI/A)**2)**0.5)*B
SETPT(1,NYB+COUNTJ,COUNTK,-COEFI,COEFJ,COEFK)
SETPT(NX+1,NYB+COUNTJ,COUNTK,COEFI,COEFJ,COEFK)
SETPT(1,NYB+2-COUNTJ,COUNTK,-COEFI,-COEFJ,COEFK)
SETPT(NX+1,NYB+2-COUNTJ,COUNTK,COEFI,-COEFJ,COEFK)
COUNTJ=COUNTJ+1
ENDDO

 Horizontal
COUNTI=1
DO II=1,NXA+1
COEFI=COEF*(1-((COUNTI-1)/NXA))
COEFJ=((1-(COEFI/A)**2)**0.5)*B
SETPT(2*(NXA+1)-COUNTI,NY+1,COUNTK,COEFI,COEFJ,COEFK)
```

```
SETPT(2*(NXA+1)-COUNTI,1,COUNTK,COEFI,-COEFJ,COEFK)
SETPT(COUNTI,NY+1,COUNTK,-COEFI,COEFJ,COEFK)
SETPT(COUNTI,1,COUNTK,-COEFI,-COEFJ,COEFK)
COUNTI=COUNTI+1
ENDDO

DOMAIN(1,NX+1,1,NY+1,COUNTK,COUNTK)
MAGIC(T)
MSWP=40
MAGIC(L)

COUNTK=COUNTK+1
ENDDO

dumpc(MGBR1)
numblk=1;READCO(MGBR+)
gview(x);view
   stop
```

APPENDIX F

Group 13 of program input file (q1) of PHOENICS

Thermal sterilization of a 3-D pouch filled with carrot-orange soup, heated by condensing steam at 121°C and cooled by water at 20°C.

```
************************************************************

 Group 13. Boundary & Special Sources

PATCH (BUOYANCY, PHASEM,1,NX,1,NY,1,NZ,1,LSTEP)
COVAL (BUOYANCY, U1 , FIXFLU , GRND3)
COVAL (BUOYANCY, V1 , FIXFLU , GRND3)
COVAL (BUOYANCY, W1 , FIXFLU , GRND3)

PATCH (UP    ,HWALL ,1,NX,1,NY,NZ,NZ,1,60)
COVAL (UP    ,U1 , FIXVAL , 0.000E+00)
COVAL (UP    ,V1 , FIXVAL , 0.000E+00)
COVAL (UP    ,TEM1, FIXVAL , 1.210E+02)

PATCH (SIDE    ,NWALL ,1,NX,NY,NY,1,NZ,1,60)
COVAL (SIDE    ,U1 , FIXVAL , 0.000E+00)
COVAL (SIDE    ,W1 , FIXVAL , 0.000E+00)
COVAL (SIDE    ,TEM1, FIXVAL , 1.210E+02)

PATCH (SIDS    ,SWALL ,1,NX,1,1,1,NZ,1,60)
COVAL (SIDS    ,U1 , FIXVAL , 0.000E+00)
COVAL (SIDS    ,W1 , FIXVAL , 0.000E+00)
COVAL (SIDS    ,TEM1, FIXVAL , 1.210E+02)

PATCH (DOWN    ,LWALL ,1,NX,1,NY,1,1,1,60)
COVAL (DOWN    ,U1 , FIXVAL , 0.000E+00)
COVAL (DOWN    ,V1 , FIXVAL , 0.000E+00)
COVAL (DOWN    ,TEM1, FIXVAL , 1.210E+02)

PATCH (WATTIE    ,EWALL ,NX,NX,1,NY,1,NZ,1,60)
COVAL (WATTIE    ,V1 , FIXVAL , 0.000E+00)
COVAL (WATTIE    ,W1 , FIXVAL , 0.000E+00)
COVAL (WATTIE    ,TEM1, FIXVAL , 1.210E+02)
```

```
PATCH (WATTIES    ,WWALL ,1,1,1,NY,1,NZ,1,60)
COVAL (WATTIES    ,V1 , FIXVAL , 0.000E+00)
COVAL (WATTIES    ,W1 , FIXVAL , 0.000E+00)
COVAL (WATTIES    ,TEM1, FIXVAL , 1.210E+02)

PATCH (UP1    ,HWALL ,1,NX,1,NY,NZ,NZ,61,LSTEP)
COVAL (UP1    ,U1 , FIXVAL , 0.000E+00)
COVAL (UP1    ,V1 , FIXVAL , 0.000E+00)
COVAL (UP1    ,TEM1, 1.546E-01 , 2.000E+01)

PATCH (SIDE1    ,NWALL ,1,NX,NY,NY,1,NZ,61,LSTEP)
COVAL (SIDE1    ,U1 , FIXVAL , 0.000E+00)
COVAL (SIDE1    ,W1 , FIXVAL , 0.000E+00)
COVAL (SIDE1    ,TEM1, 1.546E-01, 2.000E+01)

PATCH (SIDS1    ,SWALL ,1,NX,1,1,1,NZ,61,LSTEP)
COVAL (SIDS1    ,U1 , FIXVAL , 0.000E+00)
COVAL (SIDS1    ,W1 , FIXVAL , 0.000E+00)
COVAL (SIDS1    ,TEM1, 1.546E-01, 2.000E+01)

PATCH (DOWN1    ,LWALL ,1,NX,1,NY,1,1,61,LSTEP)
COVAL (DOWN1    ,U1 , FIXVAL , 0.000E+00)
COVAL (DOWN1    ,V1 , FIXVAL , 0.000E+00)
COVAL (DOWN1    ,TEM1, 1.546E-01, 2.000E+01)

PATCH (WATTIE1    ,EWALL ,NX,NX,1,NY,1,NZ,61,LSTEP)
COVAL (WATTIE1    ,V1 , FIXVAL , 0.000E+00)
COVAL (WATTIE1    ,W1 , FIXVAL , 0.000E+00)
COVAL (WATTIE1    ,TEM1, 1.546E-01, 2.000E+01)

PATCH (WATTIES1    ,WWALL ,1,1,1,NY,1,NZ,61,LSTEP)
COVAL (WATTIES1    ,V1 , FIXVAL , 0.000E+00)
COVAL (WATTIES1    ,W1 , FIXVAL , 0.000E+00)
COVAL (WATTIES1    ,TEM1, 1.546E-01, 2.000E+01)

BUOYA = 0.000E+00 ; BUOYB =−9.810E+00 ; BUOYC = 0.000E+00
BUOYD = GRND10
BUOYE = 4.000E+01
EGWF = T
**********************************************************
```

APPENDIX G

Derivation of Equation (6.3) used to minimize the distortion of grid cells in the corner of the pouch.

In the construction of pouch geometry, Equation (1) for ellipse was used for the construction of pouch grid in the x–y plane:

$$\left(\frac{x}{a}\right)^2 + \left(\frac{y}{b}\right)^2 = 1 \tag{1}$$

$$\frac{2x}{a^2} = -\frac{2y}{b^2}\frac{dy}{dx} \tag{2}$$

$$\frac{dy}{dx} = -\frac{x}{y}\frac{b^2}{a^2} = \tan\theta \tag{3}$$

$$x = -y\frac{a^2}{b^2}\tan\theta \tag{4}$$

From Equation (1), the height of the pouch, shown in Figure 6.2, can be written as follows:

$$y = \mp b\sqrt{1 - \left(\frac{x}{a}\right)^2} \tag{5}$$

$$x = -\sqrt{b^2 - \left(\frac{xb}{a}\right)^2}\frac{a^2}{b^2}\tan\theta \tag{6}$$

$$x = -\sqrt{-b^2\frac{a^4}{b^4}\tan^2\theta - \left(\frac{xb}{a}\right)^2\frac{a^4}{b^4}\tan^2\theta} \tag{7}$$

$$x = -\sqrt{\frac{a^4}{b^2}\tan^2\theta - \left(\frac{xb}{a}\right)^2\frac{a^4}{b^4}\tan^2\theta} \tag{8}$$

$$x^2\left[1 + \left(\frac{a}{b}\right)^2\tan^2\theta\right] = \frac{a^4}{b^2}\tan^2\theta \tag{9}$$

$$x = \sqrt{\frac{\left(\frac{a^4}{b^2}\right)\tan^2\theta}{1 + \left(\frac{a^2}{b^2}\right)\tan^2\theta}} \tag{10}$$

INDEX